Australian
National
University

AUTOMATED FIBRE PLACEMENT WITH IN-SITU ULTRAVIOLET CURING AND ON-THE-FLY RESIN IMPREGNATION

Adriano Di Pietro, BEng (Hons)

A Thesis submitted for the degree of
Doctor of Philosophy of
The Australian National University

August 2015

Declaration

This thesis is an account of research undertaken between July 2007 and August 2015 at the College of Engineering and Computer Science, The Australian National University, Canberra, Australia.

This thesis contains no material that has been accepted for the award of any other degree or diploma in any university. To the best of the author's knowledge and belief, it contains no material previously published or written by another person, except where due reference has been made in the text.

Adriano Di Pietro

Publications

The following publications were published during the course of this research:

Di Pietro, A, Compston, P, Hovland, G 2008, 'Toward Rapid Robotic Fibre Placement with in-situ UV Curing', *1st Annual International Conference on Sustainable Automotive Technology (ICSAT)*, RMIT Press, Melbourne, Australia.

Di Pietro, A, Compston, P 2009, 'Automated Fibre Placement with in-situ Ultraviolet Curing: Concept Testing', *2nd Annual International Conference on Sustainable Automotive Technology (ICSAT)*, Germany.

Di Pietro, A, Compston, P 2009, 'Resin Hardness and interlaminar shear strength of glass fibre/vinylester composite cured with high intensity ultraviolet (UV) light', *Journal of Material* Science, vol. 44, pp. 4188-4190.

Di Pietro, A, Compston, P 2011, 'Shear properties of a glass-fibre/vinylester composite cured with high intensity ultraviolet light for use in automated manufacturing processes', *Advanced Composite Letters*, 20 (2).

Di Pietro, A, Cardew-Hall, M, Compston, P 2014, 'A Predictive Model for the Degree of Cure in Automated Fibre Placement with in-situ UV Curing', In draft.

Schiemer, J, Di Pietro, A, Compston, P, Hovland, G 2009, 'Accuracy assessment of 3-axis robotic milling of polymer foam', *Australian National University – Internal Report*, Canberra, Australia.

Acknowledgements

Firstly, I would like to thank my supervisor Professor Michael Cardew-Hall for the opportunity to undertake this work; your enduring support gave me the strength and direction I needed to get this thesis finished and was a saving force more than once. You provided me with an example of leadership and I am forever grateful for your support and your time. I would also like to thank my other supervisors. Professor Bronwyn Fox, for your technical and academic guidance, particularly during the later stages of my thesis write-up; Robert Gresham, for your technical guidance during the build phase of my thesis; Dr. Geir Hovland for the opportunity to work and study in Norway within you dynamic team; and Dr. Paul Compston for the opportunity and supervision for my thesis during my time as a full time student. Thank you to The Australian National University for the institution within which I could undertake such a significant and life changing experience particularly during my part-time studies as a remote student many kilometres from the physical bricks and mortar.

To my brilliant and beautiful wife Natalene, your love and support was a constant throughout this thesis and you have always been my inspiration. Not only did you encourage me to start this work, but you also helped me in so many ways in finishing it. I have learnt so much from you during this thesis and I appreciate and thank you for the sacrifices you made in supporting me. It is clear to me that great work cannot come without great love and family. Siena, Aria and Mia, your arrivals all came during the time of this thesis and you have each imparted your own inspiration and love on and within me that has contributed to it.

I am also very grateful for the encouragement and confidence of my parents and my brother, Antonio, Anna and Damiano Di Pietro. You have helped me bring together ideas and thoughts along the way, you were there with me the whole way especially when the end seemed so far away, thank you. I would also like to thank all my friends for their encouragement, distractions, laughs and debates. Jeff, Jose and Rebecca, our time as office mates won't be forgotten. Iain Kendal, thank you for your support and comradery as a team mate in the InnovationACT competition. The tenacity and creativity of that experience was a highlight during this thesis.

Abstract

Vehicle emissions contribute to up to one third of the world's air pollution [1]. Reducing vehicle weight is crucial to reducing these emissions. Composite materials offer high specific strength-to-weight ratios which make them ideal for lightweight applications; however, existing composite manufacturing is slow and expensive. Automated Fibre Placement (AFP) is a state-of-the-art composite manufacturing process but is limited by the low complexity of parts it can produce; the cost, size and speed of the actuation systems; expensive and sensitive material options; and numerous pre and post-processes required in order to complete a part. This research proposes a new and efficient composite manufacturing process that addresses these limitations by combining AFP technology with in-situ ultraviolet (UV) curing and on-the-fly fibre and resin impregnation (UVAFP). The body of this thesis focused on proving the process concept and building robust predictive models for the technology.

It was proposed that reducing the size of the placement head would increase the capability of this technique to manufacture more complex parts. It was shown that by optimising the placement head clearance angle, placement head width and the compaction roller radius the minimum placement radius and arc length could be as small as 100mm and 90° respectively. It was also demonstrated that industrial robots were sufficiently accurate and repeatable to act as placement articulators for AFP. The feed rate, path interpolation point filtering and spindle speed were optimised to achieve a path following accuracy of less than 0.042mm. By increasing the tension in the tow and compaction force, dry fibre tows were shown to be a suitably dimensionally stable replacement for expensive towpregs with minimal gaps and overlaps.

Dry glass fibre tows and bulk vinylester resin impregnated on-the-fly was chosen as an inexpensive and versatile material system and consolidation approach for use in UVAFP. The material system was shown to have equivalent properties to composites manufactured by traditional techniques and good strength in comparison to aluminium and steel but much lighter. Rapid impregnation times were demonstrated up to 2160 mm/sec. High intensity UV light curing eliminated the need for post process curing and shortened the cure time and increased layup speeds. When the UV light was

applied in a ply-by-ply in-situ approach, the cure time was measured to decrease the current thermal cure cycle length by 43.75% and the degree-of-cure was increased by 1.3% (as measured indirectly by the interlaminar shear strength). By characterising the process parameters, the effect on degree of cure and degradation could be controlled and predicted. A degree of cure in excess of 99% was achieved, providing equivalent material properties to traditional thermal cured composites while minimising peak exposure temperatures, thus reducing mass loss caused by thermo-oxidative degradation.

UVAFP was demonstrated to be a viable composite manufacturing process capable of producing high quality components and addressing the limitations of current AFP systems. The technology was shown to address efficiency shortfalls and make composite manufacturing economical and accessible to vehicle manufacturers searching for manufacturing process solutions for lightweight.

Contents

List of Figures

List of Tables

List of Equations

Nomenclature

Nomenclature	Property	Unit
σ	Stress	MPa
F	Force	N
A	Area	mm^2
ε	Strain	-
E	Young's modulus	GPa
G	Shear modulus	GPa
v	Poisson's ratio	-
L	Change in specimen length	mm
L	Initial specimen length	mm
σ_T	True stress	MPa
σ_E	Engineering stress	MPa
ε_T	True strain	-
ε_E	Engineering strain	-
σ_x	Principal x-direction stress	MPa
σ_y	Principal y-direction stress	MPa
σ_z	Principal z-direction stress	MPa
τ_{sbs}	Interlaminar short beam shear strength	MPa
τ_{xy}	In-plane (xy) shear stress	MPa
τ_{zx}	Transverse (zx) shear stress	MPa
ε_1	Major strain	-
ε_2	Minor strain	-
ε_{eff}	Effective plastic strain	-
σ_0	Yield stress	MPa
T	Temperature	°C

Acronyms

Acronym	Description
AFP	Automated Fibre Placement
AHK	Alpha-Hydroxy Ketones
ANOM	Analysis of Means
ANU	Australian National University
ATL	Automated Tape Laying
BAPO	Bisacylphosphine Oxide
barg	Bar gauge pressure
CAD	Computer Aided Design
CAE	Computer Aided Engineering
CAM	Computer Aided Manufacturing
CCR	Cut, Clamp, Restart
CNC	Computer Numeric Controlled
cPs	Centipoise
CPT	Cured Ply Thickness
DAQ	Data Acquisition
DC	Dynamic Current (electrical)
DI	Digital Input
DIO	Digital Input / Output
DLPC	Double Langmuir Probe Characteristic
DO	Digital Output
DOE	Design of Experiments
DSC	Differentiated Scanning Calorimetry
DMA	Dynamic Material Analysis
EB	Electron Beam
FDA	United States Food and Drug Authority
FOD	Foreign Object Damage
FRP	Fibre Reinforced Polymer

FW	Filament Winding
HEPA	High Efficiency Particulate Arrestance
HMI	Human Machine Interface
ILSS	Interlaminar Shear Strength
IM	Intermediate Modulus
IO	Input / Output
IR	Infrared
MEKP	Methylethylketone peroxide
NASA	National Aeronautics and Space Agency
OEM	Original Equipment Manufacturer
PA	Polyamides
PP	Polypropylene
PEI	Polyetherimide
PET	Polyethyleneterephthalate
PES	Polyethersulfone
PEEK	Polyetheretherketone
PEKK	Polyetherketoneketone
PID	Proportional-Integral-Derivative
PPH	Parts per hundred
PTFE	Polytetrafluoroethylene (Teflon)
QFD	Quality Functional Development
RMIT	Royal Melbourne Institute of Technology
RMSE	Root Mean Square Error
RST	Resin Spray Transfer
RTM	Resin Transfer Moulding
RI	Resin Infusion
RFP	Robotic Fibre Placement or Request for Proposal
R^2	Coefficient of Determination
SMC	Sheet Moulding Compound
SN	Signal to Noise ratio
TCP	Tool Centre Point

TEX	Textile weight measure (g/1000m)
Tg	Glass Transition Temperature
TP	Thermoplastic
TS	Thermoset
UV	Ultraviolet
UVAFP	Ultraviolet Automated Fibre Placement
VAP	Vacuum Assisted Processes
VARTM	Vacuum assisted resin transfer moulding
VER(s)	Vinylester resin(s)
Vf	Fibre Volume Fraction
VOC	Volatile Organic Compound
WT%	Percentage by weight

1 Introduction

Government regulations around the world require aircraft and road vehicles to adhere to strict fuel and material restrictions in order to satisfy pollution emissions targets and recyclability considerations for a full cradle-to-cradle lifecycle. New regulations that are being introduced include the emissions trading schemes in Australia, Great Britain and Germany, post-Kyoto protocols [2], seeking further cuts to carbon emissions, and even lower pollution reduction targets. To achieve these goals, lightweight, fuel-efficient transport options are part of the solution. Fibre reinforced polymer material systems (or composites) offer lightweight and high specific strength and stiffness with the ability to be tailored for specific loading applications. Their superior mechanical properties of composite materials make them attractive for industries where weight in structures is critical to performance, such as the transportation industry. Their specific strength-to-weight ratio means that composites can reduce component weights by approximately up to 60% when compared to steel components, and approximately up to 40% when compared to aluminium components [3]. As such, composites are increasingly being utilised in the aerospace, automotive and high performance industries as an alternative to traditional metals. The use of these materials in the production of transportation structures offers the possibility of significantly reduced weight and higher performance specifications, therefore, reducing energy consumption and decreasing the carbon emissions and increasing the range.

While the composites market continues to grow [4], unfortunately, traditional approaches to the manufacture of composite structures are time consuming and expensive for most industries. This cost is driven not only by the high material cost (generally the cost of prepregs), but also the slow manual labour intensive processes used to produce components made from these materials. In general, manufacturing processes include numerous labour intensive lay-up and curing stages, long cycle times, use of expensive constituent materials with high scrap rates and hazardous emissions. In addition, expensive specialised capital equipment is often required, restricting the availability of the technology to large production industries. As composite

manufacturing is currently reliant upon these slow and expensive processes, current growth in global demand for composites will soon outstrip the composite manufacturing industry's output capacity. As a result, only one third of the world's demand for fibre reinforced polymers will be met by 2020 [1].

Faster, economical and more efficient composite manufacturing processes are needed to provide lightweight vehicle solutions to reduce pollution and promote zero emission modes of transport such as e-mobility [5][6]. Furthermore, accessible technologies that have reduced footprint, less capital burden upfront, and increased flexibility to service a larger number of different applications are necessary to grow the composites industry faster. Automated manufacturing technologies offer accelerated production, increased quality and repeatability, and reduced labour costs. Automated Fibre Placement (AFP) is the current state-of-the-art technology in automated composite manufacturing and offers huge potential as a cost effective composite production process.

1.1 Automated Fibre Placement

Automated manufacture of composite parts by means of AFP is a clean, quick process that improves accuracy and repeatability for fibre alignment in tailored composite parts [7]. AFP is recognised as the current state-of-the-art automated process for the production of composite structures in the aerospace industry [8]. Lay-up rates and quality are vastly improved when compared to hand lay-up. Automation offers repeatable high quality components and reduces labour costs. The process is also flexible and can be applied after offline programming to produce any appropriately designed component. The process applies reinforcement fibres with or without resin onto a tool through a predefined path, incrementally laying adjacent tows (ribbons of reinforcement fibres) to complete a ply, building up thickness ply-by-ply. This allows for direct manufacture of design intent by controlling the lay-up path of each individual tow optimising placement paths [9] and increasing efficiency while reducing waste. An example of an AFP system produced by Coriolis Composites [10] as mounted on an industrial robot is shown in Figure 1.

Figure 1 – An AFP system by Coriolis Composites

A small number of commercial AFP models are currently available for both thermoset and thermoplastic composites, and offer vastly improved lay-up times and quality in comparison to manual lay-up. Industries such as the aerospace and aeronautical industries have adopted these units in their manufacturing lines to meet fast throughput time on new high production models [11][12][13][14]. However, in spite of the potential benefits, a number of limitations exist that have implications for industrial application of the technology.

1.2   Limitations of AFP

AFP is a highly automated state-of-the-art technology however, due to a number of limitations; the technology is currently restricted to specific applications where the throughput and cost can be justified, for example, commercial and military aircraft that have high margins and low volume orders. The primary limitations of the AFP process are:

1.   Design of AFP systems – limited reach and access

Due to the design of the hardware systems of AFP, the process has limited capacity to produce 3D shapes and access tight corners. This limits the range of parts the

equipment can build [15]. Through miniaturisation of placement head design and discrete localised control of the composite at the nip point, tighter geometry should be possible. Likewise, scalable high degree of freedom, high accuracy articulation systems are also required to address this limitation. Composite manufacturing can become both safer and capable of producing complex 3D shapes and superior quality parts.

2. Type of Materials - limited properties

Currently, material options for fibre placement systems are limited to preimpregnated tows or specific bindered tows. Moreover, only a few specific types of prepregs and bindered tows can be used in AFP. While lighter than steel and aluminium, these AFP supply materials have limited properties and are generally specified for high performance, low volume applications such as the aerospace industry where high costs and long processing times are acceptable. For widespread use in transportation vehicles different material options are needed that can be tailored properties, are economical, and have faster processing for high volume production.

3. The process – slow and segmented

Most composite manufacturers build composites from prepreg reinforcement fibre fabric or tows; the same applies for current AFP systems. Prepregs require refrigerated storage handling and separation film between their layers. In AFP systems, this means that the creel system must be temperature and humidity controlled, guide systems get blocked and require constant servicing, and the placement head must contain heating and cooling systems for handling purposes all before the composite is applied by the compaction roller.

Composite manufacturing requires several steps: lay-up, bag and de-bulk, curing, finishing and cutting. Current AFP systems only provide a solution to the lay-up step, meaning that all other steps must still occur in addition either before or after AFP processing. The movement and setup and pull-down time for each additional process step increases both the factory footprint and the number of workers required to operate, which escalates the cost and production time of each part. Most composite parts require curing by heating and pressure to set the resin and the fibre together, which is often provided by autoclaves following lay-up, whether by AFP or other means. Curing is a time consuming process that typically takes up to 20 hours. In addition, composite parts

must fit into the autoclave, which restricts the size, shape, and range of parts that composite manufacturers can build. Finally, autoclaves are expensive typically costing millions of dollars. The autoclaves themselves make up the bulk of the capital cost for any composite manufacturer. Thus, autoclave curing is the single largest obstacle to efficient and economical composite manufacturing. Furthermore access to relevant industrial data in making manufacturing decisions around the use of the technology is limited due to the competitive market place and closed vendor community. As such more data in the way of process models is needed in order for wider scale adoption of the technology.

1.3 Research Objectives

Using the current AFP technology as the benchmark, the current research aims to develop a novel concept that combines the function of AFP technology, with ultraviolet (UV) light curing applied as the composite is laid "in-situ", and continuous resin impregnation at the point of application or "on-the-fly", otherwise termed throughout this work as UVAFP.

The main goal of this research is to investigate whether a novel composite manufacturing process can be used to produce lightweight, stronger, more complex vehicle structures faster than current AFP processes. More specifically, the objectives of this thesis are:

1. To understand the primary geometric parameters that define the complexity limitations of AFP that will enable AFP technology to be applied to complex parts with tight radii therefore enabling it to be utilised more broadly by industry.

2. To understand if by using in-situ UV curing and on-the-fly resin impregnation in the AFP system, composite components can be made in a faster more efficient manner while maintaining their appealing lightweight and strength.

3. To understand the fundamental process kinetics and mechanics so that an accurate model can be developed for precise application of the technology and to produce optimised part quality.

Ultimately, this work aims to demonstrate the feasibility that environmental regulations can be met by decreasing fuel consumption of transportation vehicles (such as aeroplanes and automobiles) through vehicle lightweighting. The global context of the thesis, the ultimate impact, problem, cause, cost, effect of the environmental regulation, and the drivers of this effect are presented schematically in Figure 2.

Problem	Health issues, climate change and environment damage		
Cause	Pollution		
Impact	Energy consumption and dirty fuels		
Cost	Environmental Regulations		
Effect	Vehicle Weight		
Drivers	Design	Materials	Process
Limitations	Complexity of Parts	Properties	Production rate
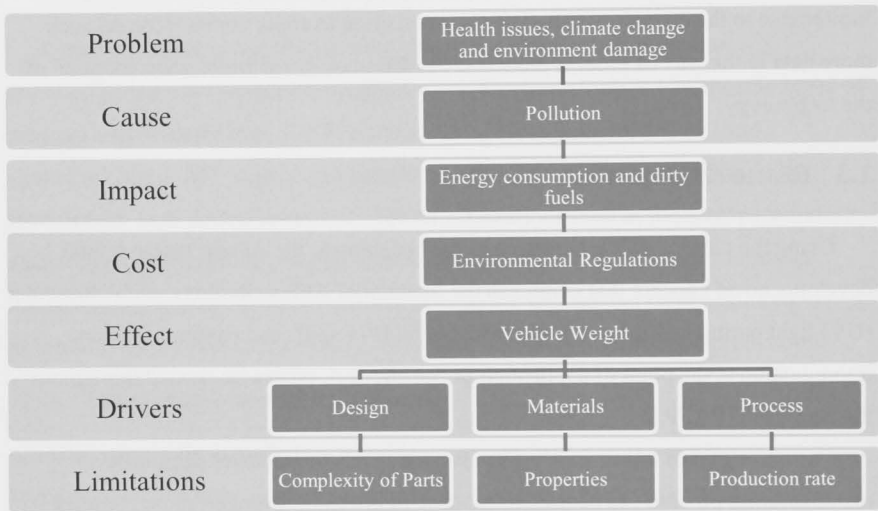
Figure 2 – Thesis context schematic

1.3.1 Research Hypothesis

The research approach for this thesis was centred on addressing the previously mentioned key limitations of current AFP processes. Nine hypotheses were tested in this work, each a driver of vehicle weight: design, materials and process.

1. **Design of Automated Fibre Placement Systems (Experiments 1 and 2)**

   a. Reducing the size of the AFP placement head will increase the reach and accessibility of the AFP placement head within the lay-up tool.

   b. By decreasing the arm extension, decreasing feed rate, increasing spindle speed, and decreasing the point filtering for the path generation

of industrial robots, will increase the path following accuracy of the industrial robot.

2. **Material Selection and Development (Experiment 3 and 4)**

    a. Increasing the tension and compaction force of the lay-up process of AFP will reduce the width and thickness variability of dry glass fibre tows.

    b. By using glass fibre and vinylester resin impregnated on-the-fly and cured in-situ using UV will result in a composite material of comparable mechanical properties to aluminium, steel and composites manufactured by traditional hand laid-up thermally cured techniques.

3. **Process Optimisation for Resin Impregnation and Curing (Experiments 5, 6, 7, 8 and 9)**

    a. By using dry glass fibre tows and on-the-fly resin impregnation, the impregnation time will be decreased in comparison to existing AFP processes.

    b. By using high intensity UV light the dose will be increased over a shorter period of time and increase the degree of cure during UVAFP.

    c. Applying the curing mechanism in a ply-by-ply in-situ approach will result in equivalent mechanical properties of the glass fibre vinylester composite cured using traditional at-once thermal processing.

    d. Testing the height of the UV light, the intensity of the UV light and the speed of the placement will define the accurate dose of UV light and degree of cure of the composite during UVAFP.

    e. Testing the height of the UV light, the intensity of the UV light and the speed of the placement will define the temperature during processing and the degradation of the composite during UVAFP.

1.4 Thesis Structure

Chapter 1 examined the key limitations of current AFP systems and proposed the research objectives and hypotheses of the current research. This thesis is structured according to each of the key limitations of AFP presented in section 1.2 where the experiments undertaken aim to address each of the AFP limitations. Each chapter focuses on a unique limitation in order of their place in the AFP manufacturing process chain and in order of precedence for driving later development.

Chapter 2 presents the literature review and the background theory surrounding AFP technology, which is essential to understand the current technology and its context. The state-of-the-art processes AFP are defined according to its history and development.

Chapter 3 presents the design and build of the prototype AFP system with in-situ UV curing and on-the-fly resin impregnation, termed UVAFP that demonstrates outcomes that meet the aims of this thesis. The context for the system design is presented as driven by experimental results as well as benchmarking research using established design methods.

Chapter 4 examines the supply materials used in AFP systems, the limitations of current materials and the case for new options. By using glass fibre and vinylester resin impregnated on-the-fly and cured in-situ using UV, a lighter composite structure was made that had comparable, if not better, strength-to-weight ratio compared to existing aluminium and steel parts.

The focus of Chapter 5 is the processes necessary prior to AFP, the pre-processes. These include the material supply from the creel and any necessary preparation and impregnation. A novel approach to impregnation is then proposed which occurs on-the-fly, and eliminates the need for pre-impregnating by utilising the continuous application technique of AFP to combine the fibre and resin at the nip point.

In Chapter 6 the limitation of AFP systems as placement devices only is addressed and the issues associated with the processes post placement via AFP in order to complete the component manufacture. A solution is proposed that combines the ply-by-ply continuous approach of AFP with the curing of the composite to produce a cured component on-the-fly, cured in-situ immediately following placement. By combining the curing with the placement the need for post-processing is eliminated.

In Chapter 7 the critical capacity driver for UVAFP – the speed of lay-up and the degree of cure of the resin by bringing together the learning of previous chapters is examined. The result is a predictive degree of cure model looking to maximise rate while maintaining quality.

Chapter 8 investigates the thermal behaviour of the composite during UVAFP process. A model to predict the temperature response of the glass fibre vinylester composite during processing using the UVAFP process was developed in order to minimise any possible degradation that could have occurred as a result. The model was based on the same primary process parameters for the UVAFP process as determined in Chapter 7; the placement speed, the set point intensity of the UV light, and the height of the UV light from the incident surface. The thermal and degradation modelling of this chapter depends on the in-situ consolidation and heat modelling work done to develop thermoplastic AFP systems although the source of the heat in this instance is generated through the radiant energy of the UV light and the heat does not contribute to consolidation except to aid wet-out and flow by reducing the viscosity somewhat of the resin as it is processed at the nip point.

Chapter 9 presents the final conclusions of the body of work undertaken for this thesis. It summarises the overall research motivation while looking back upon the work that inspired the thesis. It provides reference to the initial limitations that were identified in commencing this thesis and how these influenced the experimental aims and hypotheses.

1.5 Summary

Emissions reduction targets in the transportation sector are driving a major engineering effort in lightweighting and clean energy propulsion systems. Composite materials offer the lightest specific strength-to-weight ratio of all advanced engineering materials, and the potential to meet weight targets to reduce fuel consumption. In addition, they make electric systems that have a lower energy output more viable. Composite manufacturing however, is currently too slow and expensive to meet the needs of widespread utilisation and therefore it is currently considered unacceptable. AFP is limited to a point that it is only useful in industries where low volumes are required with large margins that can justify the cost. Clean and efficient processes are

also required. This research aims to address some of these limitations and propose a new concept in AFP that can provide the manufacturing process the industry needs to meet macro and political pressure to produce lightweight vehicles. This thesis was undertaken as an isolated study, outside any large research program. The conception, design and manufacture of the UVAFP prototype and the tests were undertaken by the author with the support of university supervisors. The project was funded by the Australian National University's internal funding for equipment and travel and the Australian Government research grants for larger investment for the industrial robots.

2 Background and Related Work

This chapter provides the background theory and related work relevant to establishing the context of this thesis. As composite materials present in various forms and can be manufactured using a multitude of approaches, it is important to understand the characteristics of the materials and each approach leading to the investigation of AFP in detail. Section 2.1 introduces the background theory relevant to composite materials and their processing. In order to identify the limitations of AFP, section 2.2 investigates the historical research and development of the technology, its predecessors and the areas where gaps in the research exist. The state-of-the-art processes involved in the manufacture of composite material components are then investigated and AFP is analysed in the context of the varying leading technologies. Section 2.3 examines the specific material implications relevant to AFP, and finally, Section 2.4 summarises the overall findings of the background and related work and the intended research focus of this thesis.

2.1 Composite Materials and Manufacture Approaches

Composite materials, as the name implies, are made up of two or more materials, namely a fibre that has been reinforced with a resin matrix. The fibre and resin are combined in varying ways to create a material system that has differing material properties to the sum of the constituent parts [16]. The fibre is used to increase the stiffness and strength of the matrix constituting the material system. This structure tends to exhibit anisotropic behaviour and composites generally out perform their metal counterparts directional load cases in terms of specific weight. Fibre arrangement in the matrix can be continuous or discontinuous. For continuous fibres, a woven or unidirectional fabric is possible. For discontinuous fibres, either a short, or long fibre arrangement can be manufactured, often a chopped matte or fleece is supplied. In some instances fibres of very minute length, too short to discern a fibre architecture, are used as a stiffening ingredient, mixed as a uniform reinforcement. Composites tend to exhibit a laminate structure through their thickness [17]. Industrial composites include bitumen,

concrete with metal reinforcement and even mud bricks. Advanced composites (the focus of this thesis) most often include combinations of thermoplastic or thermoset polymers or resins with carbon, glass basalt, and polymer or aramid fibres. The advantages of advanced composite materials are listed below:

1. **Lightweight:** Composites are lightweight, especially in comparison to materials like concrete, metal, and wood. Fibre reinforcements generally have low density yet maintain exceptional properties axial properties. Composites also provide design flexibility because many of them can be moulded into complex shapes. The downside is often the cost. Although the resulting product is more efficient, the raw materials are often expensive. In simple terms, composites are significantly lighter than steel with comparable properties. Comparing the density of an average high strength low alloy steel with a carbon fibre epoxy composite, shows densities of approximately $7.8 g/cm^3$ versus $1.6 g/cm^3$ respectively. This equates to a reduction of almost 80%. While not comparable 1:1, automotive body structures made using steel often weigh between 300 and 400kg while a CFRP body structure can weigh as little as 150kg. Ultimately, a car made from composites would require significantly less energy for propulsion, resulting in a significant fuel saving [18].

2. **High Strength**: Composite materials are extremely strong, especially per unit of weight. An example of this is the high tenacity structural fibres used in composites such as carbon, Aramid and S-Glass, which are widely used in a variety of applications. When arranged in a filament structure, such as in carbon fibre, the specific properties far exceed any metals. By choosing an appropriate combination of matrix and reinforcement material, a new material can be made that exactly meets the requirements of a particular application [18].

3. **Corrosion and Chemical Resistance**: Composites made from the appropriate polymer matrices are highly resistant to chemicals and will never rust or corrode (although their properties and integrity may degrade). This is why the marine industry was one of the first to adopt the use of composites. Boats made with fibreglass can stay in the highly corrosive salt water without rusting [18].

4. **Elastic:** Fibre reinforced composites have excellent elastic properties with high yield strengths. This feature is ideal for springs, and it is why composites are used in car leaf springs and in the limbs of archery bows [18][19].

5. **Non-Conductive**: Certain composites, such as composite made with fibreglass, are non-conductive. This is important because often a structure is needed that is strong, yet will not conduct electricity. An example of this property being advantageous is in ladders. Aluminium ladders are advantageous in that they are lighter than steel and can be easily moved. However, they are still conductive of electricity and can be an electrocution hazard. Ladders made with fibreglass on the other hand are not a risk if the ladder was to cross a power line [18].

The manufacture of composite materials often requires various stages. These include the a) preparation of the materials and tools, b) lay-up and forming of the fibre to the required geometry of the component, c) impregnation of the fibre with the resin and consolidation of the two phases in the tool, d) curing of the resin and, e) finishing the component.

Traditional approaches to the manufacture of composite materials are characterised by manual labour, which is intensive and time-consuming. The most common manufacturing methods can be categorised by eight main approaches. These include the following with each approach detailed in the following section:

1. Wet lay-up;

2. Manual prepreg lay-up;

3. Resin Infusion;

4. Resin Transfer Moulding;

5. Resin Spray Transfer;

6. Filament Winding;

7. Pultrusion;

8. Automated Tape Laying; and

9. Automated Fibre Placement.

2.1.1 Wet Lay-up

Wet lay-up (Figure 4 [20]) involves the impregnation of the resin into the fibres within an open mould tool in a manual process either through simple pouring or spraying of the resin. Consolidation is usually accomplished through rollers and brushes. Due to the high likelihood of air entrapment wet lay-up is rarely used on critical structures and components that need to withstand elevated temperatures due to the possible expansion of the air bubbles and consequent delamination. This approach is often used in low technology applications.
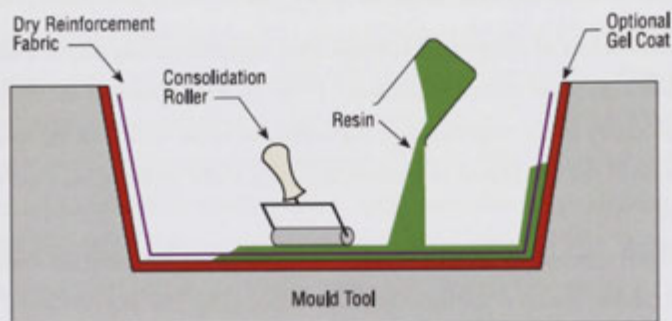
Figure 3 – Wet lay-up schematic

2.1.2 Manual Prepreg Lay-up

Manual prepreg lay-up is the standard manufacturing technique used in the composites industry for the manufacture of high quality components [21]. In its simplest form, manual prepreg lay-up involves the manufacture of composites using pre-impregnated (i.e. the name prepreg) fabrics of structural fibres and resin laid up by hand onto an open mould, as shown in Figure 4 [22]. The process is labour intensive, requiring accurate placement of each ply of material, cut to a specific shape and at a specific orientation onto the tool. Plies can be cut by hand using templates, or as is more common, by using a ply cutting machine. The lay-up is finally vacuum bagged and compacted onto the tool and then cured using any number of curing techniques such as autoclaves, ovens, press moulding or simply at room temperature under the vacuum bag. The use of heat pressure and high temperatures causes the viscosity of the resin to

drop and to the wet-out across interfacial ply surfaces and consolidation of the fibre preform and resin to form the final part thickness. Finally at the appropriate temperature the resin reacts and cures. In the aerospace industry this generally requires autoclave curing at high pressures (7 bars).

Figure 4 – Manual prepreg lay-up

The lay-up generally occurs in an environmentally controlled room where temperature and humidity are dictated by the sensitivity of the resin, which has been

partially pre-cured or b-staged onto the fabric, to dust, temperature and moisture ingress. For this reason, prepreg materials are almost always kept in sealed packaging frozen until ready to be used. Often the prepreg is rolled and stored on backing paper or film to avoid adhering to itself and/or anything else until such time as the lay-up technician is ready to apply the prepreg to the lay-up stack [21]. Operators must be trained are considered a highly skilled workforce, increasing the cost of staff and overhead to maintain expertise. Methods for adhering the prepreg to either the tool surface for the first ply or previously laid ply for every subsequent ply vary. Often a debulking step is required which uses vacuum bagging compaction to ensure correct adhesion and removal of air bubbles between plies. Figure 6 [20] demonstrates this process.
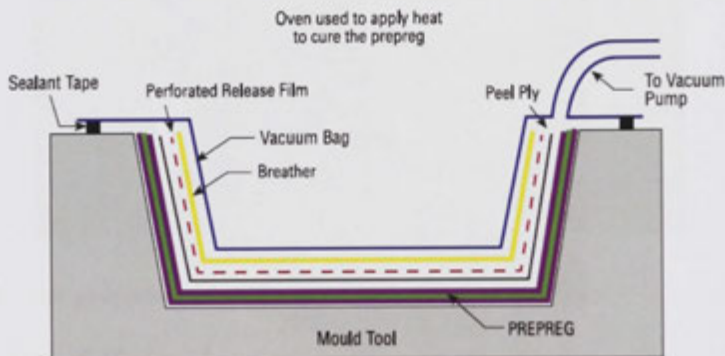
Figure 5 – Prepreg lay-up scheme

2.1.3 Resin Infusion

Resin infusion in comparison to prepreg lay-up removes the pre-processing step where the resin is impregnated onto the structural fibre fabric. Dry or bound fabric is laid up in plies in a similar fashion to prepreg lay-up, although in some instances where geometry is complex, to ensure the dry fabric maintains position and no fibre splaying occurs the lay-up a binder activation step follows lay-up, adding a step where one was removed during the preimpregnating (prepregging) phase. The bound or laid up fibre is termed a preform, due to the fact that fibres have been formed into shape prior to wet-out. Once laid up and either vacuum bagged or the tool closed, the resin is then added to

the lay-up by vacuum assist from outside the bag or tool through atmospheric pressure. The resin is drawn into the fabric wetting out the lay-up and filling voids. Because the pre-impregnating step is removed the process is considered to be more economical than prepreg, but preforming steps required for the fibres, like binder activation, reduce this advantage. Resin infusion requires resins of a much lower viscosity to ensure flow and therefore toughening agents and additives to the resin become difficult to incorporate. Further, fibre volume fraction control is less precise than prepreg where the resin laid up is controlled by the prepreg ratios (Figure 7 [20]).
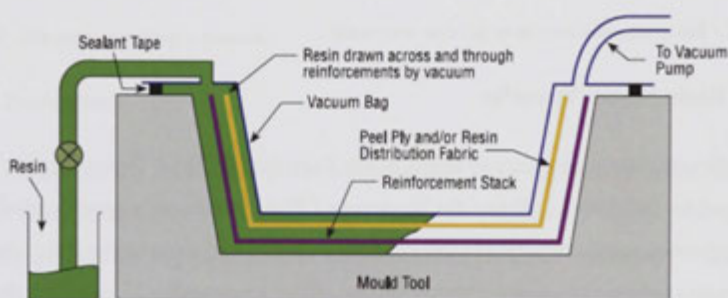
Figure 6 – Resin infusion setup

2.1.4 Resin Transfer Moulding

In Resin Transfer Moulding (RTM), a preform is manufactured as with resin infusion however the resin is injected under pressure into a closed mould (Figure 8 [20]). This resin pressure and closed mould controlled volume provides for greater control over fibre volume fraction. The process is often implemented in a press in order to withstand the resin injection pressures but variants of the process, such as RTM 'light', utilise lightweight composite tooling simply clamped together and the resin pressure are significantly lower.
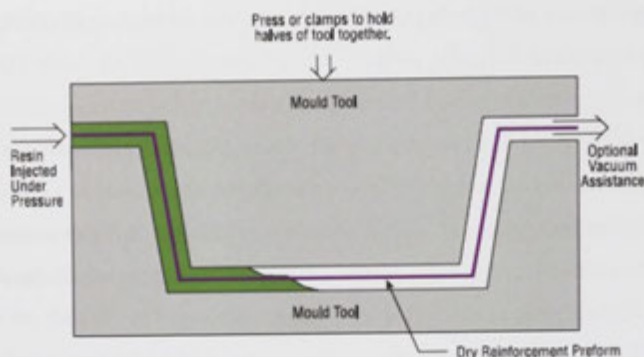
Figure 7 – Resin transfer moulding process schematic

2.1.5 Resin Spray Transfer

Newer techniques such as Resin Spray Transfer (RST) or "Spray-Up" as developed by Quickstep [23] and the Bayerpreg CSM systems are currently used in advanced composites industries to either apply or apply and wet-out the fibre tows. These resin spraying processes employ the use of the spray technology within the tooling, effectively producing a semi-impregnated preform within the tool. In the RST process, resin is sprayed onto the tool, a dry fibre preform of the shape of the part is then placed into the tool onto the resin, if necessary further spraying operations follow and the tool is then prepared for curing by vacuum bagging or closing the mould and then heat and pressure are applied in order for impregnation to occur and final consolidation and cure. The process utilises industrial robots and metering, mixing equipment to deliver the resin.

2.1.6 Filament Winding

In a typical filament winding process, fibre tows are run through a resin bath and then pulled onto a rotating tool surface, which provides tension and compaction of the tows. However, this process is limited to parts that do not contain concavities in the rotating symmetry, as the fibre tension would cause the fibres to 'bridge' over the concave sections (Figure 8 [20]).
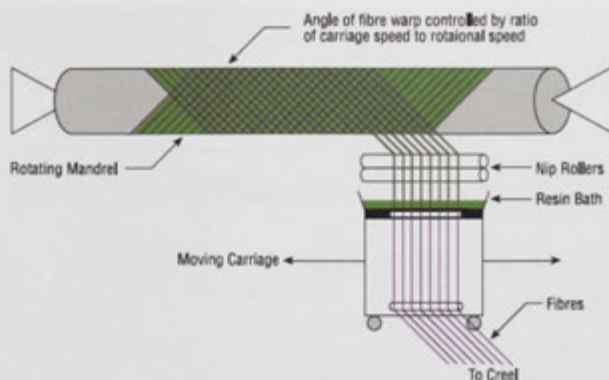
Figure 8 – Filament winding schematic

2.1.7 Pultrusion

Pultrusion is a continuous process for manufacture of composite materials with constant cross-section. As the name implies, reinforcing fibres are 'pulled' through an extrusion die in order to produce the components. The fibres are generally pulled through a resin, possibly followed by a separate preforming system, and into the heated die, where the resin undergoes polymerization. Many resin types may be used in pultrusion including polyester, polyurethane, vinylester and epoxy. An example of the process flow is represented in Figure 9 [20]. The die is situated following the polymer injection at the heaters.

The technology can be applied to both thermosetting and thermoplastic polymers. Pultrusion of polybutylene terephthalate (PBT), polyethylene terephthalate (PET) and other thermoplastics is now common practice. For thermoplastics impregnation occurs either by powder impregnation or by surrounding it with sheet material of the thermoplastic matrix, which is then heated, a technique used in the manufacture of cables.

Utilisation of the pultrusion process has grown steadily at around 8-10% in recent decades [23]. Pultrusion is a relatively energy-efficient and resource-saving process given the concentrated and localised heating as well as it continuous operation.
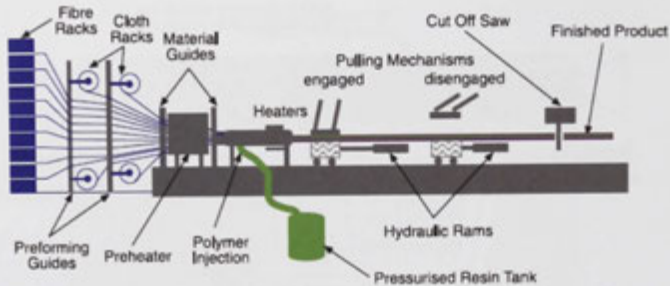
Figure 9 – Pultrusion process schematic

2.1.8 Automated Tape Laying

In Automated Tape Laying (ATL), tapes are often greater than the standard 25.4mm or 1 inch and therefore can only be placed on smooth minimal curve surfaces, such as the wing skin shown in Figure 10 [24]. In a typical ATL process, unidirectional fibre tapes (versus tows), approximately 12.7mm and wider, which are pre-impregnated with resin, are laid onto a die using a gantry or robotic system. In the ATL process, tapes are fed from bobbins and compacted using a roller. The tapes are collimated to increase the width of the tape band, and Cut, Clamped and Restarted (CCR), as the placement head is moving. This is commonly termed "*on-the-fly*". The ability to cut, clamp, stop and start tapes allows the tape bandwidth to be changed according to product geometry and the programmed tape path. Using AFP or ATL is often a compromise between the lay down rates versus the complexity of the part to be laid up. Throughput is typically seen as being higher in ATL systems and with a high degree of uniformity throughout the part. ATL can achieve this due to the reduced number of mating surfaces between tapes. Recent advancements in the speed of cutting mechanism and feed drives that match the velocity of the tow with the velocity of the placement head, comparable lay-up rates (kg/min onto the tool) to ATL have been achieved with AFP [25]. ATL is similar in its approach to AFP except for the difference in the width of the tape used versus the tows used in AFP.
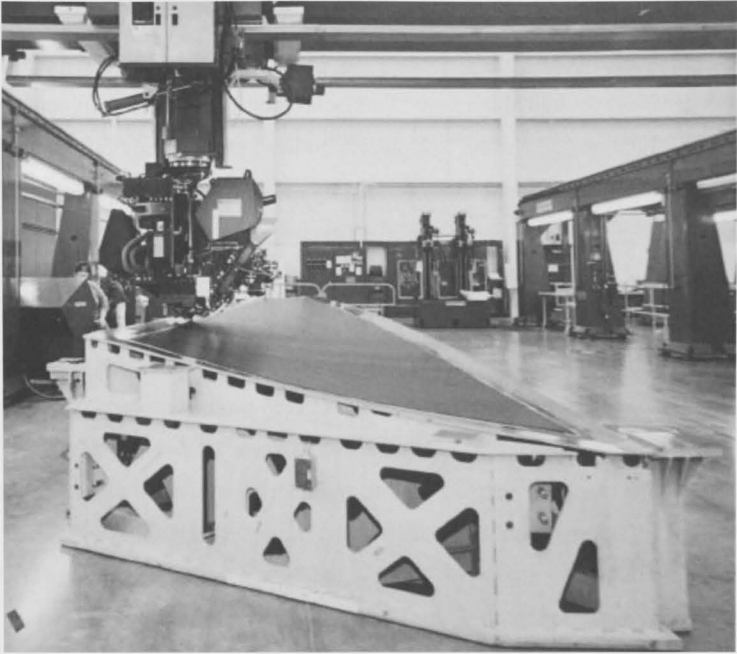
Figure 10 – ATL of a low contour surface wing skin

2.1.9   Automated Fibre Placement

In the AFP process, fibre reinforcement tows are pulled from a spool or supply creel and directed to the placement head (commonly known as the end-effector device) located at the end of an industrial robot or high accuracy gantry system [26][27] through which placement onto a mould surface is achieved. The tows or narrow slit tapes are often 6.35mm or ¼ inch wide. The narrow width is used to allow for the placement of a collimated band onto geometry with complex curvature without wrinkling, bucking or pulling occurring. Energy, usually in the form of heat, is supplied directly at the application point to allow the resin to heat and reduce in viscosity, aiding wet-out of the fibres and adhesion to the substrate or previous ply only. The heat is not sufficient to cure the resin but in some instances can b-stage (partially cure and then freeze the reaction from further progressing) the matrix. It is during the post cure, which often occurs in an autoclave, where further and much greater amounts of energy are applied across the entire laid up component to cause full wet-out, consolidation, migration of

molecules across the bond surface and in the case of thermoset resins crosslinking. This approach can be applied to both thermoset and thermoplastic processing. For the in-situ process the energy required at the time of consolidation needs to be sufficient to achieve wet-out, consolidation and curing. The placement head immediately following the compaction and consolidation device eliminating the need for post-curing can implement the high intensity energy source. This negates the need for the post-cure. For thermoplastic matrices, heating, adhesion, the fibre placement head using substantial localised compaction force can affect molecule migration and cooling. For thermoset in-situ curing, the resin must be able to cross-link and achieve a sufficient degree of cure within the consolidation timeframe, requiring not only high intensity energy sources but also highly reactive resins or a free radical reaction that continues after exposure.

Due to the width of the tow band, during steering of the tows through curved placement paths, the tows inevitably place at varying rates depending upon the placement path radius and therefore each tow requires individual CCR control. A schematic cross section of an AFP placement head is shown in Figure 11, which illustrates the main design and functional elements of a typical system.

AFP employs the use of fibre tows pre-impregnated (or prepregs) with resin and partially cured to allow for handling and storage. Thermoplastic prepregs such as polyetheretherketone (PEEK) and polyetherketoneketone (PEKK) are heated, consolidated under pressure and then cooled by the head. This gives a relatively quick processing time. Thermoset prepregs are applied to composites by heating the tows to increase tack just prior to placement. Thermoset prepregs require refrigeration and have a limited shelf life. After placement, thermoset prepregs also require a thermal curing stage to fully consolidate the layers and maximise properties.
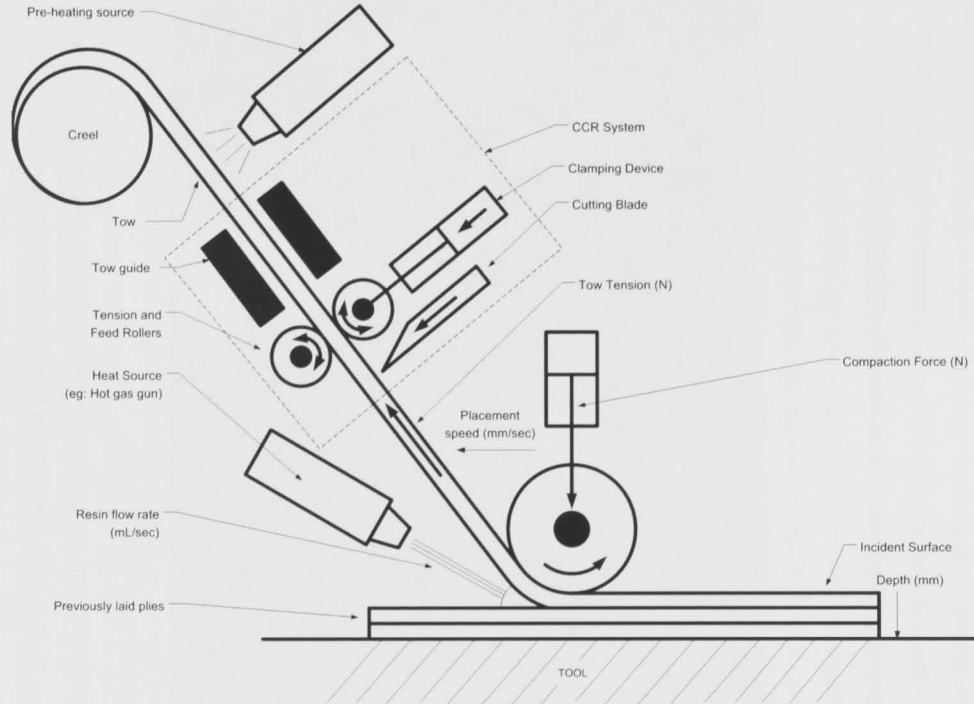
Figure 11 – AFP simplified process model[1]

---

[1] For a detailed analysis of the design and make up of an AFP system please see Chapter 3 The UVAFP Prototype Design and Build

The design and form of the AFP system is driven by the functional elements. AFP systems are functional engineering machines that are often skeletal in nature, with visibly exposed subsystem equipment. These subsystems are identified in Figure 12 [10] as the:

1. Fibre placement head;
2. Robotic articulation system;
3. Fibre and resin creel system;
4. Programming software/controller/human machine interface (HMI); and
5. Placement tool.
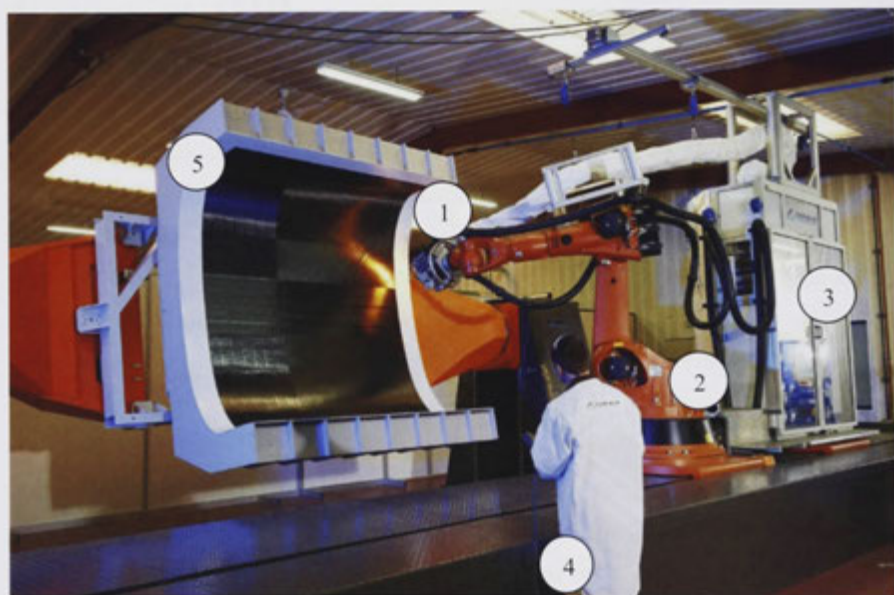
Figure 12 – The Coriolis Composites AFP system

A comparison of current composite manufacturing approaches in popular liquid moulding processes, such as resin infusion and Resin Transfer Moulding (RTM), as detailed above, fibre reinforcement preforms are placed into a mould or die and are impregnated with resin. Typically, these processes require long setup times, use large amounts of consumable materials and waste and offer limited possibilities for automating the entire process. Furthermore, the preforming of the fibre reinforcements is often undertaken in a separate process [28], which requires a significant amount of

operator intervention. AFP provides a unique solution in that preform lay-up; impregnation and curing can be streamlined and combined into a fully automated system. Other processes that require less manual touch operations and lend themselves more to automation include composite pultrusion, roll forming and stamp forming. These processes offer high throughput and excellent quality control, however, the processes are inherently limited in the components that they can produce and therefore AFP offers particular advantages around flexibility. In high pressure forming processes (such as RTM) tooling costs are doubled and often require large presses and infrastructure to support the pressure loads because preforms must be forced into place through drawing mechanisms. The tooling cost is considered too high for large low volume component production. Equally, the risk of failure within the closed mould, which is inaccessible during processing, is considered too great [29]. Therefore, these processes are inherently hard to automate, are labour intensive, and they rely on significant manual flexibility to handle each part. AFP provides lay-up on an open mould and localised consolidation, which reduces the need for tooling that, can handle the drawing stress loads to force the preform into position.

The primary limitation for both filament winding and ATL is the inability to wind onto shapes that had concavities and to lay tows onto small radii with complex non-geodesic geometries. The issue in the ATL process was primarily related to tape width and tight radii or geodesic lay-up paths which resulted inevitably in a failed product caused by tape wrinkling, pull-up or buckling of the tape. ATL therefore was mostly utilised laying components with near straight and non-geodesic surface. The increasing interest in the use of composites for aerospace production drove further developments. These included the production of separate tape slitting machines that prepared high quality feed material on separate bobbins prior to use in AFP machines, computer numeric control (CNC) and programming in general. In the mid to late 1970's a large number of government and industry research programs in the USA and Europe were funded to examine the technology and accelerate development [30]. This is evident in the large number of patents submitted by Hercules Aircraft Company and the McDonnell Douglas Aircraft Company [1] to name just two original equipment manufacturers involved in the programs. Research and development has continued to

rapidly position AFP as the current state-of-the-art technology in automated composite manufacturing.

Figure 13 - Automated fibre placement machine TORRESFIBRELAY-UP.

A comparison of all the manufacturing approaches, including types of materials, lay-up rates, and a summary of the advantages and disadvantages, is shown in Table 1 [1][31][32]. As can be seen, AFP results in the most advantages and least disadvantages and offers lay-up rates between 2 and 20 kg/hr. This is not the fastest process rate, however the flexibility of AFP, as is shown in the advantages, layable paths and surface curvatures in Table 1, compensates for the reduced maximum speed. In addition, AFP can support high-speed lay-up even with increasing complexity of the part [33]. AFP also has the potential to produce large components with the greatest accuracy of all the automated processes available [34]. Large commercial aircraft structures, such as the fuselage sections of the Airbus' A350 XWB (extra wide body), as shown in Figure 13 [4][35], as well as the tail, nose and fuselage sections of the Boeing 787 Dreamliner [35] are now commonly being produced with AFP technology. These aircraft programs,

particularly the 787 Dreamliner, are utilising AFP technology in large scale with great success. The impact of this technology on the manufacture of advanced composites, particularly in the aerospace industry, cannot be underestimated. Its adoption will address the need to produce single monocoque structures without the need for fastening and reinforcement in the aerospace industry. With increased productivity rates and quality control by utilising repeatable and accurate CNC systems, AFP allows for smarter and lighter design through the use of the specific advantages of composites around fibre orientation. That is, the system lays down complex paths specifically where the designer requires reinforcement for application loading. This will transform the aerospace manufacturing industry from its current cottage industry approach, requiring significant manual touch labour, to a state-of-the-art automated industry able to produce structures that were previously not possible to produce [1].

Table 1 - Description of composite manufacturing processes and functionality

Process	Supply Material	Advantages	Limitations	Part Size restriction	Lay-up Rates (kg/hr)	Layable Paths	Concave Surfaces	Convex Surfaces
Wet lay-up	Dry fabric of chopped fibre matte and liquid resin	Robust and easy to apply. Non-skilled labour. Quick application	Completely manual with very little quality control. Low temperature applications only.	No limit	100	Geodesic & non-geodesic	Y	Y
Manual Prepreg Lay-up	Reinforcement fabric with pre-impregnated resin	Highly articulate and flexible, in-situ inspection and rework possibilities, manipulation and manual adjustment possible	Slow, and expensive labour with health risks as well as quality and repeatability issues variation from part to part	No limit	1 to 10	Geodesic & non-geodesic	Y	Y
Resin Infusion	Dry fabric or preformed reinforcements and liquid or films of resin	Low material cost, low porosity, low temperature curing and low capital equipment cost	Requires specific low viscosity resins, slow infusion process, limited success with cores, high consumables requirement	Vacuum system and oven size	5	Geodesic & non-geodesic	Y	Y
Resin Transfer Moulding	Dry fabric or preformed reinforcements and liquid resin	High quality surface finish on all sides of part, low porosity parts, accurate geometric conformity	Expensive two sided tooling, high capital cost, requires expensive press, high pressure process	Press size and tonnage	20	Geodesic & non-geodesic	Y	Y
Resin Spray Transfer	Dry fabric or preformed reinforcements and liquid resin	High quality surface finish on all sides of part possible but generally open mould, low porosity parts, accurate geometric conformity	Low cost low pressure open mould tools possible. Limited to specific resin chemistries due to sprayability requirements. Reach of robot and spray system limits access and limited to certain thicknesses due to permeability before an additional spray layer is required	No limit	200	Geodesic & non-geodesic	Y	Y

Filament Winding	Liquid resin and dry unidirectional fibre tows or pre-impregnated tows	High rates, low cost and easily scaled	Cant lay-up concavities, add or drop or 0° ply rotations	Rotary axis and longitudinal axis length	200	Geodesic	N	Y
Automated Tape Laying	Pre-impregnated unidirectional tape	Accuracy, few gaps and angular cuts	Geodesic paths and limited contours only, reliability not secure, low rates and high machine cost	Gantry size	2 to 30	Geodesic	Y	Y
Pultrusion	Dry tows and liquid resin	High speed, high quality components, endless lengths, directionalised fibres	Fixed profile, small processing window (only while in the tool) high pressures, single fibre orientation	Thickness restrictions and tool opening	200	N/A	N/A	N/A
Automated Fibre Placement	Pre-impregnated or dry unidirectional slit tape or tows	Accuracy, high conformity, tight radiuses, adjustable bandwidth, close cut adherence to part edge, low scrap rate,	Limited reliability, low rates and high machine cost	Gantry size	2 to 20	Geodesic & non-geodesic	Y	Y

A simplified version of this comparison is shown in Table 2 [32] associated with the 9 primary differences in the processes. Namely, the surfaces that can be laid up, the direction of surface curvature, the ability to lay discrete tows, consolidation and thickness, lap/gap control, touch labour utilisation and flexibility.

Table 2 – Composite manufacturing process features summarised

AFP	Filament Winding	ATL	Hand Lay-up
Geodesic and Non-geodesic	Geodesic Path only	Geodesic Path only	Geodesic and Non-geodesic
Convex and Concave	Convex Surface	Convex and Concave	Convex and Concave
Start and Stop Fibres	Endless Fibres	Start and Stop Fibres	Start and Stop Fibres
In-process Compaction	In-process Compaction	In-process Compaction	Compaction in Autoclave
Constant Ply Thickness	Non-constant Ply Thickness	Non-constant Ply Thickness	Constant Ply Thickness
Accurate and Repeatable	Accurate and Repeatable	Accurate and Repeatable	Not Accurate and Non-Repeatable
Lap/Gap Controllable	Lap/Gap Controllable	Lap/Gap Controllable	Lap/Gap Non-controllable
Reduced Labour Cost	Reduced Labour Cost	Reduced Labour Cost	High Labour Cost
Flexible Design	Non-flexible Design	Non-flexible Design	Flexible Design

2.2 The Development of AFP

To address the limitations of AFP and understand how it can be improved it is important to understand how the technology was developed and the historic progress of the design to its current state-of-the-art. AFP has been in development for over 50 years.

The AFP technology was first developed in the 1960s [1] made possible by breakthroughs in CNC, precise electromechanical systems and the increased demand for composites for aerospace production for the Hercules Aircraft Company and McDonnell Aircraft Company [1]. At the time, the current state-of-the-art technologies in automated composite manufacturing were filament winding and ATL processes [36]. However, these processes were limited by their inability to lay tows into small radii and complex geometries, and to wind non-geodesic shapes.

The first documented attempt to address the issue was actually implemented in an ATL system patent by Goldsworthy in 1974 [37]. The invention had the ability to slit prepreg tapes into thinner 'slit tapes' to improve geodesic conformance within the ATL head, thus introducing the fundamental concept of AFP – placement of thin fibre tows or slit tapes [38]. From this point on and into the 1980's a rise in demand for composite materials led to a large number of government and industry research grants (estimates put total expenditure in the tens of millions of dollars) to examine the technology and bring forward its development [30]. These were aimed at promoting composite use in aircraft [34] and defence technologies as a lightweight high strength material, as well as a means to modernise manufacture through automation advancements [1].

While AFP technology has been used in the production of a diverse range of components such as helicopter structural elements [39] bridge sections [40], composite repair patches, boats [41], gun barrels [42][43] and cryogenic fuel storage systems [44][45], it has most commonly been utilised in the aerospace industry for the manufacture of structures such as wing skins [46] and fuselage sections [47][48]. Tows, filaments and tapes became the most popular composite material form due to characteristics that enabled tailoring of the internal structure of the composite through accurate placement of the fibre reinforcement. The first tape-laying machine was produced in the early 1970's [30] in a joint project between the US Air Force and General Dynamics [24]. Maturing from experimental technology to commercial solution has involved significant development both on site with end users and at research institutions. Initial development of AFP technology started with Original Equipment Manufacturers (OEMs) in the aerospace industry, shifting to external vendor solutions. This has allowed the airframe manufacturers to create a competitive market for commercial AFP systems, while offloading the cost of future development,

maintenance and patents to the vendors. With this transfer to a commercial technology, data on the process and its development has been limited and technical developments are highly protected.

The increasing popularity of liquid moulding processes however, has seen alternatives to prepreg manufacturing, such as RTM and RI become a target for AFP use. AFP systems are increasingly being utilised for preform manufacture using dry fibres. The dry fibres are coated in a binder and placed before then being infused with resin as part of the final curing process. The binder is activated through localised heating and pressure during the AFP process creating a completely tailored preform in a single process. By being able to manufacture the preforms for use in later processing, AFP has expanded its useable scope from just part manufacture coupled with a particular curing process to providing the fundamental constituents for other processes.
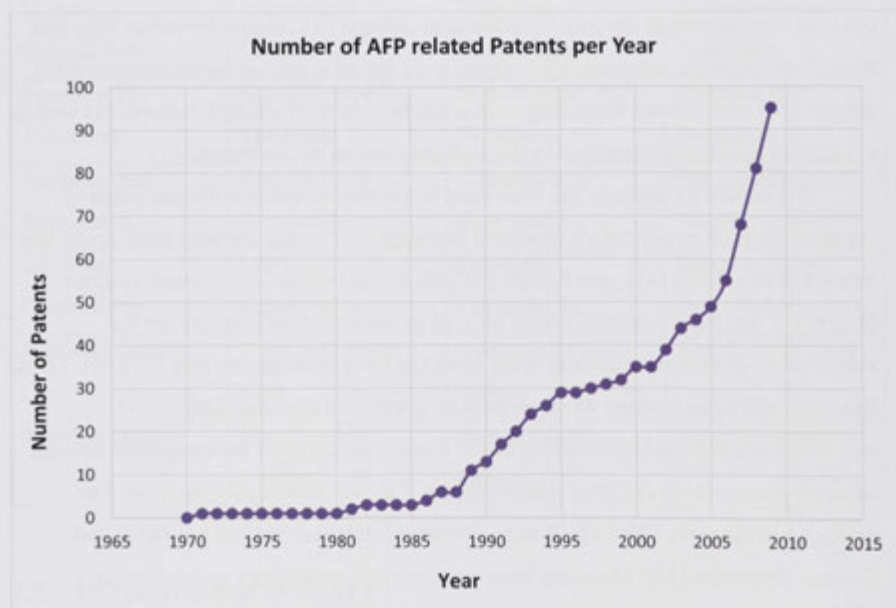
Figure 14 – Patent Statistics for Automated Composite Manufacturing Processes

While AFP technology appeared soon after ATL was conceived, development of the system did not progress rapidly until late in the 1980's. From 1980, AFP systems surpassed the number of ATL installed in production lines within the aerospace industry

[24][48][49]. Since 1990, competing technologies using broad-goods [50] and fabrics [51] instead of tows, filament and tapes were developed; however, few of the technologies have progressed to production. Ewald [52][53] developed a modular design AFP type system, splitting lay-up tasks into two individual stages. The first stage machine de-spooled, cut and re-spooled the tape lengths into courses, while the second stage laid the pre-cut courses from the spool onto the tool. The two stages are shown in Figure 15 [52][54]. Due to process complexity when attempting to design a system that integrates many tasks, such as tape cutting, clamping and re-feeding, the AFP head becomes complicated and the size of the head increases dramatically, limiting its ability to lay in tight geometries and slowing its production rate. Ewald's two-stage machine provided for simplified equipment and greater clearance and reach of the placement head. Furthermore the machine had a higher lay-up rate than current single stage AFP machines. Utilising only wide tapes, this machine shared the same limitations as ATL systems, including limited geometry, conformity and high scrap rates. While this approach offered potential benefits in terms of speed and simplicity of mechanisation, it is arguable that the total time benefits and the cost to the factory floor footprint limited production feasibility. However, limited data is available to quantitatively substantiate this.

Figure 15 – Forest-Line ACCESS System (L) and ATLAS System (R)

Another similar process to AFP is the patented process used by Fibreforge [55]. This system includes a proprietary software algorithm which determines flat net formed blanks from 3D design shapes. A tape-laying machine lays the flat blanks according to a generated flat pattern. This pattern is then transferred to a stamping press where it is

formed into the form of the required three-dimensional part. This concept could certainly be combined with AFP for the lay-up rather than tape laying [55] utilising the flattening software to program the AFP system and finally combining AFP 2D preforming with 3D stamp forming.

Commercial development of AFP technology, and the related patents filed, has increased dramatically since its conception in the 1960's. Current growth in patent filings around the technology suggest the interest and value the process offers producers driven by huge demand for such technology and a rapid pace of commercial development and refinement. For example, as can be seen in Figure 14, the number of patents filed per year relating to AFP technology has more than doubled since 2004. Development has continued at a rapid pace since the 1970's assisted by improvements and provisional patents in automation material techniques, sensors and scaled electronics and motors, actuators, control and placement algorithms and drive systems. None, however, address the use of new materials or new curing techniques other than thermal curing except for the development of electron beam curing systems. Furthermore, all AFP related patents focus on delivery of the material in its as delivered form onto the tool and do not examine on-the-fly impregnation – the patent mapping therefore presents a clear gap in the literature and general body of knowledge in the field and the opportunity for increasing the understanding around the versatility of AFP as a process concept for handling different materials requiring differing curing and application or impregnation techniques. Furthermore, while patents have increased the number of published academic works has decreased with very few recent landmark studies .

There are a claimed 40-50 AFP systems operating worldwide, not including countries such as Russia, Korea and China where this information is not readily available [5]. This figure is made up by a number of turnkey systems by a select few companies offering AFP technology. Turnkey solutions include the controller, programming software, material supply system and the placement head and actuation system (either a robot or gantry).

The aerospace industry were the earliest adopters of these systems as it has aimed to address the emerging growth of aircraft needed and the cost margins available that allowed for the increased usage of composites [48]. Accordingly, research has

concentrated on addressing issues critical to aerospace requirements and specifications. Suppliers and research bodies accessing the technology have likewise occurred closest to their biggest end-user, the aerospace industries, in the USA and Europe. While a large number of patents exist surrounding the AFP process, there are currently less than 25 different assignees of primary AFP patents worldwide. The largest holder of AFP related patents is Cincinnati Milacron, now known as MAG Cincinnati™, followed closely by Boeing Corporation and Ingersoll and Coriolis Composites. The main areas of patented development in AFP technology have been in the control and programming algorithms, the cut, clamp and restart (CCR) mechanism, the roller and the creel and guide systems. These areas are most critical to process control, repeatability and accuracy which the aerospace industry demands. In recent years a rise in macro-political and economic drivers has pushed other industries towards lightweight design and material usage. These industries have differing demands and drivers to the aerospace industry, which has meant an increased focus in areas such as lay-up speeds, lay-up rates and process chain integration, such as issues surrounding autoclave post curing. A number of patents assigned to MTorres and even MAG Cincinnati now focus on AFP systems specifically design for wind turbine blade manufacture. With further diversification of the technologies utilisation development and patenting will certainly increase and include various extensions and modifications of the process.

2.3 Composite Material Processing in AFP

The AFP process can be applied to either dry fibre tows, pre-impregnated slit tapes or pre-impregnated tows (commonly known as 'towpregs') with either a thermoset or thermoplastic polymer matrix [1][53]. The value chain for composite material processing in AFP is shown in Figure 16.
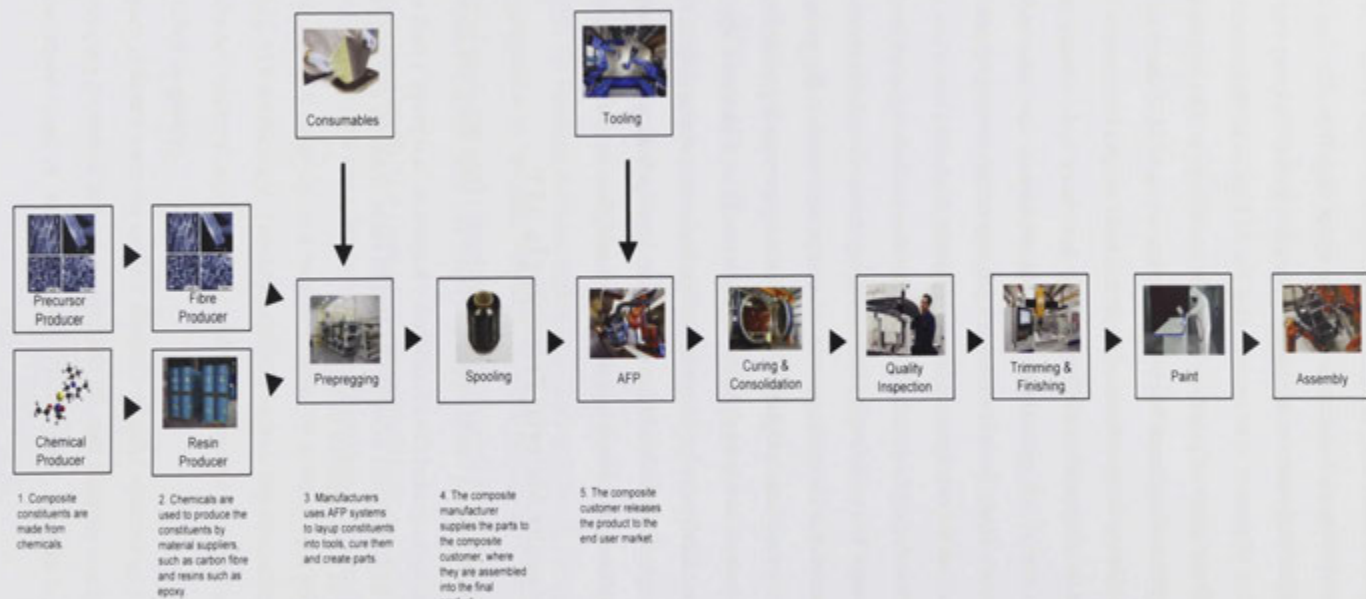
Figure 16 – The composite material value chain for AFP processing

The fibres and polymer matrices most commonly used in AFP are detailed in Table 3 [56] with the polymer-matrix determining the processing method. From the table it can be seen there are numerous materials therefore this section will review only the most common materials and associated processing, with a focus on the curing and handling methods employed to date.

Table 3 - Fibre and Resins (thermoset and thermoplastic) used in AFP

Fibre	Resin	Processing
• Glass	• Thermoset	• Thermoset
• Carbon	• Bismaleimide (BMI)	• Autoclave
• Boron	• Bisphenol-A Epoxy	• Room temperature
• Aramid	• Polyimides	• Electron beam (EB) curing
• Basalt	• Polyester	• High intensity Laser curing
• Graphene	• Vinylester	• Fluid heated tooling
	• Phenolic	• Quickstep
	• Thermoplastic	• Oven
	• Polyetheretherketone (PEEK)	• Vacuum bag only
	• Polyetherketoneketone (PEKK)	• Resin transfer moulding (RTM)
	• Polypropylene (PP)	• Compression moulding
	• Polyamides (PA)	• Microwave curing
	• Polyetherimide (PEI)	• Induction heating (eg: roctool)
	• Polyethyleneterephthalate (PET)	• Thermoplastic
	• Polyethersulfone (PES)	• Autoclave
		• In-situ heating and cooling
		• Welding
		• Vacuum forming
		• Compression moulding
		• Pressing / Forming

2.3.1 Thermoset and Permanently Cross-Linking Composites

In the AFP process, thermoset composites can be used in a number of ways. Often, 50% resin weight towpreg is used during fibre placement. Thermoset resin prepregs require pre-heating to control the resin viscosity and hence the resin tack during feeding and prior to placement onto a mould. At the application nip point, the temperature is raised to reduce viscosity, increase tack and affect wet-out and intimate bonding to the substrate, while being compacted by the compaction roller. After placement, in systems without in-situ curing mechanisms, the composite part requires the application of further energy, usually in the form of heat but other options such as radiation can be used, to cure the resin and maximise the material properties [57]. For most epoxy-based prepregs, the thermal cure stage requires an autoclave cure, which increases cost and cycle time. This extra stage compromises the potential productivity gains from AFP versus using in-situ methods [58]. Advantages of thermoset resin

systems include low cost, in comparison to thermoplastics counterparts, [59] and generally higher maximum operating temperatures. Disadvantages of thermoset resin systems include the toxicity of some ingredients, limited shelf life and complex and expensive curing processes [60]. Furthermore, their rheology and inherent tack at operating temperatures means AFP systems, using these materials, require maintenance more often to clean built up resin within the feed guide system.

Criss et al., [61] examined the concept of an AFP system with a thermoset prepreg that was B-staged within the creel system prior to reaching the fibre placement head. Pre-stage of the cure involved heating the resin to a certain temperature to initiate reaction (often below 50% degree of cure) and then slowing the reaction through chilling of the tow while still allowing the tow to be manipulated and handled for placement. Subsequent reheating of the prepreg increased tack and allowed the resin to again flow and wet-out the fibres. By advancing the cure prior to placement, the laid composite only required a very short thermal post cure to reach a suitable degree of cure with comparable mechanical performance to standard processed parts. The thinking behind this approach was to eliminate the need for pressure during cure. The concept was tested with Cytec IM7 (intermediate modulus) carbon fibre and 977-3 epoxy resin in an experimental setup that used off line infrared heaters and a multi-zone oven under a nitrogen blanket to eliminate the possibility of oxidative degradation. Void content was measured using micrographs for various temperatures, pressures and delivery rates. The results showed that void content was reduced using the pre-staging process. This confirmed the hypothesis that partial curing during consolidation encouraged cross-linking and homogeneity of the matrix. The study also demonstrated the approach on cylindrical laminates, which also had reduced fibre buckling. With the gains made post placement however, complex and bulky auxiliary equipment was necessary prior to the placement head.

Staging of the curing process prior to delivery at the nip point was also investigated by Hutchins [62] for a carbon-fibre/epoxy composite (Hexcel IM7/8552). This work examined the effect to the degree of cure using differential scanning calorimetry (DSC), dynamic material analysis (DMA) testing and the glass transition temperature (Tg). Samples were manufactured using varying configurations of pre-heating or B-staging equipment prior to fibre placement before final cure was affected.

The purpose of B-staging was to improve handling characteristics, reduce the bulk factor and improve results in consolidation. By varying the degree of b-stage curing and the cycle times overall processing times could be reduced and the material mechanical properties improved. Hutchins aimed to minimise the post curing time required, by trying to progress the B-stage cure as far as possible beyond the material producers recommended 12.5-15% prior to fibre placement. The chemical and mechanical changes in the final product were examined by means of destructive and non-destructive testing for the varying degrees of B-staging. It was found that properties reduced slightly with increased B-staging. Beyond 20% B-staging properties reduced significantly. Hutchins [62] identified various risks associated with pre-staging on the spool. For example, spreading of the prepreg tow, variation of the staging level from the outer layers to the inner layers of the spool roll and a change in bulk factor during winding due to relaxation of the tow in tension. Furthermore, during processing with increased B-staging, issues arose such as limited ability to lay-up the B-staged tow onto contoured surface (because the tack and flexibility of the prepreg tow had decreased), lofting of the plies at lay-up which resulted in poor interlaminar debonding and later delaminations as well as concerns on the ability to assure quality due to variability in the prepreg. The cost-benefit analysis deemed this process to be unsuitable for production use due to the excessive and inefficient energy consumption required to B-stage the resin as well as the additional time required to then still cure the resin completely.

The concept of in-situ curing at the point of application rather than prior or post placement eliminates additional stages and has been shown to decrease cycle times [60][63]. One approach that has undergone significant investigation is in-situ electron beam (EB) curing. The first proposal for in-situ curing a thermoset-based composite in an AFP process was by Enders & Hopkins [64]. They investigated in-situ electron beam irradiation with the tape placement process. The authors suggested the concept of in-line cure control, which is possible by using in-line sensors that could provide, closed loop control of the placement speed. This could be achievable considering the localisation of curing that occurs and the efficient response times and control of the EB curing energy.
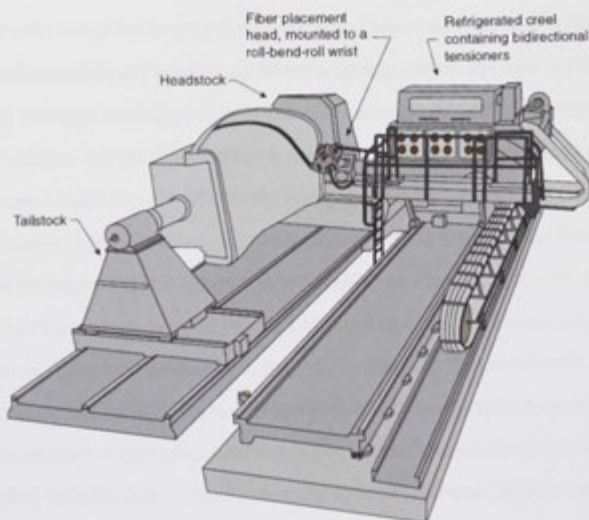
Figure 17 – MAG Cincinnati Viper horizontal gantry configuration

Goodman, Byrne and Yen [65] and Goodman, Weidman, Byrne, & Byankov [66] examined in-situ EB curing in ATL for large integrated structures using a custom machine designed to simulate EB curing ATL lay-up processes. The study developed one of the first true in-situ curing models using irradiation initiated curing in automated composite manufacturing, which could also be applied to AFP. The paper not only presented data on the mechanical and thermal properties of parts produced, but also examined the design trade-offs when incorporating EB curing and the limitations to part geometry due to the size of the EB system. Three different modes of EB energy application were tested on cationic resin systems only. For mode A, a fractional dose of EB curing of a newly laid tape occurred immediately after heat and pressure consolidation. In mode B, a full dose of EB was applied to the previous tape layer immediately before a new tape layer is applied. In mode C, the incoming tape is exposed to a full dose of EB immediately before consolidation. It was found that Mode's B and C required less EB energy and were more efficient and suited to dynamic current (DC) electron beam guns, while mode A required higher energy to penetrate through more layers and more suited to low frequency EB guns. The mode of

application was found to greatly affect the interlaminar shear strength, conformability and spring back of the cationic resin composites. This highlighted the sensitivity of the materials and the final part quality and strength. The authors stipulated further testing was required before a definitive conclusion could be made.

Goodman et al. [65] also examined the location of application of the EB irradiation in additional studies. The studies demonstrated that the in-situ cured composites displayed better resin dependant properties such as shear strength and interlaminar bond strength than those composites only cured by an at-once thermal cure. This was consistent in both exposure locations and it was also found that residual stresses were reduced using this in-situ curing approach through reduced thermal cycling of the entire part and tool. Goodman et al. [66] also successfully manufactured actual composite components using EB curing. The study went on to examine combining post cure heat with the EB curing. While the post cure heat increased the manufacturing time, the combination increased the short beam shear strength by up to 3 times when compared to samples without post cure heat. However, the typical lay-up speed was approximately 83 mm/sec, considerably slower than current commercial systems. The authors also cited work by NASA which showed a ply-by-ply curing approach that produced better interlaminar shear strength results, than an all in one step post cure.

In 1996 and 2001, Grenoble et al.[67] and Cano et al [68] also examined the use of in-situ EB curing with a modified AFP head that enabled curing on-the-fly in a ply-by-ply manner. The initial experimental unit integrated a simple roller and EB gun and could only manufacture flat panels. The unit effectively proved the concept and demonstrated the ability to lay-up and cure high quality panels. Burgess, et al [69], also studied the use of EB curable prepregs for rapid in-situ curing. Control parameters for the study included feed and lay-up rates, acceleration and deceleration of the placement head, compaction force, hot gas temperature and EB related controls. Both studies reported increased mechanical performance relative to at-once cured panels exposed to a single thermal cure cycle. The increased performance was attributed to the reduced stress of inter-ply temperature differences. The studies employed a pneumatic control system for force control and real time closed loop control. They also used a compliant rubberised roller [70] to increase coherence to complex geometries to improve quality

whilst varying application pressure across the width of the roller. This conformity, while advantageous for adhering fibres to a complex surface, is currently unqualified in terms of the application area and lack of data.

In-situ curing lasers have been posed as a possible solution to thermal response and heating ramp time delays with other in-situ heating mechanisms such as heated gas. In order to assess this theory, Wang [71], developed a heat transfer and cure kinetics model for the process of in-situ laser cured thermoset matrix composites in filament winding. The results of this study are transferable to fibre placement technology using laser curing. The laser delivered localised radiation to the application zone. Wang tested laser energy absorption of various resin systems and the effect on performance characteristics. The author found that the in-situ approach to curing reduces residual stresses in composite parts. However, to overcome the conflicting requirements of production rate vs quality of the composite, Wang [71] proposed that by increasing the laser exposure time in a manner that was decoupled from the lay-up time the quality and speed could be increased. This was achieved with a second laser system covering multiple tow rows after the lay-up point. The models and experiments demonstrated that the degree of cure could be increased further. This approach combined in-situ concepts with post curing but still maintained a dynamic continuous approach. Cycle times were drastically reduced and equivalent material properties to those manufactured with a traditional post-cure were found.

Composite curing with UV light can also reduce cycle times and solvent emissions, and produce parts whose mechanical properties are unaffected by the layering and secondary bonding that occurs with in-situ curing in a ply-by-ply process [63]. Di Pietro et al. (2008) demonstrated that an in-situ UV curing approach could be applied to robotic AFP process using a high intensity (25 W/cm^2) UV light source. The AFP machine created as part of the work of this thesis [63][72], which laid dry fibres and wet-out the fibres at the nip point is shown in Figure 18 [72]. Exposure times of less than one second per unit area were all that was required to cure glass-fibre/vinylester plies laid at a speed of 20 mm/s. The mechanical properties of the UV cured samples manufactured using the AFP process were equivalent to thermally post-cured counterparts [73].
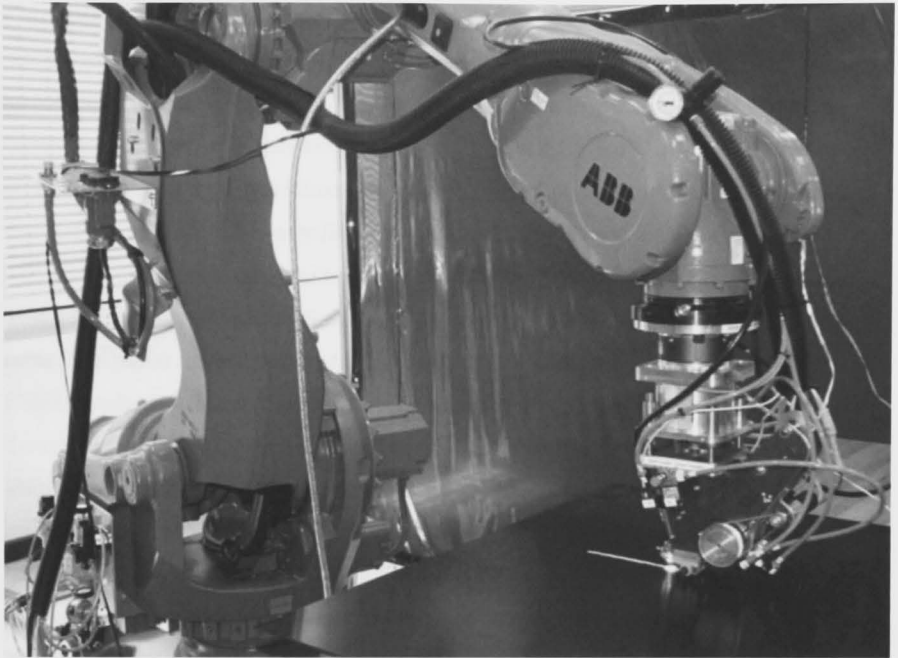
Figure 18 – The UVAFP prototype work-cell

2.3.2   Thermoplastic Composites

Thermoplastics do not permanently cross-link and therefore when heated above a critical glass transition temperature, parts can be formed, bonded and cooled in-situ. In-situ consolidation of thermoplastics is performed using localised heating of the layers to be bonded just prior to the nip point. The layer of thermoplastic to be applied to the thermoplastic substrate is then consolidated using pressure to promote bonding and chemical chain migration across the bond interface. The process is then immediately followed up with localised cooling and thus re-solidification. This negates the need for an autoclave, such as in thermoset systems, which is a major influence on composite part size, cost and throughput time [64]. A number of different technologies have been proposed in order to achieve in-situ thermoplastic bonding. These include hot gas guns, open gas torches, infrared lamps [74], high intensity lasers, and EB, microwave and high intensity UV radiation [31][63][73] [75][76][77].

The earliest approaches for developing thermoplastic lay-up in automated devices such as ATL and AFP were reported by Grove [57], Mantell and Springer [78] and Tessnow [79]. Advantages of thermoplastics in ATL and AFP are that they have a virtually unlimited shelf life, high level of chemical resistance, offer high impact resistance and can be welded and recycled. Thermoplastic raw material delivery and packing is much simpler than that of thermoset material systems. As thermoplastic prepregs are not tacky at room temperature, they do not require refrigeration during storage in the creel system or delivery system, and therefore cannot adhere to itself and rope or twist. Drawbacks include the high running costs of the devices in the head to affect in-situ heating and cooling in a very rapid timeframe. Other drawbacks include the large amount of waste energy during this heating and cooling, the inconsistent material properties including fibre volume fraction, resin content, geometric deviations and non-uniform crystallinity [60]. Early research examined the effect of temperature, time and pressure on lay-up quality, particularly bonding of plies and the effect on properties to determine precise processing windows and requirements unique to TP processing in comparison the TS AFP systems previously developed.

In 1993 a placement head for thermoplastic-based composites was designed and manufactured by Felderhoff and Steiner [80]. While the primary intent of the authors was not in the design of the thermoplastic AFP system but rather to develop the software that described the physical mechanisms involved, the head developed was very compact and ideal for use in a lab or for small part production. The design included a guide system for collimation of the fibre tows, an in-situ heating gas gun to consolidate and effect bonding of the plies and start and stop of individual fibre tows to vary ply angles. The design aimed to take advantage of ability of thermoplastic polymers to be consolidated in-situ in an automated system. Considerations for the new design included the critical distance from manipulation device (or robot mounting face) to the application roller, the cutting mechanism and preheating and application point heating of the thermoplastic. The head allowed accurate control of the preheating, nip point and temperatures, the tension in the tow, the compression force and lay-up speed. The design identified heat control as a critical area for concern in mitigating the risk of thermal degradation due to the quick start stop of fibres and the inability to couple this with an equivalently fast heating/cooling system. The head used infrared preheaters and

a hot gas torch at the nip point. The product was an initial concept paper and further work was needed to fully validate the process.

Shih [81] examined new techniques in online consolidation of thermoplastic composites. A simple filament winding system was developed for the manufacture of composite rings, which is relevant not just for filament winding, but can also be extrapolated to AFP. The controllable experimental parameters included roller speed, tow tension, compaction force, hot gas heating temperature, air flow control and control of the distance between the hot gas gun nozzle and the thermoplastic tow. Using this setup, composite cylinders from 6.35 mm wide APC-2 towpreg (carbon fibre and PEEK) were manufactured. A statistical processing window was determined looking at the most critical parameters, which were identified as speed, temperature and pressure. Quality measures for the studies were consolidated density, void content tests and micrographs of the cross sections of each part to qualitatively describe the consolidation and bonding. Differential Scanning Calorimetry (DSC) measured the degree of crystallinity. Finally, the Interlaminar Shear Strength (ILSS) of samples was measured and found to be very sensitive to speed and temperature. Analytical models were developed for the process from the experimental results. These models were used in CAD tools for predicting processing limits. The models included thermal simulations and stress simulations, and were used for predicting processing windows. Thermal degradation was not considered in the study even with the high heating rate and slow response times of the hot gas gun.

Leon et al. [82], found that thermoplastic in-situ AFP was well suited to thick section components due to the ply-by-ply, application of heat and bonding. The transmission of more energy to the bond surface and the application of large localised forces also impacted underlying plies progressing the bond. It was also found that thick structures manufactured with AFP thermoplastic processes performed better in comparison to thermosets of equal thickness and comparable material properties because they did not require a lengthy thermal post cure in an autoclave. Very slow ramp rates are required to post-cure such thick thermosets in order to mitigate the risk of exothermic reaction and degradation of the internal matrix. Furthermore, to actually see the energy penetrate the centre of the laminate thermal lag was substantial and energy

consumption was actually increased. Using AFP for TP matrices with in-situ consolidation means that a large amount of soak energy was not required.

Various heating mechanisms utilising convection, conduction and radiation have also been proposed for thermoplastic in-situ consolidation. Lichtenwalner [12] examined thermoplastic AFP with a rapid heating system using high intensity lasers and a neural based control system. The neural based control when used in conjunction with the fast responding lasers provided improved quality and adhesion and minimised the risk of thermal degradation by overheating. This was achieved through learning algorithms that mapped thermal responses and delay times. The laser process performed very well and was able to rapidly apply heat and switch off heat to the laminate on the localised area to be adhered.

Hulcher et al. [83], proposed utilising the incremental nature of fibre placement and tape lay-up processes to investigate the utility of interleafing the plies with resin to increase strength and impact resistance. The interleafed samples were prepared using PEEK/IM7 composite and a PEEK interleaf film. These interleafed laminates were compared against an equivalent PEEK/IM7 composite without interleafing. The interleafing provided promising results, improving performance particularly in impact resistance. The process however required two stages, one for the laying of the ply, the other for interleafing. This extra stage was labour intensive and slowed processing. By automating the film deposition with a spraying/coating process that is integrated into the AFP head; these labour limitations could be overcome.

Coffenberry, et al. [84], examined the effect of process parameters on in-situ thermoplastic consolidation. Over the range of 4cm/sec to 23 cm/sec, it was found that increasing the lay-up rate decreased the interlaminar shear strength of the sample in a near linear relationship. The strength reduced from approximately 100 GPa at 4cm/sec to 55 GPa at 23 cm/sec, a loss of 45%. To improve the interlaminar shear strength the material width of each tape was increased, decreasing the void content of the samples. This quite clearly identified the importance of the consolidation modes and control in thermoplastic part manufacture. It also identified the need for plastic flow of resin through heat and time was necessary to allow for adequate adhesion and ply melding. That is the process of bonding through heating and melting plies so that polymer chains migrate across the join surfaces to effectively weld the plies together. Coffenberry, et al.

[84], proposed that a cost versus performance database could be established for composites produced using this process. Process adaption, throughput and part integration were presented as the main factors affecting part cost.

Lamontia et al. [85] successfully demonstrated thermoplastic tape placement, filament winding and AFP. The system used application point heating to form the melt zone for consolidation and localised bonding in-situ. The paper proposed a thermodynamic model for the process, which examined the heating and cooling cycles for the process in two dimensions. The model examined the time dependent properties of pressure and heat and how these equated to material performance characteristics. This included the heat transfer induced temperature field, the evolution of intimate contact, the consolidation and melding, flow and void reduction of the matrix and interlaminar bond development. Lamontia found that when using optimised parametric values for process speed, consolidation pressure and heating temperature as derived from the model, mechanical performance of 85% to 100% of a fully post cured autoclave part could be achieved.

Grenoble, et al.[67], examined the use of different cross section tapes to improve laminate quality. Trapezoidal cross section PIXA thermoplastic tows were compared to the most commonly used rectangular cross sections tows. The aim of this work was to reduce void content by controlling how adjacent tows contacted and how the tows deformed during compaction for better stacking and nesting. This study showed promising results but introduced extra materiel costs in producing the trapezoidal shape. Void content was low, but the lack of consistency and dimensional variation in the trapezoidal tow inhibited consistent control and quality. Experiments found the material was sensitive to overheating causing deconsolidation after compaction. Because of the limited length (less than 5m) of the trapezoidal tow samples, the fibre placement system could not adequately hold the tow in alignment. As the tow alignment, during placement, could not be controlled sufficiently, tension control and ribbon guidance was compromised. Despite this, comparable performance was achieved when compared to samples produced with traditional tows. However, to achieve high interfacial bond strength and low void content, it was suggested that a secondary compaction roller and heating method be used.

While in-situ curing has possibilities in reduced cost and total process cycle times, in-situ curing with AFP faces a number of technical limitations and some disadvantages depending upon the part geometry. Gruber, et al. [44] cited experiences with in-situ EB curing that applies to nearly all in-situ mechanisms. These experiences highlighted the limited number of resin systems that are curable on-the-fly and the lack of commercially available equipment providing suitable performance. In particular the lack of suitably toughened systems such as compaction rollers failing when exposed to high intensity irradiation sources such as EB. The use of EB also increased the size and load of the placement head and the added need for radiation protection around equipment. All of the above highlight a lack of experience and literature on the topic even in 2001. Certainly development of optimised AFP placement controllers that could use cure control, such as the work currently being done using dielectric analysis (DEA), will be a major challenge [44].

While a significant amount of the current literature focuses on thermoplastic AFP a majority of parts made in production using AFP are made using TS matrices. Most likely the consistent issues associated with in-situ consolidation and the time, temperature and pressure sensitivity of TP processes has limited the application and the scalability of the fibre placement process using thermoplastics [86]. Current research trends suggest a large effort is taking place to rectify and understand these issues so as to take advantage of the inherent characteristics of high-localised pressures (to affect adhesion and melding) and the ability to apply heat locally in AFP systems.

2.3.3 Dry Fibre Bindered Preforms

AFP can also be applied to the manufacture of 'dry' fibre preforms with very low thermoset or thermoplastic binders [87]. These would be for use in liquid composite moulding processes such as RTM, vacuum assisted processes (VAP), resin infusion or as tailored inserts into layered sandwich style structures [88]. Dry fibres can be placed very accurately using CAD data thus providing designers with a manufacturing process that allows them to tailor the internal structure of composites to the loading requirement. Various techniques for the manufacture of preforms currently exist including manual lay-up with binding 'tackifiers'. These preforms can be formed into 3D through stitching techniques such as tailored fibre placement [89] (that create net

shaped 2D preforms), 3D technical weaving, 3D sewn preforms [89] and the use of AFP with dry fibre tows that are adhered to the shaped tools for full 3D preforms. AFP allows manufacture of preforms using dry fibre tows with minimal resin or binder (approximately 5% or less), and allows tacking and binding but not complete wet-out. Wet-out of the fibre during feeding is ideal for preform manufacture because the precise resin volume can be controlled and incorporated [63]. Complete wet-out is not initially required. Rudd, et al. [90], examined the possibility of using fibre placement technology to manufacture performs for the liquid composite moulding technique, RTM. The system was one of the first to look at dry fibre lay-up and used cheaper raw materials such as glass rovings. This potential is yet to be fully utilised. With a shift in composite manufacturing towards liquid resin processing, preform manufacture will become increasingly important in future AFP systems.

2.4   Summary and Literature Gap

An overview has been provided detailing the most prominent research into AFP technology and its many uses in composite manufacture. These include dry fibre performing, placement of thermosetting prepregs as well as the in-situ consolidation and processing of thermoplastics. The AFP approach as an integrated process provides for a complex system that is a unique process in itself. Experiments and theoretical models, are necessary to grasp the full interactions of the process kinetics.

While AFP has developed as the current state-of-the art, its intended application has been limited to the production of large scale, geometrically simple aerospace structures. There are five key gaps in the literature in regards to AFP technology and the materials they use. First, there is little or no comment in the literature on the design considerations for placement head devices and the reach and access of these placement heads. This is important for defining the complexity of the parts that can be laid-up (this applies not only to AFP but also to technologies such as 3D printing and other additive manufacturing techniques). Second, there is little or no research investigating the use of raw constituent materials such as dry fibre tows and liquid resin. Such a gap means producers and vendors have little insight into the issues (dimensional stability, uniformity of the raw material, environmental conditions and handling systems) associated with using these materials in high-tech automated systems. Third, applying

in-situ curing and impregnation techniques to AFP, such as UV photo-curing and resin nip point dispensing for on-the-fly resin impregnation. Fourth, using flexible industrial robots in such applications and utilising their six degrees-of-freedom to produce complex parts. Finally, the models of the AFP dynamic and transient process for controlling process quality and predicting processing rates. This includes impregnation, consolidation, curing and the ultimate thermal and mechanical properties. Therefore, this research focuses on contributing to the literature in these five areas to develop this beyond the current state-of-the-art for AFP.

3 The UVAFP Prototype Design and Build

This chapter presents the design and build of the prototype AFP system with in-situ UV curing and on-the-fly resin impregnation, termed UVAFP that demonstrates outcomes that meet the aims of this thesis. The context for the system design is presented as driven by experimental results as well as benchmarking research using established design methods. In Section 3.1 the Quality Functional Deployment (QFD) process used to develop the requirements and specifications is presented. The subsystems and interfaces are also defined providing the functional breakdown of the prototype. During the design phase two design hypotheses are proposed. Section 3.3 presents the design study that examined the first hypothesis looking at placement head size and access to certain component shapes that limit the AFP process. In Sections 3.4 to 3.9 the physical design the UVAFP prototype is presented in the context of the QFD and relevant background on each subsystem. The placement head is broken down into the major subsystems and each is discussed and the new design presented. The articulation system is analysed and the solution for the UVAFP system presented. Likewise, the current state-of-the-art in fibre and resin creel systems and the programming and control are presented along with the designs, their function, and the approach for the UVAFP prototype. Section 3.10 presents the experimental study examining the second hypothesis and the use of industrial robots for AFP articulation. Section 3.11 presents the literature and benchmark for AFP programming and control and the final solution developed for the UVAFP prototype. In section 3.2 the build stage of a UVAFP prototype is presented, providing details of the installation, assembly and initial commissioning. Finally, the chapter is summarised providing an overview into the design focus of the next chapter. Following chapters provide the underpinning research and experimental results for the UVAFP process using the system design and scaled experimental setups representing the system.

3.1 The Quality Function Deployment

The design of the UVAFP prototype followed the Quality Function Deployment (QFD) design process. The QFD design process was developed to ensure user demands and quality measures are achieved in the final product. The process deploys the functions forming quality in the context of the product, and the subsystems and component parts. The first phase is the definition and ranking of requirements, the high level needs of the customer. The second phase requires the translation of these requirements into specifications that allow the need to be measured. The specifications are then compared to known benchmarks and then targets for the specifications defined [91].

3.1.1 The Requirements of the UVAFP Prototype

In the UVAFP process, tows are placed onto a mould/tool, impregnated on-the-fly with resin, consolidated and cured in-situ to produce composite parts in a simple integrated process. Composite component thickness is built-up tow-beside-tow, ply-on-top-of-ply similar to a brushstroke of paint, and the coats of paint to build up the thickness. The requirements of the UVAFP prototype were derived from benchmarking current state-of-the-art AFP systems available on the market, as well as from discussions with representatives from industry. While the target market was ultimately automotive no AFP systems exist in use in auto production projects and therefore industry knowledge of the process is low. As such representatives included manufacturing engineers, program leaders for new manufacturing technology currently using AFP technology in the aerospace industry, manufacturing engineers and production staff currently producing composite components and procurement/supply chain management staff seeking solutions for composite manufacturing supply. Representative organisations included Agusta Westland, Italy, Eurocopter (now known as Airbus Helicopters), France, Eurocopter (now known as Airbus Helicopters), Germany, EADS Innovation Works, Germany, Airbus, France, Boeing, USA, Boeing Phantom Works, Australia and researchers working in the field from Royal Melbourne Institute of Technology (RMIT), Australia, University of Sydney, Australia, Universitetet i Agder, Norway, The Australian National University (ANU) and the

Advanced Composites Structures Cooperative Research Council (CRC-ACS), Australia. Due to the nature of non-disclosure agreements and permissions on what data could be released the data was cleaned and not attributed to specific organisations. In doing this some of the specific outcomes may have been lost. Representatives were asked to define what their expectations would be of a technology that could replace or improve upon the current state-of-the-art in AFP. The surveying at this stage was purposefully generic to derive high level requirements, not specifications. Some comments were inevitably specific and/or actual solutions due to the technical knowledge of the respondents surveyed. Following the surveying the collective views were summarised in a requirements list. The cleaned responses are shown in the following list prior to inference of the requirements as a consolidated set:

- Cheaper than prepreg
- Quicker than prepreg
- Use of existing material systems
- Use of new material systems – especially dry fibres
- High quality and high speed required by industry
- Control for thermal degradation
- Provide local and complete full consolidation without need for post compaction
- Void content minimised
- Come with accurate models of the process for simulation
- Consolidation of current academic and literature curing models for process control and quality modelling, not just lay-up simulation
- Varying thermal and pressure conditions during consolidation
- Auto-hesion and interlaminar contact quality high
- Control of threshold pressure for interlaminar contact
- Fully consolidated after processing hence bulk material properties after processing

- Head placement design normal to tool

- Tow tracking and centring on compaction roller important

- Interleafing effect of resin between plies could be interesting

- Separate cutting mechanism and placement mechanism

- Mount head side on to robot

- Electric drive the best as no oil contamination of composites

- Multiple tow feed

In total, 12 requirements were finally considered for the prototype as presented in Table 4. Essential or mandatory requirements were deemed as those necessary to meet the research and proof-of-concept goals at the most basic of operating levels. Prioritising of the requirements was undertaken using a pairwise comparison process as shown in Appendix 11.1. The requirements are listed in order with essential or mandatory requirements designated with the * listed first and then in order of priority. The requirements are also defined according to the three research drivers for AFP limitations, namely design, materials and process.

The highest ranked desirable requirements focused on quality and functional scope. Lower ranked requirements were those deemed as "nice to have" but not essential for a first prototype system setup and the aims of proving the technology, with the cost of the prototype being the lowest priority in that regard. The UVAFP uniquely aims to eliminate additional process steps by curing of the matrix in-situ and impregnating the tow with resin on-the-fly. It is these steps combined with the AFP concept that makes UVAFP unique.

Benchmarking of the requirements provided insight into current commercial AFP systems. While most systems address the scope for laying up composites, the systems did not address the broader manufacturing process chain issues. For thermoset matrices this requires adhesion and compaction only. For thermoplastic matrices this requires melting, adhesion and online consolidation. However, for both matrices final curing or consolidation relies on later post-processing to achieve final component quality.

3.1.2 The Specification of the UVAFP Prototype

The engineering specifications for the UVAFP prototype were derived from the requirements listed in section 3.1.1 and are shown in Table 4. The specifications provided quantifiable metrics for each requirement. The specifications were used during the design phase to define not only the physical characteristics of the placement head, for example the minimum concave tool radius and arc length, but also the functional limits of the hardware, for example the maximum UV intensity, determined by the maximum wattage of the UV bulb and power supply. This approach simplified the engineering decision-making process.

Table 4 – Requirement to specification development for the UVAFP system

Requirement	Priority	Driver	Specification	Units	Target	Validation
Lay fibre and resin uniformly and cure in-situ effectively	*	Process	Resin matrix family type	type	Thermoset or thermoplastic	By design
			Resin	type	Vinylester (with ability to handle other liquid resins)	By design
			Fibre	type	E-Glass (with ability to handle other 6.35mm or ¼ inch tows)	By design
			Material Processing	type	Separate fibre and resin	By design
Faster than hand lay-up	*	Process	Curing Method	type	Ultraviolet	By design
			In-situ	Y/N	Y	By design
			In-situ curing locations	1 - pre, 2 - post, 3 - during	2 and/or 3	By design
			Min Lay-up Speed	min mm/sec	0.5	Experiment
			Max Lay-up Speed	max mm/sec	3000	Experiment
			Flow Rates of Resin	ml/min	0.3 to 30	Experiment
			Min Tow Width	mm	3	Experiment
			Max Tow Width	mm	6.5	Experiment
			Tow Thickness	mm	0.38	Experiment
Produce higher quality parts to hand lay-up	*	Process	Voids	%	<3	Experiment
			Compaction Pressure	N	10-1500N	Experiment
			Compaction Mechanism	type	Pneumatic Actuator	By design
			Critical Distance	mm	<800mm	By design

			Fibre Volume Fraction	%	>50%	Experiment
			Internal Quality system	Type	Error passing on controllers	By design
Place fibre along programmed path	*	Design	Path Repeatability	mm	<0.03	Experiment
			Cut/ Clamp/ Restart Mechanism	Y/N	Y	By design
Easy to maintain and support	*	Design	Period between services	hrs	50	Will not be validated (future work)
			Weight	kg	<20	By design
Produce complex parts	1	Design	Minimum Convex Radius	mm	150	By design
			Minimum Concave Radius	mm	30	By design
			Arc length of minimum concave radius	degrees	180	By design
			Creel System	type	1 roving, internal pull, digital tension control – internal to placement head	By design
			Fibre Tension	N	0 to 0.6N	Experiment
			Roller Diameter	mm	30	By design
			Min cut length	mm	50	By design
			Individual tow payout	Y/N	Y	By design
			Clearance angle	degrees	45	By design
			Head offset distance	mm	<500	By design
Controllable / Adjustable Process parameters	2	Design	Programmable	Y/N		By design
			Controller	type	IRC5 internal	By design
Minimise waste	3	Materials	Waste	grams/m^2	<5	Will not be validated (future work)
			DOF external to head	#	6 - robot	By design

			DOF internal to head	#	3 -head (1 compaction, 2 roller passive)	By design
Durable	4	Design	Time to change head	min	<1	Experiment
			COTS Components	List	Cutter, roller, bearings, pneumatic cylinder	By design
			Roller Material	material	Steel with elastomer surface	By design
			Cutting Technique	type	Guillotine	By design
Accept varying material systems	5	Materials	New Features	List	Closed loop pressure control, resin viscosity control, compliant roller, Tow payout, Scraper to minimise lofting	By design
			Auto fibre feed	Y/N	Y	By design
Modular	6	Design	Time to change supply materials	sec	<60	Experiment
			Number of Tows	# to #	1 (but scaleable)	By design
			Tow width range	mm	5.5 to 7	Experiment
Low capital cost	7	Design	Cost	$	<10,000	By design

While all survey respondents and end users questioned were exclusively in the aerospace industry, for the first prototype and target market of automotive it was deemed acceptable to use a lower performance material system of glass fibre / vinylester. This was on the one hand to reduce cost but also to aid the selected curing process performance (UV curing) by increased transmissibility of glass fibre. As detailed in the specifications the system was designed to handle other resins and fibres but these investigations would be outside the scope of this thesis. Metrics with specified ranges provided the opportunity for process control and acted as the independent variables for the process optimisation study. Figure 19 shows the corresponding process window for the prototype based on the target specification.
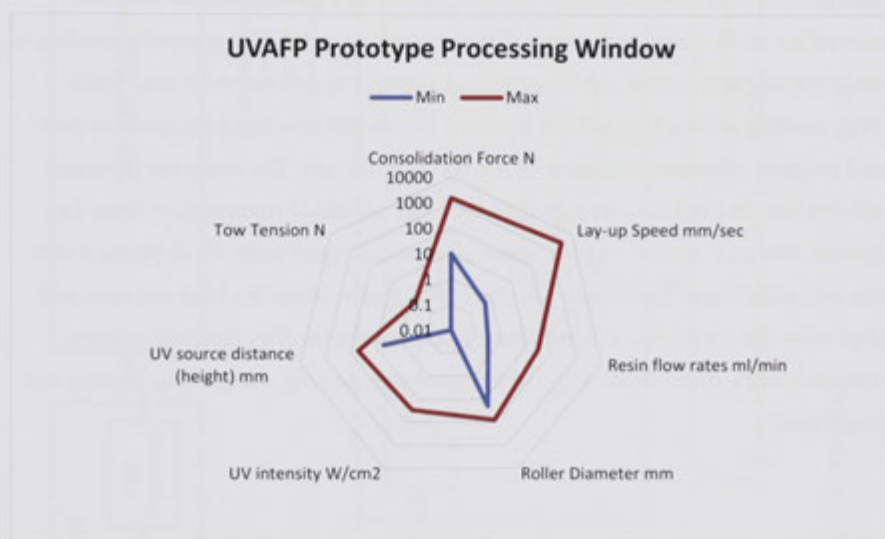
Figure 19 – UVAFP prototype processing window

In many instances, metrics were determined based on benchmarked state-of-the-art AFP systems. These included MAG Cincinnati's VIPER and FPX system [92][93][70][94][95], Coriolis composites AFP unit [96][97][10] MTorres' Fiberlayup system, ElectoImpact's AFP system and Ingersoll's Mongoose system and Automated Dynamics Corporation's V3 to V5 machines amongst others. Some metrics were defined according to limits placed on the experimental unit having only 1 tow feed system. This was the case for the resin flow rate. This was set at a maximum of 30

mL/min which equates to approximately 2 kg of resin/hr or approximately 5kg of composite/hr assuming no lost time for cutting and repositioning etc. While this is at least an order of magnitude too slow for the implied application in automotive production, keeping to the modular approach and allowing for multiple tows to be added in industrial systems the deficit could be addressed.

3.1.3   Subsystems and Interfaces

Following the development of the requirements and specifications in the design process an analysis of the AFP system was undertaken in order to identify the primary steps internal to the process. A schematic of the system architecture of UVAFP subsystems is shown in Figure 20. The direction of data passing and the fibre tow movement are indicated with arrows. The subsystems are broadly grouped according to programming and control, the material creel system and the placement head itself. Programming included the off-line planning system that developed the essential path and program command definition for the lay-up of the part. The controller processes this off-line data and uses the path definition and associated commands to drive the system. The creel system supplies material to the placement head which places it onto the tool according to the defined placement path, consolidates the fibre and resin and then cures the composite. The placement head contains the fibre handling systems including entry guide, tensioning, clamping, cutting, heating, compacting, cooling and inspection.
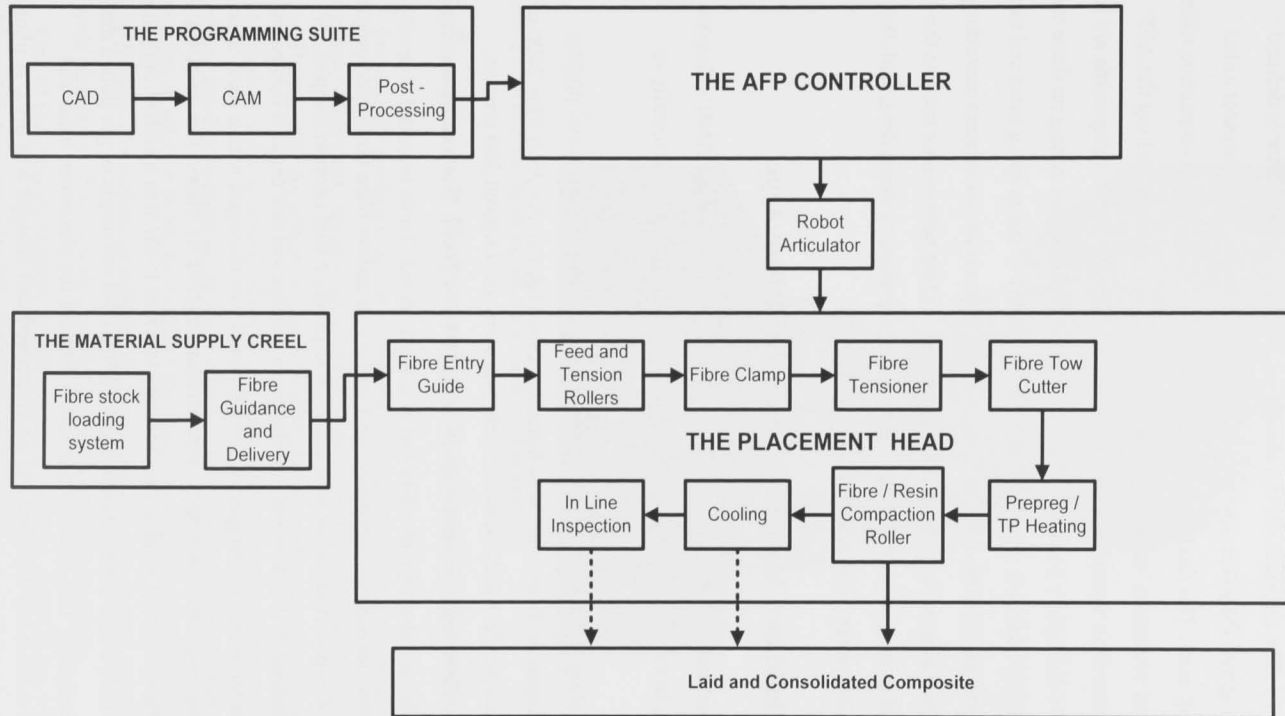
Figure 20 – The system architecture of a generic AFP System

The interface of the creel to the placement head is defined by the handling limits of the fibre tow. The interface for the placement head to the articulator is defined by the robot mounting and the placement path as programmed using the computer aided manufacturing suite. The final composite is acted upon only by the compaction roller and any in-line processes; such as cooling and inspection, thereby making the AFP process continuous in nature. Internal interfaces within each of the subsystems are in many respects defined by packaging and automation technologies acting on these two inputs. Therefore quality is dictated firstly by the quality of the prepreg tows and then by the two main tasks of the AFP process, namely the accurate movement according to the programmed placement path, and the material handling subsystems such as the CCR from the creel to the compaction roller. However the process is dependent, with the final part quality dictated by additional post processes.

3.2   The Build and Assembly of the UVAFP Prototype

The final build of the UVAFP prototype took place within the ANU's flexible robotic manufacturing workcell. The build process is documented pictorially in Appendix 2.

The tooling surface for the lay-up of fibres was a flexible industrial jigging system developed by Demmeler Maschinenbau GmbH & Co, the Profi Plus 2400 x 1200 with standard feet and a surface hardening using the Demont 500 process developed by Demmeler, product code PL28-01004-011 [148]. The tooling was rigidly mounted to the workbench and calibrated as a work object. Tools included a variety of material options including aluminium, steel and also a carbon fibre reinforced prepreg tool. For most experiments a flat tool was used to produce trial coupon samples for mechanical testing. Extraction and ventilation to manage volatile organic compounds (VOCs) from the resin system (particularly styrene) was managed with a local fume extractor using high efficiency particulate arrestance (HEPA) filters. The umbilical line connecting the placement head to the creel and services to the was installed onto the robot arm to ensure that cables, hoses and feed lines did not tangle or get pulled during complex articulation. This was made possible because the placement head was permanently mounted to the robot and no automated tool changer was used. A photo of the final system build laying up a part is shown in Figure 21.

Figure 21 - UVAFP curing of a glass-fibre/vinylester composite.

3.3   Experiment 1: Placement Head Size, Reach and Access

For an AFP system to place continuous fibre tows onto a tool surface to lay-up a composite component, the geometry of the surface must not exceed certain complexity limits. These limits are driven by the interaction between the placement head and the tool surface in order to avoid collisions and ensure the normal orientation of the placement head in relation to the tool surface. The normality of the AFP placement head orientation in relation to the tool surface has been found to be critical in ensuring a high quality lay-up. The normal orientation ensures adequate compaction, no wrinkles, and accurate placement of tows with controlled spacing onto the tool [98].

One of the primary features of AFP technology is the ability to lay fibres into concave geometries not just convex geometries of the filament winding process. It is the

radius and arc length of these concave features that limits access of any AFP system. The minimum radius and maximum arc length that any AFP system can place fibres into is determined by the size of the placement head. Specifically the size represented by the independent design features of the radius of the compaction roller, the width of the placement head from front to rear and the clearance angle of the tow CCR guide chute.

Whilst many existing AFP systems have limited head clearances this is primarily due to the fact that to date, many have been built for the manufacture of specific parts and in many cases head clearances have not been required so other design requirements have been prioritised. This however means that moving forward current AFP systems can only be considered for a small number of part types due to the relatively large minimum radius and small arc lengths they can access to place fibres onto. This has ultimately restricted the uptake of AFP systems in industry as demonstrated by the case that to date almost 100% of AFP sales have gone to aerospace applications with a small number of systems now seeing application producing wind turbine blades. Many aerospace components and structures exhibit by default smooth sweeping geometries due to their aerodynamic function and therefore are naturally well suited for AFP manufacture. However, these types of parts have limited production volumes and are generally limited to exterior components and not structures [99]. The highest carbon fibre composite consuming program in aerospace is set to be the Boeing 787 Dreamliner at 47 aircraft per month in 2017. While this single program will consume a large quantity of carbon fibre composite material the rate of output (takt time) at such volumes is still quite long in comparisons to the likes of the automotive industry. A far greater number of opportunities at higher production volumes exists in other industries, however these applications demand complex forms driven by tight design envelopes for lightweighting components.

Some wing spars are manufactured with AFP by placing tows directly onto the final shape tool. However, due to the limited clearance angle of the placement heads, rotating tooling or additional axes must be used. Mounting the tooling on a rotating additional axis permits a greater clearance angle range to access all three sides of a C-shaped spar. This solution of course can only be applied in limited situations where the tooling is suitable to mount on a rotator. That is, the component must have a primary

longitudinal axis that is straight with a length that is within the limits that allow it to be suspended between a pair of rotators. To make these parts practical, they must be divided into smaller parts, and later joined post-lay-up, this inevitably adds weight to the design and diminishes the properties and appeal of a composite solution [98]. Debout, Chanal and Duc [100] found that in most cases ATL and AFP machines are limited to 10m and 3m minimum tool curvature radii respectively due to the design of the placement system.

Some studies have been undertaken to develop part-smoothing strategies in order to reduce the necessary movement and kinematic challenge in maintaining normality to the part surface in particular through tight radii [101]. This leads to the compromise of lay-up rate over part quality. Faubion [101] showed that machine life and operating costs could be reduced by using "road grader" type smoothing whereby placement head orientation drifts to nearly 85° in comparison to the tool surface instead of the nominal 90° while managing higher lay-up rates and reduced machine wear but at a cost to quality with possible insufficient compaction in concave radii. Stamen noted that head size must be minimised in order for tight geometry to be laid by AFP systems. In this case spar elements having 2 flanges and a web at 90° to each other [98]. The spar geometry demanded up to 45° clearance angle while a mono wing geometry up to 52° clearance. The work undertook a categorisation of part geometries and the required angular motion through each rotational axis of the placement head, as shown in Table 5.

Table 5 – Part placement head rotation requirements

Part	Roll (X axis rotation, °)		Pitch (Z axis rotation, °)		Yaw (Y axis rotation, °)	
	+	-	+	-	+	-
Straight spar	90	90	0	0	180	180
Bent Spar	105	122	45	40	180	180
Winglet/Sharklet	62	22	8	22	180	180
Mono-wing	0	35	50	52	180	180

ElectroImpact [102] developed a modular placement head with optimised clearance around the nip point in order to maximise such clearances, an example is shown in Figure 22 [98]. The placement head design focuses on clearance at the nip

point, however the modular design incorporates the entire creel system within the end effector itself, meaning the overall placement head is very wide amongst benchmarks, this ultimately limits the clearance of the placement head and the complexity of parts that can be produced.
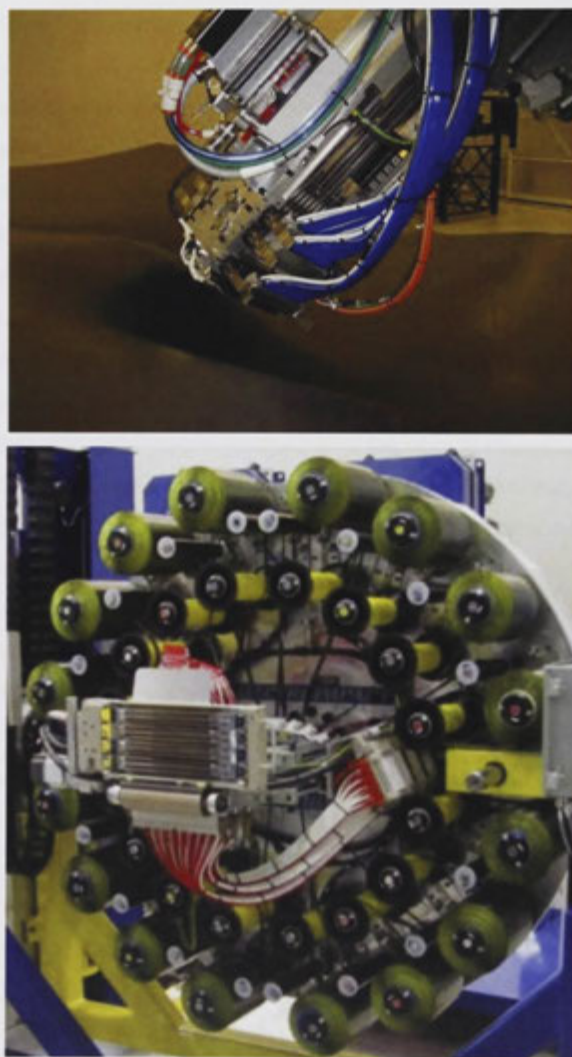
Figure 22 – ElectroImpact Modular AFP head

Rower [103] proposed a novel compact head design capable of complex part production. The head design mounted onto an industrial robot with a universal base plate incorporating creel and CCR equipment. To achieve complex part lay-up Rower proposed a low profile tool centre point that could place 90° internal corners with corner radii as small as 12mm and tangential (off-normal) lay-down. The design was also capable of bi-directional lay-down and with independent compaction axes that was considered important for complex parts that would contain a greater number of shorter placement runs. Rower found that by maximising nip point clearance (for example by keeping tow guides as close to the roller horizontal centreline as possible maximised corner clearance) and likewise by ensuring a bi-directional lay-up capability (using mirrored clearances) and a very small compaction roller geometry (19.125mm diameters polyurethane rollers) complex parts could be produced. The study did not characterise the access or reach of the system but identified design features important to high accessibility placement heads.

While the literature discusses design features, functional elements and the internal automation, nowhere in the literature is the impact on the placement head packaging envelope examined in order to optimise the complexity of parts that can be produced. While certainly placement head design optimisation must occur within the vendor market, proprietary software systems are improving. This software can sometimes address design limits by identifying potential collisions and optimising approach and departure of the placement path programming and in some instances deviating from the program logic of maintaining placement head normality to the part surface in order to reach a certain feature. That said, the user is ultimately restricted to in produceable part complexity by the placement head design. In order to address these design limits and develop modularity and customisation, an understanding of the driving dimensions and characteristics that determine reach and access in the multi-body kinematic problem.

3.3.1 Experiment Aim and Hypothesis

The aim of the study was to determine the optimal head geometry to allow the most reach and access to the widest variety of component geometry categories. In order to quantify the access limits of AFP placement head design and ultimately inform the design process for the UVAFP prototype, a study was undertaken examining the effect

of roller radius, head width and clearance angle on the minimum layable radius and the maximum arc length achievable. It was hypothesised that reducing the size of the AFP placement head will increase the reach and accessibility of the AFP placement head within the lay-up tool. It was proposed that by reducing the size of the placement head (decreasing the roller radius, the placement head width and the clearance angle) the minimum layable radius and maximum arc length can be achieved. It is further proposed that by calculating such an optimal design that the access of the optimised head will exceed current state-of-the-art systems.

3.3.2 Experiment Apparatus

As a design study, the experimental apparatus was a constrained geometry set as per Figure 23. The geometry set represented the placement head end effector of an AFP system. The geometric set detail included a circle representing the compaction roller, a triangular shape representing the clearance angle defining the approach of the tow guide chute and packaging of the placement head up to the robot wrist axis (pitch or rotation of the z axis as per this 2D representation) and a circle and triangular tangent shape representing the wrist. The independent variables of the set included the roller radius, r_{roller}, the placement head clearance (angle of attack of the tow guide) β, the head width, w, measured from the centreline of the head to the widest point along the clearance angle and the head offset measured from the widest point on the placement head to the robot wrist access, O. The dependent variables of the study were defined as the minimum tool radius, r_{min}, and arc length of said radius, θ and together defined the access limits of the placement head.
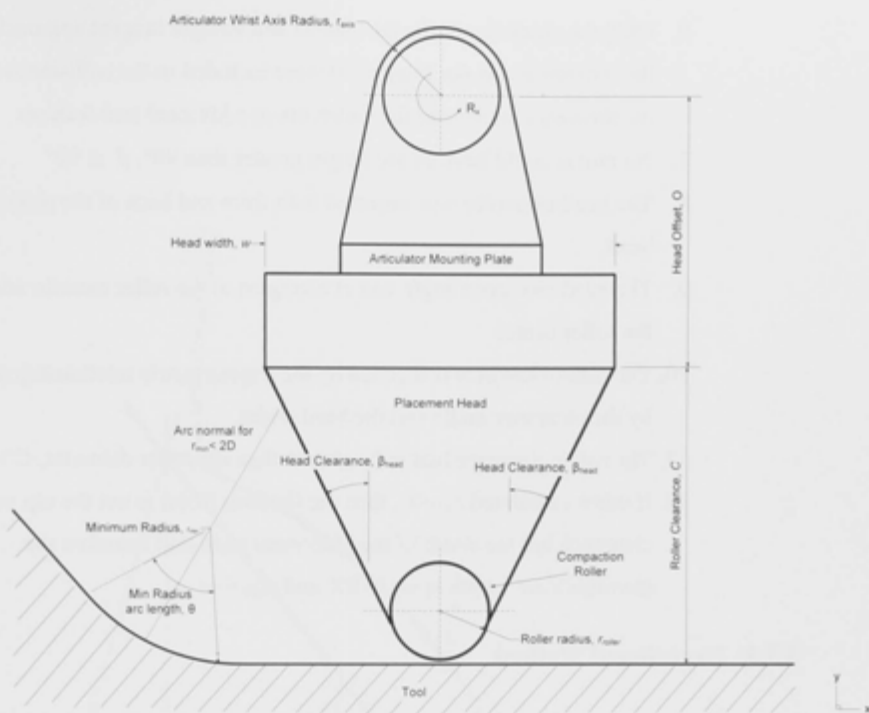
Figure 23 – Geometric study parameters and constraints

In order to fulfil the process limits of AFP, the study maintained certain process conditions, namely:

1. The compaction roller had to maintain contact with the surface, ie: roller radius and tool surface maintained a tangent contact.

2. Contact occurred beyond the point where the placement head geometry and the tool radius coincided. Coincidence signified the limit of the experiment scenario.

3. The placement head had to maintain a normal angle to the tool surface.

4. The minimum tool radius could not be less than the roller radius

5. The centreline of the placement head (drawn between the compaction roller axis and the articulation wrist axis) maintained a perpendicular relation to the articulator mounting collar.

6. Only the geometry of the tool radius and straight tangent approaches to the tool radius (as per Figure 23) were included in the collision studies, no allowance was made for undercuts or additional tool features

7. No radius could have an arc length greater than 90°, $\beta \leq 90°$

8. The head clearance was mirrored both front and back of the placement head.

9. The head clearance angle was at a tangent to the roller exterior and not the roller centre.

10. The roller clearance is dictated by the trigonometric relationship defined by the clearance angle and the head width.

11. The roller clearance had to be greater than the roller diameter, $C > 2r_{roller}$

12. If when calculated $r_{min} < C$, then the limiting factor is not the nip point clearance but the width of the placement head and therefore the maximum arc length is set to 90° and $r_{min} = w$.

3.3.3 Experiment Method

The experimental method involved a number of steps. The first step involved forming the mathematical model based on the geometric set. The second step involved running analyses to determine the optimal design parameters that would define the size of the placement head, within physically feasible ranges. Finally, a benchmark analysis was undertaken using the optimised design in comparison to commercial AFP systems to compare the access improvement and the groups of parts that can be produced.

3.3.3.1 Formation of the Model

The geometric model was drawn using the Solidworks 2008 CAD system as a 2D sketch as shown in Figure 24. In the CAD environment the process conditions were defined as geometric constraints. Once modelled, the set was setup for variation of the independent variables and measuring the effect on the dependent variables.

$\theta = \sin^{-1}\left(\dfrac{w}{r_{min}}\right)$

r_{roller}

w

$\left(w, w\tan(90-\beta) + r_{roller}(1 - \dfrac{1}{\sin\beta})\right)$

$y = x\tan(90-\beta) + r_{roller}(1 - \dfrac{1}{\sin\beta})$

$(x-0)^2 + (y - r_{roller})^2 = r_{roller}^2$

$(0, r_{roller})$

r_{roller}

$(x-0)^2 + (y - r_{min})^2 = r_{min}^2$

$\dfrac{r_{roller}}{\sin\beta}$

β
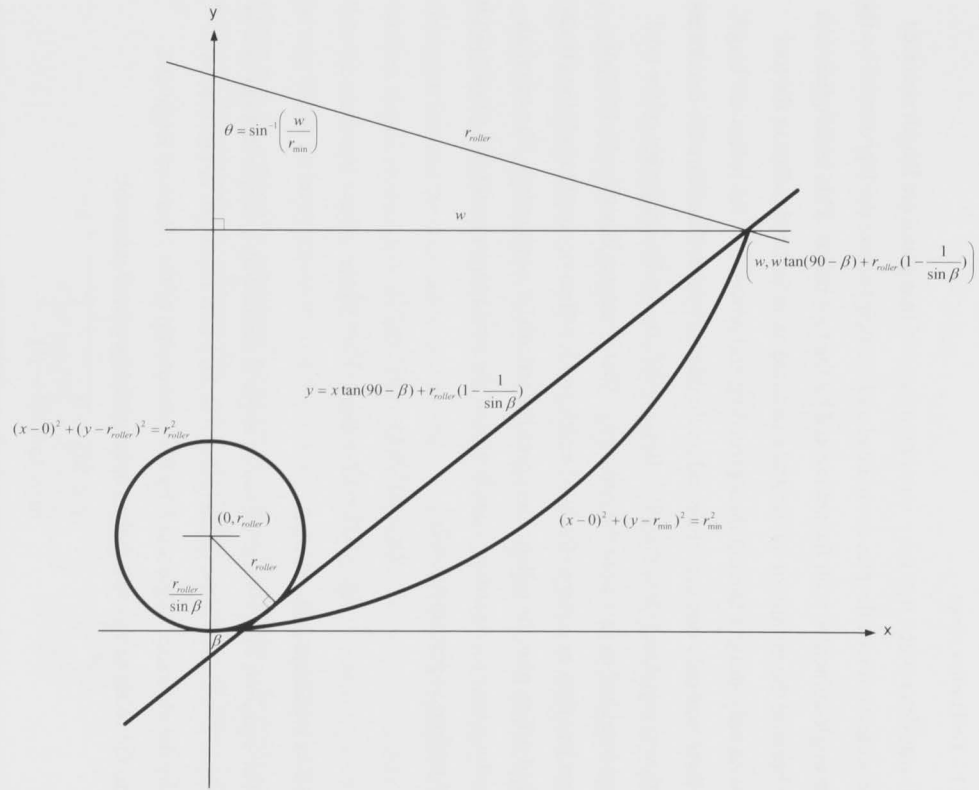
Figure 24– **Placement head reach and access geometry simplified**

The formulae defining each of the coordinates and functions were derived using the trigonometric definition of the process conditions and geometric constraints. The limits on the range of the minimum tool radius is shown in Equation 1.

$$r_{roller} \leq r_{min} \leq (w) \; || \; \frac{(O + r_{roller} + r_{wrist})}{2}$$

Equation 1 – Tool radius range

It was determined that the minimum radius and maximum arc length occurred when the widest point of the placement head and the point where the line created by the clearance angle coincided with the arc created by the tool radius. This assumption was possible because the minimum radius was examined as an isolated radius in the tool surface with only straight tangent lines preceding and proceeding the radius arc length. That is, there was only one curvature and no double curvature. Therefore the maximum arc length was equal to or less than 90°. Beyond 90°, the width and height of the total placement head had to fit within the concavity. That is (as per Equation 1), the tool radius was less than or equal to the head width and less than or equal to half the distance of the head offset, plus the roller radius plus the articulator wrist radius. The equation for the roller where (a, b) are the coordinates of the circle centre point and r is the circle radius, therefore as per Equation 2.

$$(x - a)^2 + (y - b)^2 = r^2$$
$$(x - 0)^2 + (y - r_{roller})^2 = r_{roller}^2$$

Equation 2 – Compaction roller function

The equation for the head clearance angle is defined by a simple straight line as per Equation 3, where m is the gradient and b is the y axis intercept. In this case m is defined by the clearance angle and b by the relationship of the clearance angle as a tangent to the roller radius which then determines the y-axis intercept:

$$y = mx + b$$
$$m = \tan(90 - \beta)$$
$$b = r_{roller} - \frac{r_{roller}}{\sin \beta}$$
$$b = r_{roller}(1 - \frac{1}{\sin \beta})$$
$$y = x \tan(90 - \beta) + r_{roller}(1 - \frac{1}{\sin \beta})$$

Equation 3 – Head clearance angle function

The equation for the minimum radius of the tool is defined as Equation 4 from the standard equation form of a circle with its centre at the position $(0, r_{min})$ and radius r_{min}.

$$(x - 0)^2 + (y - r_{min})^2 = r_{min}^2$$
$$x^2 + (y - r_{min})(y - r_{min}) = r_{min}^2$$
$$x^2 + y^2 - 2r_{min}y + r_{min}^2 = r_{min}^2$$
$$x^2 + y^2 - 2r_{min}y = 0$$
$$x^2 + y^2 = 2r_{min}y$$
$$r_{min} = \frac{x^2 + y^2}{2y}$$

Equation 4 – The minimum radius function

For determining the minimum accessible radius of a placement head and the maximum arc length the problem can be approached in two different ways. That is, by either setting the radius as the driving dimension and having the arc length driven or by setting the arc length and having the minimum radius driven. For the formulation of the minimum tool radius and maximum arc length in this work, the coincidence point of the clearance line and the tool radius arc was determined to optimise both parameters. While a simple approach to the minimum radius could have been used that determined that the minimum radius of was equal to the roller radius the arc length would usually be very small, or more precisely equivalent to $90°$-β. As per the simplified geometry, where $x = w$, y could be calculated according to the clearance angle therefore r_{min} would be determined according to Equation 5 according to substitution from Equation 4.

$$r_{min} = \frac{w^2 + \left[w \tan(90 - \beta) + r_{roller}\left(1 - \frac{1}{\sin \beta}\right)\right]^2}{2\left[w \tan(90 - \beta) + r_{roller}\left(1 - \frac{1}{\sin \beta}\right)\right]}$$

Equation 5 – The minimum radius according to the clearance angle, roller radius and placement head width

The mathematical model explained the dependence between the minimum radius and the arc length. In this case the dependency was inverse, meaning that the minimum

radius occurred and the minimum arc length while the maximum arc length occurred at the maximum radius.

$$\theta = \sin\left(\frac{w}{r_{min}}\right)$$

Equation 6 – The formula for the arc length as a dependency of the minimum radius

3.3.3.2 Design optimisation

To optimise the design of the placement head to both minimise the accessible tool radius and maximise the arc length of this radius, a full factorial analysis of all independent variables was undertaken. The chosen ranges for the study for each independent variable are shown in Table 6.

Table 6 – Reach and access independent variables and their ranges

Variable	Range	Units
Head clearance, β	5 - 85	°
Head width, w	100-1000	mm
Compaction Roller radius, r_{roller}	12.5-100	mm

To examine the effect of each parameter individually, 2 of the 3 variables were fixed to the mid-range value for the range under examination and the final variable was varied across the tested range. Following collection of the data across the full factorial dataset a ranking algorithm was run in order to identify the design with the smallest minimum radius and the largest arc length. The results are presented in section 3.3.4.

3.3.3.3 Benchmarking Study

Following the optimisation analysis, a benchmarking study was undertaken to determine the minimum radius and maximum arc length that could be reached by particular commercial state-of-the-art placement head designs. The benchmarks selected (in alphabetical order) included Automated Dynamics Corporation, Coriolis Composites, ElectroImpact, Ingersoll, MAG Cincinnati and MTorres. The placement head models for each benchmark was selected based upon quality of images and data available on the system in the literature. Each benchmark was measured in order to capture the independent variables. The data was gathered by photographic analysis

using the ImageJ open source software package [104], as no data was publically available for the specific design variables of this study. Scale measurements were taken from known distance references within the photos to calibrate the pixels/unit length. Using the scale calibrated images measurements were taken for the head offset, the head clearance and the roller radius. The benchmark data was then compared to the optimisation result to validate the performance improvement.

Part complexity as defined by the geometry of the lay-up surface and the steering paths the fibre tows and the interaction of surface and placement head is driven by clearance and conformance, referred to as 'access', to enable compaction into the geometry and the scale of the component and the relation of the geometry access to the 'reach' of the articulation system. Therefore, target components for composite application in the automotive and aerospace were assessed according to their minimum concave radius seen on such parts and the arc length of the minimum radii. The groups were then broadly defined in a process limit chart for the benchmarked AFP systems and the optimised design.

3.3.4   Experiment Results and Discussion

The results of the design optimisation and benchmarking study are presented in the following sections. As was hypothesised, it was found that by reducing the size of the AFP placement head the complexity of the part that can be produced maintaining process rules increased.

3.3.4.1   Design Optimisation

The three primary independent variables, namely roller radius, head width and clearance angle were analysed in a full factorial analysis with minimum tool radius and maximum arc length. The full factorial analysis calculated the minimum radius and maximum arc length of the tool according to Equation 5 and Equation 6, respectively. Where the process conditions were breached because the roller clearance was less than the minimum radius, the placement head width was used as the minimum radius and therefore a maximum arc length of 90° was achieved.
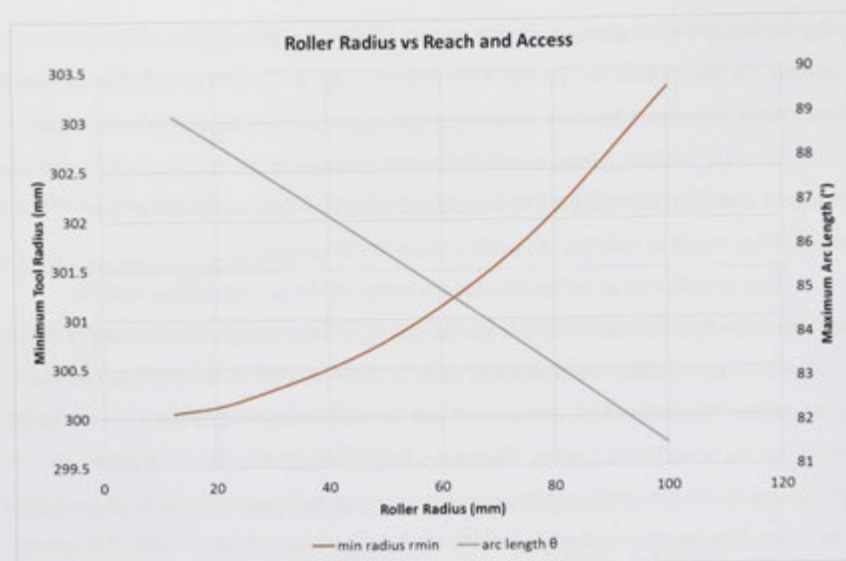
Figure 25 – Roller radius versus minimum tool radius and maximum arc length

Figure 25 shows that by increasing roller radius the expected outcome of increased minimum radius and a decreased maximum arc length occur. Therefore the smallest roller radius is best for optimisation of reach and access as defined by minimum tool radius and maximum arc length. In many commercial designs of AFP systems, the roller radius is increased for a number of reasons, going against the findings of this work. These reasons include increasing the contact area of the roller onto the tool aiding adhesion and consolidation and reducing lofting of the tow immediately after the roller due to the high upward shear forces caused by small roller radius and small contact area. It is evident however from this work that the gains in consolidation come at a cost to reach and access and therefore should be considered in the design of placement heads and their target applications.
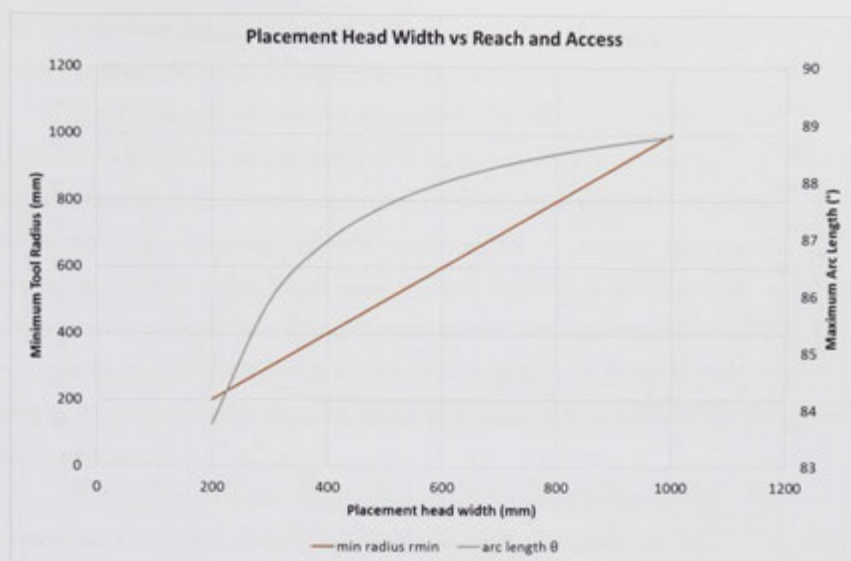
Figure 26 – Placement head width versus minimum tool radius and maximum arc length

Figure 26 details the effect that the placement head width has on the minimum tool radius and maximum arc length. There is a linear relationship between placement head width and minimum radius. The relation to arc length surprisingly exhibits a positive logarithmic nature. This suggests that increasing the placement head width actually increases the possible arc length for the mid-range values chosen for the other design parameters. These influences suggest that while minimising the width of the placement head has a significant impact on the access in terms of the minimum tool radius, the smallest width is not the optimal design for ensuring maximum arc length of the radius. For the example, for a 45° clearance angle and 50mm roller radius as was set in this case, the width can be up to 400mm with significant gains made in arc length. Above 400mm the arc length gains diminish and therefore exceeding this width should be avoided.

Figure 27 – Placement head clearance angle versus minimum tool radius and maximum arc length

Figure 27 indicates that the optimal design range for the clearance angle is less than 45°. Clearance angles greater than this very quickly diminish accessibility in terms of tool radius and arc length. Due to the geometric constraints, the overall height of the placement head increases given the same width as the clearance angle decreases. This leads to larger and larger minimum tool radiuses as the clearance angle decreases. In this case, the width was set to 300mm, leading to a maximum arc length of 90° at clearances angles less than 45°. This was because beyond 90° the height of the placement head would have led to a collision with the tool radius tangent surface.

Utilising the full factorial data set a search was undertaken on the optimal design that minimised the tool radius and maximised the arc length. A bipartite parameter ranking technique was used to score all parameter combinations. The highest ranking was applied to the parameter combination that scored highest in each quality measure as an aggregate by adding the individual ranks. The highest scoring combination for the design parameters were a roller radius of 75mm, a head width of 100mm and a clearance angle of 25°, achieving a minimum radius of 100mm and a maximum arc length of 90°. The reason for this selection is based on the process conditions limits and not directly from the calculated trigonometric problem. Certainly other variable sets

also met the same radius and arc length but these designs had a smaller roller radius and required greater clearance making packaging more difficult.

The design optimisation results suggested that the roller radius was less important in achieving the smallest tool radius compaction as possible if the geometric constraints of normal oriented compaction is to be maintained, that is, a smaller minimum radius is certainly achievable with a smaller roller radius, however the minimum to maximum arc length range while trying to maintain the normal orientation condition was reduced. Seemingly other parameters play a greater role and therefore roller radius can be maximised to a value as large as the minimum radius of the tool as long as the roller does not exceed the placement head width and a clearance of at least 45° is maintained.

The biggest influence on the clearance of the optimised head design was determined to be the head width and clearance angle. The small width of the optimised design would be a challenge for incorporating CCR systems and therefore may not be realistic for actual AFP system design. Given however the results demonstrated in Figure 26 the width could be increased to account for packaging and improve the arc length even with diminishing access for smaller tool radii. For convex curvature radii the roller diameter has little impact exception possibly increasing the contact length due to the roller conformance. On concave features however the roller radius would be the same as the minimum radius that can be laid as long as the arc length was no more than 180°. For the fibre tow steering limits, the curvature by which tows must turn is also limited by the width of the tow (usually ¼" or 6.35mm) and the flexural properties of the tow. Studies have been undertaken to determine the minimum steering radius of 1/4" tows, this is usually in the order of 500-600mm [105].

Kim, Potter and Weaver [105] developed a new technique of induced fibre shearing within the tow in order to reduce the minimum steering radius. The results were successful in demonstrating the potential to reduce the steering radius down to approximately 30mm. This was achieved by removing the compaction roller and using a compaction shoe that 'slide' over the tow causing compacting but allowed for differential speeds across the tow width and therefore allowing the shear to occur. The width of the tow, the ability for the fibres to shear (ensuring fibres are either heated or

dry to allow binder or resin flow) was important to reducing the steering radius without inducing wrinkling or gaps [105].

The compaction roller width and the number of tows being laid side by side on the tow band both drives the production capacity of the system but also the complexity of parts that can be produced. A wider roller and more tows means greater throughput but reduced flexibility for complex geometries.

3.3.4.2 Benchmarking Study

For the benchmarking study design variables measurements were collected for the six most common state-of-the-art placement heads. Photographs were collected from public sources and using the ImageJ image analysis software and reference scale lengths contained at the same depth within the photo field to collect measurements. An example of the photographic analysis is shown in Figure 28 [104].

Figure 28 – Design variable benchmark analysis

Because the measurements were taken using photographs and scaling techniques the tolerances on all measurements should be considered very large. The results give only an indication of the access that current systems have and allow for a design

comparison to be made. The results of the photographic studies are summarised in Table 7. Included in Table 7 is the design optimisation result for the comparison study.

Table 7 – Design variable benchmarking data

Variable	Units	Automated Dynamics Corporation	Coriolis Composites	ElectroImpact	Ingersoll	MAG Cincinnati	MTorres	Optimised UVAFP head
Model		V5	Unknown	Unknown	Mongoose V1	Viper	Fiberlayup	
Image								
Image source		ADC Corporation	Coriolis Composites	Electroimpact	Ingersoll	Fives Machines	Google image search	
Head clearance, β_{head}	°	40	73	72	73	60	60	30
Head width, W	mm	485	335	425	250	262.5	400	100
Head offset, O	mm	775	870	775	900	1500	1300	
Compaction Roller radius, r_{roller}	mm	25	37.5	25	55	50	60	75

The access limits of each benchmark system is shown below in Figure 29 plotting minimum radius against maximum arc length. The design with the most access is defined by the series closest to the upper left of the processing window. For future work, examination of a sample tool set for a representative structure and the reach and accessibility of each machine in 3D would be useful. It can be seen that from the data gathered the design with the least accessibility and the ability to produce the least complex parts is the ElectroImpact design [102]. This can be attributed to the width of the head design by incorporating the creel system within the placement head. While minimising travel paths of the tows and mitigating tension issues as well as allowing for quicker head changes the design configuration clearly limits the access of the system. An alternate design aiming for the same concept is the Ingersoll Mongoose head design with the vertically mounted creel system within the placement head. The Ingersoll system however is limited by its poor clearance angle due to tow guide equipment that is situated just prior and post the consolidation area of the compaction roller. Of all the design the Automate Dynamics Corporation V5 head design shows the greatest accessibility due to its steep clearance angle and small compaction roller radius.
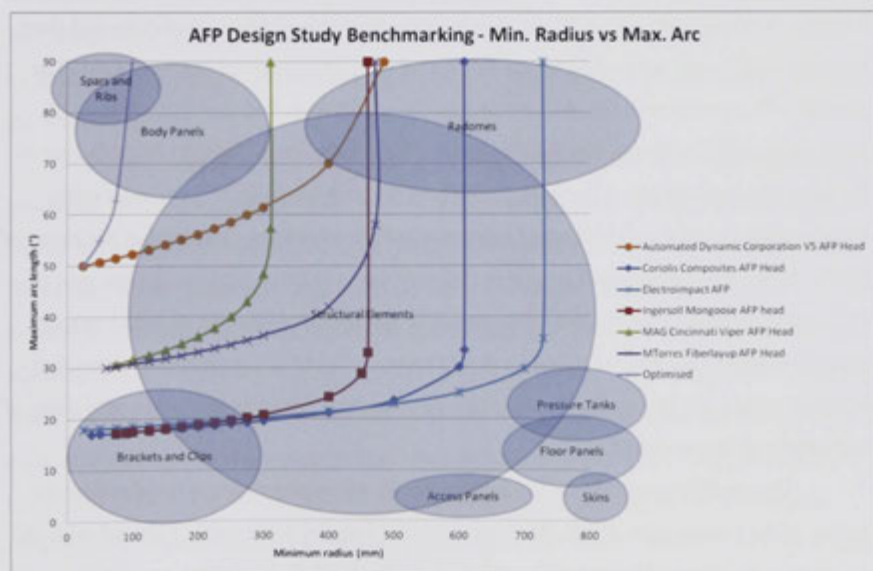
Figure 29 – Head design geometric study benchmarking results

Within the target industries for UVAFP (automotive and aerospace) part scales vary significantly, from wing skins and fuselage sections with single dimensions over 5m to brackets and clips that have single dimensions no bigger than 100mm. In qualitative analysis AFP systems can currently produce parts with dimensions both less than and greater than 2m and components with geodesic and non-geodesic fibre paths. The differentiating factor restricting manufacture of all components is the minimum radii and the arc length of said radii. The range of parts used in the two target industries (aerospace and automotive), are shown within Figure 29. These are spars and ribs for aerospace, body panels for automotive, radomes for aerospace, structural elements for both industries, brackets and clips for both industries, access panels for aerospace, skins for aerospace, floor pans and panels for both industries, and pressure tanks. Part definition regions that either overlap or are under the AFP system design limits are producible using the system. Those not overlapped or above the design process limit cannot be produced. The significance of this finding is that most complex parts cannot be produced by current AFP systems and also proportionately only half of the current structural elements designed using composite can also be produced using current AFP systems. In some instances AFP strategies involve a combination of placement and forming. Starting with a "2.5D" placement geometry with simple complexity and then forming using matched tooling to the full complexity of the actual 3D form [10]. The current AFP system with the greatest accessibility and therefore the widest range of producible parts is the Automated Dynamics Corporation unit. This is primarily due to the high clearance angle of the unit's design which differentiates it from most other commercially available AFP systems. Most other systems have clearance in the range of 60-75° while the Automated Dynamics Corporation unit had a measured clearance of 40°, approximately 30% greater clearance. The significant influence of the clearance angle is demonstrated by the fact that the MTorres and MAG Cincinnati systems that have 60° clearance angles are the next two systems in order of access and complexity of parts that can be produced.

The smallest possible radius achievable for all systems was determined by the radius of the compaction roller. At this radius, arc lengths were vastly reduced with the smallest radius being 25mm and the greatest arc length 50°, again this result was achieved by the Automated Dynamics Corporation system due to its small roller radius

and higher clearance. The MAG Cincinnati system was however able to achieve a full 90° arc length for a smaller radius than the Automated Dynamics Corporation system, due to its narrower head width. This occurred at a minimum radius of 311.47mm.

Using the design optimised design variables all composite target parts currently producible by the benchmarks were shown to be producible even those structural elements only partially producible by the benchmarks. Furthermore, certain body panels and spars and ribs with minimum radii above 100mm were also shown to be producible. This outcome confirming the hypothesis that a smaller and optimised design for the placement head would allow for more complex parts to be produced as defined by minimum radii and maximum arc length.

3.3.5 Experiment Conclusion

The reach and access of AFP placement head determines the limits of the part complexity that can be laid up by AFP. This study defined part complexity by minimum radii (concave) and arc length. The results showed more complex shapes can be laid up with optimisation of the placement head design, this makes the technology more accessible and more versatile. By increasing the access of AFP systems, the flexibility and complexity of the parts that can be made using AFP technology will be increased expanding the number of AFP producible parts and increasing utilisation and access of the technology.

The challenges in AFP design are primarily related to the size of the part to be produced, the part's geometry and the maximum allowable size of the placement head before the clearances required to avoid collisions limit the ability of the system to place fibres. Increased placement head size also limits the reach and access of the system, due to increases in weight and the minimum radii the tows can be laid onto. However larger placement heads generally have a greater lay-up rate (kg/hr) and have greater capacity requiring less spool changes and reefed downtime. As a consequence, the clearance of the placement head and ultimately the complexity of the parts that can be produced using AFP systems is determined by the assembly and packaging of the subsystems. Ideally, AFP systems should be designed to produce the widest variety of part geometry sizes and complexities. In practice, outside of small trade moulders, it is probably more appropriate that in a production environment, where a very limited number of different

products (often a single component type) will be made on an AFP, AFP should be optimised for just that specific application. A lack of customisation options for the AFP machine to the specific part being produced is a common issue. Understanding how to deliver this customisation rather than making a more generically capable AFP machine is an area for further research. By understanding what new components could be made using increasingly flexible systems it is assumed that the technology will become more attractive and viable to more industries and applications thus proliferating the use of composites in achieving weight reduction and thus meeting environmental emissions targets. Therefore, a compact and simplified end effector design is proposed for the UVAFP prototype. The philosophy used in the compact design would rely on the following requirements:

1. Reduced size of AFP head (by not using towpregs) for (i) no heat source for processing and (ii) no cooling in the creel or guide system for protecting;

2. Increased clearance angle of attack;

3. Thinner roller width;

4. Scalable design; and

5. Reduced cut distance.

The results determined that, in order to meet the specifications defined in the QFD process of the previous chapter, the design of the nip area would require clearance around the roller to allow diving into the concave feature. The arc length as a function of the minimum concave radius was also determined and the step wise degradation of the access but then gradual improvement as the radius increased.

In undertaking this experiment and investigating the results it is recommended that in future work the design analysis be expanded to investigate in a simulated environment an appropriate design envelope in 3D for a placement head capable of producing a representative complex 3D part. Likewise, the study should be extended to cover analysis based on actual 3D components of differing scales in order to assess the optimal solution in terms of production rate. This should consider larger placement heads capable of placing many tows and increasing production rate but possibly limiting component complexity versus smaller heads of lower production rates but capable of

producing more complex components. In examining the further applications for AFP the argument stands that AFP systems should be designed in such a way that allows them to produce the widest variety of part geometries, sizes and complexities. Such systems are unfortunately often characterised by high capital cost and a large factory footprint [34] with very low production rates. These systems are not configured for industries other than the aerospace industry where the drivers that determine production choices are quality, repeatability and traceability. In instances where speed and cost reduction are required different configurations are required [106]. The alternate argument presents that entirely flexible systems will never be the optimal configuration for production components. Instead, machines designed specifically for the geometry, size and complexity would perform better and achieve higher throughput and quality. This work has found that whether examining flexible generic systems, or a customised specific machine, miniaturisation of placement head design and increased clearance and degrees of freedom will improve the complexity of parts that can be produced.

The benefits of AFP technology are clear and industry's desire for such systems is evident in the increasing number of purchases. However, the limited types of components with simple geometries that can be produced using AFP is restricting further uptake of the technology in new industries and for new applications. Currently AFP machines are restricted due to the operational reach and access limits of the placement head design.

3.4   The Design of the UVAFP Prototype

The equivalent system architecture of the UVAFP system is shown in Figure 30 in comparison to the generic system shown in Figure 20. The architecture includes the additional sub-systems for in-situ UV curing, on-the-fly resin impregnation and integration with a 6 degree of freedom industrial robot. These subsystems require the UV light box and its control system, the resin spray system and the robot. The selection of each subsystem was based off of the system specification. The design challenge for the UVAFP system involved the compact and efficient packaging, integration and assembly of the subsystems as well as the control of devices simultaneously during placement in real time. The following section examines each sub system of the design.
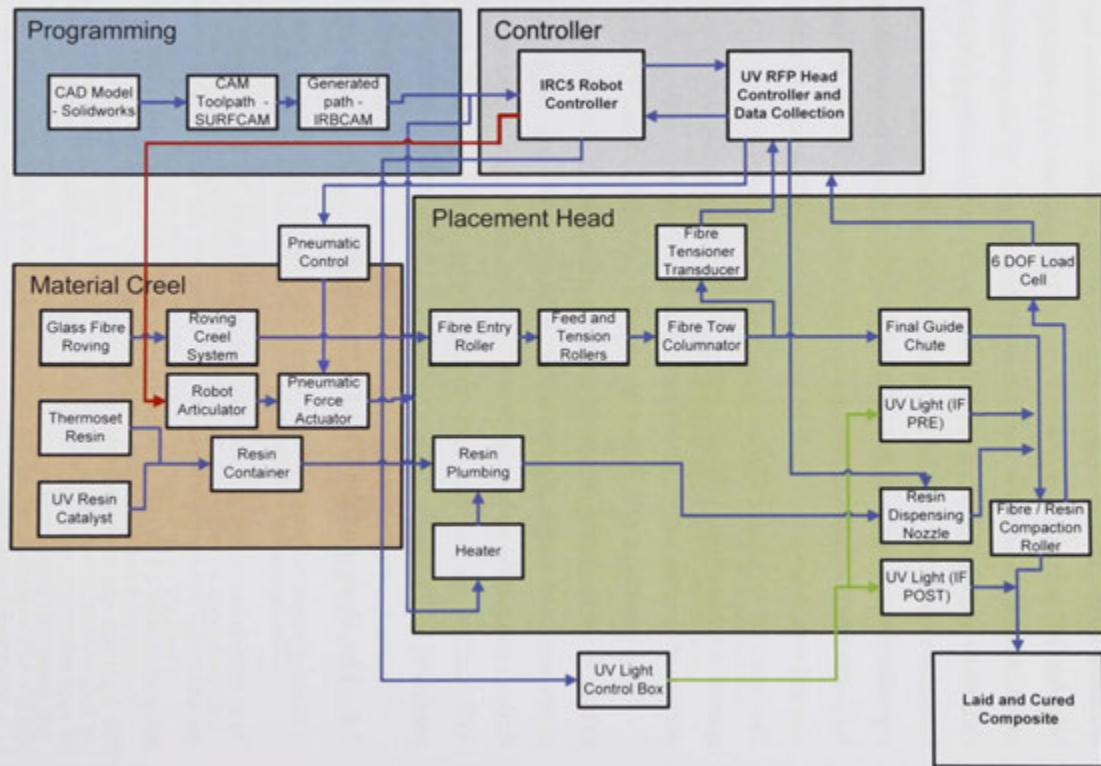
Figure 30 – The system architecture of the UVAFP prototype

In the UVAFP process, final part quality is dictated entirely within the single process step and in comparison to standard AFP systems includes the addition of the curing mechanism and the combining of the materials. The placement head is vital in both cases and is discussed below in section 3.4.1.

3.4.1 The Placement Head

The placement head sits at the end of the articulation device that moves the head through the programmed placement path. The primary functions of the AFP head are to:

1. Feed, collimate and control the tension of the fibre tows/tapes;
2. Control the temperature of the tow and the consequent rheology of the polymer matrix during placement;
3. Compact the tows (and matrix) onto the tool using a roller or other compaction device;
4. Effect cure or b-staging of the composite; and
5. Cut, clamp and restart the tows/tapes.

The design of most fibre placement heads takes on a V-shape with tangential feed of the fibre tow to the roller. Tows are often feed onto the roller from two different clearance planes, alternating the tows in each plane to create space for CCR devices to operate on each tow without collisions. This is shown in Figure 31 [47]. This design concept dominates fibre placement head design. The fibre approach path to the roller along the tangent angle must incorporate most of the primary systems within a very short distance. The guide chute must incorporate access to the tow for cutting, clamping and drive pulley restart rollers. The electro mechanical systems are predominantly servo-electrically driven or pneumatically driven. The feed angle is critical for access to the geometry of the tool and in this work referred to as the head clearance (on both sides of the placement head).

In some instances the feed of the tow may approach the compaction roller from a vertical tangent to allow the compaction roller to be placed on an additional rotation axis perpendicular to the roller axis. This is to allow for redirection of the roller for bidirectional lay-up, thus eliminating the need to reorient the entire placement head at the end of a placement path run and thus shortening overall placement times.
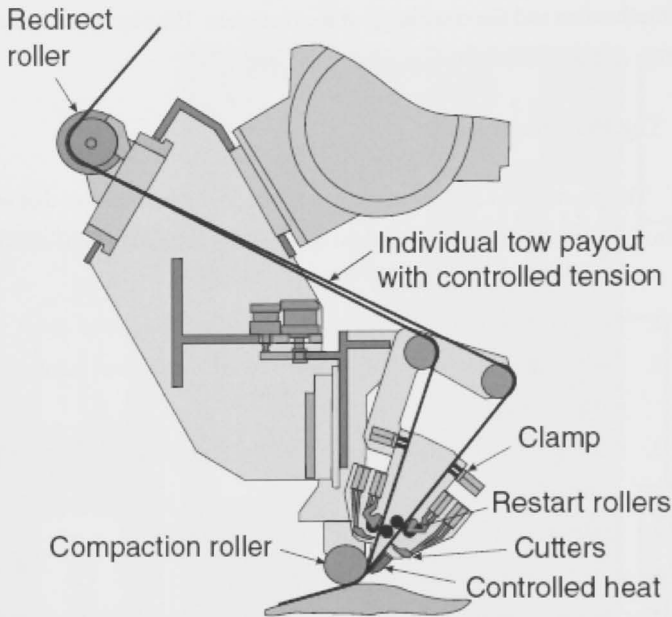
Figure 31 – A generic embodiment of an AFP placement head

The clearance angle and design of the UVAFP prototype was based upon results of a design study experiment detailed in section 3.3. With a tangential fibre approach for only 1 tow no second tangent plane was necessary, however all of the sub system elements were incorporated as well as additional features to standard fibre placement systems, namely the UV light curing and the resin dispensing spray nozzle.

Automated fibre placement heads come in a variety of sizes from small systems laying only 1 tow at a time [107] to large scale industrial units that can lay-up to 32 collimated tows simultaneously [92]. AFP can be scaled to produce large composite components with great accuracy [108]. Conversely, while AFP systems can also be scaled to produce small size components with lower throughput [109] functional packaging limits mean that most AFP systems currently have limited clearance for quite large minimum concave tool radii. Abdalla et al., [110] developed a low cost FW machine for experimental use and highlighted the need for cheaper, smaller, scaled

machines in order to easily undertake experiments as well as manufacture more complex components. Reducing the size of the AFP placement head according to a scale that matches the part would not only increase the accessibility of AFP systems but could also reduce the cost. An indirect benefit of this could be improved access to the technology for smaller enterprises and research institutions thus propagating the technology and its development. Currently, research institutions such as universities use scaled down versions of commercial systems [111] that have a smaller footprint and less throughput capacity. This allows research to be undertaken more freely and modification and development to be made rapidly, accelerating research outcomes and providing the possibility for small-scale technology demonstrations. With such reductions in cost and scale and increased dexterity and flexibility, AFP will be a more accessible and be able to manufacture a wider variety of parts.

3.5   The UVAFP Placement Head Design

Design concepts for the UVAFP placement head began with schematics and sketches. The first concepts for the placement head focused specifically on the in-situ UV curing and on-the-fly resin impregnation. Figure 32 [63] shows the basic 2D concept proposal [63] and the differing resin dispensing locations and the UV curing locations that could be applied to the UVAFP technology.
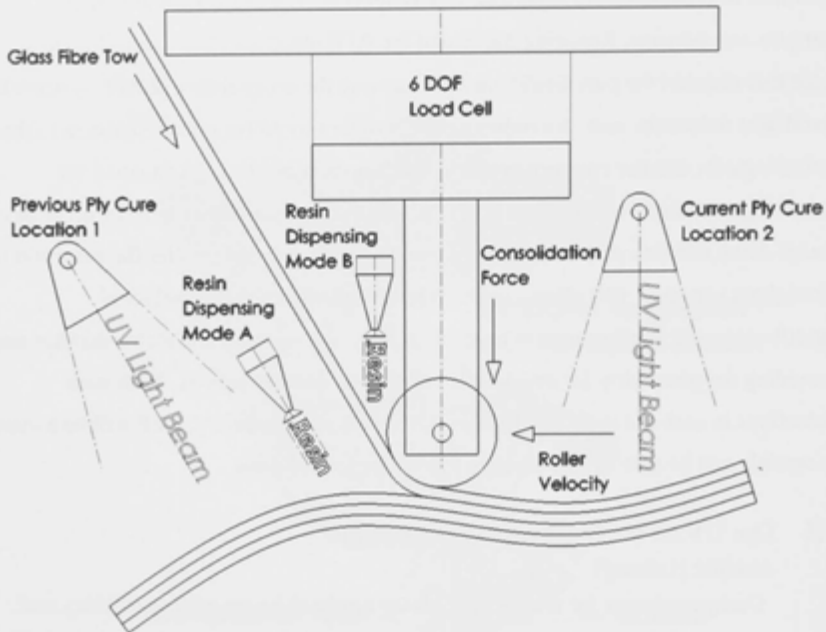
Figure 32 – UV RFP Model including both resin dispensing and UV locations

This design concept was used as the first conceptual steps towards the prototype design. The locations of the resin delivery and the UV curing were particularly important as not only were they independent process variables but also defined the work package envelope. The prototype was designed as a flexible system with adjustable mounts for UV lights both prior to the placement roller and preceding the placement roller. Likewise resin application mounts were made flexible and with multiple positions, including application directly onto the tool application or onto the fibre tow. The mounting of the UV system was also made flexible with positions both before and after the roller the prototype allowed for the possibility for curing to be initiated on the previous ply, while following the roller the laid ply could be cured. Likewise by spraying resin onto the tool, the tow was placed into the resin, with wet-out was aided by capillary effect. On the other hand by spraying onto the resin onto the fibre the resin was forced into the tow by the spraying pressures and velocities as well as the capillary effect acting to help the resin track along the fibre length. The placement head for the UVAFP prototype undertook all the basic functions of other AFP systems, however in

accordance with the specification included a number of extra features. The placement head included:

- The load cell and mounting plate;
- The compaction cylinder;
- The placement assembly, including the compaction roller;
- The UV in-situ spot curing orifice; and
- The resin spray nozzle and head, and piping.

The construction of all assemblies was CNC machined 6061-T6 Aluminium alloy billet and plate with global tolerances according to specified decimal places. For dimensions specified to 2 decimal places a tolerance of ±0.25mm was defined. For dimensions specified to 1 decimal place a tolerance of ±0.05mm was defined. Finally for no decimal places ±0.1mm was defined. Angular dimensions were tolerance to 0.1 degrees. All designs were analysed using static finite element analysis studies and optimised for weight saving and stiffness.

The placement head final design section is shown in Figure 33. The design incorporated all elements of the process map and design concepts in a compact and simple assembly that allowed for easy maintenance, the easy addition of mounts and extra sensors and precise control and measurement of process parameters.
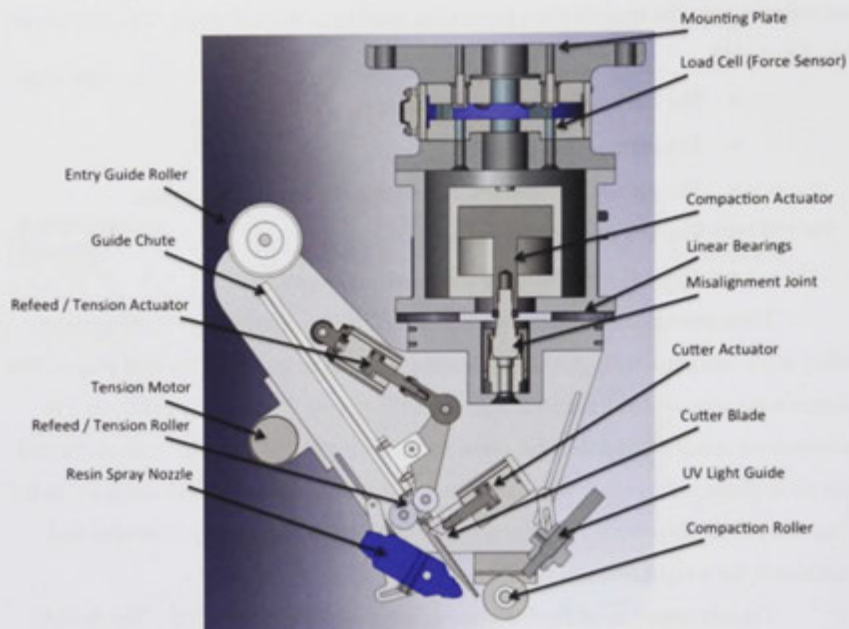
Figure 33 – The UVAFP prototype placement head cross section

The prototype places single tows onto the tool while resin is sprayed directly onto the tool or tow. The tow is compacted and consolidated with the resin using the compaction roller and force control system and then cured using UV light supplied from a spot curing system delivered by a liquid filled light guide. The system is capable of cutting the tow, re-feeding for the start, and end of placement paths, and can control the tension of the tow during placement. Below the mounting platform sat the placement head assembly containing the fibre tow guides, the CCR, the UV curing system, the resin spraying system and the compaction roller. The following sections discuss the CCR system, the curing system, the resin impregnation system and the compaction system in detail.

3.6 The Cut, Clamp and Restart System

The cut, clamp and restart (CCR) system is an integral part of an AFP placement head. It is found just prior to the nip point where the tows are collimated into a single band and pressed onto the tool/mould by a compaction roller. The CCR mechanism

must accommodate a large number of mechanisms into a streamlined and accurate unit. The positional accuracy of any cut and the control of the gap are crucial to achieving quality parts, reducing scrap and ensuring repeatability. The CCR must also handle these requirements at high speeds with tight tolerances in order to ensure production rate is not impacted adversely. These tolerances and lap gap control are the crucial elements that define, in part, the complexity of the CCR and ultimately determine the tool geometry that can be used and how fast the placement can be made. Most AFP systems operate controls on each individual tow, allowing for differing feed rates of the individual tows, to account for the different placement speeds necessary during path placement when steering tows around a radii (tow at the outside of the radii will be laying faster than inside tow). This is referred to as individual tow payout [112] and minimises wrinkling and fibre buckling around the radii as well as allowing for the width of the collimated tow band to be changed while placement head movement. This is possible because each tow has an individual cutting blade, tensioning system and restart feed mechanism. This also minimises waste and ensures the collimated band follows, as close as possible to the component edge.

The primary mechanical elements within the CCR system are an entry guide mechanism, often a roller (Figure 34, left hand edge of cross section [92]), the entry port to the guide chute, a clamping roller device to stop and hold the tow during cutting and non-feeding (Figure 34, labels 32 and 39), a feed roller system for re-feeding the fibre after cutting down to the compaction roller and controlling tension (Figure 34, labels 21 and 34), the cutting blades (Figure 34, label 18) and the heating/cooling system for controlling tack through the CCR system and aiding wet-out at the exit of the CCR.
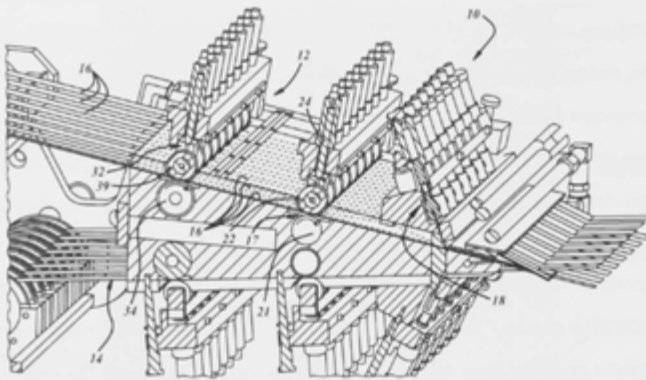
Figure 34 – CCR system within a fibre placement system cross section

Steiner, et al. [112] designed a compact cutter and re-feed mechanism, as well as changing the construction to reduce the critical distance between the roller and the articulation device's final axis, known as the head offset, and the minimum cutting distance, the distance the cutting blade is from the compaction roller. Steiner's design was significantly smaller than traditional AFP units, because it was built from an integrated manifold block, with actuators and feed rollers mounted within the solid design. This construction ultimately reduced the cost and increased the flexibility of the system.

De Vlieg [25] examined the issues with high placement speeds in an ElectroImpact AFP system with the intention to achieve placement speeds over 50 metres/minute. The focal areas of the research included the mechanics and actuation of the cutting and adding tows at high speed and the processing speed and timing of the cutting and re-adding of tows, the accuracy of the servo controls, servo lag and mould following errors in the programming system. At these high speeds significant issues with timing and on-the-fly real time control were shown to be critical for accurate lay-up. To address these issues, a novel cutter design was implemented with a reversed facing shear plane to conventional cutters. Development of new mechanics for the actuation of the cutting and tow adding systems, including the roller conformance, control systems, servo systems and programming were undertaken. Different cutting mechanisms were assessed such as rotary cutters, guillotine cutters and the timing of

their actuation, the control system for the device and the actuators exceeded the average CNC scan rate (4ms) using real time high speed controllers. The design of the cutter blade clamped down on the tow, the tow did not have to be stopped because the moving force actually pulled the blade closer to its opposing shear plane making the cutter more effective. The design also included a flexible material as the bottom mandrel for the guillotine to penetrate to. This meant that the guillotine cutter could completely penetrate the entire tow, have the bottom mandrel flex as it was hit and then have it return to its position guiding the tow straight through the guide chute so that there was no edge for the tow to be caught against. The system effectively allowed the speed of the fibre placement head to be maintained while cutting occurred, minimising stop time [25].

One of the crucial debates of today is whether large general purpose fibre placement machines and tape layers are the panacea for the aerospace industry or whether part-purposed machines should be built instead, utilizing components and features learned from fibre placement and tape placement, but arranged to make only one part, more quickly, with less investment, and with less real estate committed. As proposed by Hulcher [83] by modifying the material and laminate construction part properties can be improved. Modification of general AFP systems to include features such as a spraying system or coating system combines the flexibility of AFP with product/material specific advantages distinct from standard AFP solutions. Likewise, Grenoble [67] suggested addition of a secondary roller and heater to improve TP consolidation of certain materials that require a larger processing window. Again, as previously discussed the use of AFP for dry fibre preforms and machines designed specifically for this purpose are currently very much underutilised and under developed. Such modifications to handle dry fibres would benefit the process significantly.

3.6.1 The UVAFP CCR System

The intricate controls and mechanisms, for cut, clamp and restart are fixed to a single tow width in order to allow for the collimation of tows. A straight tangent design approaching the compaction roller nip location simplifies the design but its size is driven by the operations that must be undertaken as the tow approaches the nip point. Therefore by reducing the number of guide chute or CCR operations the head

clearances are increased. The largest and most cumbersome of systems usually required in the CCR is the heating and cooling systems to protect the towpregs and keep them within their operating ranges. In addition large ducting systems for convective heating and cooling or conductive heating systems requiring large surface areas with large power electronics elements are needed adding significant volume, mass and complexity to the placement head. By removing the need to heat or cool towpregs a significant saving in the head size and particularly clearance just prior to placement can be achieved, ultimately leading to greater access.
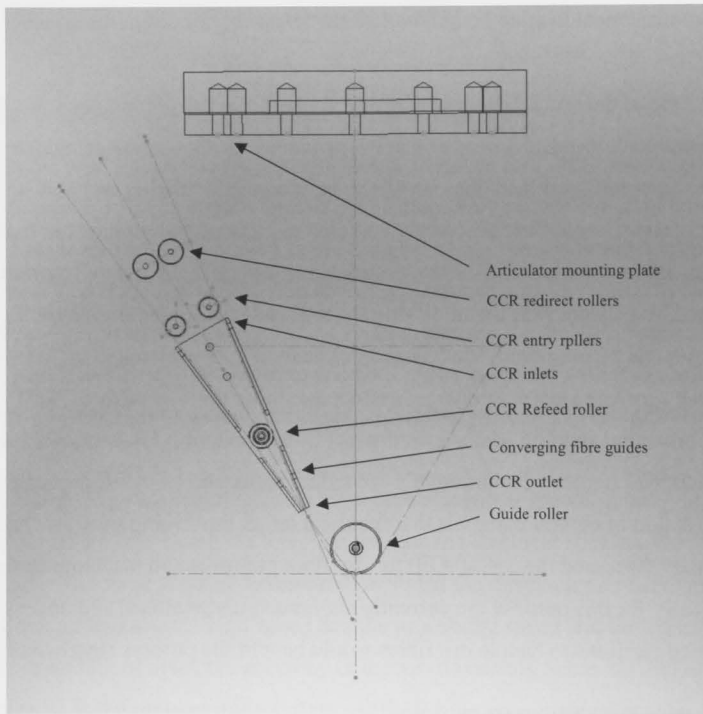
Figure 35 – Fibre guide, compaction roller convergence and robot wrist noting height of end-effector

Figure 35 shows one of the initial design sketches for the compaction roller system and the supplying CCR system. The articulator wrist is also identified at the top of the figure. The figure shows the considerations made for the clearance angle and the head offset distance in order to maximise reach and access for the lay-up of complex

components. The tangent lines are highlighted and the slight divergence of the converging tows onto the compaction roller. The feed roller is identified within the triangular section guide chute as well as the entry and guide rollers. For the prototype the decision was finally made to allow for collimation and handle multiple tows but not build with. Therefore the triangular section CCR system was removed and a simple straight channel guide was used.

The CCR unit for the UVAFP prototype was a simple design incorporating learning from the literature. The fibre was contained in a guide chute channel with a simple entry guide roller. Along the guide chute were machined access points where firstly the feed roller, driven by a small DC motor and gearbox controlled the tension and re-fed the tow to the roller. This feed roller only acted upon the tow when a small pneumatic cylinder actuated a second free spinning roller onto the tow clamping the tow between the two rollers. Following the feed and tension roller was a guillotine style cutting blade actuated again by a small pneumatic cylinder. The guillotine edge was made from hardened steel and mounted on two miniature linear bearings. To reduce the risk of the re-feeding of the tow getting caught at the entrance to the guillotine the guillotine was mounted in the other direction to that recommended by De Vlieg [25]. This was because if the guillotine blade was before the shear edge there was the possibility the tow could get caught on the shear edge. Following the guillotine cutter was a run off guide that feed the tow at a tangent to the roller. A section of the design is shown in Figure 33.

3.7 Compaction and Consolidation Devices

As discussed in previous sections, another area requiring development is in the design and choice of the feed and compaction mechanisms, such as rollers. While the current benchmark design of a compliant roller is widespread across most AFP research little operational research is available in relation to roller compliance and its effect on pressure uniformity. Fibre buckling and fracture due to excessive distortion in tight radii and feed mechanism efficiency to name a few. Surely OEM's and vendors of AFP systems are investing a great deal in this area that directly determines quality but it is clear that published work is very limited. With the introduction of possible other fibres such as basalt, organics and even nano-particles the transient and local application

nature of AFP presents unique load cases that have not been modelled at a micro level. This in turn should affect design and the embodiments of AFP systems that will become available in the future.

Various approaches have been taken for compacting and consolidating the tow and resin onto the tool. The most common is a rigid steel roller. Other possibilities include a conformable polymer roller; segmented rigid rollers for each tow and even compaction slide mechanisms known as 'compaction shoes'. A compaction shoe design does not rotate like rollers but uses a solid sliding compactor that slides over the tool/mould surface. Conformable compaction mechanisms, whether as one piece or segmented, allow greater adhesion and conformity to the tool and have been found to offer significant advantages in their ability to consolidate the tows and increase part quality [50][113][114][115]. Numerous patents exist protecting this technology [70], and a number of studies have been undertaken to assess the control of the temperature of the conformable roller and how this effects tow buckling, alignment and adhesion.

A necessary mechanism for compaction to occur and be maintained is tension in the tow. The design and control of tension systems internal to fibre placement heads has also been the focus of a number of papers [116]. Tension is most often controlled by servo driven motors and combined feed systems within the CCR and creel systems. With the reduction in the size of servo motors over recent years, the size of AFP heads has also decreased allowing for greater access of the placement head.

Compaction force is most commonly actuated via a pneumatic piston located within the fibre placement system that either sits between the gantry and the placement head entirely, or between the placement head and the compaction roller itself. The compaction roller runs immediately after the tows, as they are exposed to heat, which liquefies the resin and induces tack during consolidation. The compaction is done in a particular manner so as to control fibre path and orientation in accordance with the digital model of the internal structure of the part. Rollers are often conformable so as to maintain contact with non-geodesic surfaces to increase adherence and remove trapped air in concave features. A large amount of research has been undertaken looking at how to regulate uniform pressure on each tow across the collimated width when a conformable roller is used [32].

Conformability of the compaction device allows AFP machines to lay tows on part moulds that contain surfaces of non-geodesic or double curvature [57], while maintaining constant compaction force. In 1991, Enders [64] examined and highlighted functional features of the Cincinnati Milacron FPX system. This unit included bi-directional tensioners, a conformable compaction roller with the ability to lay on curvatures with radii as small as 152 mm, resin tack control, servo controlled tension to eliminate tow twisting, individual tow payout and online cut, clamp and restart on-the-fly. Enders identified the most critical process parameters that effected quality and the speed of the process, including resin tack, tow width, spooling tension, number of tow feeds, heating mechanisms, compaction force [64] as part of necessary qualifications for the aerospace industry.

The concept of using a segmented shoe as the consolidation device instead of a roller was proposed by Lamontia, et. al. [113][117]. The goal of the NASA Phase II Small Business Innovation Research (SBIR) program was to develop and prove out a number of innovative conformable compactors for assembly into deposition heads. The final outcome for the project incorporated a segmented compaction shoe containing three separate modules that drag over the surface and compact the fibre tow band to the mould. The modules act as distinct thermal zones with different temperatures and pressures causing a unique thermal profile during dynamic placement. PEEK thermoplastic composite samples with undulating geometry, including pad ups and pad downs were produced and showed good microstructure and reduced void content. The study identified further areas for research in optimising for throughput and compactor design as well as limits in the conformability to the surface of a shoe device. Issues with using conductive heating as a heat source for curing because of the thermal lag and the risk of overheating, possibly causing thermal degradation were identified despite achieving proof of the concept. The study suggested that there is a direct relationship between increased compaction pressure and reduced void content. Therefore, the system was designed able to achieve normal compaction forces reaching up to 2800N [113][117].

3.7.1 The UVAFP Compaction and Consolidation System

The UVAFP prototype was designed using a compaction roller mechanism. The design allowed for the easy and quick change of the roller which meant that in experimental studies the material, the diameter (while maintaining the tangent fibre tow feed) and if desired the use of a segmented rollers could be easily tested. This was achieved by using a quick release axle system (similar to that used on a bicycle wheel) and an adjustable axis position easily changed by using spacer blocks. The roller first chosen and used for all the studies in this thesis was a PTFE coated steel sealed ball bearing roller. The PTFE coating was chosen to aid in the cleaning and removal of resin and to try and minimise sticking of the fibres to the roller instead of the tool. The PTFE also had some compliance, which provided improved compaction of the tow and resin.

The design of the load cell and mounting plate was a simple mounting plate, to load cell to compaction cylinder mounting plate assembly. The loadcell was a JR3 45E15 6 degree load cell, capable of measuring loads up to 1000N for F_x and F_y and 2000N for F_z, with F_z as the normal axes to the compaction roller, that is the compression force. Moment loads, for each axes was limited to 125 Nm. The mounting of the load cell was designed according to ISO 9409-1 63mm bolt pattern, allowing for easy mounting.

45E15A4-U760-A
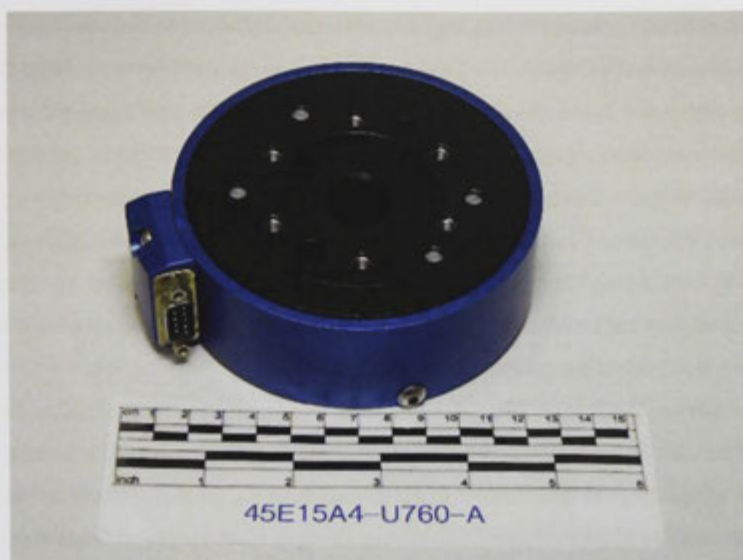
Figure 36 – The JR3 45E15A4 6 degree of freedom load cell

The compaction cylinder assembly provided an additional vertical degree of freedom to the placement head and robot system. This assembly comprised of the compaction cylinder itself, a Festo high load, short stroke pneumatic cylinder, model ADN-63-25-A-P-A, connected to a proportional pneumatic regulator, model VPPM-6L-L-1-G18-0L6H-V1N by Festo. The compaction cylinder was a large bore short stroke unit designed for high pressures and high speeds. The 4 linear bearings were included to ensure linear motion and maintained stiffness between the robot and placement assembly and inhibit rotation of twisting. The 4 linear bearings linked the cylinder housing to a mounting platform forming the interface to the placement assembly was moved by the compaction cylinder. The connection of the mounting platform to the cylinder end was coupled with a misalignment joint to compensate for any possible misalignment in the assemblies. The mounting platform incorporated a large number of mounting holes for auxiliary systems such as the pneumatic actuators.

3.8 The Fibre and Resin Creel System

The material supply creel system (the creel) incorporates both the material supply and spooling source, The creel can either be mounted externally and separate

from the placement head [97], mounted integral to the placement head or within the articulation system [49][98]. The creel is also often responsible for controlling the tension in the tow as it is fed to the placement head as well as conditioning the tows for adhesion and consolidation. Tension is measured through the tow guide and can be controlled to a set value by resistive devices that brake or clamp the feeding tow. Alternatively, the tow can be actively fed to minimise tension and residual stress in the tow [93]. Controlling tension is crucial to the success of any fibre placement because it ensures conformance and uniform lay-up, as well as controlling tow spread and any induced localised stresses in the final laminate.

Tow guides feed the fibre tows from the creel system to the placement head. There are various types of tow guide mechanisms being implemented. In some systems, a guide chute made from a flexible material runs from the creel system to the placement head through an umbilical tube [96]. In other designs, tows are pulled from the creel through guide hoops or rollers that direct the tow to the placement head during movement of the head. In these designs the tows maintain their direction and movement through tension and are generally exposed and uncovered allowing access for re-feeding (see the Torresfiberlayup system by MTorres in Figure 13).

AFP systems most often use pre-impregnated fibre reinforced composites of either thermoset (TS) or thermoplastic (TP) matrix. Thermoset resins are often still partially reactive at room temperature; therefore creel systems must control the temperature and humidity. Temperature controls the tack of the resin and therefore affects considerations such as clogging, resin build up and sticking. To maintain shelf life, the air needs to be filtered for particulate matter to inhibit foreign object damage prior to use. Most prepregs are supplied with separation film on the back of the tow to stop bonding or sticking between layers. Therefore many AFP systems include hefty refrigerated creel systems [97] as well as heating systems and consumable uptake systems to capture release films. Thermoplastic prepregs require less control and protection at ambient conditions due to their inert nature. During processing they require accurate control of temperature, time and pressure within the guide system to ensure flexibility of the tow through the feed mechanisms and during articulation of the placement head.

While fibre tows have high flexural yield strength, they can be susceptible to shear, compression and fracture causing them to be fragile and prone to breaking. 'Stringers' are individual filaments that have broken; these can cause blockages and further breakages if not managed. Placement head feed systems must the tows from breakage and stringing as well as their environmental hygroscopic nature, therefore requiring temperature and humidity control. Both requirements are handled through encasement from the creel all the way to the placement head and smooth guide curves with low friction guide rollers and environmental conditioning. In-line inspection is often used to check the tow integrity and occurrence of stringers while tensiometers measure for breakage [118]. The requirement is amplified for the use of towpregs in order to protect the resin, controlling its rheology to ensure no adhesion or resin flow as well as protection from foreign object damage and resin build-up in the guide systems. All of these creel environmental control systems add to weight and bulk of the placement head.

3.8.1 The UVAFP Fibre and Resin Creel System

Tension is an important parameter in the AFP process to ensuring fibre direction, consolidation and to avoid lofting and wrinkling. The design of the tow creel supply must consider the changes in orientation, position and distance from the creel during placement and the impact this can have on tension. The tows being used for the UVAFP prototype were all supplied in a centre-pull roving (in excess of 20kg), it was evident early in the design process, that a centre pull offtake system inevitably induces a twist in the roving. It was therefore decided for simplicity, to place the material creel in a stationary location remote to the placement head. Tows were fed up to the head along the robot arm or suspended them to allow the free movement of the tow with twist to minimise its effect on layup quality and feeding directly to the placement head.

The creel design for the prototype consisted of a simple stand and guide hoop arrangement to direct the fibre tow from the roving up to the height of the robot arm in the correct orientation and allow free movement to remove twist. The orientation was ensured by using simple tension rollers that were acted upon by a small electro mechanical clutch that applied a broking force on the tow movement based on a specified speed of pull out using encoders in the rollers themselves. All guiding to the

placement head was done either using redirect rollers (steel or Teflon ball bearing rollers), and guide hoops made with Teflon sheaths. The design lends from chopper gun and filament winding systems that also use dry fibre and benefit from the stability of the material and lack of a need to store and handle the fibre tow in temperature and humidity controlled conditions like towpregs.

The resin feed system utilised pneumatic atomising spray technology for non-moving part delivery of resin at pressure. Resin was stored in a lightproof pressure pot with the photo initiator pre mixed into the liquid. The pressure pot had a 4 L capacity and sat clear for the system so that it was safely and easily accessible by the operator. The pressure pot feed resin to a spray nozzle mounting internal to the fibre placement head through PTFE lines that were easily cleanable and reusable or if clogged replaceable for future trials. The spraying system specification was developed according to the specification in Table 8. The system was designed using Spraying Systems Inc. components and Festo pneumatics. The spray gun was a Spraying Systems Inc. spray nozzle specified as a small JJAU model.

Table 8 – Spray system specification

Operating parameters for 1 nozzle	Minimum	Maximum
Total Spray width	6mm	7mm
Resin pressure	30 kPa	100 kPa
Atomizing air pressure	30 kPa	100 kPa
Atomizing air flow	10 Nl/min	25 Nl/min
Resin Flow rate		6L/hr
Resin Temperature	10 °C	30 °C
Resin viscosity	200 cPs	400 cPs
Resin density		1046 kg/m^3
Solvent resistance	Acetone	IPA
Pressure pot material	304SS	
Pressure pot volume	4L	
Fittings materials	brass	
Supply pressure	6bar	7bar
Supply air flow	400 Nl/min	675Nl/min

Supply quality	DIN ISO 8573-1	
Supply Solid content	Class 5	
Supply water content	Class 4*	
Supply Oil content	Class 5	
Operating temperatures	5°C	40°C
Operating humidity	45%RH	90%RH
Electrical supply	24Vdc	

3.9   The Articulation System

The manipulation of the AFP head is handled either by a gantry system or industrial robot with up to 6 axes. Gantry systems are the most common articulation devices used in AFP and can either be vertical (as shown in Figure 37) or horizontal (as shown in Figure 17). The gantry system must move the placement head through the programmed placement path, ensuring placement head and tool relations. The gantry system must also provide a rigid position reference so that the placement head can apply the compaction force required to consolidate the tow and resin.

Gantry systems have a large work area and footprint and are suited to the production of large components and where high loads are experienced (for example when the creel system is contained in the placement head and carries a large weight. They have seen use as the articulation system primarily in the production of large aerospace structures and even in wind energy structures. Such scale of machinery requires high tolerances over large distances, which increase the complexity in maintaining accuracy, and adds considerable cost to the equipment as well as its ongoing upkeep. Furthermore, due to their size, gantry systems often require foundation works or significant building works to accommodate the super structure.
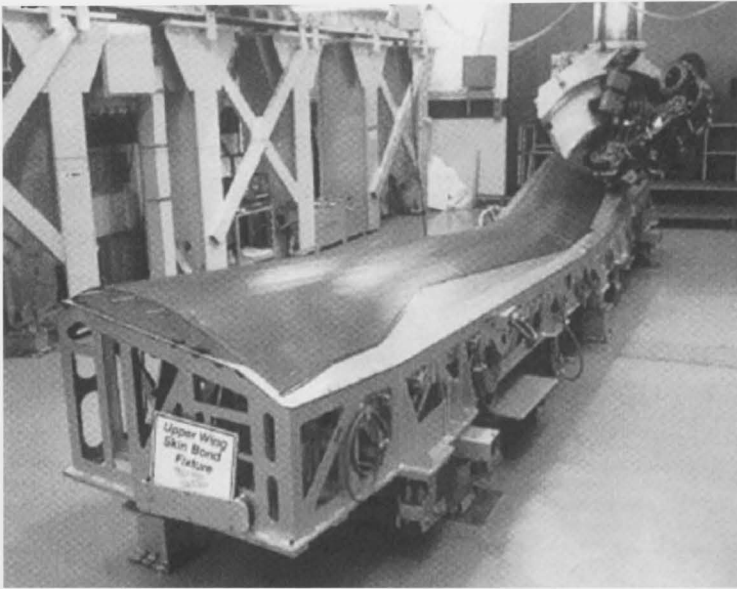
Figure 37 – Production of the V-22 Upper wing Skin-using Fibre Placement Technology

For example, the production AFP system shown in Figure 38 [119]. Figure 38 is a MAG Cincinnati system used for producing FA -18 E/F Super Hornet fuselage skins by Northrop Grumman Corporation [48].
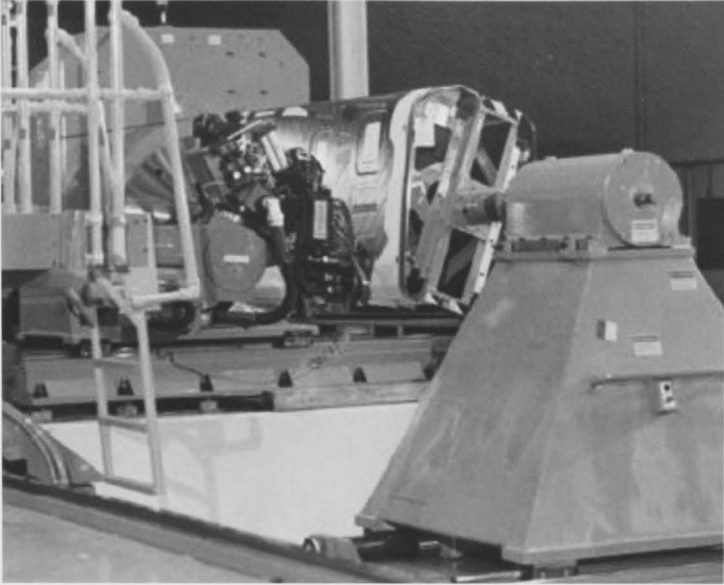
Figure 38 – Fibre Placement of the Northrop Grumman F/A-18 E/F Fuselage Skin

Alternatively, industrial robots articulation setups offer a more economic, smaller footprint and higher flexibility in the kinematics (commonly 6 degrees of freedom). Traditionally utilised for point to point, pick and place and welding applications, industrial robots are now seeing use in path critical applications such as AFP. Industrial robots also offer the added benefit of reduced size and increased degrees of freedom. While robots cannot often support the same loads as a gantry system they are capable of supporting loads in the ranges required for AFP – primarily the compaction force. The high degree of freedom of industrial robots and the relatively small arm and interface to the placement head improves the reach and access of the placement head and therefore are well suited to smaller, more complex parts with tight geometries. Several approaches have been used to investigate the possibility of applying AFP as a general purpose process, with generic machinery. Most of these studies focus on the use of anthropomorphic robots installation [120] adding degrees of freedom, reducing cost and increasing reach and access. Recent AFP installations for research and low volume production such as at NASA Langley [121] and in The Automated Composite Manufacturing Technology (ACM) Centre at the National Aerospace Laboratory NLR, Netherlands [122] and the Fraunhofer, Functionally Integrated Lightweight Structures

(FIL) Coriolis Composites AFP installation have taken advantage of industrial robots with for the articulation of the placement system.

AFP articulation systems can, and are often, combined with an additional external axis, either rotary or linear, which increases the reach and coverage of the articulation system and allows a work-cell size tailorable to the part [123]. With more axes comes the potential for greater placement acceleration and deceleration speeds by using axes in opposition to each other and not restricting the performance to the maximum capability of just one axis motor.

3.9.1　The UVAFP Articulation System

At the time of the commencement of this thesis, The Australian National University College of Engineering and Computer Science had been awarded an Australian government Large Equipment Infrastructure Fund (LEIF) grant for the purchase of two ABB industrial robots. The robots were an IRB6600 series and IRB1600 series with a robot control system that incorporated the ABB Multimove feature for the simultaneous control of the robots and synchronised kinematic programming. The purpose of fund grant was to establish a flexible manufacturing workcell for research into novel manufacturing techniques. The larger of the two robots (the ABB IRB6600 robot) was chosen for the articulation and movement of the UVAFP prototype because it provided the most reach and working envelope and offered the force resistance and stiffness to counteract compaction loads being applied by the placement head onto the tool. The smaller IRB1600 robot was used for initial trials and proof of concept tests as shown in later chapters. This robot provided easier mounting of equipment while still controlling the path and speed of the end effector.

Therefore, the selection of robots for the UVAFP prototype was based on existing infrastructure and was designed around the functionality of these two robots.

An image of the robot workcell is shown in Figure 39. The design of the robotic research work-cell was established to maximise accuracy; maximise available work area; maximise effective collaborative work area of both robots and minimise overall footprint while maintaining maximum flexibility of the work-cell for all other operations to be performed with the robots besides fibre placement. A simulation model

of the workcell was developed in the ABB offline-programming environment, Robot Studio.

Figure 39 – The ABB IRB6600 and ABB IRB1600 robot workcell.

The load capacity of the IRB6600 robot was 175 kg, and the reach was nominally 2.55 metres. The workspace limits of the robot are shown in Figure 40. The accessible area is shown in blue and because of the continuous rotatable nature of the first axis (the base) the area can be revolved in 360°.
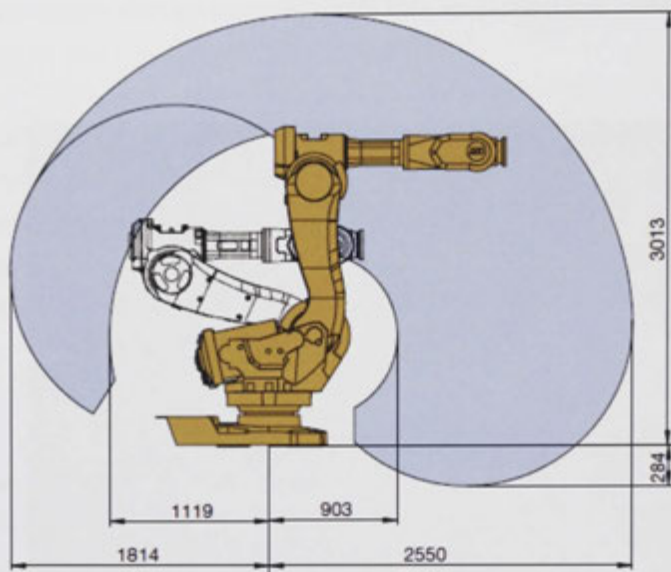
Figure 40 – IRB6600 work area and part size calculation

Prior to establishment of the UVAFP prototype design the suitability of the robots in terms of accuracy and reach had to be determined. An experiment examining accuracy for tool centre point (TCP) path following was undertaken as described in Section 3.10 [124] . The experiment was based on robotic milling but provided insight into the effect of specific process conditions related to the use of an anthropomorphic robot on accuracy. As with any structure moment forces become greater with distance. ABB provides design guides for end effector load limits, to ensure the robots can maintain path and point accuracy drive motors and the couplings.
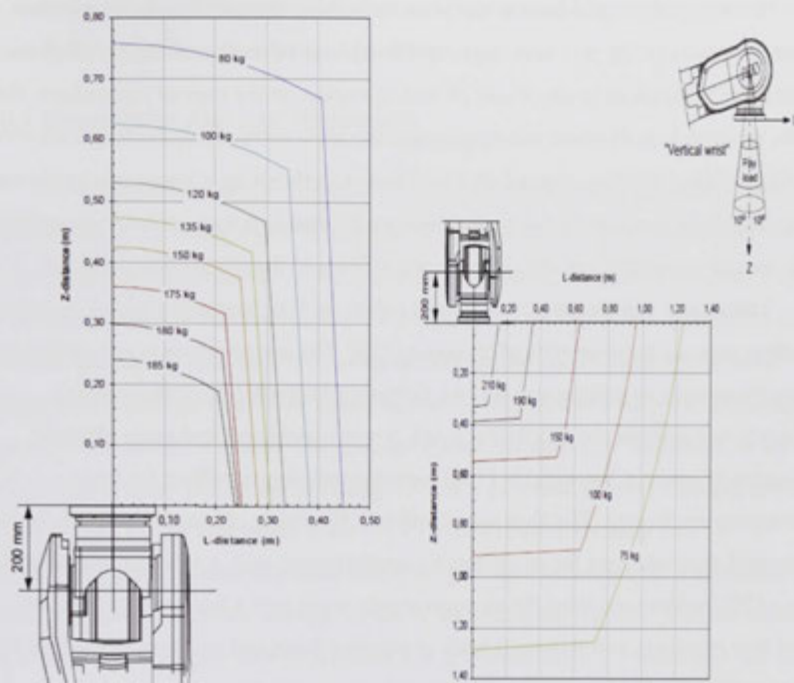
Figure 41 – Load limits for a horizontally alignment and vertical alignment of the 5th axis wrist

The orientation of the robot wrist (the 5th section counting from the base axis up the arm) has different load limits when used in different orientations. This is particularly important for AFP where the 5th axis acts to ensure normal perpendicular orientation of the placement head in relation to the tool surface. The horizontal and vertical limits are shown in Figure 41. In the vertical orientation, higher payload limits are shown indicating a stiffer configuration of the robot in this orientation and therefore a vertical mounting configuration was chosen for the UVAFP placement head.

3.10 Experiment 2: The Degrees of Freedom of AFP Articulation Systems and Reach

Note: This work was undertaken in conjunction with Jason Schiemer and Paul Compstom of the Australian National University, College of Engineering and Computer Science as part of a joint collaboration project.

Several studies have been undertaken examining the use of anthropomorphic industrial robots [120]. It is very important to understand the nature of the allocation of the degrees of freedom in any workcell and its impact on the type of components that can be produced. In filament winding system the most common embodiment involves a rotating mandrel (degree of freedom 1) working together with a linear axis guidance head (degree of freedom 2). Such machines are limited to convex circular structures with limited variability and the ability to steer fibres to the risk of fibre slippage.

Traditional applications of industrial robots such as spot welding and material handling account for over 80% of their use [125]. The use of robots in non-traditional applications such as milling and surface following technologies is an emerging approach that exploits the flexibility, reach, lower capital cost and more efficient utilisation of space. Chen and Hu [126] investigated robotic milling for rapid prototyping machining. The high speed and task flexibility offered by industrial robots were cited as advantages for small batch manufacturing, with a space saving of 40% over a CNC milling machine for an equivalently sized part. Chen and Hu [126] also noted that relatively soft materials such as polymer foam and wax are appropriate for robotic milling as the low stiffness due to linkages in the robot arms should have a smaller effect on accuracy.

To realise the potential of industrial robots, it is important to understand the effect these articulators and their particular multi axis arm design has on quality. Simoes et al. [127] used surface flatness to characterise milling accuracy of a plaster part milled with an articulated robot. A decrease in surface flatness was found to be linearly proportional to an increase in extension of the robot arm and the feed rate. The authors also concluded that the path error stated by the robot manufacturer is significantly more than the point error and a straight line could be expected to have a higher accuracy than a specific repeat point accuracy. The study did not analyse complex surfaces whereby on the one hand the 6 degrees of freedom of industrial robots could have an advantage for reach but on the other hand could reduce accuracy even further due to the complex kinematics of many axes simultaneously. A curved surface generated in a computer aided design (CAD) model will have multiple points; therefore the tool-path for the robot could include many small linear moves that may affect accuracy. This indicates

that curved surfaces could give a more thorough view on the limitations of robots for surface following task such as AFP and milling.

3.10.1 Experiment Aim and Hypothesis

This experiment aimed to examine the accuracy of industrial robots when used in complex surface following tasks. In this case, a milling process was used to test the effect of four major parameters on the accuracy of a robotically milled polymer foam part designed with a double curvature. It was hypothesised that by decreasing the arm extension, decreasing feed rate, increasing spindle speed, and decreasing the point filtering for the path generation of industrial robots, will increase the path following accuracy of the industrial robot. The milling experiment approach was taken for its applicability to many processes, including AFP as it provided a direct a measureable accuracy figure on the tool centre point (TCP) which is used for most robot programming tasks, particularly those concerning surface following. It is proposed that industrial robots are accurate enough for use as an articulator for AFP. Furthermore, following on from the previous experiment it is proposed that their flexibility and high degrees of freedom will increase reach and access for the production of complex shapes containing double curvature and tighter minimum radii. Four robot design and process parameters were tested, these were arm extension, feed rate, spindle speed and point filtering for path generation. The filtering is set during post-processing of the tool-path data file in a format that is readable by the robot controller. It is hypothesised that accuracy will decrease with increasing arm extension, feed rate and point filtering spacing. Spindle speed was varied to ascertain the specific machining effect on quality relating to resistance of the stock material to the TCP movement as it machining away product.

A design of experiments approach [128][129] was used to assess the parameter effects. The milling accuracy was characterised by mean error vector values, which were determined through comparison of a laser scanned image of the milled part with the CAD model file.

3.10.2 Experiment Apparatus

The robotic milling set-up is shown in Figure 42. The robot was an ABB IRB1600 with IRC5 controller. The robot has a reach of 1.45 m, payload capacity of 5kg and repeatability of +/- 0.05 mm. The maximum feed rate is 1000 mm/s. A 140W spindle from Dremel's 400 series [130] with a speed range of 5,000–33,000 rpm was mounted to the robot. The total mass of the adaptor and spindle was 1.578kg with a centre of gravity at the coordinates (0,-2.32,101.91) from the 0,0,0 of the robot wrist mounting face, thus giving a mass distance of 101.91mm.

Figure 42 – Robotic milling setup of the ABB IRB1600 with spindle and foam sample

The cutting tool was an 8 mm diameter high speed steel ball-mill with 14 flutes. The foam blocks for milling were adhered to a table placed directly in front of the robot. The sample was positioned with its origin at a Cartesian coordinate of $(x, 0, 200)$, with x being varied as the arm extension within the robot co-ordinate frame.

3.10.3 Experiment Method

3.10.3.1 Sample design

A sample with a double curvature was designed using computer aided design (CAD) software SolidWorks 2006, and is shown in Figure 43. The double curvature was created through the centre of the sample and surfaces were lofted out of this area symmetrically. The double curvature was used to test the ability of the robot to mill surfaces through simultaneous joint angle changes and to test the effect of the linearization of complex surfaces on accuracy. The sample was designed so that all surfaces could be milling during roughing and finishing stages. The polymer foam for the milling tests was 50 mm thick extruded polystyrene of density 32-35 kg/m^3. Blocks with dimensions 300 x 200 mm were prepared for milling.
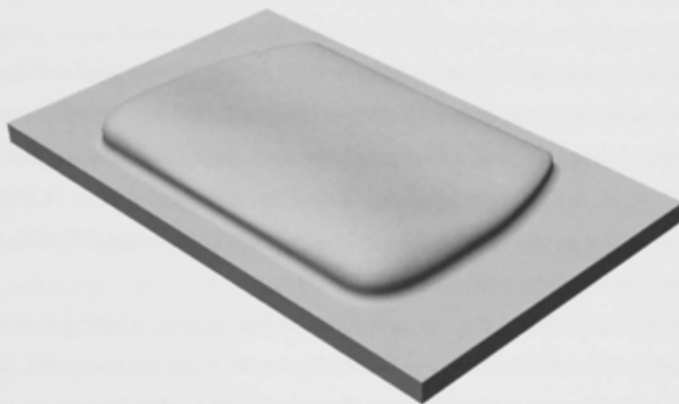
Figure 43 - Solid model of the sample for milling

A tool-path was generated using computer aided manufacturing software SurfCAM Velocity, Version 3. The tool-path consisted of a 3-axis z-roughing stage followed by a 3-axis planar z-finish. In both stages, the cut was set for climb milling with the tool aligned vertical to the surface. For the roughing stage the x, y and z-step size was 3.2 mm and the stock-to-leave was 1 mm. The z-finish then removed the remaining material in a 1 mm step. The computer aided manufacture software output in APT-CL format was exported to post-processing software (IRBCAM GmbH) for

conversion to the ABB programming language (RAPID). The arm extension, feed-rate and minimum distance between points were set using the IRBCAM software.

3.10.3.2 Experiment test array and accuracy measurements

The milling experiments were conducted using a design of experiments (DOE) approach [128]. An L9 fractional factorial orthogonal array was used. Using this array allowed a balanced comparison of process parameters and their level settings from a significantly reduced number of milling operations. In this study, the L9 array allowed four parameters to be tested at three levels, as outlined in Table 9.

The arm extension was defined by the distance radially out from the origin of the robot co-ordinate frame which was located at the centre of the robot mounting stage. The distances of 750 and 1350 mm are close to the arm extension limits. The arm extension and robot feed-rate were set at the post-processing stage using the IRBCAM software.

The behaviour of the foam sample material influenced the level settings for the feed rate and spindle speed. Low feed rates (<100 mm/s) and high spindle speeds (>22,000 rpm) caused the material to soften and melt, most likely due to friction generated heat. High feed rates (>800 mm/s) and low spindle speeds (< 18,000 rpm) caused the material to tear. Hence, the feed rate was set in the range 200-800 mm/s and the spindle speed was set in the range 18-22,000 rpm.

The post-processing stage included a point filter option, whereby a minimum distance between points in the tool-path data file for the robot were selected. A larger distance reduces file size but led to larger distances of interpolated movement and it was proposed that this could influence accuracy as the robot arm makes a smoothed linear move between the points. The points in all cases were fly-by points with zone accuracy of 0.03mm. For this study, the point filter was set in the range 0.2-3 mm.

Table 9 - Experimental array (L9) for the robotic milling and average sample shape error for each experiment

Experiment #	Arm extension (mm)	Feed-rate (mm/s)	Spindle Speed (10^3 rpm)	Point filter (mm)	Average error (mm)

1	750	200	18	0.2	0.062
2	750	400	20	1	0.069
3	750	800	22	3	0.081
4	950	200	20	3	0.060
5	950	400	22	0.2	0.067
6	950	800	18	1	0.091
7	1350	200	22	1	0.062
8	1350	400	18	3	0.100
9	1350	800	20	0.2	0.065

After milling, each sample was scanned using a laser scanner mounted on a Faro ScanArm to produce digitised point cloud data. The Faro ScanArm device had an accuracy of $\pm35\mu$ ($\pm.0014$ in.) and a scan rate up to 45,120 points/sec. This data file (ASCII format) was imported into the Polyworks software suite and aligned to a best fit position on the surface of the original CAD file of the test sample using the IMCompare component of the Polyworks suite. Error vectors were then generated between the original design and the point cloud. The final result was an error map for each sample. An example of an error map, overlaid on the solid model, is shown in Figure 44. Error ranges were highlighted visually using a colour scale gradient across the evident error range of each sample. For each experimental run, the mean error was calculated using the error vectors. The maximum error was also noted.
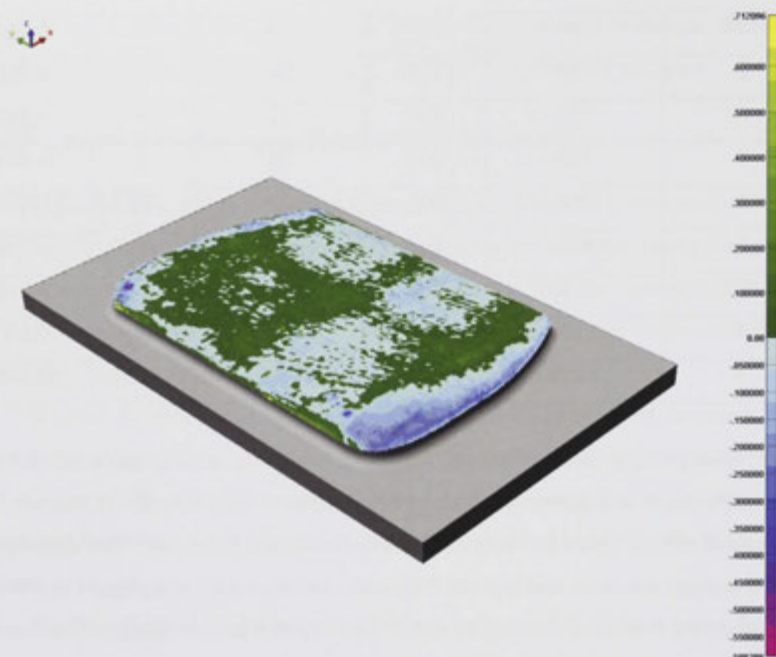
Figure 44 – Error vector comparison to CAD example

3.10.4 Experiment Results and Discussion

An analysis of means (ANOM) was applied to the results to elucidate the parameter effects. The mean and maximum error values were averaged; for example, the error values from experiments 1, 2, and 3 were used to find the average errors for arm extension of 750 mm; and the errors from experiments 1, 4, and 7 were used to find an average error for feed rate of 200 mm/s, etc. These average errors were plotted against the parameters settings. The average shape error from each experiment is given in the final column of Table 9. Two representative error maps, from experiments 2 and 8 are shown in Figure 46. For clarity, the top view is shown and the error patterns are typical for all samples. The main errors occurred in centre of the sample and were caused by insufficient material removal. Nevertheless, good accuracy was achieved with average error ranging from 0.06 mm (experiment 4) to 0.10 mm (experiment 8). By decreasing the arm extension, decreasing feed rate, increasing spindle speed, and decreasing the point filtering for the path generation of industrial robots, the path following accuracy

and hence surface accuracy of the milled samples were improved concurring with the experiment hypothesis.

(a)
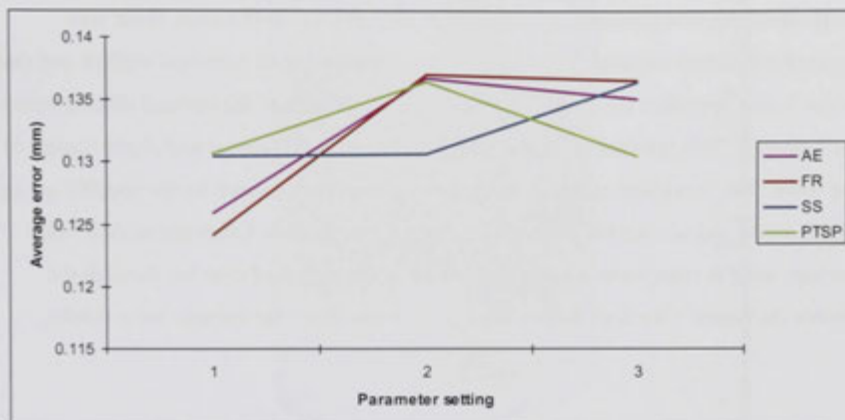
(b)
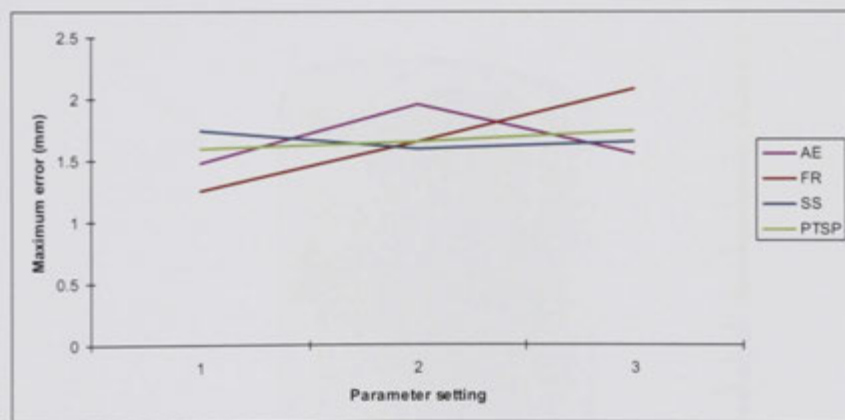
Figure 45 - Parameter effect (interaction) plots for (a) average error and (b) maximum error (AE = arm extension, FR = feed rate, SS = spindle speed, PTSP = point to point filtering)

A greater understanding of the effects of the parameter and level settings can be gained from the ANOM results which are plotted in Figure 45. The greatest error in Experiment 8 agreed with the hypotheses that at the greatest reach and comparable feed rate and highest point filter spacing the greatest error would occur. In the DOE findings

it is clear that the point filtering had a greater effect on the accuracy than the feed rate. For AFP surface following applications, such errors concerning the TCP accuracy are well within the desired tolerance ranges for tow positional accuracy.

The maximum shape error, ranging from 0.796 mm (experiment 2) to 1.430 mm (experiment 8), was recorded at the edges of the samples. In this case, there was excessive material removal. The edges of the model included a vertical surface and due to the 3-axis operation the contact on the surface was outside the optimal cutting zone of the ball-mill. This resulted in poor scalloping of removed material and slight tearing of the foam. The maximum errors at the edges are, therefore, caused by the specific set-up in this study and are outside the region of interest for surface following in AFP. The average error is representative of the situation in the region of interest, through the double curvature; therefore further analysis is made using the average error results.

(a)

(b)
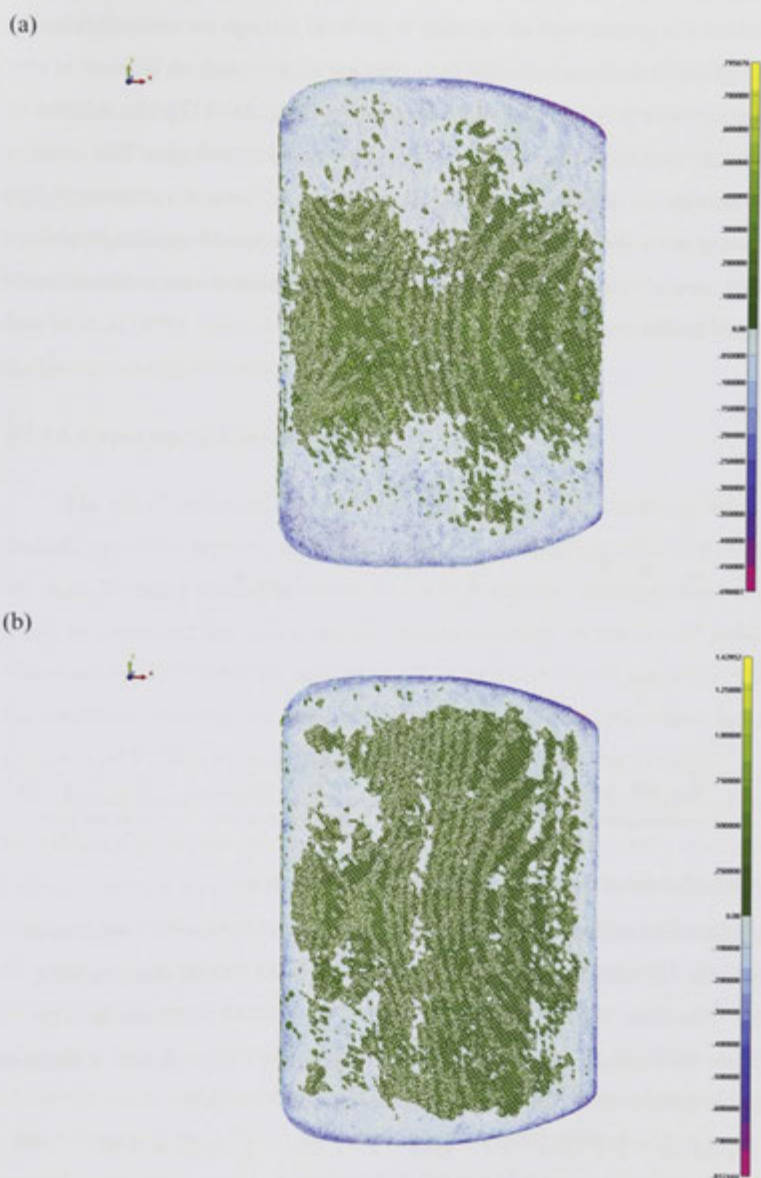
Figure 46 - Error maps from (a) experiment 2 and (b) experiment 8

A greater understanding of the effects of the parameter and level settings can be gained from the ANOM results which are plotted Figure 47. There appears to be no

significant parameter effects as the error ranges from approximately 0.062 to 0.085 mm. However, the error is greater with an increase in the level settings for arm extension, feed-rate and point filter. The conclusion that accuracy reduces with an increase in arm extension and feed-rate is consistent with earlier work [127][131][132]. The ANOM results for spindle speed indicate an optimum level setting of 20,000 rpm. This is not surprising given that the response of the polymer foam to milling at the extreme settings, as noted in section 2.3. Overall though, there are no clearly opposing trends. Therefore it is concluded that there are no significant interaction effects exhibited by the parameters used in this study.
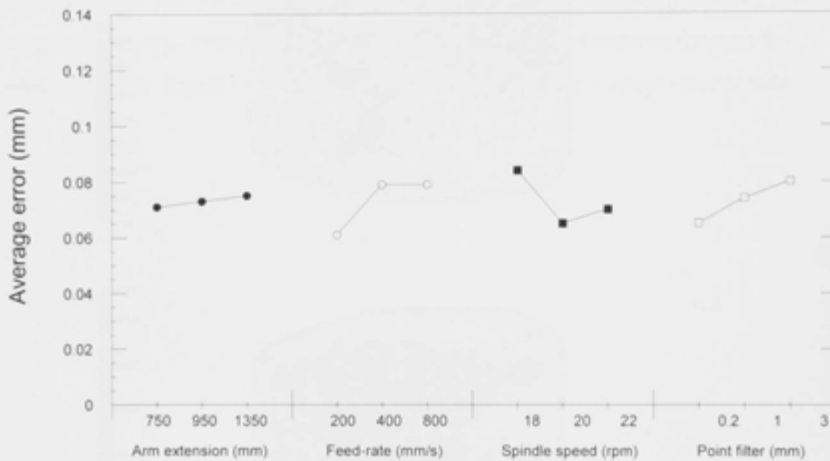
Figure 47 – Analysis of means data for each of the process parameters

The results indicate that the ideal settings required to produce the lowest error are arm extension 750 mm, feed-rate 200 mm/s, spindle speed 20,000 rpm and point filter 0.2 mm. Therefore, a predictive model based on the ANOM [128] was used to predict the error for a sample milled with these ideal settings. The prediction is based on the deviation from the overall mean for each ideal setting, as follows:

$$\bar{y}_{predicted} = \bar{y} + (\bar{y}_{AE} - \bar{y}) + (\bar{y}_{FR} - \bar{y}) + (\bar{y}_{SS} - \bar{y}) + (\bar{y}_{PF} - \bar{y})$$

Where $\bar{y}_{predicted}$ is the predicted error, $\bar{y}$ the overall mean, and $\bar{y}_{AE}$, $\bar{y}_{FR}$, $\bar{y}_{SS}$ and $\bar{y}_{PF}$ are the mean errors from the experiments with the ideal settings for arm extension, feed-rate, spindle speed and point filter, respectively. The predicted error was 0.042 mm

however due to time constraints a further experiment using the optimised settings was not conducted.

Overall, the lowest error and hence greatest accuracy was achieved with the lowest arm extension. This indicates that milling close to the robot and where arm stiffness will be highest gives the most accurate results. The feed rate also had a significant effect. Lower feed rates gave more accurate milling results and it was hypothesised that vibration at higher feed rates due to the climb milling cutting could have been the cause. Furthermore, greater feed rates require greater acceleration and deceleration of the robot axes and therefore overshooting and sudden changes in momentum could also affect path following quality.

3.10.5 Experiment Conclusion

The use of industrial robots in the articulation of AFP placement heads has been feasibly proven as accurate for milling applications requiring tolerances of less than ±0.1mm. By using milling as a measure for TCP accuracy during programmed path runs it can be concluded that robots are also accurate enough for use in AFP applications where similar TCP loads are applied and TCP path accuracy is important. Furthermore, the results also showed that industrial robots will meet the requirements as a placement device in AFP. With extra degrees of freedom this can increase versatility

Future research should certainly include testing of the theoretical optimal settings to validate if the model produced settings actually do provide higher accuracy. A focus on the degrees of freedom the entire placement system with the use of additional axes acting on the work object could should also be assessed to better understand the effect of compound articulation on robot accuracy. This would increase the reach and access of AFP machines and enable fibres to be laid into tight radii on parts with complex geometry. This in turn however requires further development of robotic systems capable of further reach, and the ability to apply a greater positive pressure or resistive force (depending upon the type of compaction force mechanism used). These two requirements are however in conflict with the need for greater accuracy and at such lengths and forces this becomes difficult to manage at extended reach. By utilising stiffer structural designs in the articulation systems and utilising stiffer materials, such as composites, this could be possible.

3.11 Programming and Control

Composite design processes and tools are developing rapidly, providing designers with the opportunity to exploit the full advantage of composites by defining tailored ply schemes with fibres oriented exactly along the load paths the components application requires. AFP technology allows this design intelligence to be manufactured in an accurate and repeatable manner using automation. Such additional design information requires complex programming and control in order to ensure design intent is enacted by the programmed machinery. This process information includes individual tow payout, cutting, tow drop and addition require additional processing in order to define correctly [133]. This is most often achieved in post processing environments using proprietary software matched to the AFP machine; such systems include FiberSim by Siemens [134], Vericut and CGTech [135].

Designing for the manufacturing process is critical to the success of the part production. In order to take advantage of the unique ability to maximise weight and strength gains using individually tailored fibre tow placement manufacture of AFP generic design rules exist [136]. Such rules can and have been built into development environments, in the case of the Tailored Composite Design Code (TACO) the software was embedded into the MSC PATRAN/NASTRAN environment [137]. In comparison to traditional composite design practice for quasi isotropic balanced woven or unidirectional fabric, AFP design rules focus on specific process limits and usually always require specific processing according to the specific AFP machine and material combination being used for manufacture. Such process limits include the individual fibre tow path steering radius, minimum cut lengths, minimum concave lay-up radius, placement strategies such as whether to use continual tows paths, tiled paths or incremental strips [138], the tow bandwidth radiuses for individual tow payout and tow add/drop for variation in the number of tows being laid on-the-fly, kinematic accelerations and decelerations of the placement head according to the component geometry. Material limits include flex and twist to minimise tow buckling, wrinkling and overlapping, to achieve the designed paths [28][47][89].

Steiner and Wiest [139] looked at the development of algorithms to facilitate AFP manufacture at the design stage and to integrate a number of custom software controls into the computer aided engineering (CAE) environment. In this case the

algorithms were applied to a filament winding process but there appears no reason this could not be applied to AFP. By reducing the design for manufacture burden in relation to know-how and experience the technology utilisation is simplified dramatically. With programming captured in standard computer aided manufacturing environments, learning and commissioning time will be significantly reduced and industry acceptance will be facilitated by the need for less training and less supporting software requirements. To do this, and remove the need for parametric control at every level, smart sensory and feedback systems for in line monitoring of process quality were recommended for integration into AFP hardware.

Ahrens [13] identified the need for simple and efficient Computer Aided Design (CAD) and computer aided manufacture (also known as CAM) software for the manufacture processes. In the transition from CAD models to digital manufacturing data, specialised tool path controllers and post processors are required for each brand of AFP system. Converting a generic CNC machine language to an AFP specific programming language requires specific post-processing software as well as operator expertise. Some studies have used commercially available software with industrial robotics including IRBCAM, Vericut and FibreSIM [140]. The problems of path programming, planning and trajectory control from geometry and sensory feedback have been a major focus of robotic manipulation studies. These studies have provided solutions that utilise complex custom software that is highly specialised and limited in flexibility [59].

Shirinzadeh, et al. [141][142] examined fabrication of open surface composites by using robot articulation to look at the programming and kinematic requirements of such a system. The methodology for process planning and programming included simulation of path generation for both open and closed contours. A new approach from the traditional robotic control 'teach' method was taken with CAD data which was defined by a surface and robotic motion was generated from tag points assigned to the surface was used to determine a normal direction equally spaced in the X and Y directions. Numerical algorithms were then used to define B-spline paths using these tags depending on the part requirements. This algorithm was also extended to closed surfaces with closed geometry or axes of symmetry similar to winding processes. New strategies in open surface path generation, through simulation as well as fibre steering

and sensory-based contour tracking, were also examined using a 6 degree of freedom robotic AFP research system focusing on process planning and control [139]. Various path and trajectory generation algorithms were examined with a number of different kinetic control models. The work presented models for AFP systems that improved control and which included the degrees of freedom internal to the AFP head. The flexibility provided by using 6 degree of freedom industrial robots advanced techniques by representing the fibre placement head, as more than just a solid body in a 3D environment.

Beyond design rules and specific part programming, accurate control during the AFP process in real time (on-the-fly), is a complex task and requires dedicated real time controllers with fast processing and response times as well as robustly designed mechanical systems that can also respond and maintain performance at such speeds. Cutter timing in high speed runs as well as clamping and restart feeding are crucial for accurate location accuracy and placement of tows (to achieve minimal waste) and usually must be calculated by predictive and adaptive systems in order to meet quality requirements. Control of the gap between tows is also an area where AFP controllers and sensors are critical. Improvements in hardware and controllers have facilitated much of the development and utilisation of microelectronics that have resulted in reduced size and cost of controllers.

Lichtenwalner [12] examined neural based, feed forward control of a robotically articulation AFP system with a laser heating system. Higher speeds and additional degrees of freedom using an industrial robot, as well as the introduction of closed loop or feed forward control [12] proved that industrial robots offer a feasible and precise means of manipulation in both path and point dependant processes such as AFP [12].

Meier [133] looked at simplifying AFP programming by using a mould-surface tracking feature internal to the AFP head. The surface-tracking feature enhanced head rotation flexibility, component history data collection, tow flaw detection and flaw disposal. Cincinnati Milacron, the original equipment manufacturers of the AFP head, treated their AFP head as an adaptively controlled unit [139]. The head was fitted with ultrasonic sensors to monitor mould curvature. Utilising the mould surface tracking feature programming of fibre placement paths was simplified allowing for two

dimensional lay-up schemes to be applied directly to 3D surfaces and also correcting for setup errors by adjusting according to surface position versus the offline programmed position.

Most research systems are fitted with extra sensors and modified for the accurate control of the key process parameters and data collection for modelling and simulating the process [81]. However, utilisation of real-time control and increased process monitoring is yet to be introduced widespread. Developments in technologies such as dielectric analysis for in-line measurement of degree of cure should be considered in future research. Control of the supply material quality is also particularly important for automation systems, which rely upon set parameters during operation. Hence the need for in-line quality inspection and control of the fibre tows during placement

Precise closed loop control of both the consolidation force and temperature are critical to the bond quality in AFP, particularly in thermoplastic applications [143]. A large amount of research has been undertaken in examining the heating and heat transfer during the process, and how this affects voids, consolidation and modelling [32][114][144][145][146]. Experimental results by Tierney and Gillespie [147] presented a model that predicted the through-thickness heat transfer and the resultant bond strength based on intimate contact and heating at the ply interface. Experiments showed that model based predictive control can be used as a method for process optimization. The numerical results showed that bond strength development was significantly affected by the process set points (e.g., velocity, bonding temperature and roller pressures). Further research is needed that focuses on the improved useability and easier programming of such 'smart' systems through software solutions while also incorporating similar concepts to design allowable or design rules within the software processing, capturing current and future understandings of the composites themselves and the cure kinetics at play during the process. Furthermore, location specific information about the exact orientation and location of the placement head through feedback systems such as optical coordinate measuring machines or even highly accurate encoders now available on the market.

3.11.1 The UVAFP Programming and Control System

With the program completed in the RAPID language and including input/output (IO) commands for triggering events the two simultaneous functions of the UVAFP system could be connected. The UVAFP prototype required two controllers – the path controller for the articulation of the placement head through the defined placement path and the task controller for the actuation of internal devices to the head at the right time along the path to ensure correct operation. The path controller was the ABB IRB controller while the task controller was a PC based data acquisition configuration using National Instruments' Labview software package. Connection was handled using an ABB Devicenet Data Acquisition (DAQ) Digital input and output (DIO) card internal to the robot controller, namely a DSQC 327A. The DSQC 327A could handle 16 x 24VDC digital inputs, 16 x 24VDC digital outputs and 2 5V analogue outputs and integrated easily into the master Devicenet structure of the ABB controller. The electrical circuit for the prototype linked the robot path controller to the Labview task controller as per Figure 48.
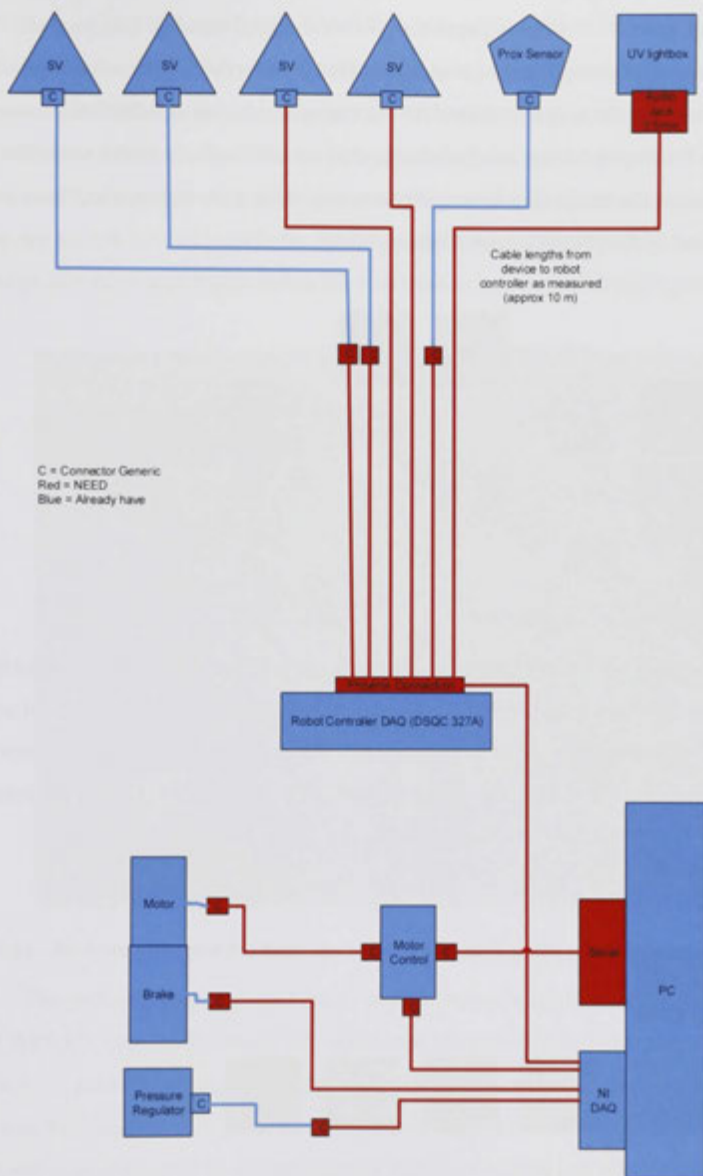
Figure 48 – UVAFP electrical control circuit (SV = solenoid valve)

The Labview control software was devised using a series of event-triggered algorithms. Events were called within move commands and timed according to position from the start or end of a placement path run. These algorithms are presented as block

diagrams in Figure 49. As the sequences explains, a digital input (DI) is received from the robot controller through a data acquisition (DAQ) interface. The motor controller would then initiate the output required for the motor to run through the DAQ to serial connection. During operation integrated encoders would feedback to the controller and determine when the motor should stop, for example after a set distance had been rotated for the re-feed of the tow to be complete.
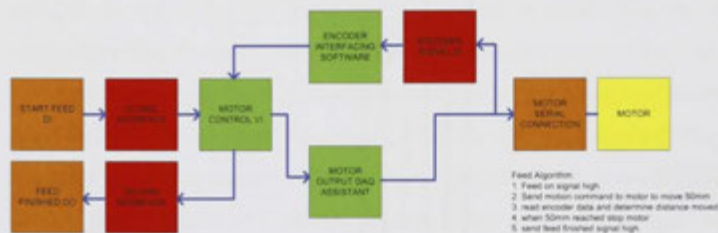
Figure 49 –CCR task control algorithm

The force control algorithm is displayed in Figure 50, as per the CCR algorithm the force controller proportional-integral-derivative (PID) would manage the set point via feedback from the load cell that provided the control variable to a PID pneumatic regulator that provided the driving pressure within the compaction actuator in order to provide the force required for consolidation.

Figure 50 – Force control algorithm

To program and control the UVAFP prototype, a novel "CAD to CAM" approach was developed. The digital surface geometry was imported into a standard computer aided manufacture environment, in this project SurfCAM was used for its inbuilt 5 axis machining capability. A placement path was generated, as per the in-built "machining" path programming tools but using the machining parameters to simulate placement parameters. For example, straight paths across a flat face with run off over part edge as well as spacing to match the tow band width as shown in Figure 51.
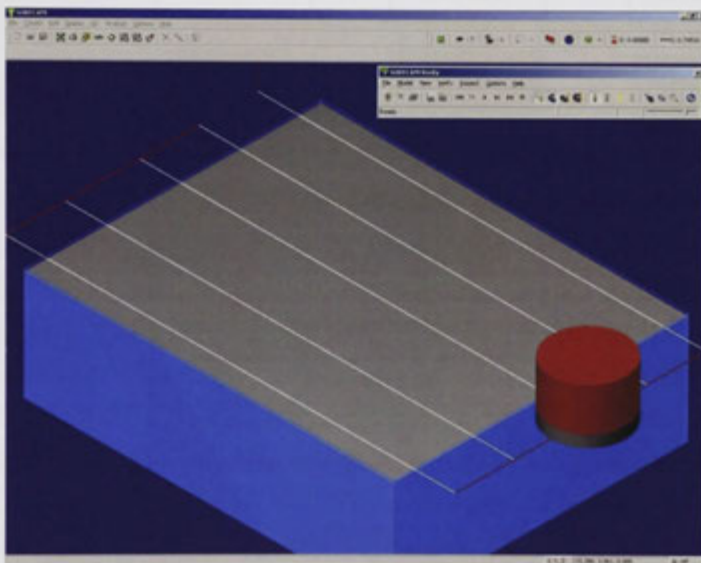
Figure 51 – Surfcam generated flat face "machining path" used as flat placement path for AFP

The path was then exported into a generic numeric control format known as CAM APT-CL code. APT stands for Automated Programmable Tool and includes simple x,y,z point data that came outputted with i,j,k orientation data. This APT-CL code was then imported into an NC to robot language converter known as IRBCAM. IRBCAM was developed to convert the tool point coordinate and orientation commands as well as the G code event handling commands (eg: on/off) into ABB's RAPID move command language with x,y,z and quaternion orientation data needed for ABB robot controllers. In order to do this global strategy options had to be selected for handling of the 6th axis. The resulting RAPID program was then loaded into a custom post processor

written by the author of this thesis specifically for the UVAFP process, that examined the program for placement move commands and added UVAFP path trigger events that would initiate certain IO channels used for device control such as CCR during placement. The process flow is shown in Figure 52.
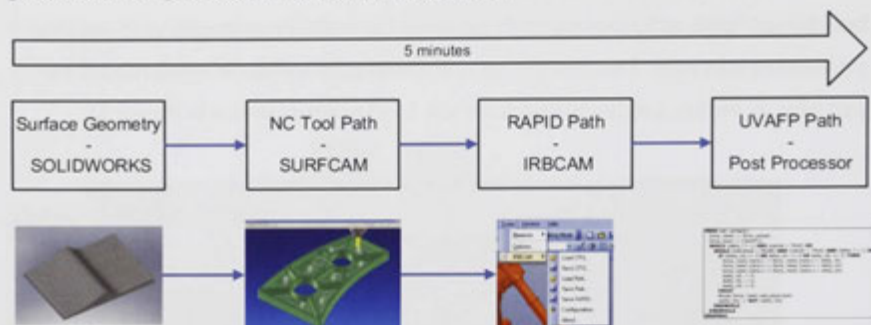
Figure 52 – The fibre placement path generation process

This process kept the intelligence of path generation algorithms within the functionality of the computer aided manufacture package used and allowed a quick and highly flexible approach to converting CAD to the appropriate IRBCAM path program [63] with minimal additional learning curve for CNC programmers. The time to generate a path using this post processor approach depended upon the size and geometric complexity of the CAD model. Programming time for generating a path for the UVAFP prototype on a simple mould (a flat tool similar to that shown in Figure 51 500 x 500mm) for a single ply using a single tow approximately 6.35mm wide with a straight section and then a steering radius of 500mm half way along the part length took less than 5 minutes [7][63].

3.12 Summary

This chapter detailed the design, development and building of the UVAFP prototype and the QFD design approach and experimental validations undertaken in consideration of the final product. The QFD approach was detailed showing the focus on compliance to the requirements and therefore quality expectations for the UVAFP prototype. Each sub-systems was considered individually for the prototype and the final system provided the full functionality of an AFP system for a single tow, suitable for research and proof-of-concept purposes. The design of the prototype was undertaken as

one of the first technical undertakings of this thesis and was a substantial piece of work in itself. Two design hypotheses were tested and the results presented providing agreement to the hypotheses. Subsequent chapters and tests utilise the prototype developed within this chapter where appropriate and efficient. This subsequent testing proved the value of the system and its design for the purpose of proving and testing the UVAFP concept. The prototype is still in commission and service at the Australian National University and is being used for further research into AFP technologies, 5 years after its original design and construction.

In the first analysis examining the design envelope for the placement head the first hypothesis proven was that decreasing the size of the placement head increases access to more complex tool geometry and thus increases the range of parts that can be made using AFP. The increased access was proven and thus used as a design guide in the development of the UVAFP prototype. The reduction in size was only possible however due to the compact and simple packaging required from their various subsystems of the UVAFP system but also because the UVAFP process requires no heating or temperature control systems as is required for systems using towpreg. The design optimisation of the placement head physical characteristics led to a design that offered greater access than current state-of-the-art placement systems. One acknowledged opportunity for cost reduction using AFP not specifically defined as a requirement, is through design for manufacture of the composite component. Metallic structures are often designed as sub-assemblies that are subsequently joined or fastened. Alternatively, composites can be designed and manufactured as monocoque or net structures that would eliminate the need for joining [149] and reduce cutting waste, hence increased design envelope coupled with design for manufacture according to the materials and process would both contribute to significantly increasing the versatility of the process.

The CCR unit as integral part of any AFP system was detailed showing the complexity of the system and the vital role it plays in waste reduction, accuracy, minimum cut lengths and the speed of the AFP lay-up. Likewise the compaction system and its impact on quality was also examined showing the various concepts that have been previously considered and the reason for the choice of a compaction roller for UVAFP. The fibre and resin creel concepts of current benchmarks was also presented

and the various concept of head mounted or remote floor mounted systems in service today, ultimately the remote floor mounted design was selected to minimise the placement head size as much as possible.

The second hypothesis that industrial robots with their 6 degrees of freedom are suitable articulation devices offering sufficient accuracy for AFP placement was also proven in a study examining tool centre point accuracy in operations that provide reacting loads and require path accuracy not just point accuracy. The advantage of using such robots being the increased reach such high degree of freedom systems offer. Increasing the dexterity and flexibility of the articulation systems used with AFP placement heads allows for an increased working envelope and reach and the ability to manufacture a larger variety of more complex parts, accelerating the adoption of AFP.

As a necessity for programming the UVAFP prototype without access to expensive and proprietary software packages a simple approach to AFP path programming was developed that was both cost-effective and quick, closely mimicking the NC programming of other industrial equipment. By using an integrated Computer Aided Engineering (CAE) solution called SurfCAM as a standard computer aided manufacturing package and IRBCAM to post process and convert tool path output to robot code and then a final post processing to add the AFP specific commands an easier programming and control solution was developed by using existing design and computer aided manufacture software.

4 Automated Fibre Placement Materials

This chapter examines the supply materials used in AFP systems, the limitations of current materials and the case for new options. By using glass fibre and vinylester resin impregnated on-the-fly and cured in-situ using UV, a lighter composite structure was made that had comparable, if not better, strength-to-weight ratio compared to existing aluminium and steel parts.

Section 4.1 examines each of the raw constituents of the AFP system; namely the fibre reinforcement, the structural matrix, and the hardener that initiates reaction to cure the composite and provides the combined mechanical properties greater than the sum of the parts. In section 4.2 fibre reinforcement options currently available to AFP are discussed and a deeper analysis of low-cost dry fibre material sources is provided. This section presents alternate constituent parts that were considered for AFP and the advantages and disadvantages of each. To assess the suitability of the new fibres for AFP, in section 4.2.3 the selection process for fibre options was presented. In section 4.3, dry fibres were tested experimentally for their suitability as an AFP supply material, specifically in their dimensional stability and handling in automation systems. In section 4.4 the resin options available for AFP were examined and the selection of an appropriate resin chemistry to address the cost and curing time of current AFP systems was analysed. Section 4.5.1 details the selection of the curing catalyst, in this instance an alternate to thermosetting chemistries is provided that cures upon exposure to UV light, known as photo-initiators. Finally, section 4.7 summarises the findings of the chapter and the context that the selection of the materials provides for studies undertaken in subsequent chapters (although not always used in experimental studies due to availability and variables being tested).

4.1 AFP Supply Materials

The list of supply materials for AFP technology is short and exclusively made up of aerospace grade towpregs that are generally expensive. The most common materials are fibre tows, supplied as tapes, tows, towpregs or slit tapes pre-impregnated

with thermoset or thermoplastic resin matrices. The tows are usually highly consolidated and are difficult to impregnate, except via specialised pre-processes. Fibre and resin combinations currently used include carbon fibre and epoxy resin, carbon fibre and polyetheretherketone (PEEK) or polyetherketone (PEK) and even polypropylene (PP). Towpregs offer advantages for AFP processing which is why they are currently the material of choice for AFP systems. The materials are formed in such a way that makes them stable and uniform for automated handling in AFP creels and handling systems. Unfortunately, the variety of fibre and resin options is small and designers are limited to a small subset of composite materials. These materials offer high performance mechanical properties excellent quality and repeatable results, servicing the needs of aerospace applications but generally do not suit automotive, industrial and other composite applications. These materials are restricted by their stringent processing windows using thermal treatment and curing mechanisms. The materials are highly sensitive to environmental effects such as humidity and temperature as well as foreign object damage (FOD) / contamination.

Thermal heating processes are by far one of the most popular curing and activation options available in composites manufacturing. But new more efficient chemistries capable of curing using radiation are now available and an opportunity exists to apply them to AFP. By examining the full spectrum of radiation curing mechanisms available and their applicability to AFP, significant process gains can be made. By introducing more materials into the range of those currently available for use in AFP systems, both in thermoset and thermoplastic matrices, designers will have greater design freedom and AFP could be applied to a larger number of components. The material considerations for AFP includes the fibre, the resin, the catalyst/initiator or hardener, the sizing on the fibres to protect them during placement, the form of the fibres including width, thickness and sectional shape and the required thickness uniformity and cross section uniformity, and finally the form in which they are supplied, whether as pre-impregnated or separate dry fibre and liquid resin. Material standards defining common materials used in robust and flexible processes, such as dry rovings in filament winding, would make for a greater design freedom, but this relies upon a universal process platform that can handle a wider variety of material tolerances.

To avoid the use of preimpregnated tows and reduce cost and necessary pre and post-processing, an appropriate dry fibre, bulk liquid resin and photo-initiator material system were selected. In order to test the use of UV curing in conjunction with AFP the fibres needed to be transparent to UV light for maximum degree of curing and eliminating the need for 'dark-curing', therefore at the commencement of the material selection only glass fibre options were considered. Using glass fibre would ultimately mean that the process is going to make the parts that are significantly heavier than carbon fibre, but the glass fibre/UV curable resin materials system is more versatile and the cost is a magnitude of order cheaper.

The short listing of fibre and resin types was based on a number of requirements. Table 10 details these requirements and the specifications metrics. For the photo-initiator, while a number of options were considered no comparative testing was undertaken and the known Ciba Irgacure 819 was used. Table 10 also identifies the requirements determined for the materials of the UVAFP prototype.

Table 10 – The material selection criteria

Requirements	Material	Specification	Metric target
Low cost	Fibre	Cost	≤ E-glass
	Resin		≤ SMC matrices (poly and vinyl ester)
	Photo-initiator		≤ MEKP
No material preparation and easy to load	Fibre	Supply form	Single end Roving
	Resin		Bulk liquid (drum, pail etc.)
	Photo-initiator		Soluble powder/liquid stable in dark
Optimal properties at lowest $/kg	Fibre	Fibre resin content	50:50
	Resin		
Can cure using UV light when combined with fibres	Fibre	Transparent	Glass
	Resin		Vinylester
Fast curable in-situ	Resin	Cure time	< 10 seconds
	Photo-initiator	Tack time	<1 second gel (ASTM D3167)
Can be used in automated systems	Fibre	Tow thickness tolerance	± 0.05mm
	Resin	Tow width tolerance	± 0.3mm
	Photo-initiator	Low viscosity	100 cPs
		Ratio	< 1 pph
Able to conform to complex geometry	Fibre	Single tow width	0.25" or 6.35mm
Comparable mechanical properties to traditionally laid up and thermally cured glass fibre reinforced polymers	Fibre	Mode I mechanicals	> E-glass
	Resin	Mode II mechanicals	> Vinylester
	Photo-initiator		

4.2   Fibres

The fibre placement process, as the name implies, is primarily focused on the placement of continuous fibres through a programmed path according to the reinforcement design of a part. The controlled placement of fibres allows for the optimisation of properties through load paths. Further weight reductions in components is possible by taking advantage of the anisotropic nature of fibre reinforced composites and defining fibre paths through specific load paths.

Fibres used in AFP must be continuous in supply through the creel system, up through guide systems to the placement head. This requires that the tow have uniform flat cross section, be stable through feeding to the placement head, resistant to stringing and fraying especially under possible shearing caused by feed and redirect rollers, be flexible enough to go through guide systems, steer through fibre paths and strong enough to handle compaction without fracturing. Common fibre materials include carbon, glass and Aramid. Each material can come in two forms, a towpreg, where the resin is preimpregnated, or dry fibre tows.

4.2.1   Slit tapes

As previously discussed in Section 2.3 and Section 4.1, the current baseline material supply form used in AFP systems is preimpregnated tows that are slit from UD materials, otherwise known as slit tapes. The advantages of slit tapes are that the fibres are pre-impregnated and the matrix pre-consolidated within the fibre tow. The tape geometry and cross section is usually stable, depending on the resin viscosity through the working temperature range. The tapes usually have uniform cross section and that the void content is below an acceptable level to ensure acceptable composite properties. In application, the size of the tape is often defined by the filament count, namely 3000 filaments (or 3k), 6000 filaments (or 6k) and so on but most often are usually a uniform ¼ inch wide. This reduces the need for flexible guidance and tow forming systems to ensure uniformity at the nip point. The task of the AFP system is therefore simply to ensure accurate placement of the slit tape against the adjacent tow and ensuring interfacial adhesion of the ply being laid. In thermoplastic systems consolidation and bonding must occur at the point of application, which requires precise control of the

temperature and pressure as well as position. Without adequate pressure and melding at the interfacial surface, delamination and 'pulling' or debonding of the tape can occur.

The disadvantage of tapes (slit or unslit) as well as towpregs (preimpregnated single tows) is that they are expensive and require precise temperature control and storage. Twist and self-adhesion is an issue for all preimpregnated fibres and makes handling operations time consuming even if the resin impregnation eliminates some of this tendancy in the fibre tow. Thermoset prepregs require refrigeration storage until they are used to inhibit cure progression of the pre-mixed resin and catalyst that have been applied onto the fibre. Even with refrigeration shelf-life is limited, usually no more than 12 months, and with a limited working life at room temperature of often no more than 30 days. These stringent storage requirements in themselves carry a significant overhead in terms of quality control and factory infrastructure. Furthermore, binding or build-up of the resin within the handling system due to resin tackiness can cause blocks and sticking, requiring regular routine maintenance. All prepreg tapes or tows are heated to increase tack prior to placement and aid adhesion adding significant equipment requirements within the placement head. After placement, thermoset prepregs still require a thermal curing stage to fully consolidate the layers and maximise properties, this usually occurs in an autoclave where the high pressures and elevated temperatures are exerted to consolidate, remove entrapped air and cause cure.

Thermoplastic prepregs (such as carbon-fibre/PEEK or glass-fibre/polypropylene) can be heated during placement and consolidated under the pressure of a compaction roller and then cooled by the placement head [121]. Following placement of some thermoplastics (such as PEEK), a long and slow post cure is required to achieve final consolidation and full material properties. The drawbacks with the process are the high material costs, low operating temperatures of the materials of some TP's, energy consumption and the running costs of the localised heating.

4.2.2 Dry Fibre Tows

Dry fibre tows in advanced structural materials come in carbon, glass, aramid, basalt and graphite to name a few, and are a constituent material to towpreg. During processing, dry fibres are wound onto a bobbin or roving of some form and mass produced resulting in a lower cost. Because the resin has not yet been impregnated into

to the fibre the storage and handling requirements are greatly reduced. The disadvantages of using dry fibre as a supply material is impregnation must occur within the processing equipment, this will be discussed in Chapter 5.

Dry fibres exist in a number of forms including single and multi-end rovings, mattes, veils, woven broad goods and fabrics. Single-end rovings are most often used in filament winding, long-fibre thermoplastics, pultrusion, knitting and weaving applications. These are produced by pulling individual fibres directly from the 'bushing' and winding them onto a roving package ready for shipment. The sizing coating applied to fibres that is used to protect the fibres from fracture and stringing does not entirely protect against tow break-up and the risk of fibre blockage in automation systems is increased when using dry fibres. Furthermore, the sizing chemistry is formulated for specific resin chemistry and effects fibre resin adhesion properties, therefore requiring specific selection of sizing for both protection and resin chemistry.

While the term 'dry' fibre tow implies no resin content, often tows are coated with a binder matrix in order to maintain the uniformity and stability of the tow. The binder is applied to the tow by either dipping, powder coated or spraying during winding of the tow onto the rovings. The binder is heated at the time of placement or preforming to aid in 'binding' the tow into position for later loading of the preform into the tool. The binder is usually no more than 5% the total weight and can either be thermoset or thermoplastic. In some instances binders are used as diluent tougheners within the bulk structural matrix once infusion occurs. Alternatively, binders can act as wetting agents to encourage fibre matrix adhesion and impregnation. Twisting in dry fibres is a regular issue due to the lack of stiffness provided by the matrix. Rovings depending on their winding technique contain inherent twists within the tow due to the way in which they are manufactured. This is a serious concern for any process using such materials but can be managed by tow guides and rollers.

By using dry fibre tows with AFP the process could be applied in non-traditional roles such as in the manufacture of dry fibre performs [100] [150]. By using dry fibre tows in AFP significant reductions in material costs could be achieved as well as increased options in fibre/resin combinations and the mechanism for curing providing greater design and process flexibility.

4.2.3 Fibre Selection

To maximise the benefits of the UV curing technology, a fibre transparent to UV light was required, such dark curing or hybrid curing systems would not be necessary. Only glass fibre offers the transparency or refractive index required in light curing processes. Glass fibre however does not offer the highest specific properties in advanced structural fibres, surpassed by carbon and aramid fibres for example, but given its widespread use, long history of development and lower tech production technique (in comparison to the carbonisation process of carbon fibre) it offers, especially in considering S-glass excellent properties for the price of the material. The automotive and aerospace industries, currently utilise glass fibres in glass matt thermoplastics (GMT), sheet moulding compound (SMC) or injected short fibre, glass fibre reinforced plastics using wovens (GFRP), chopped fibre and other forms. While carbon fibre has seen increased utilisation in recent years the cost of the material alone is prohibitive to its uptake in comparison to the weight saving. In applications where higher volumes and lower margins, the material cost is critical to its viability. The reduced mechanical properties of glass fibre in comparison to carbon and aramid can be offset by the cheaper price and ready availability. The cost to performance compromise therefore means that target applications include structures and components requiring intermediate tensile and compressive properties (in comparison to carbon fibre) but higher flexural, impact absorbing or elastic properties where the cost of the high performance fibres cannot be justified.

Of the glass fibres commercially available there exist a number of standard specified fibre types, namely E-glass, S-glass, R-glass as defined by ASTM D578-05, "Standards Specification for Glass Fibre Strands" [151]. Figure 53 [152] shows the typical stress strain behaviour of the different glass fibre types in the elastic region, including Owens Corning's proprietary Advantex glass and other advanced structural fibres.
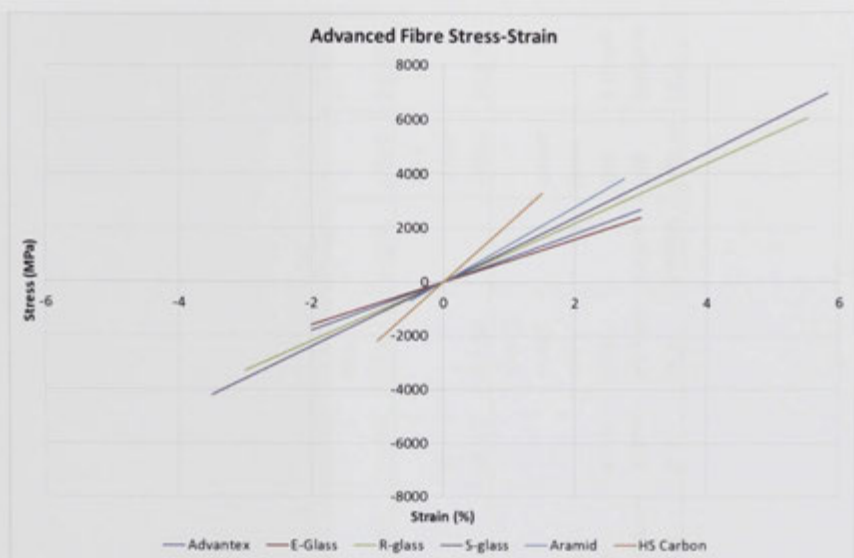
Figure 53 – Typical structural fibre stress-strain curves

The filament winding process requirements closely reflects the AFP process and therefore fibres developed for this process were short listed as potential candidate fibres. Tows must be continuous and uniform in dimension, high tensile properties, very low stringer and fuzzing and appropriate sizing to protect the fibre during delivery through guide system where high abrasion or wear can occur. Table 11 [153][154][155] shows the mechanical and thermal properties for the various glass fibre candidates examined for use in the UVAFP system.

Table 11 - Fibre tow properties

Property	Units	Test Method	R&G Hollow Glass Fibre	OCV WindStrand H EPW17	OCV XStrand Roving	OCV Advantex Single End Roving Type 30	Standard E-Glass	Jushi E6 CPR 386T Direct Roving	OCV FliteStrand Roving
Product Code			190 050-X		MCX S 21	SE1200		E6DR17-1200-386T	MCF 14
Fibre Designation		ASTM D578-05	H-glass	R-Glass	S-Glass	E-CR glass	E-Glass	E-glass	S-Glass
Cost	$US/kg		60	14		4	2		
Average filament diameter	microns		12	17	17	17	17	17	9
Tex	g/km			2400	2400	2400	2400	1200	675
Roving Width	Mm		3.175	6.35	6.35	6.35	6.35	6.35	6.35
Roving Thickness	Mm		0.26	0.35	0.35	0.35	0.35	0.35	0.35
Density (@ 25°C)	g/cm³	ASTM C693		2.55	2.45	2.62	2.55-2.58		2.45
Refractive Index (bulk annealed)	NA	ASTM C1648	1.42	1.54	1.522	1.565	1.547-1.562		1.522
Resin Compatibility	Resin		Polyester, Vinylester, Epoxy, Phenolic	Epoxy	Polyester, Vinylester, Epoxy, Phenolic	Polyester, Vinylester, Epoxy	Polyester, Vinylester, Epoxy, Phenolic		Epoxy, BMI, Phenolic
Thermal Conductivity (@ 25°C)	W/mK	ASTM C177	0.21	1	1.34	1.22	1.0-1.3		1.34

Coefficient of Thermal Expansion @23-300°C	$\times 10^6$ cm/cm°C	ASTM D696		4.1	3.4	6	5.4		3.4
Specific Heat Capacity @ 23°C	kJ/kg.K	ASTM C832		0.75	0.816	0.79	0.807		0.819
Pristine Fibre Tensile Strength	MPa	ASTMD2101		4510	4955	3790	3490 3790		4955
Young's modulus	GPa			87	88	81	69-72	70	88
Specific Modulus	x10⁶ m	Calculated		3.48	3.67	3.15	2.75/2.85		3.67
Elongation at Break	%			5.35	5.5	4.9	4.8		5.5
Tensile Strength	MPa	ASTM2343 with Epoxy						2673	
Tensile Modulus	MPa	ASTM 2343 with epoxy						81126	
Score		Green = 3, Amber = 1, Red = 0	12	28	31	24	21	12	30

Of the candidate fibres Owens Corning Advantex E-glass Single end Roving type 30 was selected for proof of concept testing. Owens Corning E-glass Single end Roving type 30 was chosen due to its low cost and comparable performance properties in relation to other glass fibres. As presented in Table 11, the fibre has middle of the range to optimal properties in cost, TEX (weight in g per 1000m), width and thickness, Young's modulus, specific modulus and elongation at break. While the glass had slightly lower performance in refractive index (important for UV curing the difference was considered negligible to other glass fibres. Most important however was its supply form, as a single end roving. This allowed for easier integration and design of the creel system for the UVAFP prototype. In order to quantify this assumption and confirm that the single end roving was suitable for AFP and not just its originally intended purpose in filament winding a study of the fibre cross section was undertaken as detailed below in section 4.3.

4.3   Experiment 3: Evaluation of Dry Fibre Tows in UVAFP

Automation systems are centred on repeatable process control. Understanding the uniformity and regularity tolerances of supply materials is vital to designing an appropriate electromechanical systems for any automated system that can repeatedly and accurately undertake a task. Flexibility and adaptability are sacrificed for speed, consistency and repeatability which ultimately drives the process costs.

Figure 54 – Precision Feed End Effector (PFE)

Proprietary processes such as the Precision Feed End Effector, shown in Figure 54 [115], and other broad width material placement systems [94] have been developed as an extension of AFP and ATL and have focused heavily on the supply material geometry, properties and consistent quality particularly due to the large variation seen in the supply material when a prepreg is not used. It seems little reference literature exists on the dimensional properties of dry glass rovings (and perhaps other roving materials) for use in designing machinery to handle such materials particularly for AFP.

In the AFP process where consecutive tow are laid side-by-side and subsequent plies then laid over the top, the dimensional uniformity of the tows are vital for ensuring part quality. In AFP one of the reasons for using towpregs is the tighter dimensional tolerances, uniformity and stability of the preimpregnated tow. This is because any variation in the individual tow dimensions can lead to gaps and laps in the case of the width and fibre volume fraction variation and ply undulating and distortion in the thickness. In both cases the mechanical properties of the composite laminate are diminished and the part performance versus the design model performance is possibly compromised. It was hypothesised that because the selected glass roving was designed for filament winding where tow dimensional accuracy is less critical that the tow would have large dimensional variations. It was further hypothesised that by controlling tension and compaction force the variation could be reduced.

4.3.1 Experiment Aim and Hypothesis

The aim of this experiment was to determine the suitability for dry glass fibre tows for use in the UVAFP process. It was hypothesised that increasing the tension and compaction force of the lay-up process of AFP will reduce the width and thickness variability of dry glass fibre tows. This was done by characterising the effect of AFP process conditions (control factors) on the width and thickness (quality response) variation of the Owens Corning Advantex E-glass Single End Roving Type 30. In order to design a robust creel / tow handling system the goal was to reduce width and thickness variance. In order to produce a high quality final laminate the goal was also to define the optimal tension and compaction settings to control the mean to target nominal dimensions to achieve consistent and uniform tow lay-ups [156].

4.3.2 Experiment Apparatus

The apparatus used in this experiment was designed to simulate loading conditions of the tow during processing in the UVAFP system and allow non-intrusive measurement of the tow. A 10m length tow was used for the experiment, with 10 measurements taken every metre along its length. The width was measured using photographic analysis so that the tow would not be deformed by any physical measurement device (as shown in Figure 61). Thickness was measured using Vernier callipers. The gap between the callipers was set so that the calliper was only touching the tow and not applying any compression in order to minimise compaction of the fibre stack caused by the measurement device.

To provide the tension, the tows were clamped at one end and using a tensile spring scale attached to the other end of the tow a controlled tensile force was applied. Compaction forces were applied by rolling the tows down onto a tool using a compaction roller mounted to a pneumatic compaction cylinder attached to an ABB IRB6600 industrial robot. This setup was designed to be similar to AFP compaction. The roller was a solid Teflon roller of 30mm diameter. The roller compaction force was measured using a JR3 45E15 6-degree load cell integrated within pneumatic compaction cylinder and roller assembly. A very small amount of resin with hardener, Ashland's Derakane 411-350 Vinylester Resin and Ciba Irgacure 819 (IC819) was applied onto the tool surface (less than 10% by weight of the fibre) prior to laying the tow and compacting so that the tow rolled into the resin and was wet-out by compaction and capillary effect. The resin was used simply to bind the fibres in position 'as applied' by the compaction for later sectional analysis. After lay-up and compaction a low-intensity UV broad application mercury-arc lamp was used to cure the resin. The experiment setup is shown schematically in Figure 55.
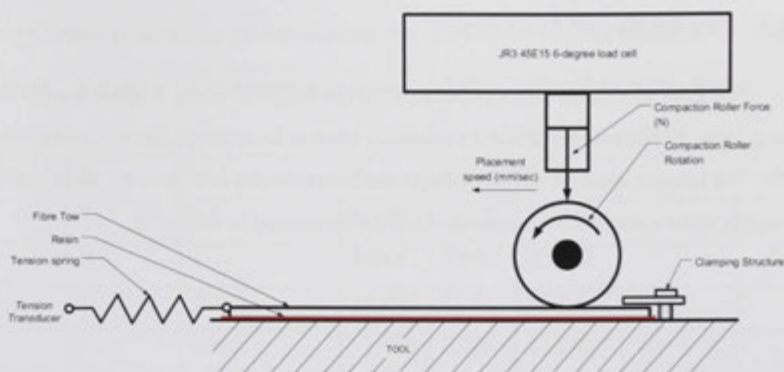
Figure 55 – Fibre lay-up simulation experiment setup

4.3.3 Experiment Method

A design of experiments test matrix was established as a column reduced L16 Taguchi orthogonal array [157] with two dependent variables: the tow width and thickness; and, two independent variables: tow tension and compaction roller force. Four levels for each independent variable were selected. Tensions were varied over a range benchmarked with other AFP systems (as per [63]), from no tension applied, or 0 to 1, 40 and 70 N. Compaction forces were varied from uncompacted, or 0 to 1, 100 or 1000N. Only normal loads (F_z) were measured as shown in Table 12.

4.3.4 Experiment Results and Discussion

The results of the experiment are split into two sections. The first section summarises the fractional factorial experiment according to the L16 Taguchi orthogonal array. The second section includes the gap/lap analysis based upon optimised settings and a prediction of average gap and lap in order to quantify average placement quality.

Average variance and signal to noise ratio variance were analysed and presented. The selection of optimal settings of the tension and compaction to provide a stable and robust process achieving a nominal target width and thickness with minimised variance was also presented. Prediction of the optimised setting effects were made and validated in the gap and lap analysis. Increasing the tension and compaction force of the lay-up process of AFP reduced the width and thickness variability of dry glass fibre tows as hypothesised.

4.3.4.1 Tow Width and Thickness

The fibre tow dimensions of the Owens Corning Advantex E-glass Single End Roving Type 30 showed significant variability even in its original form over the 10m length. The images used for width measurements are shown in Figure 61 and Figure 69. The width measurements were recorded and are presented in Table 12.

Table 12 – Fibre cross-section analysis experiment L16 fractional factorial matrix for tow width

Sample	Tension	Compaction	Mean	StDev	Signal to Noise Ratio (nom)
Units	N	N	$\hat{y}_i$	$\hat{s}_i^2$	SN_{nom}
1	0	0	6.530	0.537	21.702
2	0	1	8.863	0.579	23.693
3	0	100	11.172	1.331	18.478
4	0	1000	11.182	2.795	12.042
5	1	0	6.149	0.383	24.101
6	1	1	5.549	0.009	55.371
7	1	100	6.997	0.003	66.406
8	1	1000	7.975	0.010	57.973
9	40˙	0	5.928	0.160	31.375
10	40	1	5.436	0.003	65.379
11	40	100	6.749	0.001	82.445
12	40	1000	6.709	0.000	83.055
13	70	0	4.929	0.143	30.729
14	70	1	4.329	0.003	63.921
15	70	100	5.885	0.001	75.267
16	70	1000	6.863	0.000	84.526

The '0' tension and compaction levels referred to the static unloaded form. The mean was calculated according to Equation 7 [157]. Where $\bar{y}_i$ is the mean, i is the experiment number, N_i is the number of trials for experiment i and u is the trial number.

$$\bar{y}_i = \frac{1}{N_i} \sum_{u=1}^{N_i} y_{i,u}$$

Equation 7 – Mean calculation of design of experiment data

The mean unbiased variance, s_i^2, was calculated by applying Bessel's correction as per Equation 8.

$$s_i^2 = \frac{1}{N_i - 1} \sum_{u=1}^{N_i} (y_{i,u} - \bar{y}_i)^2$$

Equation 8 – Mean variance calculation for design of experiment data

To analyse the variance and robustness of the dimensional response to the tension and compaction process parameters the signal to noise (SN) variances were analysed. For a "larger is better" goal, the signal to noise ratio, SN_i, should be calculated according to Equation 9 [157] in order to maximise the ratio.

$$SN_{max,i} = -10 \log \left[\frac{1}{N_i} \sum_{u=1}^{N_i} \frac{1}{y_u^2} \right]$$

Equation 9 – Design of experiments signal to noise ratio for maximising the performance of the signal

For a "smaller is better" goal, the signal to noise ratio, SN_i, should be calculated according to Equation 10 [157] in order to minimise the ratio.

$$SN_{min,i} = -10 \log \left[\sum_{u=1}^{N_i} \frac{y_u^2}{N_i} \right]$$

Equation 10 – Design of experiments signal to noise ratio for maximising the performance of the signal

Because the aim of the experiment was to target the response according to a "nominal is best", the signal to noise ratio, SN_i, was calculated according to Equation 11 [157].

$$SN_{target,i} = 10 \log \left[\frac{\bar{y}_i^2}{s_i^2} \right]$$

Equation 11 – Design of experiments signal to noise ratio for achieving a target performance of the signal

The nominal width for a dry tow is 6.35mm or ¼ inch [154]. This width is not only the standard for dry glass rovings but also for slit tapes, towpregs and dry tows of carbon fibre used in AFP today. The results of the study show significant variance from this nominal width, with averages ranging from 4.329mm up to 11.182mm. The Taguchi [156] matrix analysis is shown in Table 13. These results display the effects of the various parameters.

Table 13 – Tow width Taguchi analysis results

	Tension Effect (mm)	Compaction Effect (mm)
$\hat{y}1$	9.437	5.884
$\hat{y}2$	6.667	6.044
$\hat{y}3$	6.205	7.701
$\hat{y}4$	5.502	8.182
Effects	**3.935**	**2.298**
$\hat{s}1$	1.311	0.306
$\hat{s}2$	0.102	0.149
$\hat{s}3$	0.041	0.334
$\hat{s}4$	0.037	0.702
Effects	**1.274**	**0.553**
Rank$_{ave}$	**1**	**2**
SN$_{nom}$1	18.979	26.977
SN$_{nom}$2	50.963	52.091
SN$_{nom}$3	65.563	60.649
SN$_{nom}$4	63.611	59.399
Effects	**46.585**	**33.672**
Rank$_{SN}$	**1**	**2**

The signal to noise ratio of the tow width response to the controls of tension and compaction is shown in Figure 56. The variable with the highest signal to noise ratio was tension. Therefore, ensuring higher tension levels would ensure a stable tow width thus providing for a more robust design and process, reducing variance. In this case the

peak SN ratio occurred at 40N tension, indicating an optimal setting for reduced variance.

Figure 56 – Tow width signal to noise effect response

Likewise, the variable providing the highest average effect, as shown in Figure 57, was again tension. Therefore tension has the greatest effect on the average width of the tow and therefore is the most important parameter in controlling the width to a nominal target. In the case of achieving the 6.35mm or ¼ inch industry standard this implies 40N tension force is required. The variable providing the highest average effect was again tension, meaning that tension had the greatest effect on the average width of the tow and therefore the most important parameter in controlling the width target. 40N was considered quite high as a tow tension for use on concave surfaces, but was not tested in practice on 3D geometries.
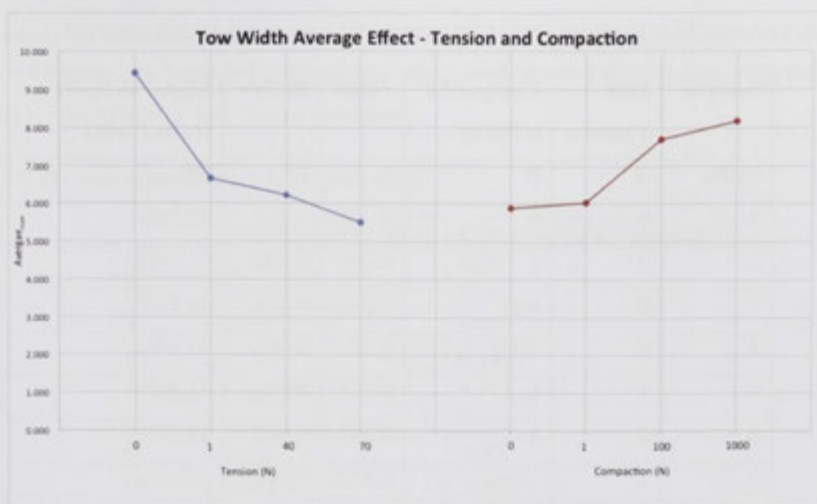
Figure 57 – Average effect response for tow width

The results for the analysis of thicknesses are shown in Table 14. The nominal average thickness of the dry glass fibre tow was determined to be 0.275mm, this is slightly higher than that of current standard AFP materials, which are usually between 0.185 and 0.2mm. The difference can be attributed to the larger filament diameter and high TEX of the chosen single end roving.

Table 14 - Fibre cross-section analysis experiment L16 fractional factorial matrix for tow thickness

Sample	Tow Tension	Compactio n Force	Mean	St Dev	Signal to Noise Ratio (nom)
Units	N	N	$\hat{y}_i$	$\hat{s}_i^2$	SN_{nom}
1	0	0	0.320	0.002	43.243
2	0	1	0.256	0.001	52.148
3	0	100	0.233	0.002	43.124
4	0	1000	0.221	0.005	33.359
5	1	0	0.318	0.003	41.347
6	1	1	0.332	0.002	43.533
7	1	100	0.312	0.001	46.945
8	1	1000	0.290	0.000	71.513
9	40	0	0.325	0.000	63.149
10	40	1	0.308	0.000	69.401
11	40	100	0.291	0.001	54.650
12	40	1000	0.242	0.001	48.433
13	70	0	0.305	0.003	40.641
14	70	1	0.364	0.000	58.412
15	70	100	0.266	0.001	53.829
16	70	1000	0.231	0.002	42.864

Averages for the thickness of the tow varied from as low as 0.221mm to as high as 0.364mm. The Taguchi [156] matrix analysis is shown in Table 18. These results display the effects of the various parameters.

Table 15 – Tow thickness Taguchi analysis results

	Tension Effect (mm)	Compaction Effect (mm)
$\hat{y}1$	0.258	0.317
$\hat{y}2$	0.313	0.315
$\hat{y}3$	0.291	0.275
$\hat{y}4$	0.291	0.246
Effects	**0.055**	**0.071**
$\hat{s}1$	0.002	0.002
$\hat{s}2$	0.002	0.001
$\hat{s}3$	0.000	0.001
$\hat{s}4$	0.001	0.002
Effects	**0.002**	**0.001**
$SN_{nom}1$	42.968	47.095
$SN_{nom}2$	50.835	55.873
$SN_{nom}3$	58.908	49.637
$SN_{nom}4$	48.936	49.042
Effects	**15.940**	**8.778**

The signal to noise ratio of the tow thickness response to the controls of tension and compaction is shown in Figure 58. The control variable with the highest signal to noise ratio was tension, the same as for tow width. Therefore ensuring higher tension levels would ensure a stable tow width thus providing for a more robust design and process, reducing variance. In this case the peak SN ratio occurred at 40N tension, indicating an optimal setting for reduced variance. Notably, from the observably near flat trend for the signal to noise ratio effect observed for compaction, appears that

compaction provides for a very good stability or robustness due to the fact that little variance to the ratio occurred across the tested range.
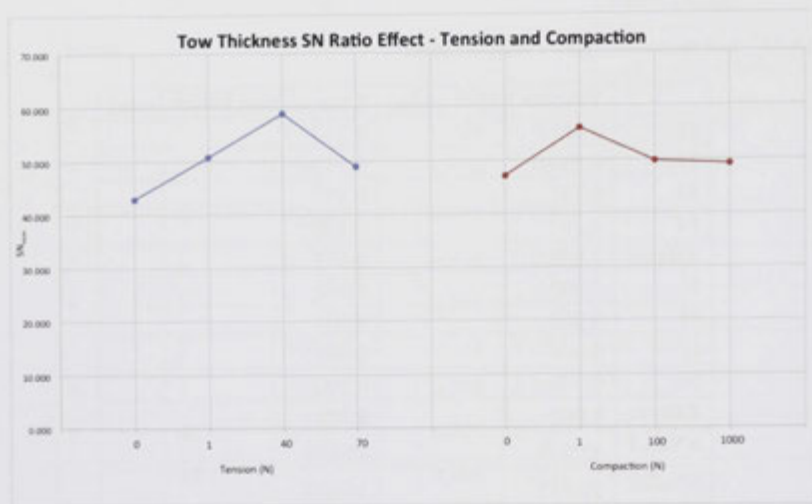
Figure 58 - Tow thickness SN effect response

The highest average effect for thickness was compaction, as shown in Figure 59. This result is to be expected given the direct action compaction has on a materials thickness. Therefore compaction is the most important parameter in controlling the thickness of a tow to a nominal target. In the case of achieving 0.275mm thickness a compaction of 100N is required.

Significant to any composite processing is the permeability of the fibre stack or tow. The results indicate shuffling and reorganisation of the fibre packing under the various load conditions as reflected by the change in dimensions. By increasing load cases tighter and tighter fibre packing occurs. This packing while good for higher fibre volume fractions could drastically effect permeability and final laminate quality. An optimal setting that minimises variance, consolidates the tow but does not overload or pack the fibres is therefore an important finding of this experiment.
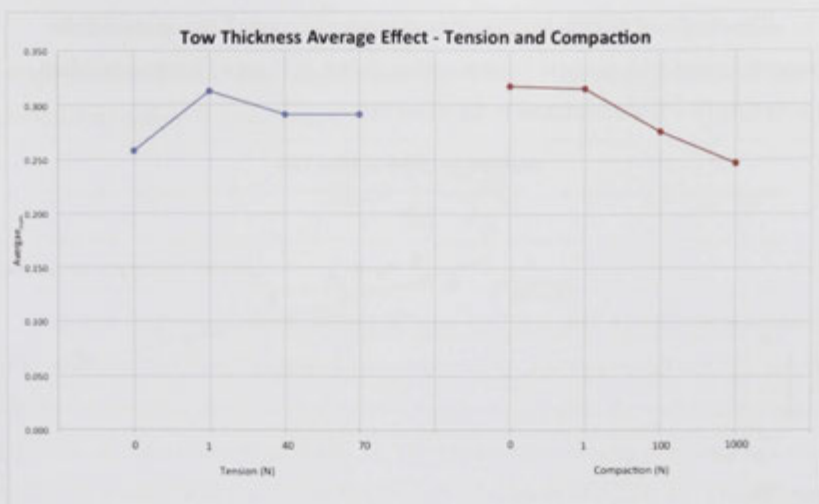
Figure 59 - Average effect response for tow thickness

Using the results of the study the optimal configuration for meeting the nominal width and thicknesses requirements for the AFP system and ensuring minimal variance and robustness are presented as below in Table 16. The optimised settings examining all findings provides that a setting of 40N tension and 100N compaction would provide for the best tow dimensional response.

Table 16 – Optimisation of settings for robustness and control to nominal for tow dimensions

Dimension	Robustness	Control to nominal
Width	Tension = 40N	Tension = 40N
Thickness	Tension = 40N Compaction > 0N	Compaction = 100N

The concomitant relationship between width and thickness of the tow was plotted as shown in Figure 60. Most models investigating fibre spreading show a negative exponential relationship between thickness and width [157][158].

$$y = 0.4241e^{-0.057x}$$

Equation 12 – Thickness vs width of tow exponential trend line

The results of this study showed large scatter according to a second order exponential trend with the best fit relationship shown in Figure 11 only providing an R^2 value of 0.5675 – low correlation to the trend line.
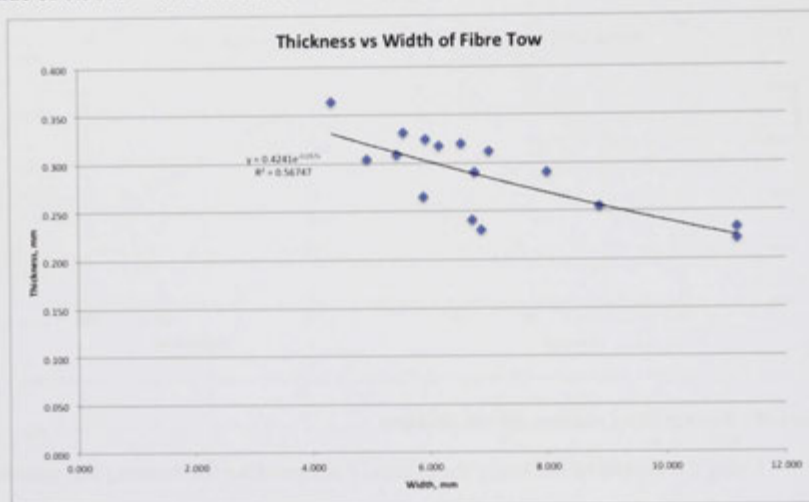
Figure 60 – Thickness vs width of fibre tow and all load (tension and compaction) conditions

The significance of this result is the lack of reasonable correlation between the width and thickness of the tow and the stability of fibre bundle. In an idealised form when a tow is tensioned and compacted by the round compaction roller two mechanisms occur [158]. Initially the upper most layers of fibres are forced downwards into the bundle of lower fibre layers and secondly the lower layers spread outwards, widening or spreading the overall tow dimensions. The overall result is a thinner, wider tow.

In order to validate the study predictions and verification tests were performed, this was done by assessing the contributions of the optimised variable levels. The average of the average was also calculated; this was done according to Equation 13.

$$\bar{T}_{\bar{y}_i} = \sum_{u=1}^{N_i} \frac{\bar{y}_i}{i}$$

Equation 13 – Average of the averages

In this study the $\bar{T}_{\bar{y}_i}$ was calculated to be 6.953 and 0.2993 for the average of the average width and thickness measurements respectively. The average SN ratio was calculated according to Equation 14.

$$\bar{T}_{SN} = \sum_{u=1}^{N_i} \frac{SN_{nom}}{i}$$

Equation 14 – Average SN ratio

In this study the $\bar{T}_{SN}$ was calculated to be 49.779 and 47.419 for the nominal SN of the width and thickness measurements respectively. The individual variable levels were then subtracted from the average of $\bar{T}$ figures to calculate the individual predicted contributions. This is shown in Table 17. The final optimal setting predicted values produce an average width tow of 6.953mm and a thickness of 0.278mm. The optimal variable levels identified are those that will be used as the pre-set process parameters for first AFP trials, likewise the tow width and thickness values represent the optimised tow dimensions with minimised variance and optimised width that will be used for the tow creel and guide designs.

Table 17 – Predicted contributions of the optimised variable levels

	Variable	Variable Level	Values		Predicted Contributions	
			Average	SN	Average	SN
Width	Tension	40N	6.205	65.563	-0.747	15.784
	Compaction	100N	7.701	60.649	0.748	10.870
				TOTAL	0.000	26.654
OPTIMAL PREDICTION VALUE				TOTAL + T$_{SN}$	6.953	76.433
Thickness	Tension	40N	0.291	58.908	0.003	8.496
	Compaction	100N	0.275	49.637	-0.013	-0.775
				TOTAL	-0.010	7.721
OPTIMAL PREDICTION VALUE				TOTAL + T$_{SN}$	0.278	58.133

Figure 61 – Photographic width measurements of OCV Advantex Single End Roving Type 30 glass fibre tows

Photographic analyses showed stringer fibres in the Owens Corning Advantex E-glass Single end Roving type 30, as can be seen in the close-up of Figure 61 and even Figure 63 where tension and compaction had been applied. While increased tension did not reduce the amount of stringers it improved the uniformity and the stability of the tow bundle reducing the occurrence of further stringing or 'fluffing' when handling the tow which would be advantageous during guidance in the creel system.

Figure 62 – Dry glass fibre tow "straightness" test for single tow placement

Increased compaction force increased the width of the tow band, spreading tows more compactly across a greater distance. This also decreased the thickness of the tow filament stack. The increased compaction force improved the top or bag side surface of the tow. The flatness of the tow top surface and the spread of fibres was much greater, producing significantly less undulations in the laid up tow and overall ply.

Due to the measurements taken, only the rectangular form could be equated for the tow section and therefore no change in the shape could be measured. It was observed that as the tow thinned (or became wider) the uniformity diminished and stray tows and undulations in the density of the filament increased. As the volume of fibres in the filament does not change it would be correct to assume that the thickness most likely tapered at either edge and possible a curved section profile would be observed if samples were sectioned and examined under the microscope. As previously mentioned, the analogy of the Poisson's ratio in the conservation of mass is relevant for tow cross sections given the results observed. Fibre packing within the tow section is optimised by applying a combination of tension and compaction forces to the tow. Tow width and thickness consistency is best controlled through consistent tension and compaction forces. In order to specify such dimensions tow guides that dictate the width would appear to the best strategy for setting the width and thickness. In some instances large variances were seen where the tow as a consolidated pack of fibres was destroyed or placed under compaction forces only. Future work should focus on the examination of the section shape and the movement of filaments in the tow stack.

Figure 63 – Tensioned and compacted fibre tow with a very small amount of resin cured to fixed the stack in the 'as applied' form. Note the gap in the tow and stringer filaments

The results show with increasing tension the width decreases in a linear faction according to the trend line with good correlation, as expressed in the R^2 value of 0.8766 shown in Figure 64. Increasing compaction increased the width of the tow in a logarithmic trend. Linear best fit trending showed poor correlation as expressed in an R^2 value of 0.3509 as shown in Figure 65. These two variable work in opposition on the tow width. On the one hand tension decreases the width and from the variance analysis stabilising the tow width the added compaction works to spread the tow and widen it accordingly.
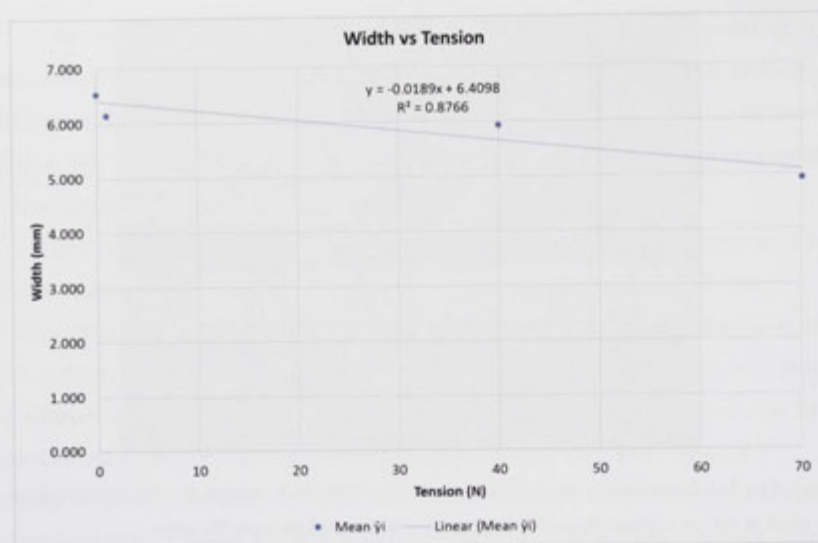
Figure 64 - Width versus tension
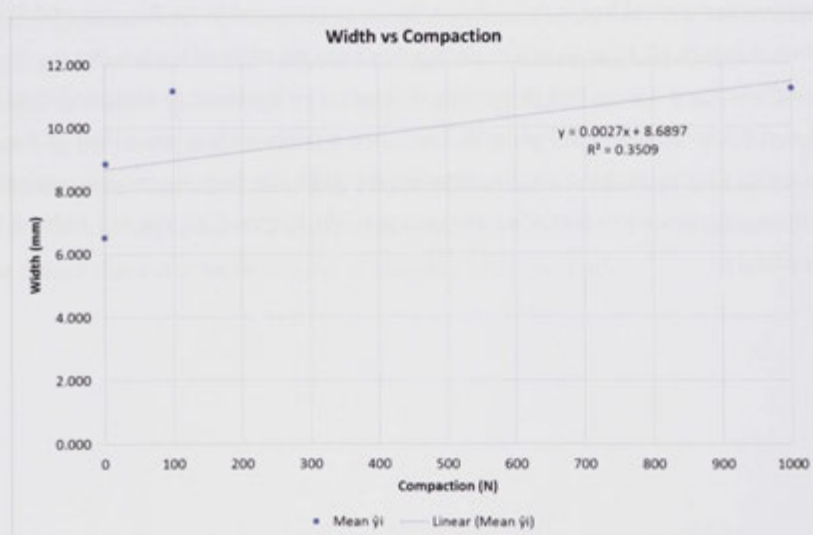
Figure 65 – Width versus compaction

In regards to thickness, tension also works to thin the tow, it is presumed through tighter fibre packing. Compaction likewise thins the tow. The effect of compaction on thickness was observed to be much greater than tension.
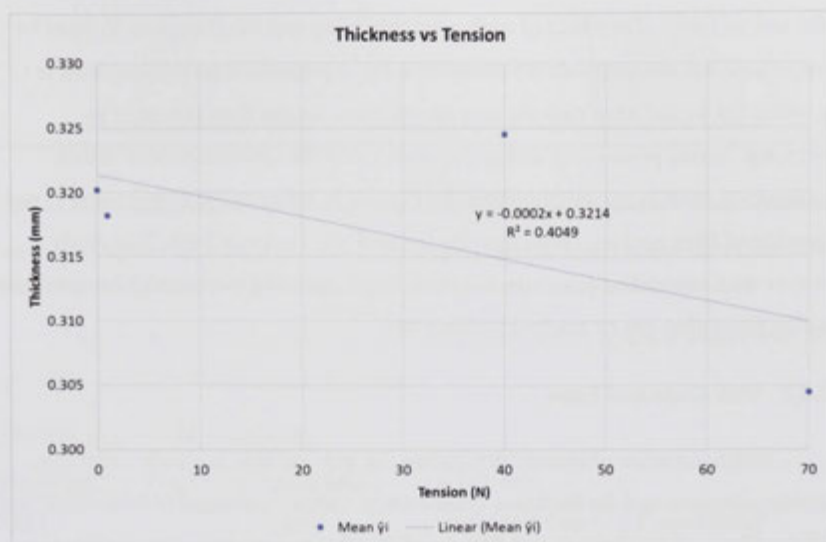
Figure 66 – Thickness versus tension
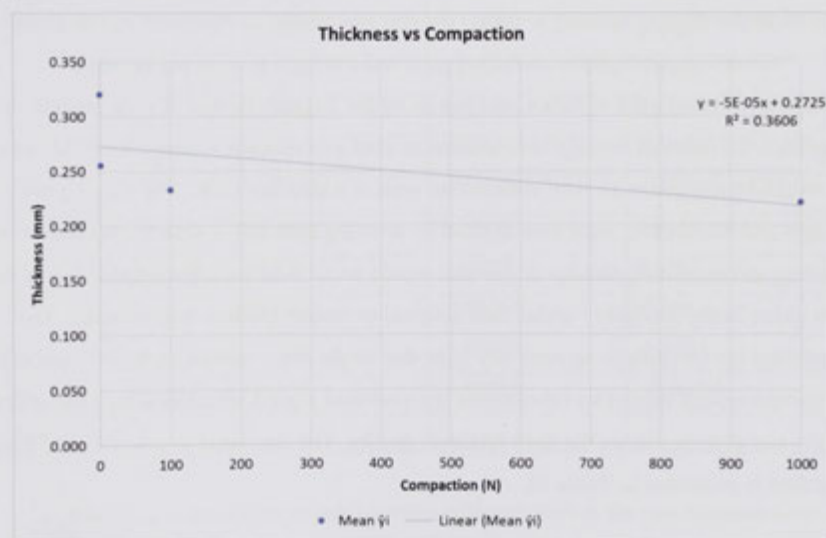
Figure 67 – Thickness versus compaction

The implications of this result to the V_f of the material were not studied in this work. The compression of a fibre tow during consolidation and the reduction in thickness indicates an increased fibre volume fraction and tighter packing of fibres. Therefore with increasing V_f is directly related to the square root of the pressure applied

to the tow or fabric. The effect of such compressibility and the change in V_f must be incorporated into the permeability calculation for impregnation modelling. That is to say, while the V_f and fibre packing may be one form for the fibre tow prior to processing, during processing, compression occurs at the specific point at which impregnation must occur and therefore the V_f must be taken as the compressed V_f and consolidated fibre packing rather than the original tow or fabric form. This study however was undertaken primarily in a static setup, ignoring tension and the maximum packing factor that can be reached within a tow.

4.3.4.2   Tow Gaps and Laps

Width variation ultimately determines the gap and laps in a collimated tow placement process and the thickness cross-section variation ultimately determines non-uniform fibre volume fraction and flatness of the ply lay-ups. Therefore a study was undertaken to predict the average gap and lap occurrences using a nominal (average) tow width for the tow spacing in taking the real tow widths as measured in this study.

Close-up photographs identified gaps and overlaps in most ply lay-ups, therefore, following the variance analysis using the Taguchi design of experiments approach the nominal average tow width was used as a spacing increment for the tows, as would be applied in an AFP collimation system within the CCR. The varying tow widths and thicknesses were then applied by centring each tow within the nominal tow spacing and examining the lap or gap that would occur with the adjacent tow due to the tow either being narrower / wider than nominal or thinner/thicker than nominal. The simulated lay-up analysis ignored any gaps that might occur within each tow itself due to the tow spread caused by compaction but provided a good visualisation of the effect of the tow dimensions on the final laminate quality. The data used to calculate the gaps and laps is presented in Table 18.
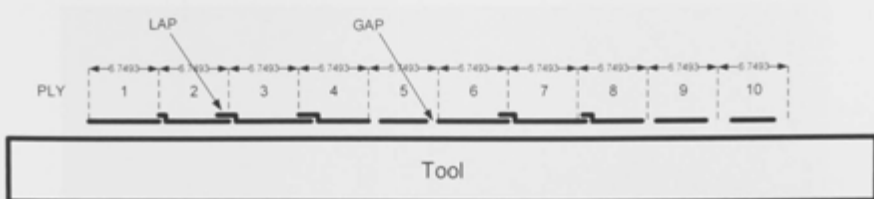
Figure 68 – Gap and lap simulation analysis showing the possible occurrence of the quality defects using the tensioned and compacted tows as per the measurements captured in this study

Figure 68 shows the schematic produced using actual versus nominal data. As can be seen 5 laps would occur and 5 gaps.

Table 18 – Gap and lap analysis data

Mean spacing (Tension & Compaction)		6.7493mm	
Tow	Actual	Individual Gap / Lap (-/+)	Consolidated Gap/Lap (-/+)
Edge			0.00035
1	6.750	0.00035	0.0007
2	6.750	0.00035	0.0257
3	6.800	0.02535	0.0257
4	6.750	0.00035	-0.0078
5	6.733	-0.00815	-0.0078
6	6.750	0.00035	0.0107
7	6.770	0.01035	0.0057
8	6.740	-0.00465	-0.0143
9	6.730	-0.00965	-0.0243
10	6.720	-0.01465	-0.01465
Edge			

The closest gap or lap match between adjacent tows is the gap between tows 1 and 2 at 0.007mm, the largest gap or lap being between tows 2 and 3 and 3 and 4 at 0.0257mm.
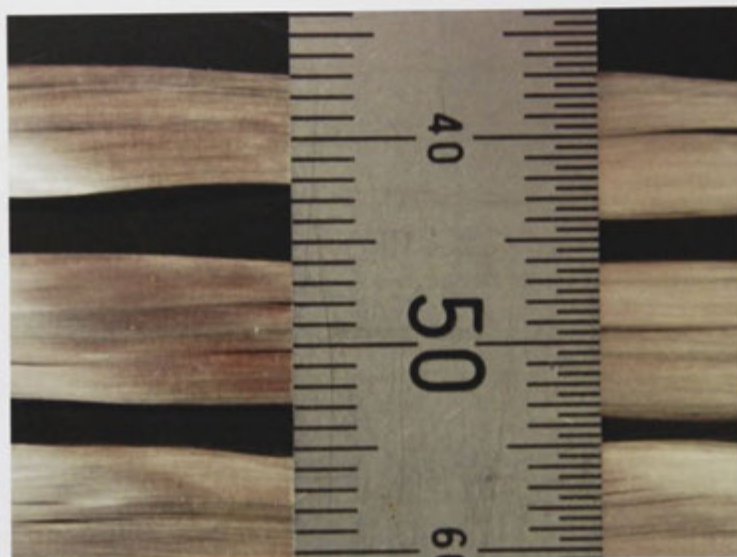
Figure 69 – Close up photographic scale of OCV Advantex Single End Roving Type 30 glass fibre tow analysis

From visual inspection, no width or thickness trend could be identified over the 10m length suggesting that dimensional variation was a short range or local phenomena. Figure 70 shows a trial lay-up of adjacent tows in a short section length (50mm). The gaps and overlaps seen are caused entirely by the width and thickness variations of the tows across short ranges. A combined fibre spreading and fibre coating system to go on the placement head to improve fibre spreading control pre-placement, this was not considered as part of this work but could be made as a modular addition in future work. This would be more complicated, but give more options for resin systems.
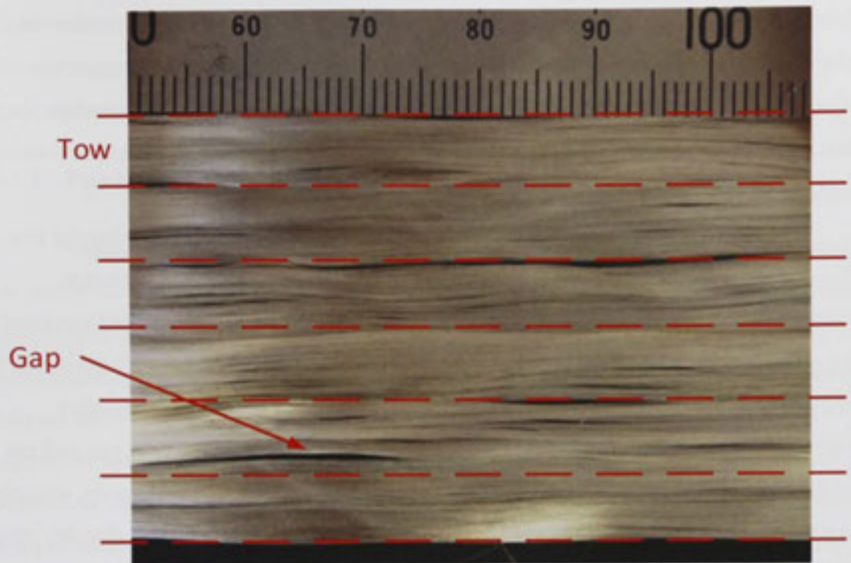
Figure 70 – Dry fibre tow lay-up gap and overlap test samples

Experimental lay-up trials following the simulated gap/lap analysis highlighted other issues in ensuring a well aligned and uniform lay-up. An apparent 'twist' in the tow which caused lofting and a lack of conformance to the part surface as visible in Figure 69 was seen throughout most lay-ups. It was clear from the close-up photos that the twisting presented as waves and kinks in the tows with clear fibre misalignment where the twisting occurred. It is unclear if the twisting was caused by the placement head and if the creel system was successfully handling the twist, however the effect appeared to only be reversible if a counter twist was applied but could often still be observed in wet-out and cured panels even though the effect was significantly reduced by counter twisting and applying tension and compaction during lay-up. For future work an external pull-off bobbin would be a better material supply solution in order to avoid twist.

4.3.5 Experiment Conclusion

The functional tolerance limits for the creel, guide, tension and compaction for the UVAFP prototype were determined from simulation and experimental work. The results of this work shows a maximum possible width and thickness section of 8mm x

0.4mm thick without causing distortion or 'rubbing' of the tow. The optimised settings examining all findings provides that a setting of 40N tension and 100N compaction would provide for the best tow dimensional response. Further work must examine the feasibility of these parameter settings on 3D shapes, especially the tension over concave features to ensure fibre pullup does not occur.

This work also showed that processing conditions can drastically alter the tow dimensions in terms of the width and thickness. This experiment has shown that materials and process can have significant variability leading to dimensional variation in the tow. This has a resultant impact on the design of AFP systems, particularly the CCR and needs to take into account these tolerances in order to produce a high quality repeatable laminate structure. Specifically, width variation can impact the gap and lap of the fibre placed tows and the thickness the fibre volume fraction uniformity, interplay voids and the smoothness and consistency of the plies. The results proved that dry glass fibres may be handled by automation systems so that they can be used in UVAFP. While the argument to use glass came down to cost moreso than properties use of wider band lower cost commodity glass tows could also be used, however they were not available during this work and would have required engineering of a wider, less flexible system that could handle the usual ¼ inch carbon fibre tows.

4.4 Resins

Resin systems come in a variety of chemical families, each with differing chemical and mechanical properties and adopted by different industries according to their needs. These include cost, mechanical performance requirements, resistance to various factors, legislation compliance, etc. In addition to binding the composite structure together, the resin protects the composite from impact, abrasion, corrosion and other environmental factors. In comparison to resins offered in towpregs, liquid resin in bulk form are less expensive than the preimpregnated volume and easier to handle in regards to bulk storage and processing. Furthermore, the options of resins that can be used are vastly increased. Towpreg requires a particular rheology in the resin to ensure the resin will remain bound within the fibres and as such reduces the available options and chemistries. Thermoplastics were not considered extensively in this work due to their cost, inherent difference in performance properties, processing and generally

higher viscosities. The most common resins of the thermoset family used in composite structures are described below, these are polyester (orthophthalic and isophthalic), epoxy, phenolic and vinylester [159].

4.4.1 Polyesters

Unsaturated polyester resins are the simplest chemistry and most economical of the readily available resin systems with long curing times. They are easy to prepare and exhibit good performance for their cost. They are manufactured by the condensation polymerization of various diols (alcohols) and dibasic acids (e.g. maleic anhydride or fumaric acid) to give esters, a very viscous liquid that is then dissolved in styrene, a reactive monomer. Styrene lowers the viscosity to a level suitable for impregnation or lamination. Generally, polyesters exhibit limited thermal stability, chemical resistance, and processability characteristics. Two types of polyesters exist in high volume mainstream production to date, orthophthalic and isophthalic [159].

4.4.1.1 Orthophthalic Polyesters

This general purpose polyester was the original polyester formula developed and remains the lowest cost. It is commonly used in applications where high mechanical properties, corrosion resistance, and thermal stability are not required. Although the upper temperature limit is usually only 50°C, it performs satisfactorily in hydroscopic environments, including sea water, and as such see's significant usage in boat building. However the chemical resistance of the polymer is poor and it is normally not recommended for use in chemicals environments [159].

4.4.1.2 Isophthalic Polyesters

Isophthalic polyesters are an advanced chemistry similar to the orthophthalic polyester backbone but with a denser molecular chemistry and thus having improved strength, thermal stability ($\approx$55°C) and mild resistance to corrosion conditions. Isophthalic resins generally have a slightly higher cost. Improved resistance to water permeation has prompted its use as a gel barrier coat in marine applications. The improved chemical resistance has led the use of this polymer in underground petroleum

tanks (in gas stations) with satisfactory service life. They are also used in applications where contact with salts and mild acids may occur [159].

4.4.2 Bisphenol-A Epoxy

Epoxy covers are a broad family of resin chemistries. The most common are prepared from the reaction of bisphenol-A (BPA) and epichlorohydrin and contain a reactive functional group in their molecular structure. Epoxy resin systems show extremely high three dimensional crosslink density which results to the best mechanical performance characteristics of all the common resins. The most demanding strength/weight applications often use epoxy almost exclusively. It has excellent strength and hardness, very good chemical heat and electrical resistance. Disadvantages include higher cost, processing difficulty including the need for precise resin and hardener ratio control and. often heat curing is required [159].

4.4.2.1 Vinylester

While often categorised as a resin chemistry of its own, vinylester is actually an enhanced polyester polymer. The chemistry is a bisphenol chlorinated, or a combination of polyester and epoxy. If the vinylester is an epoxy combination it is often referred to as a 'vinylester epoxy'. Some advanced vinylester chemistries have also been produced with even further improved properties. It's curing, handling and processing characteristics are similar to those of polyester, but it often exhibits higher properties for mechanical strength, corrosion and temperature resistance. While vinylesters generally cost more than standard polyesters, they are widely used due to their attractive compromise between cost and performance [159].

4.4.2.2 Resin Selection

Hybrid thermal and UV systems were initially considered for the UVAFP prototype, including peroxides, 1,1-di-fe/t-butyl peroxy-3,3,5-trimethylcyclohexane, and sec-isopropyl percarbonate or a combination thereof. This excluded phenolic resins and most polyester resins, however all were quickly discounted due long elevated thermal dwell temperatures needed. In the end, resin options were limited to those resins

known to work with IC819 from prior studies [75] and have the potential to meet the target requirements as outlined in Table 10.

Ashland's Derakane 411-350 vinylester resin was chosen as the system to use in the UVAFP prototype because it provides excellent resistance to wide range of acids, alkalis, bleaches, and solvents. This resin is a bisphenol-A epoxy vinylester and has good toughness, thermal resistance and holds up in corrosive environments. Mechanical properties and good fatigue strength mean that the resin also tolerates heavy design loads and often in assemblies where bearing or fastener load transfer occurs. High elongation and toughness in comparison to standard vinylesters provides better impact resistance and less cracking due to cyclic temperature, pressure fluctuations, and mechanical shocks providing a safety factor against damage during process upsets or during shipping installation. When properly formulated and cured the resin also complies with the United States Food and Drug Authority (FDA) regulation 21 CFR 177.2420, which covers materials intended for repeated use in contact with food [160].

Table 38 [153] in Appendix 3, shows the comparative properties of a number of resins identified for use in the UVAFP prototype. Some of the resin properties referenced are based on thermal catalysts and therefore a different chemistry to that which would be used in the UVAFP system. For example, Ashland's Derakane 411-350 epoxy vinylester resin mixed with Norox brand MEKP-925H Methylethylketone peroxide (MEKP) or equivalent low hydrogen peroxide content MEKP, Cobalt Napthenate-6%, Dimethylaniline, and 2,4-Pentanedione.

Ashland's Derakane 411-350 Vinylester Resin exists in two forms, the baseline chemistry and a higher reactive version that is also clearer than the base chemistry. This next generation of the Derakane line resins is known as Derakane 411-350 Momentum Vinylester Resin. The Momentum series vinylester has lighter colour than the standard Derakane vinylester that makes defects easier to see and correct while the resin is still workable and the has improved reactivity by way of pre-incorporated accelerants yet has a longer shelf life [161].Unless otherwise stated, the base chemistry version Derakane 411-350 Vinylester Resin was used, not the MOMENTUM version so as to eliminate the effect of the accelerant (formulated for thermal cure treatments) on the UV curing.

4.5 Initiators

Catalysts participate in a chemical reaction to increase the rate of that reaction. Unlike other reagents in the chemical reaction, a catalyst is not consumed and less applied energy is required to reach the reaction point, but the total reaction energy from reactants in converting to products does not change. A catalyst may participate in multiple chemical transformations and hence a number of types of catalysts exist for structural resins in advanced composites. The effect of a catalyst may vary due to the presence of other substances, known as inhibitors (slowing activity) or promoters (which increase the activity). Resins may be reacted (cross-linked) either with themselves through catalytic homopolymerisation, such is the case for epoxies, or with a wide range of co-reactants including polyfunctional amines, acids (and acid anhydrides), phenols, alcohols, and thiols. These co-reactants are often referred to as hardeners. Reaction of polyepoxides with themselves or with polyfunctional hardeners forms a thermosetting polymer, often with strong mechanical properties as well as high temperature and chemical resistance. The cross-linking process forms a molecule with a larger molecular weight, resulting in a material with a higher melting point. During the reaction, the molecular weight has increased to a point so that the melting point is higher than the surrounding ambient temperature, the material forms into a solid material. Cross-linking and the chemical reaction of structural resins is usually a thermal process whereby a 'cure cycle' is applied to the resin in order to achieve pre-determined cross-linked properties. Changing the cure cycle often changes the cured properties.

Both catalysts and hardeners can be referred to as initiators. Acting as a trigger for the chemical reaction whether in combination with heat or another mechanism, the initiator is a necessary constituent to the composite structure. Their significance is apparent when changing the initiator changes the properties. Cross-linking reactions other than thermally triggered initiators include photo or radiation reactions whereby the application of certain wavelengths of light or radiation causes a chemical reaction, usually the breakdown of saturant to provide reaction sites to free causing cross linking.

4.5.1 Photo-initiators

Photo-initiated or UV curable resins consist usually of these same multi-functional monomer and oligomer matrices, with small amounts of photo-initiator that generates reactive species upon exposure to UV radiation. These reactive species or sites either occur to cause a cationic or free radical reaction [162].

In cationic reactions, the photo-initiator reacts upon exposure to UV light and ionises. For the photo-initiator to react, it must be exposed to light of the correct wavelength and of sufficient intensity. This creates catalysts or cations as a by-product. By definition, these catalysts promote a chemical reaction to occur that begins catalytic polymerization [163]. These cations promote polymerization of multi-functional epoxides and vinylesters [164].

4.5.1.1 Cationic Photo Reactions

In cationic reactions the catalyst is not consumed in the reaction. Hence, a consequence of this is that UV-curing epoxy adhesives with catalytic photo-initiators can exhibit shadow or dark curing capability, meaning that the cure will continue to progress even after exposure to UV light has ceased. Most conventional cationic-cured UV coatings are based on cycloaliphatic epoxy compounds because they cure faster than glycidyl epoxy type resins. The formulation of cycloaliphatic epoxies has been extensively studied, and they have been shown to be compatible with a wide range of resin types [165].
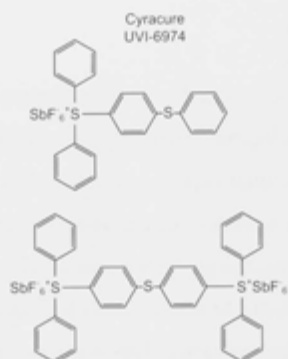
Figure 71 – Structure of a typical photo-initiators, Cyracure UVI-6974, mixed triarylsulfonium hexafluoroantimonate salts
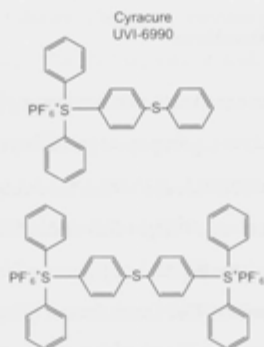
Figure 72 – Structure of a typical photo-initiators, Cyracure UVI-6990, mixed triarylsulfonium hexafluorophosphate salts

Triarylsulfonium hexafluoroantimonate salt (Cyracure UVI-6974) and triarylsulfonium hexafluorophosphate salt (Cyracure UVI-6990) are two highly tested cationic photo-initiators [165]. Another photoinitiator is diaryliodonium hexafluoroantimonate salt (SarCat-CD-1012) [165] [166]. For cationic resin systems full cure can be achieved but cure times are significantly increased due to the poor propagation speeds of 'dark curing'. However it is possible to increase the speed of dark curing by increasing the temperature at which the curing occurs [167].

4.5.1.2   Free Radical Photo Reactions

A second type of photo-initiated reaction results from a free radical curing mechanism. The free radicals are produced as the photo-initiator decomposes when it is exposed to UV light. However, the free radicals are consumed in the adhesive cure process, and propagation continues until the growing chain radical is deactivated by chain termination. Termination occurs when a polymer chain radical reacts with another radical. These systems can therefore only cure where UV light is delivered and more free radicals with unpaired electrons are generated. A majority of UV curing reactions involve such cross-linking of unsaturated monomers by a free radical mechanism. The monomers are generally acrylates or methacrylates. For free radical reactions to effectively occur, at least one of the components being bonded must be UV-transparent in order for the UV light to penetrate and react with the initiator throughout the mixture, hence no shadow or dark cure capability is evident. The soluble photo-initiators require relatively small amounts to be added to the monomers [168]. The optimum concentration of photo-initiator to achieve a minimum cure time depends on the type of initiator and the sample thickness. It has been found that the optimum concentration decreases with increasing thickness [163]. Likewise, the optimum concentrations of the photo-initiator were found to be typically in the range between 0.2% and 0.4% [163] of the weight of the resin [169]. While a wide range of initiators are available, the use of bisacylphosphine oxide (BAPO) is currently seen to be the optimum solution to achieve minimum cure time and maximum conversion for photo-polymerisation of thick samples [169]. BAPO absorbs wavelengths greater than 380 nm and thus allows deep penetration into the material and cure of relatively thick composite laminates. Combination of BAPO with alpha-hydroxy ketones (AHK) was suggested to facilitate both surface and through cure. In these cases resins of epoxy-acrylic nature are blended causing both catalytic and free radical reactions to occur.

Chartoff detailed some important characteristics of these polymers in his thermal analysis of free radical cured photo-initiated resins [168]:

1. The polymers are heterogeneous and have more than one phase present even when only one monomer is involved

2. Because of this heterogeneity they have unusually broad glass transitions

3. The degree of conversion achieved in many UV cured systems is in the 60–80% range due to vitrification, so that considerable residual monomer is often present;

4. Partially cured, vitrified samples contain trapped free radicals that will continue to react slowly;

5. When a partially cured photopolymer is heated above its current T_g a reaction exotherm is evident

4.5.1.3 Hybrid Photo cured & Thermal cured Reactions

Another option in formulation is the inclusion of two types of initiators requiring differing reaction mechanisms so that a dual curing resin is created. In application this may see UV curing combined with thermal curing. Following initial gelation and curing using UV radiation, a relatively quick (up to 30 minutes) post-cure stage [170] can be applied. Resin properties similar to those with a full thermal cure and post-cure have been achieved in a number of studies. This approach may be useful for parts that cannot be exposed directly to UV light during an initial processing or moulding stage.

4.5.1.4 Photo-initiator Selection

Lackey et al. [171] examined the production of glass fibre composites manufactured by filament winding with in-situ UV curing. The system used an in-line resin bath to wet-out fibres which were then wound and cured. Two photo initiators were trialled, including bisacylphosphine oxide (BAPO) and alpha-hydroxy ketones (AHK). Experiments were conducted examining a number of process parameters and the overall effect on material properties. No significant difference was found with respect to the tensile strength. However, specimens with various concentrations of BAPO photo initiator tended to have slightly lower tensile strength than those for specimens with mixtures of BAPO/AHK. Also this tensile strength tended to be slightly lower than those of thermally cured specimens, due to the added through thickness cure advantage of AHK.

For the resin dependant shear strength, more distinct differences were observed by Lackey et al [79]. Decreasing the concentration of BAPO increased the shear strength of the specimen, although still lower than those thermally cured with MEKP.

Specimens cured with a combination of BAPO and AHK had a higher shear strength than those thermally cured with MEKP. This effect was again explained by the better through thickness cure reaction generated by the AHK. Lackey et al. also found that surface finish was influenced by where and when the composite was subjected to UV light. Samples exposed to UV light after winding was completed had a better surface finish than those cured ply-by-ply. This was attributed to the increased surface tension created during the rapid curing of each thin ply and the subsequent shrinkage caused by the rate of cure.

Gupta and Ogale [172] proposed a hybrid solution of acrylate epoxy resin with both a photo-initiator and thermal initiator to combat the issue associated with the opaqueness of carbon fibres to UV light. The authors aimed to address an issue with the thermal and mechanical properties of an established stereolithography process for injection mould and die manufacture. These dies were to be reinforced with carbon fibres but the issue of how to cure resin applied beneath carbon layers remained. The dual curing formulation was successfully demonstrated allow a carbon fibre composite to be manufactured using a sequential UV cure step followed by thermal curing. The UV cure provided stability and greater ease of handling but tackiness and uncured resin remained an issue. The thermal post cure allowed for full cure to be achieved and tackiness of the surface to be eliminated. The application in this instance, fibre reinforced SLA samples was demonstrated allowing for increased thermal conductivity and mechanical performance although the accuracy and repeatability of the process using the fibre reinforcements was limited to poorly controlled wet-out of strip samples.

Previous work in developing UV curable prepregs by Stachurski, Coman and Compston [173] identified Ciba Chemical's (now BASF), Irgacure 819 as a highly reactive curing agent that can cure with exposure to UV light in a matter of seconds. IC819 was selected as the photo-initiator for its low part per hundred (pph) weight requirement, easy solubility and rapid cure. The target for the UVAFP prototype was extremely rapid curing times and it was considered that at such rates there was simply no time available to heat the significant thermal mass of tools.

IC819 undergoes a free radical reaction that causes cure only when exposed to UV light. A fixed ratio of 0.5 wt% of IC819, was used with the chosen resin. The properties of IC819 are summarised in Table 19.

Table 19 – Irgacure 819 property table

Property	Value
Chemical group	Bis-Acyl Phosphine (BAPO)
Chemical name	Phosphine oxide phenyl bis (2,4,6-trimethyl benzoyl)
Colour	light yellow
Form	powder
Particle size	D50 25.46 µm
Melting point	127–133 °C
Specific gravity	1.19 g/cm^3
Absorption peaks in methanol 295	370nm

IC819 is a commercially available photo-initiator and had been successfully proven as the photo-initiator to create a rapid photo-curing resin system in a prepreg sold by Australian Composites as AUSPREG [173]. The patent for the prepreg described the UV prepregging and pre-curing or pre-staging process and offered a number of example resin systems. In the example using IC819 the prepreg was pre UV staged immediately following wet-out by first exposing the prepreg to 4.7 mW/cm^2 for 10 seconds. The pre-staged prepreg was then rolled onto a bobbin and stored ready for later final UV curing. The advantages of a UV curing prepreg meant that prepregging and pre-staging were both quick and energy efficient, later curing was extremely quick (a matter of seconds) and required only low energy UV lamps. The prepreg could be stored for an extended periods (up to 6 months) at room temperature as long as the material was kept from UV light by placing the prepreg into a non-transparent storage bag. The research covered polyester, vinylester, vinylester epoxy and bisphenol-A epoxy resins [173]. While other photo-initiators were examined, including Ciba Geigy Irgacure 184 (1-hydroxy cyclohexyl phenyl ketone), Ciba Geigy Irgacure 654 (benzildimethyl ketal), Ciba Geigy Irgacure 907 (2-methyl-1-{4- (methylthio)phenyl}-2-morpholino-propanone-1), Merck Darocur 1664, Rohm Catalyst 22, Alcolac Vicure 10 (isobutyl benzoin ether), Alcolac Vicure 30 (isobutyl benzoin ether), and Alcolac Vicure-55 (methyl phenyl glyoxylate phenyl ketone), little improvement in cure time

and properties were noted in regards to the final resin dependent mode II mechanical properties.

4.6 Experiment 4: Glass Fibre / Vinylester Composite Mechanical Properties – Strength vs Weight

In this work it is hypothesised that glass fibre and vinylester resin impregnated on-the-fly and cured in-situ will result in lighter and stronger components compared to existing aluminium and steel parts. Aluminium and steel are the current benchmark materials in the construction of automotive and aerospace structures although new aircraft are utilising composites more and more. Fibreglass vinylester composites are a strong lightweight material that are used for many products in industrial applications but less so in mass produced vehicle structures. Applications include, aircraft, boats, bath tubs and enclosures, hot tubs, septic tanks, water tanks, roofing, pipes, cladding, casts, surfboards, and external door skins. Although it is not as strong and stiff as composites based on carbon fibre, it is less brittle, and its raw materials are much cheaper. Its bulk strength and weight are known to be better than many metals, and it can be more readily moulded into complex shapes [174].

Therefore, following the selection of the specific glass fibre, initiator and vinylester resin, a set of trial experiments were undertaken in order to validate the material systems mechanical properties. In order to validate a lighter and stronger material a normalised approach to comparing mechanical properties must be undertaken based on specific weight as per the density. Composite samples were produced using the selected materials and tested for their mechanical properties. Reference material samples were not produced due to the extensive databases that exist listing the standard material properties. In some instances different tests are used to quantify strength and performance between a composite and a metal and therefore sometimes direct comparison cannot be made. Therefore, only the most common and appropriate mechanical properties were tested.

4.6.1 Experiment Aim

The aim of the experiment was to determine the mechanical properties of the chosen composite material system produced mimicking the steps of the UVAFP

process. The properties would then be normalised by weight (density) and compared to traditionally manufactured glass fibre and vinylester (thermal cure using an MEKP catalyst) and the benchmark metals (aluminium and steel) to determine if the glass fibre, vinylester was lighter and stronger than the metals.

4.6.2 Experiment Apparatus

During first commissioning and running of the UVAFP prototype it was noted that resin content and impregnation was hard to control and therefore a Polytetrafluoroethylene (PTFE), otherwise known as Teflon, tool with a machined channel was used for the producing mechanical test specimen samples. This contained the resin and controlled the fibre volume fraction by constraining the sample cross section dimensions and ensured conforming sample dimensions for test specimens. Samples were produced using the Owens Corning Advantex E-glass Single End Roving Type 30 fibre, Derakane 411-350 vinylester with the Ciba Irgacure 819 photo initiator at 0.5 parts per hundred (pph). Fibre tows were hand laid and cut using standard glass scissors to the appropriate length. Resin was applied pre-catalysed with the photo-initiator using a blacked out (to ensure no exposure to ambient UV light until lay-up) fine dose dispenser. UV curing was performed using an OmniCure S1000 spot curing system with a liquid filled light guide and wattages set using a calibrated Exfo R2000 radiometer integrated into the UVAFP system. For the composite reference samples made using thermal cure, the composite was hand laid up and oven cured using a standard fan circulating oven at the ANU, College of Physical Sciences. Mechanical tests were performed on the ANU, College of Engineering Instron 4505 Universal Testing Machine (UTM). Metallic reference samples were not manufactured or tested instead properties were sourced from recognised databases as cited for each material.

4.6.3 Experiment Method

Fibre and resin composite samples were manufactured by in a hand lay-up, ply-by-ply approach. Each ply had the resin dispensed within the tool channel, then the fibre placed and simultaneously consolidated with the resin using a standard hand lay-up compaction roller. Lay-up of fibre and resin quantities were calculated for a target 50% V_f. Efforts were made to compact fibres adequately to avoid fibre waviness by use of

the compaction roller. Following lay-up of the fibre and resin the ply was then cured using the UV spot curing system, passing the light orifice over the channel and at a constant speed. Each ply was exposed to 11.5 W/cm² of UV radiation energy with the spot curing system light guide 20 mm from the surface producing a 20mm diameter exposure area moving at 20mm/sec. This arrangement effectively providing 1 second of exposure, or a step wise determined dose of 11.5 J/cm². On the final ply an additional pass of UV light at a slowed speed of 5mm/sec was made to ensure the highest degree of cure possible. This provided 4 seconds exposure or a dose of 46 J/cm². The samples were built up to the appropriate thickness according to the test specimen requirements for mechanical testing. The channel mould a nominal 7mm width, with a channel depth of 10mm and total tool depth of 25mm placed on top of the 1inch thick hardened steel layup table (Demmeler). This ensured no deflection of the tool surface. A minimum of 5 samples were tested for each property. The mechanical properties tested included weight and strength specific properties such as density, tensile strength and short beam shear strength. All mechanical properties were determined according to the relevant ASTM test method.

4.6.4   Experiment Results and Discussion

The fibre volume fraction was calculated to be approximately 30-40%, lower than the target volume fraction. The reduced V_f is attributed to the retention of resin and restricted resin bleed due to the manufacture of samples in a channel tool. Given the trials did not use the UVAFP prototype, process variables such as compaction force, speed and wattage of the UV light were not optimised. The ideal variables would be determined in future experiments. Nevertheless, the results showed that a composite of acceptable quality could be produced with the process approach based on dry-fibre and liquid resin delivery, and rapid in-situ UV curing.

The achieved mechanical properties of the samples are shown in Table 20. The interlaminar short beam shear strength (sbs), MPa, was evaluated using Equation 15.

$$\tau_{sbs} = \frac{3P}{4wt}$$

Equation 15 – Equation for the calculation of short beam shear strength

Where P is the maximum load, w specimen width and t the thickness of the specimen. Although ILSS depends heavily on void content this test was not performed in this experiment as process quality was not the primary goal in this experiment but rather the material properties themselves, as the actual UVAFP head was not used. Mechanical properties of the UVAFP produced glass fibre and vinylester sample were comparable or higher than a hand laid-up, thermally cured (convection oven, metal tool according to [201]) composite of similar materials. Compared to the metals investigated, the shear strength and tensile modulus were lower but all other properties of strength were higher as normalised by weight (density). The recorded tensile modulus was much lower than expected, raising questions about the V_f and the strain measurement method. No comparable data was readily available for flexural strength and modulus due to the significant difference in material constructions between the Aluminium and Steel and the composite, particularly in thickness. Likewise, directional properties influenced the composite results for these properties and these cannot be compared to the metallic materials in a normalised fashion that would be representative.

Although the ply-by-ply curing approach should reduce cure shrinkage strain through the thickness of the laminate the final longer dose exposure on the last ply could have also caused a non-uniform degree of cure through thickness, again diminishing the shear strength. Possibly by reducing the dose or slowing the cure, higher shear strength can be achieved. Alternatively, the single ply doses could be increased and the final ply dose kept the same as all other plies to ensure uniformity of cure. The inclusion of glass fibres appeared to assist in the penetration and dispersion of radiation energy through thickness with all samples achieving a high degree of cure. No specific degree of cure data was recorded.

Table 20 – UV ply-by-ply cured glass fibre vinylester composite mechanical properties in comparison to thermal cured composite properties and common BIW metals, AA6111 and AISI1008 steel

Property	Density	Short Beam Shear Strength, τ_{sbs} (normalised)	Tensile strength, yield $\sigma_{tensile}$ (normalised)	Tensile Modulus, $E_{tensile}$ (normalised)	Flexural strength, yield σ_{flex} (normalised)	Flexural Modulus, E_{flex} (normalised)
Unit	g/cc	MPa	MPa	GPa	MPa	GPa
Standard	ASTM D792 (A)	ASTM D2344	ASTM D4762	ASTM D4762	ASTM D790M (3 point)	ASTM D790M (3 point)
Dimensions		50 mm (L) x 7 mm (w) x 7 mm (t)	200 mm (L) x 26 mm (w) x 2.8 mm (t)	200 mm (L) x 26 mm (w) x 2.8 mm (t)	10 mm (w) x 2.1 mm (t)	10 mm (w) x 2.1 mm (t)
UV cured GF / VE	1.61	52 (32.3)	222 (137.9)	12 (7.5)	538 (334.2)	17.8 (11.1)
Thermal cured GF / VE [201]	1.62	50.3 (31)	195 (120.4)	12.2 (7.5)	500 (308.5)	16.4 (10.1)
Aluminium 5182-O [208]	2.65	150 (56.6)	130 (49.1)	70 (26.4)		
Steel AISI 1020	7.88	315 (40)	350 (44.4)	205 (26)		

4.6.5 Experiment Conclusion

A glass fibre, vinylester composite cured in-situ using UV photo curing was produced mimicking the UVAFP process steps. The final composite system chosen for the UVAFP prototype is detailed below in Table 21.

Table 21 – Final composite construction

Component	Composition (V_f)	Material
Fibre	40	OCV Advantex Single End Roving Type-30 SE1200
Matrix	60	Ashland Derakane 411-350 Vinylester Resin + CIBA Irgacure 819 (0.5% wt)

The properties of the composite were tested and compared to other structural materials used in automotive structures, namely, the BIW. The benchmark materials, Aluminium AA5182-O and steel AISI 1008 data while generally stronger, in fibre driven properties such as tension the composite outperformed the aluminium. Looking at the density difference however, shows that the composite is lighter than the benchmarks. The density of the glass fibre vinylester composite was much lower than both the aluminium and steel benchmark materials. While the as tested tensile strength of the composite was higher than aluminium it was lower than steel. In design applications were working envelopes are tight and geometry cannot be changed to account for higher normalised properties metals still have the upper hand as the material of choice.

The mechanical properties tested demonstrate that the composite system laid-up ply-by-ply and cured in-situ using UV is a material system with strength properties exceeding metals for automotive applications. While the stiffness of the material system was well below that of isotropic metals, by weight a comparison could be made. Alternatively using the properties in flexural applications such as leaf springs and or energy absorbing structures appears optimal. The material is lightweight and takes advantage of specific fibre direction properties achievable using tailored fibre placement that could out-perform existing metallic materials and be produced in a streamlined automated process.

4.7 Summary

To address the high cost materials currently available for use in AFP applications, a range of low cost raw materials, such as dry glass fibres and bulk intermediate grade resins, were analysed for their suitability to use in UVAFP for in-situ non-thermal curing and on-the-fly impregnation. By using separate dry fibre and liquid resin, not only was it demonstrated that the system is more flexible in offering further material options, but the need for preimpregnated tows was eliminated. Likewise, with the use of new materials that did not require thermal curing processes cycle times, energy consumption was shown to be drastically reduced. The selection of these new materials for AFP requires development of new feed and delivery mechanisms in the prototype as well as the creel system used for material storage and delivery to the placement head [96].

For the in-situ UV curing process proposed for the UVAFP prototype, a UV transparent fibre was selected to avoid the need to use cationic photo-resins and shadow curing. This eliminated the possibility of using more advanced and higher performing fibres such as carbon and aramid.

For the resin and photo-initiator, a number of options were examined to determine the ideal combination of material properties and processability for UVAFP. Keeping in mind the low cost requirement in addition to the design intent that no additional material preparation should be required, an easily mixable resin and initiator combination was selected that undertook a free-radical reaction so that it could be stored in a darkened supply tank ready for use. The final system was a vinylester resin with intermediate properties capable of providing the performance required in most automotive applications. On balance, the vinyl-ester and glass material system provides additional toughness over polyester and is likely to be worth the cost for automotive applications. Glass fibre generally keeps the parts in the realms of semi-structural components

While such a material combination in industry most often sees use in large structures such as marine vessels due to the trade-off of weight and shear volume costs, the development of the UVAFP system for other fibre and resin choices could also be undertaken quite easily in order to expand the scope to more technical and higher performing structures requiring carbon fibre and epoxy composite properties for

example. UV curable epoxies exist, although generally with a slower curing time. Commingling of glass and carbon fibres could also be a solution but will not be considered in this thesis. Likewise hybrid curing systems can also be applied in order to address the lack of UV transparency of other fibres or alternatively using comingled glass and carbon fibre composite structures [175] in order to use the glass fibres to allow for UV penetration. Future work should look at examining such concepts of alternate material options and the possible benefits and limitations. Further, trials using the UVAFP prototype specifically should be performed covering an extensive test matrix of material properties to not only characterise the materials but verify the operation and reliability of the UVAFP head and system.

5 AFP Impregnation Systems and Pre-Processes

Through the findings of Chapters 1, 2, 3 and 4, one of the key issues that has not been addressed with AFP has been the number of individual steps in the manufacturing value chain, both preceding and following the AFP lay-up step. As previously stated, this increases the overall time and cost to manufacture composite materials. In Chapter 4, the selection of a suitable low cost dry fibre and photo-initiated resin that could be used in the UVAFP concept was detailed. The aim of this was to eliminate the need for towpregs by using raw constituents, however, the impregnation process was not discussed or tested. The focus of this chapter is therefore the processes necessary prior to AFP. These include the material supply from the creel and any necessary preparation and impregnation. A novel approach to impregnation is then proposed which occurs on-the-fly, and eliminates the need for pre-impregnating by utilising the continuous application technique of AFP to combine the fibre and resin at the nip point.

Before presenting results and data on impregnation studies and in order to understand the current state-of-the-art in impregnation processes and technologies, a literature review was undertaken and is presented in Section 5.2. This section describes the process of impregnation and consolidation and includes prepregging as well as the current methods of resin impregnation (for example, open, closed and on-the-fly impregnation systems. The merits and drawbacks of each method is discussed in order to benchmark the best solution for a new concept for on-the-fly resin impregnation. Section 5.1 examines the mechanisms of impregnation and the modelling of the process of fibre wet-out. Permeability is examined according to the relevant literature and summarised by the driving metrics that characterise the flow of resin through the fibre. Section 5.3 presents the experimental findings of testing of the on-the-fly impregnation and consolidation concept using resin spraying. In this experiment a number of considerations were made for the novel steps including application technique, management of waste, void and gas evacuation, fibre volume fraction control and the creel system that feeds the dry fibre tows. Finally, in section 5.4 the results of the literature review and benchmarking for the new on-the-fly impregnation process and the

impregnation modelling and experimentation are summarised. The final outcomes in the context of the UVAFP prototype are then discussed and concluded.

5.1   Impregnation of Fibre reinforced Composites

The impregnation of fibre reinforcements (such as glass or carbon fibre) with a matrix material (such as vinylester or epoxy resin) occurs when a pressure difference acts on the resin to force it into the free spaces existing between fibres, at a rate and to a degree that is determined by the permeability. The pressure acting on the resin can be caused by injection pressure, vacuum or even velocity, and at the same time every composite manufacturing process has slightly differing impregnation mechanisms or ranges of the mechanisms that effect impregnation. Complete impregnation by the resin wetting-out the fibre is critical to the quality of the composite. During the impregnation of the fibre, the fibre to resin ratio is defined (otherwise known as the fibre volume fraction). Likewise it is during this process step that air can become entrapped causing voids. The cured ply thickness (CPT) is determined depending on the fibre packing and fibre volume fraction.

In composite manufacturing and impregnation these include resin pressure, tow tension, thickness, surface tension, viscosity and geometry [158].
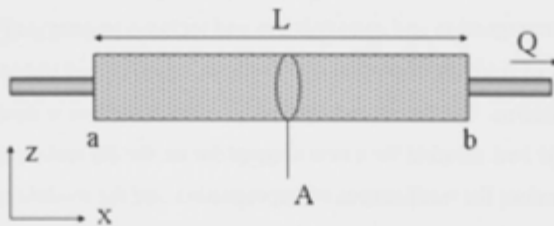
Figure 73 – Schematic section of 1D flow as described by Darcy's law

The permeability of the preform is described by Darcy's law for 1D flow for a given fluid viscosity, μ, (often according to ASTM D2196-10) as explained in Figure 73 and shown in Equation 16.

$$\frac{Q}{A} = -\frac{K\Delta P}{\mu \varepsilon L}$$

Equation 16 – Darcy's law for 1D permeability

Where Q is the flow rate (as measured from the visible macro flow front), A the cross sectional area of the fibre preform, ΔP the pressure difference applied, ε is the porosity, L the length, in the dimension being observed, across which the pressure difference and flow occur and K the permeability factor in the direction of the fluid flow.

Darcy's law only applies in steady laminar flow environments. That is, flows with a Reynolds number typically less than 1, although in some instances laminar flow has been determined with Reynolds number's up to 10. Therefore, in order to check the validity of Darcy's law under those conditions, the Reynolds number must be determined according to Equation 17. Where ρ is the density of the impregnating resin, d is the distance between fibres, v is the fluid intersticial velocity and μ is the resin viscosity.

$$Re = \frac{\rho v d}{\mu}$$

Equation 17 – Reynold's number

The distance between fibres, d, and therefore the porosity, ε, of Equation 16, can be calculated according to the fibre packing arrangement [176].

The main factors driving impregnation are the permeability and process and material pressures. These are discussed separately in the following sections and where appropriate specific and new considerations have been made for mechanisms unique to UVAFP in order to develop a final impregnation model and determine the impregnation time, degree of impregnation and quality of impregnation regarding void removal.

5.1.1 Fibre Volume Fraction and Fibre Packing Arrangement

Geometry plays a significant role in impregnation. The thickness to be impregnated and the width relate largely to the free space available for movement and compression of the tow filaments and the effect this has on fibre packing. Furthermore, the geometry also drives the applied pressure and the effect surface area over which the pressure is applied. The effective cross section dimensions of a fibre tow can be used to determine the V_f of the tow by determining the total rectangular area in 2D and applying a 3D calculation to determine volume. First the area must be calculated according to Equation 18 and then the fibre volume fraction can be determined by Equation 19 using

the number of fibres within the tow and the size of the fibres. Where A is the area, t is the thickness, w is the width, N is the number of fibres in the tow, r_f is the radius of the fibres and V_f.

$$A = tw$$

Equation 18 – Fibre tow cross section area by thickness and width

$$V_f = \frac{N\pi r_f^2}{A}$$

Equation 19 – The fibre volume fraction by the fibre tow cross sectional area, filament number and diameter

The fibre volume fraction can also be determined for a unit area of a laminate, of thickness d, containing n plies of reinforcement with areal weight of w_{areal} as per Equation 20.

$$V_f = \frac{n w_{areal}}{\rho_f d}$$

Equation 20 – Simplified Fibre volume fraction according to areal weight and density

Fibre spreading during processing can have a significant impact on the tow dimensions as the tow cross section changes from circular to rectangular, as previously shown in Chapter 4 experimental results and explained schematically in Figure 74 [158]. The figure demonstrates the change that can occur in a tow due to fibre spreading (A) in an un-spread fibre tow bundle (B) and is flattened with a marked difference to thickness and width.
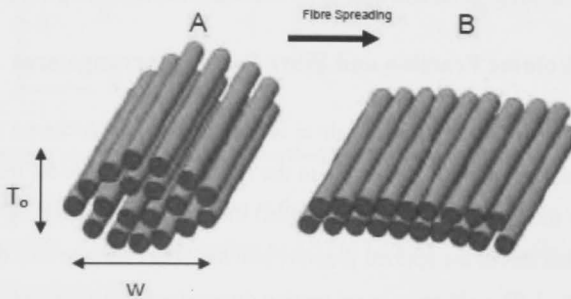
Figure 74 – Fibre spreading (A) in an unspread fibre tow bundle (B) schematic

During spreading the arrangement of the fibres or fibre packing changes, often going from a loosely contained bundle to an ordered and repetitive arrangement. The fibre packing factor greatly influences the calculation of the V_f. The fibre packing factor is an idealised repeated unit cell of incompressible circles (for 2D analysis) of the same diameter representing the fibre cross sections and free space in a thin section laminate (whereby the laminate width is many times larger than the thickness) volume. The arrangement of the fibres is based upon the fabric type and stitching, the compaction pressure the filament diameter and tow width, weight and thickness [176]. Equation 21 [177] shows the formulae used to calculate the V_f according to two different fibre packing arrangements, namely close hexagonal and square array [176]. The idealisations of these common packing arrangements, referenced often in the literature are also shown [177].
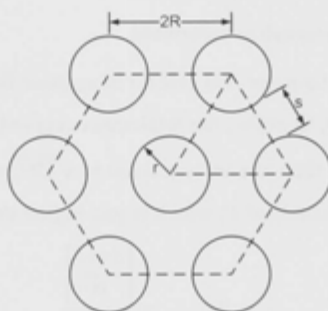
$$V_f = \frac{\pi}{2\sqrt{3}} \left(\frac{r}{R}\right)^2 \qquad \qquad (close\ hexagonal)$$
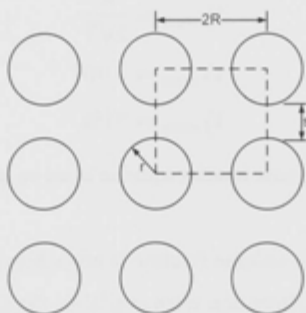
$$V_f = \frac{\pi}{4}\left(\frac{r}{R}\right)^2 \qquad\qquad (square\ array)$$

Equation 21 – Fibre volume fractions for hexagonal and square array fibre packing arrangements

In reality most composite cross sections show a variety of fibre diameters and a somewhat randomised distribution of fibres (as per Figure 75 [177]) and as such fibre packing is usually less than optimised. The theoretical maximum fibre volume fraction that can be achieved in an idealised model is through the hexagonal close packing.
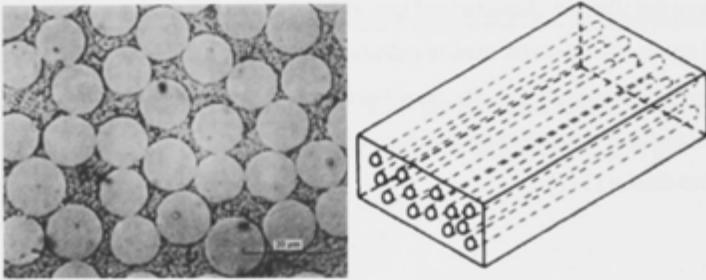
Figure 75 – Fibre packing micrograph and schematic

In the equilateral triangular unit cell for hexagonal fibre packing, the sides are of the length 2R, when d=0, therefore the total area occupied by fibre is equal to three 60° segments. The unit cell then has an area equal to $\sqrt{3R^2}$, so that Equation 22 stands true to for the maximum theoretical V_f which is just higher than 90%.

$$V_{f,max} = \frac{\left[\frac{3\pi r_f^2}{6}\right]}{\left[\sqrt{3r_f^2}\right]}$$

$$V_{f,max} = \frac{\pi}{2\sqrt{3}}$$

$$V_{f,max} = 0.907$$

$$V_{f,max} \approx 91\%$$

Equation 22 – Maximum fibre volume fraction equation based on hexagonal fibre packing idealisation

Of course, such a high volume fraction is not achievable in practice – even if such a high degree of fibre collimation were available, the fact that fibres are touching would result in an ineffective composite where fractures due to lack of binding matrix

could propagate. Of all the manufacturing process filament winding is usually associated with the highest fibre volume fractions due to the high fibre tension and ability to use open impregnation resin baths often with around 70% fibre volume fraction.

5.1.2 Permeability

The permeability of a single fibre tow, multiple fibre tows or plies (otherwise known as a ply stack or preform) describes the porosity or free space between fibres and how the preform allows a fluid to flow through it. Permeability is calculated differently in each direction and effected by different variables. Shotton-Gale (2012, [158]) summarised a number of permeability factor models for both axial and transverse permeability, as presented in Table 22 [158][178][179][180][181][182][183].

Table 22 – Axial and transverse permeability models for composites

Authors	Model for Axial permeability K_x	Model for Transverse permeability K_z
Amico and Lekakou [178]	$K_x = \dfrac{\mu \varepsilon}{P_c} a_h$	
Carman-Kozeny [179]	$K_x = \dfrac{r_f^2}{4k} \dfrac{\left(1 - V_f\right)^3}{V_f^2}$	
Cai and Berdichevsky [180]	$K_x = \dfrac{r_f^2}{8V_f} * \left[\ln\left(\dfrac{1}{V_f^2}\right) - \left(3 - V_f\right)\left(1 - V_f\right) \right]$	$K_z = \dfrac{r_f^2}{8V_f} * \left[\ln\left(\dfrac{1}{V_f}\right) - \dfrac{\left(1 - V_f^2\right)}{\left(1 + V_f^2\right)} \right]$
Berdichevsky and Cai [181]	$K_x = r_f^2 \dfrac{e^{(B(V_A) + C(V_A)V_f)}}{V_f^{(m(V_A))}}$	
Bruschke and Advani [182]		$K_z = \dfrac{r_f^2}{3} \dfrac{(1 - l^2)^2}{l^3} * \left(3l \dfrac{\arctan\left(\sqrt{(1+l)/(1-l)}\right)}{\sqrt{1 - l^2}} + \dfrac{l^2}{2} + 1 \right)^{-1}$ $l^2 = \dfrac{4}{\pi} V_f$
Gebart [183]	$K_x = \dfrac{8 r_f^2}{c} \dfrac{\left(1 - V_f\right)^3}{V_f^2}$	$K_{z,quadratic} = \dfrac{16 r_f^2}{9\pi\sqrt{2}} \left(\sqrt{\dfrac{V_A}{V_f}} - 1 \right)^{\frac{5}{2}}$ $K_{z,hexagonal} = \dfrac{16 r_f^2}{9\pi\sqrt{6}} \left(\sqrt{\dfrac{V_A}{V_f}} - 1 \right)^{\frac{5}{2}}$

Where V_A is the maximum packing capacity of the fibre bundle and r_f is the fibre radius, c is a fibre arrangement constant and is equal to 57 and 53 for quadratic and hexagonal fibre packing patterns respectively and V_f is the fibre volume fraction. μ is the resin viscosity (often according to ASTM D2196-10) and ε, is the porosity. $B(V_A)$, $C(V_A)$ and $m(V_A)$ are maximum packing capacity curve fitting constants.

Other factors can also influence the permeability of the fibre. Sizings can influence permeability. The function of the sizing is to lubricate the fibres to minimize abrasion damage during production. Important to the impregnation process, sizing can influence the surface tension and/or wettability or receptiveness of the resin system towards the reinforcement [185]. The presence of a 'binder' in the fibre bundles can also be an important factor, particularly at the macro flow level [184].The function of the binder is generally to act as a bonding agent to hold the tow filaments together. Binder can be applied to the tow of fabric in different form, most often either yarns or powder. Binder yarns can act as infiltration points through thickness, aiding in transverse permeability. While the presence of the binder powder can also aid infiltration and impregnation it also fills otherwise free space in the tow as well as affecting the fibre packing and geometry by "binding" the fibres together. In most permeability constant calculations the presence of binder is ignored and little information exists in the literature regarding binder permeability impact as a variable except in experimental permeability characterisation studies where the binder is simply considered a part of the fibre tow being tested.

5.1.3 Pressure

During composite manufacturing, a number of different process pressures contribute to the impregnation of fibre with resin, the consolidation and compaction of the composite and in order to form and cure the resin controlling out-gassing and other chemical reaction forces. A number of models have been developed for calculating these pressures (generally covering the capillary pressure and the applied pressures) and their overall effect on impregnation for use in predicting degree of impregnation and wet-out time. These are defined as negative pressures, assisting the infiltration of resin, whereas the entrapped gas pressure is considered to be a positive pressure, inhibiting the infiltration. The pressure also changes as the flow front of the impregnating resin moves

forward. Therefore the pressure differential term, ΔP, can be expressed varying over time as Equation 23 [186], with the entrapped gas pressure, P_{gas}, dependent upon the infiltration radius into the tow bundle which varies throughout the impregnation and the capillary pressure, $P_{capillary}$, and the applied pressure, $P_{applied}$, being constant.

$$\Delta P = P_{gas}(r_i) - P_{capillary} - P_{applied}$$

Equation 23 – The pressure differential equation as developed by Foley and Gillespie

5.1.3.1   Entrapped Gas Pressure

Although not relevant to UVAFP, when comparing to vacuum assisted processes, the vacuum pressure applied during vacuum assisted processes is considered to be contained in the entrapped gas pressure term. If the vacuum is perfect, there will be no air left in the tow to limit the flow front, whereas if the vacuum is less than perfect, air will remain and inhibit the infiltration. If air becomes trapped within a tow the universal gas laws applies to the air. The actual amount of air (gas) will depend on the level of vacuum applied to the materials and how well this vacuum evacuates the initial air entrapped in the tow. The impregnation radius, r_i, will go from a maximum of the tow radius, r_0, to zero as the resin completely infiltrates the tow. Taking the radial equations developed by Foley and Gillespie [186] and applying them to 1 dimensional thicknesses, the entrapped gas pressure is a function of the depth of impregnation according to the initial tow thickness and current impregnation thickness, as expressed in Equation 24. A critical radius of the entrapped bubble is defined as the thickness at which the gas is entrapped.

$$P_{gas} = a^2 b P_{atm} \left(\frac{T_0}{T_i}\right)^2$$

Equation 24 – Entrapped gas pressure at the critical radius as defined by constants a and b

Where a is the proportion of the initial thickness at that point in the impregnation, b is equal to the proportion of entrapped air initially at T_0 which calculates the resulting entrapped gas pressure as a coefficient to the atmospheric pressure when trapped, bP_{atm}. aT_0 is equal to the critical thickness where the entrapped air pressure occurs. Because the entrapped gas pressure changes with the depth of impregnation according to Equation 24 the ideal case of full vacuum or rather no

entrapped air was taken for this work in order to allow an impregnation time to be calculated based on constant pressures during impregnation. This approach was not too far from reality in a void free laminate, in that infiltration was driven axially and the flow front allowed an open escape path for any gas and impregnation occurred entirely in an open environment in comparison to other processes where a vacuum bag might be used.

5.1.3.2 Capillary Pressure

The capillary pressure for a tow and resin combination was described by Ahn and Seferis [187] using a Young-Laplace relationship [158]. In this model the capillary pressure, $P_{capillary}$, is described as a function of the resin surface tension, ζ, the contact angle θ and the equivalent diameter of the pores in the fibre bundle, D_E, as described in Equation 25.

$$P_{capillary} = \frac{4\zeta cos\theta}{D_E}$$

Equation 25 – The Ahn and Seferis model for capillary pressure using a Young-Laplace relationship

In anisotropic fibrous preforms for composites, there is a distribution of porosity pore sizes and shapes, which makes the determination of the diameter of the pores, D_E, extremely difficult. Pore variation and non-uniform distribution leads to "fast tracking" of the resin flow front towards smaller pores and can even lead to resin being "pulled" from previously filled pores. Ahn and Seferis [187] consolidated many of the models and merged all different anisotropic and geometric configurations of materials to form a formula for D_E as described in Equation 26.

$$D_E = \frac{8r_f\varepsilon}{F(1-\varepsilon)}$$

Equation 26 – The equivalent diameter of pores in the fibre bundle as described by Ahn and Seferis

The relationship is a function of the fibre radius, r_f, the porosity, ε, and the form factor, F. The form factor is equal to 2 for transverse and 4 for axial flow for simple 1D flow in a unidirectional fibre material [188]. From this equation it can be seen that that a larger capillary pressure is seen with a smaller contact angle and the smaller the equivalent diameter of the pores (D_E). This being said, smaller equivalent pores have a

lower fluid retention. In many studies [178] axial flow has been proven to by orders of magnitudes faster than transverse, with results documenting up to 19 times faster [189].

5.1.3.3 Applied Pressure

The applied pressure can be calculated as the sum of all process pressures acting upon the tow and resin within the impregnation zone. In most composite processes these are the tow tension, the environment pressure, the resin pressure and the compaction pressure. The total applied pressure is therefore calculated according to Equation 27.

$$P_{applied\ (total)} = \sum \left(P_{tension}, P_{compaction}, P_{environment}, P_{resin} \right)$$

Equation 27 – Total applied pressure in the impregnation zone

5.1.4 Impregnation Models

Impregnation as a process has been the focus of many studies and a number of models exist describing the relationship between the process parameters and the impregnation time and degree of impregnation. Binetruy et al. [190] proposed a model for tow impregnation and the formation of voids within infusion/injection processes such as RTM. They proposed that impregnation occurs at two levels, the macro – between tow fibre bundles, and micro – inside the tow fibre bundle. It was proposed that voids form when the advancement of the impregnation flow front between the two mechanisms are different. The longitudinal flow front differences mean that the edges of the macro front start to come into contact before the micro front can wet-out the fibre and allow gas escape, as described in Figure 76 [158]. The Figure shows the macro flow front accelerate past the slower micro front, top left, then, the micro flow front starts to impregnate inwards at the accelerated macro flow front, top right. The micro flow front then comes into contact from both sides, trapping a void within the micro flow, bottom left, and finally, the void forms, bottom right.
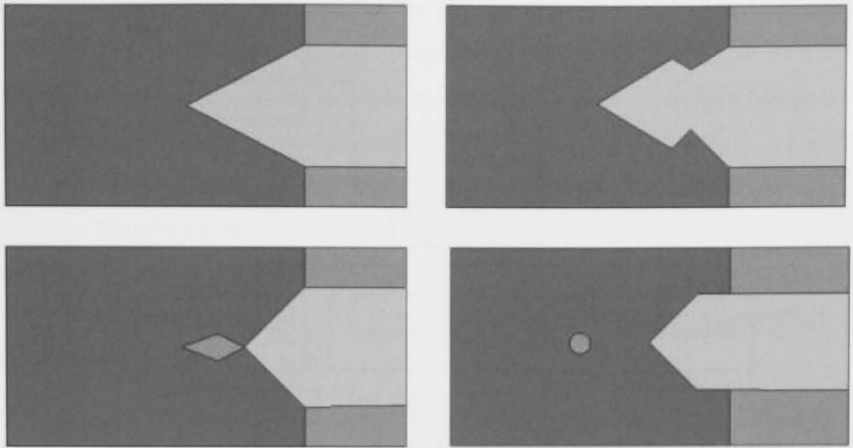
Figure 76 – A diagram showing void formation caused by differential micro and macro flow fronts

Shotton-Gale [158] presented an impregnation model in his dissertation on the design of a 'clean' filament winding impregnation unit. The model considered the various permeability and impregnation parameters governing the impregnation time and degree of impregnation based on the foundation of Darcy's law for fluid flow, as shown in Figure 77. Permeability was considered both in the axial and transverse directions and the pressure functions considered capillary and applied pressure from processing. Shotton-Gale's model was derived from two models previously developed models. The first by Foley and Gillespie [191] and the second by Gaymans and Wevers [192]. The models of Foley and Gillespie [191] and Gaymans and Wevers [192] allow for the theoretical calculation of the residence time versus the resulting degree of impregnation for various methods of impregnation, namely pin-assisted (rolling the fibre tow over a radius introducing a pressure difference in the tow), immersing the tow to utilise capillary pressures and/or applied pressure impregnation techniques.
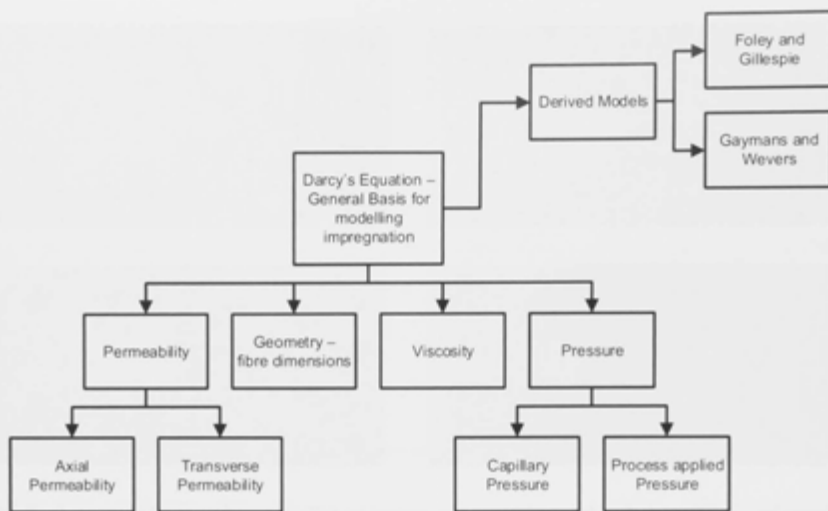
Figure 77 - Schematic illustration presenting an overview of the various models that were considered for the design of the resin impregnation unit

Foley and Gillespie utilised Darcy's law to derive an expression for the rate of impregnation, as presented in Equation 28 [191].

$$\dot{r}_i = \frac{-K_z}{\eta(1 - v_f)r_i} \left[\frac{P_{gas}(r_i) - P_{capillary} - P_{applied}}{ln(r_i/r_0)} \right]$$

Equation 28 – rate of transverse impregnation into idealised circular tows and therefore change in impregnated radius $\dot{r}_i$ according to Foley and Gillespie

Equation 28 defines that the rate of change of the transverse impregnated radial distance in idealised circular tows, $\dot{r}_i$, is defined by the transverse permeability. The Foley and Gillespie model [191] was modified by Shotton-Gale [158] for rectangular fibre bundles is shown in Equation 29, as the integral over time of Equation 28, where the circular radial measurements, r_0, were substituted for thickness measurements, T_0.

$$t_i = \eta(1 - V_f)T_0^2 \left[\frac{c_1^2 \left(\ln\left(\frac{1}{c_1}\right)^2 + 1 \right) - c_2^2 \left(\ln\left(\frac{1}{c_2}\right)^2 + 1 \right)}{4K_y(\Delta P)} \right]$$

Equation 29 – Foley and Gillespie model for impregnation infiltration time as modified for rectangular fibre bundle geometry and a phased time approach to infiltration

t_i is the infiltration time, η is the viscosity of the resin, T_0 is the initial thickness of the fibre tow, are constants, K_y is the transverse permeability and ΔP is the pressure differential. It was assumed that the infiltration takes place over an arbitrary change in infiltration radius or in this case thickness, from $T_i = T_1 = T_0 c_1$ to $T_2 = T_0 c_2$, where T_i is the initial thickness that has been impregnated into the tow and T_0 is the tow thickness. Therefore c_1 and c_2 are constants that can be varied from the tow being empty ($c_1 \approx 1$) to the tow being full ($c_2 \approx 0$).

The degree of impregnation is then calculated for the time phases according to Equation 30.

$$D_l\% = \left[\frac{T_i}{T_0}\right] \times 100$$

Equation 30 – Degree of impregnation as defined by Foley and Gillespie

Gaymans and Wevers also defined degree of impregnation, as shown in Equation 31, where T_i is the infiltration time and T_0 is the thickness [192].

$$D_l\% = \left[\frac{T_i}{T_0}\right] = \sqrt{\frac{2K\Delta P t_i}{\eta \varepsilon T_0^2}}$$

Equation 31 – Gaymans' and Wevers' model for degree of impregnation

Where K is the permeability in the direction being investigated, η is the viscosity of the liquid, T_i is the infiltration thickness, T_0 is the thickness of the fibre tow, ε is the fibre tow porosity and ΔP is the pressure differential.

5.2 Impregnation Systems

In the composite material manufacturing value chain, impregnation is the processing step whereby dry fibres are combined with the liquid resin. This process requires the flow of resin through a fibre stack whether the stack is a single ply of fabric, a single tow or multiple plies that have been preformed. At the same time as flow should occur so to must air and gases be expelled or extracted. The impregnation step can strongly affect the overall process efficiency. Process parameters such as speed, temperature, roving yield, and material waste, along with quality aspects like fibre volume fraction and laminate void fraction, are all directly affected by the impregnation process [193].

5.2.1 Prepregging

Pre-impregnation or prepregging, is the process of impregnation of the resin matrix into the fibre reinforcement either in the form of a woven fabric, unidirectional fabric or even single tow or collimated band tape to form a pre-wet-out and combined composite material in a value added form. The prepreg, as it is often referred, is usually in an uncured or B-staged (semi-cured) state ready for lay-up, consolidation and later complete curing. Prepregs are supplied as either rolls for fabric, bobbins for tows or spools for tape and are the most common material form used in the production of advanced composite structures at the time of writing. Prepregs are laid up, ply-by-ply (or as a continuous tow), consolidated through heat and pressure, placed in a vacuum environment to extract entrapped gases and then cured through the application of a specific cure cycle recipe (usually controlling temperature, pressure and part vacuum). Prepreg materials are generally extremely expensive (in comparison to raw constituent costs). Because the impregnated resin must wet-out the fabric but not run off or drip, which requires particular resin rheology, prepregs can only be formed from a limited number of resins that have been tailored accordingly. Likewise as a continuous process prepreg comes in either a roll with fixed width, tape, slit tape (where wider tapes are slit into thinner tapes) and tows. This restriction in the material options also restricts design choices and often prescribes costs that are beyond what can be justified for the end product. The rheology and pot life of prepreg resins also usually require slow ramp rates in their cure cycles. Further, due to the tack of prepreg and the limited drape of the reinforcement fabrics they require highly skilled technicians to lay them up. For bulk ply lay-up generally only manual lay is adequate, adding significant labour costs. In processes such as filament winding, ATL and current AFP labour costs are removed but speeds are generally much slower than the capability of the equipment (driven mostly by the processing requirements of the prepreg in regards to resin melt) wet-out, flow and compaction.

Figure 78 – Preimpregnating machine using hot melt and knife-coaters / filmers for resin coating

5.2.2 Open Impregnation Systems

The most basic resin impregnation systems are open impregnation systems using resin baths. Resin bath systems can be divided into two main types, drum and dip (Figure 79 [193] & Figure 80 [194]). In the drum type (Figure 79), the dry fibre tows are compacted over a roller drum onto which a resin film has already been applied by partially submersing the drum into the resin bath and using surface tension and a doctor blade to draw up the resin to come into direct contact with the tow. The quantity and thickness of the resin draw is usually controlled by temperature and speed of the drum – working with the rheology and surface tension of the resin. The resin and tow are then compacted at the drum and through additional rollers in later steps to ensure impregnation. Additional rollers downstream of the drum then apply further pressure to impregnate the fibres and then strip excess resin.
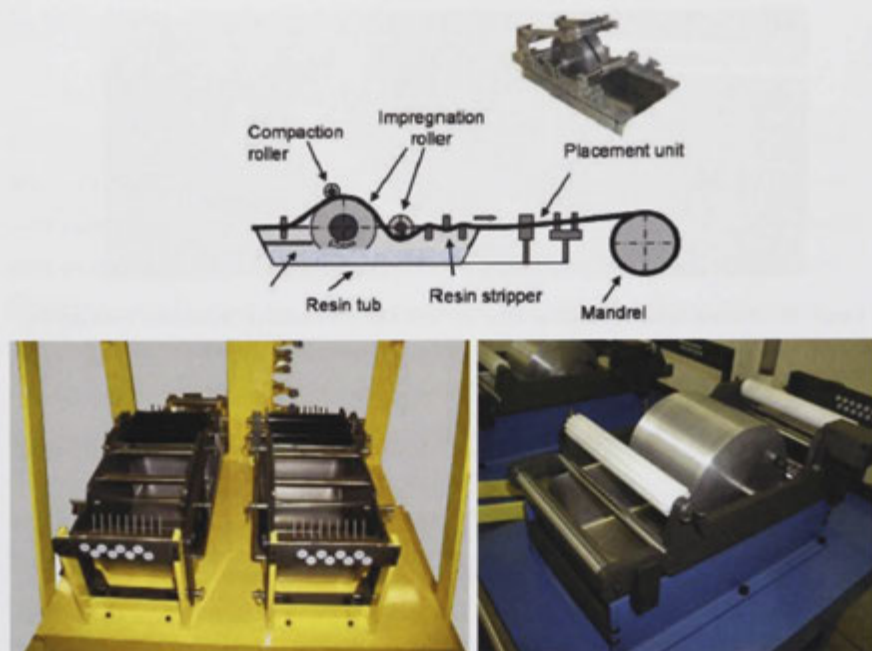
Figure 79 – Drum style resin bath system

In dip-type resin baths (Figure 80 [195]), the tow is dipped below the surface level of a bath of resin. Following dipping, the tow is then drawn through a series of pressure rollers submersed in the bath to impregnate the fibres. The wet tow then passes over a series of smaller diameter rollers out of the bath to complete the impregnation and remove excess resin.
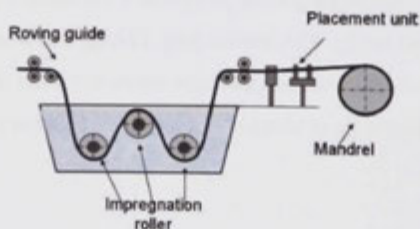
Figure 80 – Dip style resin bath

Another style of impregnation system often used in prepregging machinery is hot melt 'knife coaters' or 'filmers' (as shown in Figure 78 and Figure 81). In these systems

the reinforcement is not actually dipped or drawn through the resin but rather a curtain film of resin is applied to the fibre before passing through a variable gap determined by a doctor blade or knife. As the moving reinforcement moves under the doctor blade or knife the thickness is controlled allowing for the resin content to be determined.
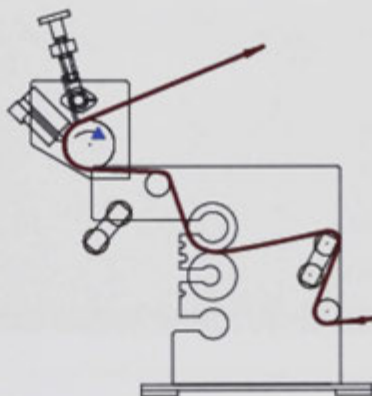
Figure 81 – A knife over roller system.

In order for impregnation to occur a number of consolidation options are available. These include nip rollers, multi-nip rollers and S-Wrapping [196], as shown in Figure 82.

NIP ROLL METHOD OF IMPREGNATION

MULTIPLE NIP ROLL COMPACTION PROCESS

HEATED ROLLS

PAPER
RESIN
FIBER
RESIN
PAPER

FLOW

HEATED ROLLS — Heating and Compaction Zone .125" per Roll Set

"S" WRAP IMPREGNATION PROCESS

HEATED COMPACTION ROLL

PAPER
RESIN
FIBER
RESIN
PAPER

FLOW
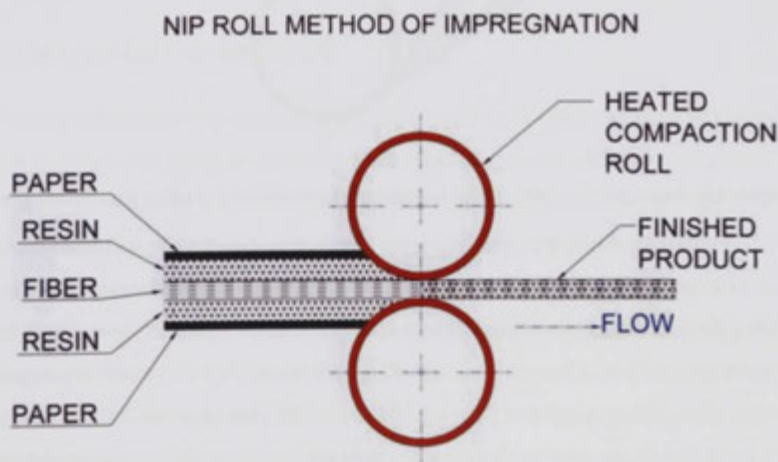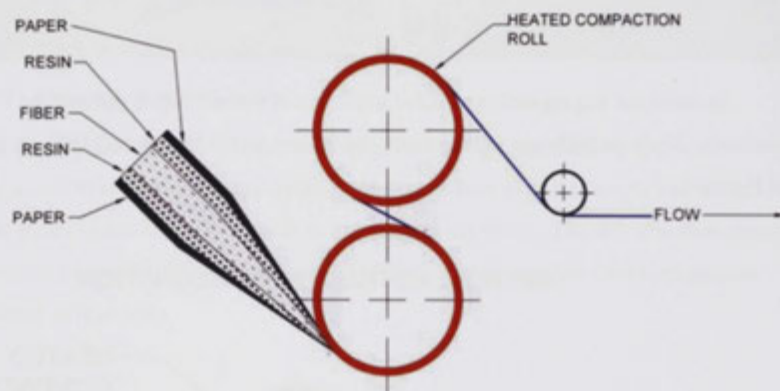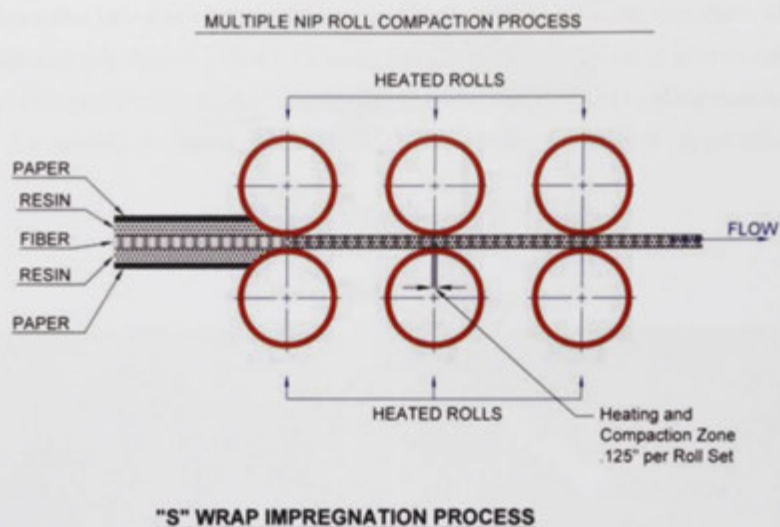
Figure 82 – impregnation options used in prepregging machines including nip roll, multi roll and S

One of the main drawbacks of resin bath and hot melt systems is that the resin's viscosity changes over time as temperature and humidity from the open environment affect the processing parameters. The doctor blade is set while the system is idle, and cannot generally be adjusted while the fibres are being drawn over the impregnation roller. The pulling speed and fibre tension affect the impregnation roller speed, which varies the hydraulic pressure of the resin between the doctor blade and the resin impregnation roller, so there is no possibility to predefine the fibre/matrix ratio.

Figure 83 – A preimpregnating machine used for coating woven and unidirectional textiles such as composite fibre reinforcements

A further disadvantage is that a large surface area of resin is exposed to air, causing a release of monomers into the production environment. The monomers, usually styrene, not only have an impact on the resin's viscosity and pot life, but also raise concerns for workplace health risks associated with volatile organic compound exposure [193].

5.2.2.1 Spraying and Curtain Coating

An open impregnation concept that is often used in the application of gel coats or in bulk wet lay-up is spray coating technology. In some instances this technique is called "spray-up" whereby the resin is sprayed onto the fibre reinforcement either within the tool or in a pre-process step. Spray laminating systems include curtain coating machines as used to produce electronic circuit boards. Curtain coating is an automated method of applying liquid industrial coatings to planar surfaces. During the curtain coating process, a horizontally flat surface passes on a conveyor underneath a steady stream of coating material [197]. This technique of impregnation dates back many centuries but modern process using impregnates and curtain coating machines

dates back to the start of the industrial era in leather impregnation applications (Figure 84 [198]).

Figure 84 – Manual curtain coating being used in leather impregnation

5.2.3 Closed Impregnation Systems

Development in impregnation systems has looked at substituting open resin baths with closed impregnation systems such as siphon systems, closed die pultrusion systems and continuous injection systems [193]. This type of impregnation usually only applies to single tows or multiple collimated tows and direct dosing of resin linked with the speed of the fibre as it passes through the closed system. The fibre/matrix ratio is actively controlled using closed loop systems. Closed impregnation involves a series of steps: the resin is brought into contact with the roving and a pressure difference then forces the resin to flow through the roving. Closed impregnation systems minimise waste and use simple mechanical forces to achieve impregnation. They offer a compact design and seal the impregnation from outside foreign objects as well as keeping the resin volatiles within the composite. With reduced exposure to air, issues associated

with temperature and humidity changes are also mitigated. Closed systems however require regular servicing and the down time associated with disassembly in order to access the closed areas reduces efficiency. Slot-die and knife systems work using this principle, however the application of the resin (in excess) occurs in an open system.

There are two main ways to impregnate a fibre tow in a closed system, one using high pressure and the other, low pressure. A high pressure design requires guiding the tow through a die that has a specific geometry that causes a pressure build-up as resin is injected at high pressure. This consolidates the fibres and resin while at the same time controlling the output fibre geometry, fibre/resin ratio and removal of gases. These systems are used in pultrusion, extrusion and injection moulding. The main disadvantages of such designs are the resin backflow, the fibre abrasion caused by the high compaction as the fibres pass through the die or mould, and the fixed fibre/matrix ratio.
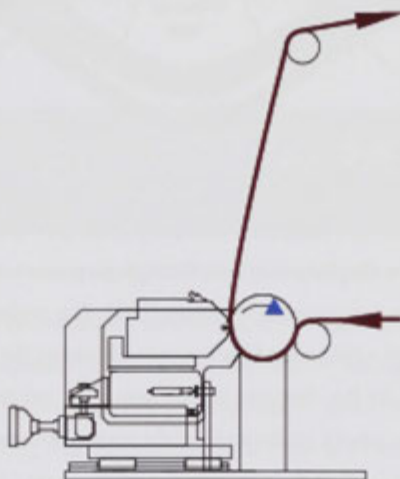
Figure 85 – Slot die film coater

For the closed impregnation of fabrics or broad goods, a variant of the system is slot-die coating, shown schematically in Figure 85 [195]. A slot die gradually reduces in geometry drawing resin in with the fibre at high pressures. This drawing process produces a pressure front causing some impregnation through the fibres. These systems are generally classified as 'filmers', however the difference is that resin is delivered by

a dosing system and the applicator geometry, generally a knife blade, applies resin at the exit. The exit has a controlled thickness to ensure the appropriate fibre content and removing excess resin. These coaters can either impregnate the fibres fully or coat the fibre on one side or both depending upon the slot geometry and resin rheology. Knife applicators generally provide better coating thickness control with less impregnation, while slot dies provide some pressure but thickness control is more complicated. A low pressure design impregnates the fibre by applying a low hydrostatic pressure on the resin and accelerating fibre bed wetting through the action of capillary pressure.
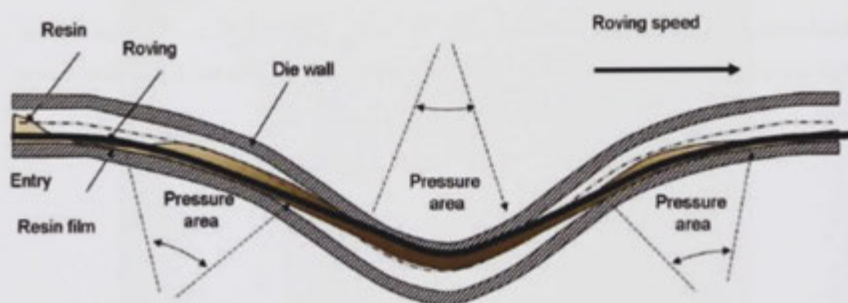
Figure 86 – The siphon closed impregnation system design

One such low pressure design is the siphon impregnation mechanism. Impregnation occurs as a single roving runs through three curves in a closed path as the required amount of resin is injected at the entry [193]. The rovings slide over the curved surface of the siphon and a thin resin film is created between the rovings and the siphon surface. This is induced by the changing siphon geometry and the change to the roving path. The roving tension causes an increase of the resin pressure on the film layer. The fibre pack is impregnated due to the pressure rise on the resin film. The pressure on the resin layer causes the resin to flow through the permeable roving.
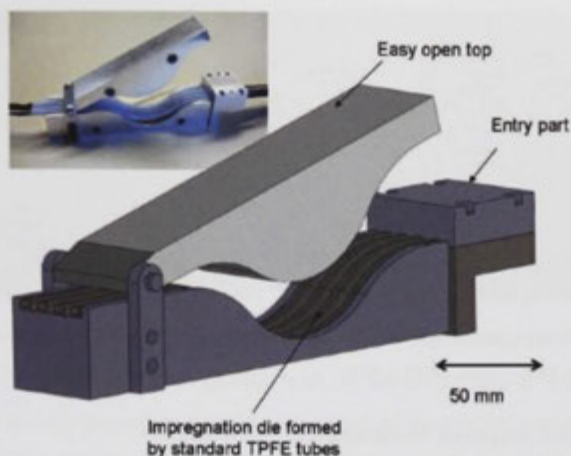
Figure 87 – A siphon impregnation design as produced by Institut fur Verbundwerkstoffe, IVW

The siphon concept was prototyped (Figure 87) and successfully tested by Miaris at Institut fur Verbundwerkstoffe [193] with a wide spectrum of processing parameters.
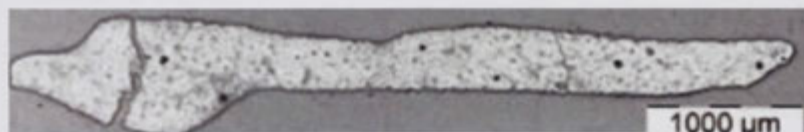
Figure 88 – 24k carbon fibre roving impregnated with the siphon prototype

Figure 88 [193] shows cross sections of carbon fibre rovings that were fully impregnated using the siphon system. One of the main advantages of this impregnation method is the ability to actively control the fibre/matrix ratio simply by controlling resin metering (Figure 89 [193]). The siphon system has also been tested in the pultrusion process, to fully impregnate tows prior to pulling though the die profiles to form the part.
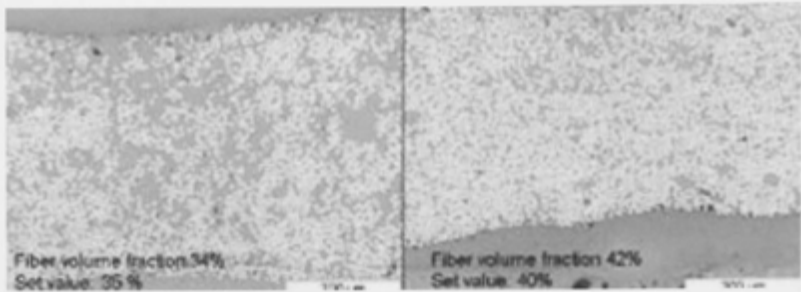
Figure 89 – Metering control applied to the siphon impregnation system to achieve different fibre volume fractions. LHS – 34%, RHS – 42%

5.2.3.1 Liquid Composite Moulding

Liquid composite moulding comprises all composite manufacturing methods where the liquid matrix (e.g. epoxy resin) is forced into the dry preformed reinforcement (e.g. carbon fibre fabric) within the moulding tool that will produce the final component shape. The main objective is to reach a full impregnation as the resin propagates between the fibre bundles and fibres. The impregnation force is usually driven by pressure differences causing resin flow and fibre wet-out. Resin transfer moulding (RTM) utilises positive resin pressures, while in vacuum infusion the pressure of the tool or mould cavity is lower than atmospheric, drawing the resin into the mould. Vacuum assisted resin transfer moulding (VARTM) combines positive resin injection pressures, while the mould cavity is kept under vacuum. Positive resin injection pressure techniques require matched moulding (two or more part moulds) in order to react the resin pressure and are usually contained within large presses to ensure the moulds stay closed. Vacuum infusion processes are usually considered open mould process, with one rigid mould and one flexible membrane (e.g. vacuum bag) as the atmospheric pressure reacts the flexible membrane to ensure consolidation [199].

These impregnation techniques require resins of extremely low viscosities to aid flow as the resin must wet-out in some cases across large distances through the fibre preform. The processes generally suffer from issues relating to air entrapment, dry spots due to fast tracking of the resin or encapsulating of gases and expensive lay-up and tooling costs. Setup time is generally high for infusion type LCM processes occurring within the moulding tool. Likewise for injection processes where impregnation occurs

within the moulding tool also. For production this is a key concern as the moulding tool cycling time is often the critical production bottleneck – limiting production capacity.

5.2.4 On-the-Fly Impregnation

AFP systems currently require a number of preceding processes prior to fibre placement. The mostly costly of these in terms of time and cost is the pre-impregnation step. In order to increase the versatility of AFP and reduce cost it is proposed that these separate value chain steps be consolidated into one process, namely on-the-fly impregnation. By combining impregnation with the lay-up process at the point of application, on-the-fly impregnation takes advantage of the tow by tow, ply-by-ply approach of AFP and the localised compaction that necessarily occurs during in the process. As discussed in Chapter 3, using dry fibre tows and liquid resin is less expensive than preimpregnated materials and is a more stable and versatile form. The variety of resin and fibre combinations can also be increased by removing the need for pre-impregnation and the issues associated with this such as resin rheology, shelf life and tack. In on-the-fly impregnation materials could be stored separately all the way up to the placement head and delivered in the required doses just prior to lay-up, reducing waste and allowing for precise control, even at a localised level for fibre volume fraction variation. The concept of on-the-fly resin impregnation can be applied to both open and closed impregnation processes. However, in contrast to liquid composite moulding where impregnation occurs at once within the tool, on-the-fly impregnation is a continuous process. Examples of on-the-fly impregnation systems include open resin baths, pultrusion and extrusion and the siphon approach. Mills [200] examined in-line pre-impregnating in the creel and the use of binder coated tows. The work addressed three key points: reduced assembly fixture cost and labour time by producing components moulded to net thickness; replacing prepregs with lower cost materials; and use of automatable material deposition processes to achieve higher deposition rates than current machines. This work successfully demonstrated the possibilities of separate resin and fibre feeds that in certain cases could eliminate the need for prepregs.

To capture the advantages and disadvantages of each of the impregnation concepts a desktop study was performed on the current benchmarks, as captured in Table 23.

Table 23 – Resin impregnation advantages and disadvantage options

Category	System	Advantages	Disadvantages
Open	Drum Resin Bath	High throughput	Exposed resin
		Large impregnation surface area	Environment control required
		High impregnation pressures	Sensitive to foreign object damage
		Controlled resin content	Minimum quantity run required
		Minimal air introduction	Mess
		Variable roll width impregnation	Large amount of waste
		Low part count – easier to service	Fume health risk to operators
		Continuous process	Risk of clogging from fibre stringers
			Speed limited due to surface tension used to apply resin film to drum
			Fixed path serial process
			High capital cost
			Large factory footprint
	Dip resin bath	High throughput	Exposed resin
		High tension impregnation	Environment control required
		No air present during impregnation	Sensitive to foreign object damage
		Variable roll width impregnation	Minimum quantity run required
		Controlled resin content	Mess
		Continuous process	Large amount of waste
			Fume health risk to operators
			Risk of clogging from fibre stringers
			Compaction controlled only though tension
			Fixed path serial process
			High capital cost
			Large factory footprint

Film coaters – multi nip rollers	High throughput		Exposed resin
	High tension impregnation		Environment control required
	No air present during impregnation		Sensitive to foreign object damage
	Variable roll width impregnation		Minimum quantity run required
	Controlled resin content		Mess
	Very high compaction and impregnation		Fume health risk to operators
	Continuous process		Risk of clogging from fibre stringers
			Compaction controlled only though tension
			Highest part count, hard to service
			Fixed path serial process
			High capital cost
			Large factory footprint
Film coaters – S-Wrap nip rollers	High throughput		Exposed resin
	High tension impregnation		Environment control required
	No air present during impregnation		Sensitive to foreign object damage
	Variable roll width impregnation		Minimum quantity run required
	Controlled resin content		Mess
	Extremely high compaction and impregnation		Fume health risk to operators
	Large impregnation surface area		Risk of clogging from fibre stringers
	Continuous process		Compaction controlled only though tension
			Highest part count, hard to service
			Complicated fibre routing
			Slower speeds
			Fixed path serial process
			High capital cost
			Large factory footprint
Spray / curtain coating	High throughput		Possible air introduction during spraying / coating
	Flat process path		Environment control required
	Variable roll width impregnation		Sensitive to foreign object damage
	High compaction and impregnation		Fume health risk to operators

		Large impregnation surface area Continuous process Less mess and waste Variable speeds	Regular cleaning required Fixed path serial process High capital cost
	RST	Moderate throughput Impregnation at the tool Any width/size reinforcement Less mess and waste	Possible air entrapment during spraying Requires later consolidation using pressure and temperature Resin
Closed	Pultrusion and Film coaters – slot die	High throughput High tension impregnation No air present during impregnation Variable roll width impregnation Controlled resin content High compaction and impregnation Continuous process Closed impregnation environment	Minimum quantity run required Mess Risk of clogging from fibre stringers Compaction controlled only though tension High part count Speed limited due to surface flow front Fixed path serial process High capital cost Large factory footprint
	Siphon	Closed environment Low mess Low waste Minimal fumes Controlled resin content Low pressure Simple design No moving parts Scalable – single tow to full roll High tow tension Excellent impregnation due to pressure differential siphon Can be applied on-the-fly	Low pressures possible poor impregnation Requires re-tooling for different fabric widths Speed limited Closed die requires downtime for servicing and cleaning Unable to watch or see the impregnation area Recalibration required for different resin viscosities and shear stress

		Metering of only resin required – low minimum quantity	
		Cross section shape variable	

5.3   Experiment 5: The Permeability and Impregnation of Tows using on-the-fly Resin Spraying and Roller Compaction

Many studies have been undertaken characterising the impregnation and through thickness (z-direction) permeability of composite laminates on a global constant parameter basis. A number of models for determining permeability exist as detailed in Table 22 in section 5.1.2. Each model accounts for various process and material parameters in determining the K factor for permeability in the fibre axial and transverse directions. The permeability of dry tows at the point of impregnation in dynamic processes has received remarkably little experimental attention given processes such as filament winding, pultrusion, prepregging and continuous laminating all function under a dynamic but continuous processing configuration and the impact this stage of the composite process has on the final laminate quality.

Characterising the permeability of dry glass fibre tow and determining the impregnation of the tows in the UVAFP process is critical to the development of the UVAFP prototype. In Experiment 3 of Chapter 4, it was identified that significant tow dimensional changes occur during processing according to UVAFP. Specifically the tow tension and compaction force have a significant impact on the tow dimensions and ultimately spreading the tows, increasing the width of the tow over which the compaction force acts, increasing the fibre packing, decreasing the thickness of the tow and increasing the fibre volume fraction, all such changes generally reduce permeability and slow down impregnation [191]. The impact of such changes have not been quantified in regards to their effect on impregnation.

For any AFP type process open impregnation systems such as resin baths would be unsuitable. Because resin baths utilise gravity to contain the resin, generally the system cannot move during operation except along horizontal axes with controlled acceleration and deceleration. This is due to the open bath causing a spill hazard and the difficulty in controlling the resin volume and impregnation quantity during motion. An alternate could be to place the impregnation system as close as possible to the placement head in a location that remains stationary or moves only along one axis. However by separating the impregnation system from the placement system impregnated tows must travel from the impregnation system through the guide systems

up to the nip point in the placement head with wet or uncured resin contacting a large portion of the feed system. Depending on resin viscosity and degree of b staging (if any), any wet fibre however would drip resin during movement and cause serious messing issues.

Most filament winding setups determine a fixed path for fibres from the resin bath to the nip point by mounting the resin bath on the tow guide trolley feeding the rotating mandrel and therefore drips are caught underneath the mandrel. Most filament winding processes are considered messy, leading to specific work to try and develop 'clean' filament winding systems [158]. They also present an environmental hazard for resin contact and fumes [201] as the resin sits in open baths and drip trays releasing VOC's and other solvents into the operating environment.

Coating systems such as knife coaters or curtain coaters that require waste capture and removal are also unsuitable for most AFP applications as these would cause significant design challenges in containment of resin and quality concerns. The siphon system developed by Miaris [193] is considered a good option for application in the UVAFP prototype, but the added size and extra equipment in-line up to the nip point at the same position as the CCR within the end-effector increase the physical design envelope determined in section 3.3 and restricts reach and access. Furthermore, it is still uncertain whether locating the siphon within a moving placement head would cause impregnation issues due to accelerations, decelerations and movement of the resin within the siphon geometry as the placement head moved. While not in existence at the time of undertaking this work, RST demonstrated the potential of spraying technology. However this process still requires post-processing for actual wet-out to occur leaving additional process steps.

Based on the findings of the benchmarking of impregnation systems, a new concept for resin impregnation was conceived using on-the-fly resin spraying and dry fibre placement compaction of the dry fibre and liquid resin using a compaction roller. The concept aims to eliminate pre-processes and post-processing time. The system combines elements of both open and closed impregnation systems by way of applying liquid resin to the tool surface in front of the tow as it is placed and the pressure differential similar to pin assisted impregnation it induces due to the roller, the tow

tension and the compaction pressure. The resin spraying, tow placement and compaction roller concept is shown schematically in Figure 90.
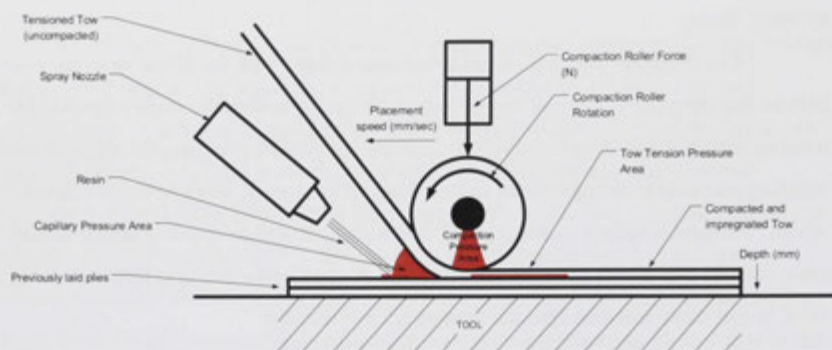
Figure 90 – Resin spraying and compaction roller experimental setup

To aid impregnation and reduce the time for full impregnation three pressure zones were devised within the concept as highlighted in Figure 90. First, pressure is created by the capillary effect as the tow is brought down into contact with the resin already applied to the tool surface. Second, the compaction roller consolidation pressure drives the fibre and resin together. Working simultaneously is the change in geometry as with pin assisted impregnation due to the fibre bending around the roller. This, as with the siphon impregnation system design, the tow tension draws resin into the tow band after the roller. The concept relies on the moving pressure front caused by the compaction roller, the tow tension and the application of resin on the opposite side of the tow to the pressure front. The concept lends from the wet lay-up approach involving first spraying and capillary impregnation then consolidation and compaction. The resin spraying approach ensures accurate metering of only the required resin volume and likewise precise delivery of the resin at the precise location it is required just prior to consolidation.

While optimisation of the process settings has been undertaken previously in Chapter 4 to assess the stability of material for automated handling and feeding, these results need to be validated against an ultimate quality measure of the final product, in this case the degree of impregnation and the impregnation time. The differing

requirements for material stability and ultimate quality need to be balanced in order to determine the operating window of the process while keeping in mind productivity.

5.3.1 Experiment Aim and Hypothesis

The aims of this experiment were to characterise the permeability and process parameters effecting impregnation time for the new concept for on-the-fly resin impregnation during the UVAFP process for the dry glass fibre tows and resin selected in Chapter 4 according to current reference models, validate the model results by experimental trials and understand if the new concept could accelerate impregnation time and quality to produce composites in a faster more efficient manner while maintaining their appealing lightweight and strength. It was hypothesised that by using dry glass fibre tows and on-the-fly resin impregnation, the impregnation time will be decreased in comparison to existing AFP processes when taking into account the total process time for impregnation of the tow or tape prior to loading of the material into the AFP system – comparing the value chain time from raw materials to impregnated composite.

5.3.2 Experiment Apparatus

The experimental apparatus centred on the UVAFP prototype placement head, comprising a fully automated resin spraying system for on-the-fly impregnation. The spray system was comprised of a Spraying Systems Co. small automated stainless steel spray gun (product code B1/8JJAUCO-SS) with a fine spray nozzle for precise dosing (stainless steel nozzle set SU2 with a Fluid Cap 2050, 0.020" or 0.51mm orifice diameter and Air Cap 70, 0.7" or 1.778mm orifice diameter) and a 3.8L stainless steel pressure tank (product code 22140-1-304SS). The spray head was positioned at approximately 60° to the tool surface and a distance of 30mm. The force control system used for the compaction roller included a 6 degree loadcell (made by JR3, model number 45E15), capable of measuring loads up to 1000N for F_x and F_y and 2000N for F_z, with F_z the normal axis to the compaction roller. Applying the compaction force was a Festo high load, short stroke pneumatic cylinder (model ADN-63-25-A-P-A), connected to a Festo proportional pneumatic regulator (model VPPM-6L-L-1-G18-0L6H-V1N). The structure supporting the cylinder stroke and direction included a

mounting frame for high rigidity during compaction and floating platform connected to 4 cylindrical linear bearings to eliminate twist and deflection caused by lateral loads from roller friction and resistance (Figure 33). A Teflon coated steel compaction roller with a 30mm diameter was mounted onto the floating platform. A high intensity spot curing system manufactured by Exfo [202],the S2000 including liquid filled light guide and 5mm orifice was mounted to expose the fibre and resin immediately after compaction within the placement head. The placement head was mounted on an industrial robot, an ABB IRB 6600, which controlled the speed and path of placement. The nip point of the UVAFP prototype is shown in Figure 91, identifying the tow, the resin spray head, the compaction roller and the UV light.

The materials used were the glass fibre tow (Owens Corning E-glass Single end Roving type 30) and vinylester resin (Ashland Derakane Vinylester 411-350) with photo-initiator (Ciba / BASF Irgacure 819) as selected in Chapter 4. These were fed from the creel through a conduit contained in the robot dress pack up to the placement head. Resin was delivered in PTFE vacuum/pressure tubing that was non-UV transparent and fibre was feed through rectangular section flexible tubing 10 x 3mm in order to protect the fibre and maintain its form and alignment to minimise twisting during robot movements. The tooling was a 12mm aluminium plate coated with Frekote 770NC release agent and maintained at a constant room temperature.
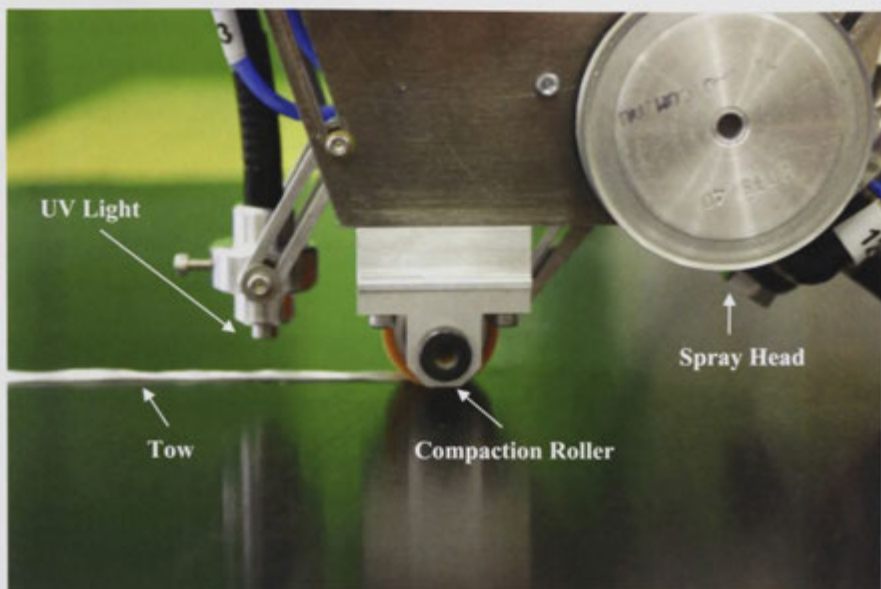
Figure 91 – Resin spray and compaction roller experimental setup

5.3.3   Experiment Method

The experiment method followed the sequential characterisation of the process variables effecting impregnation either according to the models developed by Shotten-Gale [158]. First, the materials were characterised during processing. A design of experiments test matrix was established as a column reduced L16 Taguchi orthogonal array [157] with one dependent variable: the tow area; and, two independent variables: tow tension and compaction roller force. Four levels for each independent variable were selected. Tensions were varied over a range benchmarked with other AFP systems [63], from no tension applied, or 0 to 1, 40 and 70 N. Compaction forces were varied from uncompacted, or 0 to 1, 100 or 1000N. Only normal loads (F_z) were measured.

Following the material characterisation, the process pressures were characterised. All data was then used in the complete models to predict degree of impregnation and impregnation time.

Following modelling, experimental impregnation trials were undertaken to validate the model predictions. A number of commissioning trials were undertaken to "dial in" the experimental method. Different setups were tested during these

commissioning trials and were considered relevant to the outcomes of the experiment and recorded in the results and discussion.

Impregnation trials were performed by feeding the glass fibre tows from the roving in the creel, through to the placement head mounted on the industrial robot to the compaction roller. Within the placement head the fibres were tensioned at the nip point (measured at the pinch rollers within the CCR), resin was sprayed onto the tool just prior to the compaction roller, the fibre and resin were compacted onto the tool causing impregnation.
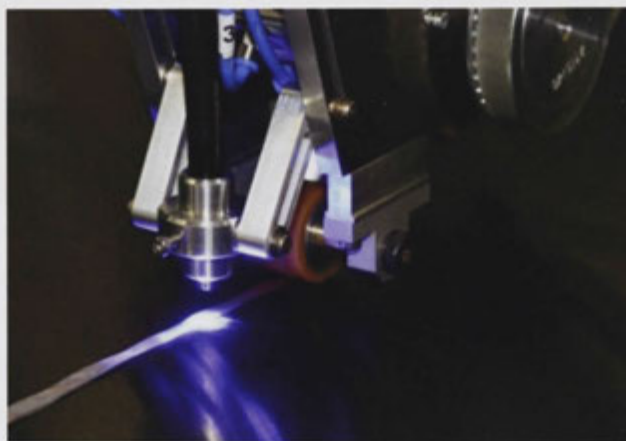
Figure 92 – Fibre and resin placement, impregnation, consolidation and UV curing in-situ using the UVAFP prototype

Immediately after compaction the resin was cured using high intensity UV light from the light guide mounted immediately after the roller. UV light and the curing settings were not optimised in this study. Curing was only undertaken in order to solidify the lay-up for examination of the impregnation quality. The samples were exposed by passing the light guide over the vinylester resin as it was sprayed onto the mould, as shown in Figure 92. The samples had the thickness built up ply-by-ply placing the tows and impregnating with resin simultaneously and curing building up the thickness to 8mm or 6 plies. All plies except the final ply were exposed to approximately 11.5 W/cm^2 and laid at a speed of 10 mm/sec with an exposure area of 20 mm in diameter. This meant that each unit area of resin was exposed to 23 J/cm^2 per

pass. To ensure full cure and that all layers in the sample received at least a dosage of 375 J/cm^2 the robot arm speed was reduced to 1mm/sec for the final ply.

5.3.4 Experiment Results and Discussion

The impregnation characterisation was undertaken according to the model developed by Shotten-Gale [158] based on his modifications to the models by Foley and Gillespie [191] and Gaymans and Wevers [192] in order to convert the formulae from circular tows and circular coordinates to flat tows and rectangular coordinates. All calculations were made assuming a single tow fibre placement application according to the UVAFP prototype. By using dry glass fibre tows and on-the-fly resin impregnation, the impregnation time was decreased in comparison to existing pre-processing combined with AFP lay-up.

5.3.4.1 Fibre Volume Fraction and Fibre Packing Arrangement

To determine the effect of the tension and compaction on the tow cross sectional area, A, a full factorial design of experiments approach was undertaken. The tow area was used as a direct correlation to the tow's V_f by the fixed number of filaments and their diameter as per Equation 19. The test matrix for the experiment is shown in Table 24.

Table 24 – Tow V_f according to tension and compaction test matrix

Sample	Tow Tension	Compaction Force
Units	N	N
1	0	0
2	0	1
3	0	100
4	0	1000
5	1	0
6	1	1
7	1	100
8	1	1000

9	40	0
10	40	1
11	40	100
12	40	1000
13	70	0
14	70	1
15	70	100
16	70	1000

The results of the design of experiment are summarised in Table 25 using the Taguchi approach for determining the variable effects on the cross sectional area. The results show variance from the approximate nominal area of $2mm^2$, with averages ranging from $1.556mm^2$, approximately -22%, up to $2.346mm^2$, approximately +17%. The mean effect $\hat{y}_x$, at each of the 4 different levels for tension and compaction are shown along with the signal to noise ratio of the means at each level $\hat{s}_x$.

Table 25 – Taguchi analysis on tow area due to changes in Tension and Compaction results.

	Tension Effect (mm²)	Compaction Effect (mm²)
$\hat{y}_1$	2.346	1.856
$\hat{y}_2$	2.066	1.841
$\hat{y}_3$	1.794	2.071
$\hat{y}_4$	1.556	1.994
Effects	**0.791**	**0.230**
$\hat{s}_1$	0.261	0.048
$\hat{s}_2$	0.037	0.053
$\hat{s}_3$	0.020	0.063
$\hat{s}_4$	0.045	0.198
Effects	**0.240**	**0.150**
SN$_{nom,1}$	21.952	35.012
SN$_{nom,2}$	39.419	39.094
SN$_{nom,3}$	42.171	32.903
SN$_{nom,4}$	34.553	31.086

Effects	20.218	8.008
Rank	1	2

The signal to noise ratio effect of the tow area response to the controls of tension and compaction is shown in Figure 93 according to a desired nominal. The variable with the highest signal to noise ratio was tension. Therefore, ensuring higher tension levels would ensure a stable tow area; providing for a more robust process and reducing variance. The peak SN ratio occurred at 40N tension, indicating an optimal setting for reduced variance according to a desired nominal area target.
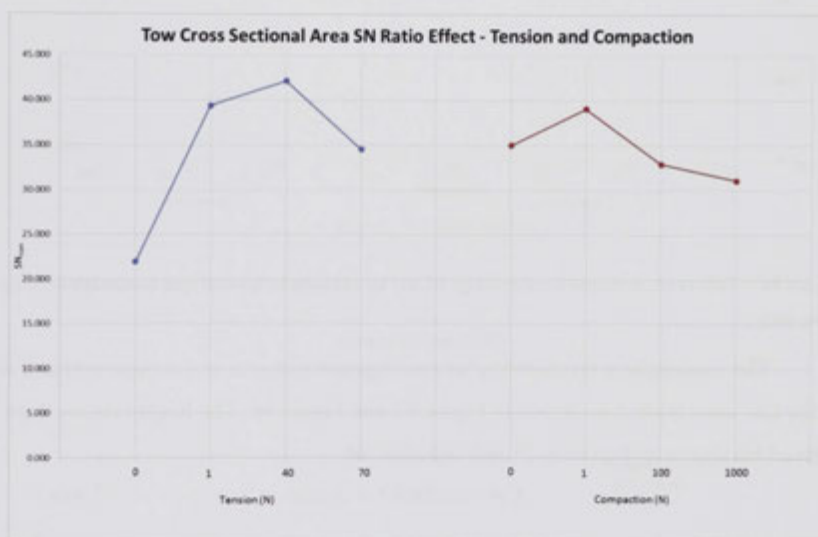
Figure 93 – Tow cross sectional area signal to noise ratio effect correlations for tension and compaction

Likewise the variable providing the highest average effect, as shown in Figure 94, was again tension. Therefore tension has the greatest effect on the average area of the tow and therefore is the most important parameter in controlling the area to a nominal target. In the case of achieving the 2mm^2 area or approx. 45% V_f a tension force of 10.428N is required, according to linear interpolation based on Equation 32.

$$A = -0.007T + 2.073$$

Equation 32 – Tow tension to average area

The variable providing the highest average effect was again tension. This shows that tension had the greatest effect on the average area of the tow and therefore is the most important parameter in controlling the area to a nominal for a consistent V_f.
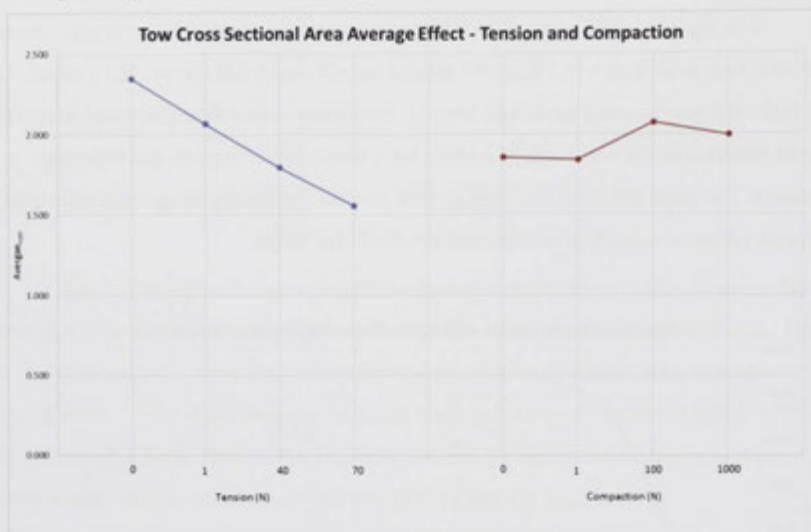
Figure 94 – Tow cross sectional area average effects by changes in tension and compaction separately

The concomitant relationship between tension and area and compaction and area of the tow were plotted as shown in Figure 95 and Figure 96. The linear relationships derived are shown in Equation 35 and Equation 34.

$$A = -0.0066T + 2.038$$

Equation 33 – Area vs Tension of tow linear trend line

$$A = 0.0002F_{compaction} + 2.2964$$

Equation 34 – Area vs Compaction of tow linear trend line

The results showed reasonable to low correlation to the trend for tension – as expected with its higher impact on stability and average effect providing an R^2 value of 0.7863 whereas for compaction the results showed very low correlation if not no correlation, providing an R^2 value of 0.1636, as well as a very low coefficient value (0.0002) suggesting little influence on process stability in terms of controlling the cross

sectional area to a nominal or average figure. This suggests little increase in area with increased compaction force.
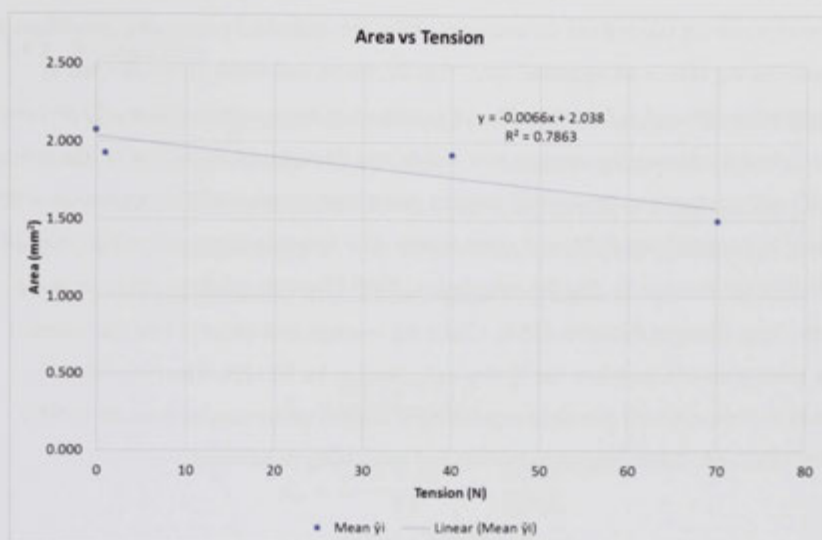
Figure 95 – Area change versus tension
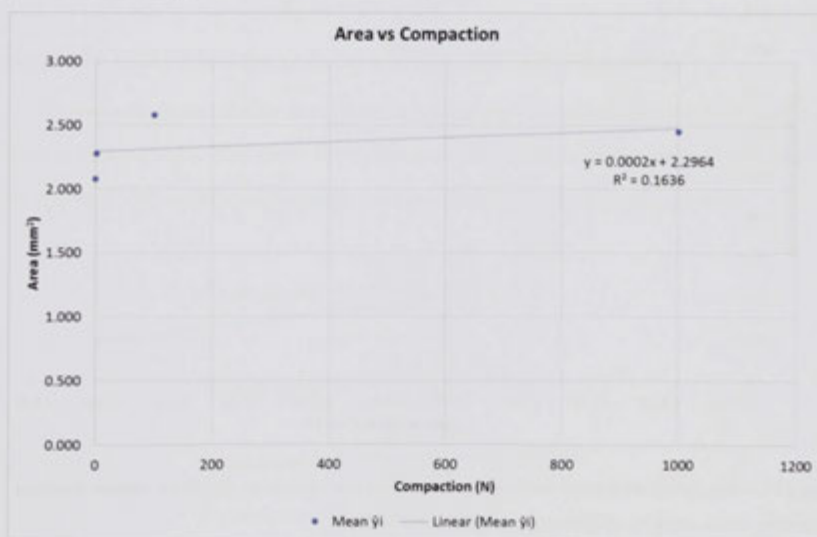
Figure 96 – Area change versus compaction

Dimensional changes related directly to the fibre packing and compressibility of the tow and a relationship to tow tension and compaction was calculated. To determine the fibre volume fraction of the dry glass fibre tow during impregnation, the fibre dimensions were taken from the averages under the optimised processing conditions to determine the tow cross sectional area. The thickness and width data collected in Chapter 4 were used in Equation 18. An average tow cross sectional area of 1.961mm^2 was determined using the average tow widths and thicknesses. Individually, the average width and thickness at the optimal process parameters (tension 40N, compaction 100N) was 6.749mm and was 0.291mm respectively. The area was then used in Equation 19 to calculate the average V_f. For the calculation, 4000 filaments per tow was used along with 17μm filament diameter [154]. Using the average area observed for the selected dry glass tows in Chapter 4, the V_f was calculated to be 46.31%. The calculated V_f correlated closely with previous experimental studies where results from 30 to 50% were achieved, depending upon tooling and processing parameters.
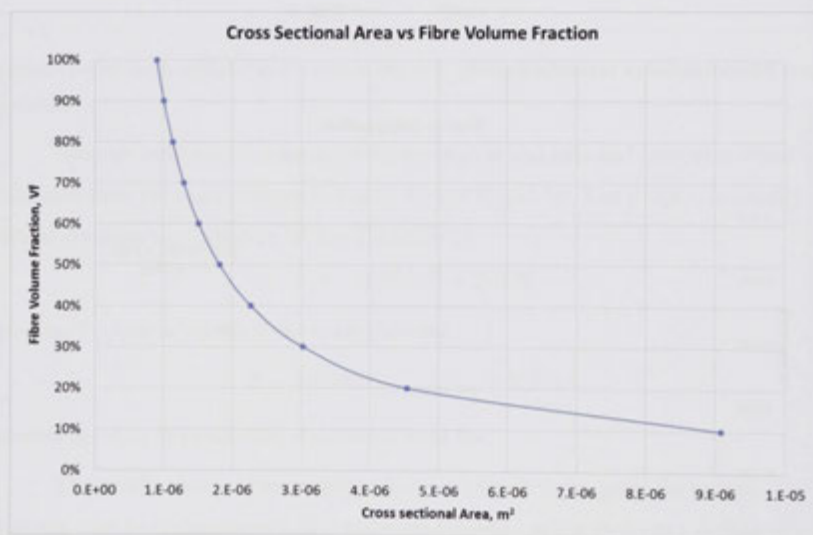
Figure 97 – The calculated cross sectional area of fibre tows based on the fibre volume fraction according to the number of filaments and filament radius.

For the selected glass fibre diameter and TEX, the changing cross sectional area of the tow was plotted according to changing V_f as shown in Figure 97 in order to

understand the areal and volume relationship. As expected, as the area increases and the tow spreads apart, the fibre volume density decreases. The relationship was negatively exponential according to power of 2 of the filament diameter.

5.3.4.2 Permeability

Axial permeability was predicted by applying Gebart's model. The calculated axial permeability is shown below in Equation 35. The fibre radius, r_f was taken as 8.5μm [154]. The fibre bundle architecture was assumed to have a hexagonal and the constant c was taken accordingly as 53 for such a fibre bundle. The V_f was taken as 46.31% according to the results of previous trials in Chapter 4.

$$K_x = \frac{8r_f^2}{c} \frac{\left(1 - V_f\right)^3}{V_f^2}$$

$$K_x = \frac{5.78 \times 10^{-10}}{53} \times \frac{0.155}{0.214}$$

$$K_x = \frac{8.946 \times 10^{-11}}{11.366}$$

$$K_x = 7.87 \times 10^{-12}$$

Equation 35 – Axial permeability as characterised for the UVAFP tow materials

Transverse permeability was likewise calculated according to Gebart's model, as shown in Equation 36. The same fibre radius as well as V_f as the axial permeability were applied. The maximum possible packing factor (V_A) of 0.9 was applied.

$$K_{y,hexagonal} = \frac{16r_f^2}{9\pi\sqrt{6}}\left(\sqrt{\frac{V_A}{V_f}} - 1\right)^{5/2}$$

$$K_{y,hexagonal} = \frac{1.16 \times 10^{-9}}{69.257}(1.384 - 1)^{5/2}$$

$$K_{y,hexagonal} = \frac{1.16 \times 10^{-9}}{69.257} \times 0.0915$$

$$K_{y,hexagonal} = 1.527 \times 10^{-12}$$

Equation 36 – Transverse permeability as characterised for UVAFP materials

Due to the layering application of fibre and resin and the resulting through thickness impregnation that occurs in UVAFP, the transverse impregnation and hence transverse permeability data was used in this study.

5.3.4.3 Viscosity

The viscosity was measured as 350 mPa.sec as measured at room temperature (22 ±2°C) according to ASTM D2196-10. This data point correlated well with the manufacturer published data of 370 mPa.sec as measured at 25°C [162]. The resin viscosity was assumed to be constant throughout processing, even though the UV light application was noted to increase the temperature of the resin and fibre but this mainly occurred after the nip point.

5.3.4.4 Pressure

During the UVAFP process a unique combination of applied pressures exist that had to be understood in order to accurately model the applied pressure. Capillary pressure was of course evident, aiding in wetout along fibres and consequently through thickness and applied to the model using known formulae. The pin impregnation physical model was likened to the nip point of the UVAFP prototype where the compaction roller acted as the pin and the tow is fed at an approach angle and then leaves contact with the roller with tension in the tow. A geometric idealisation of the pressures and forces at play during impregnation are shown in Figure 98.
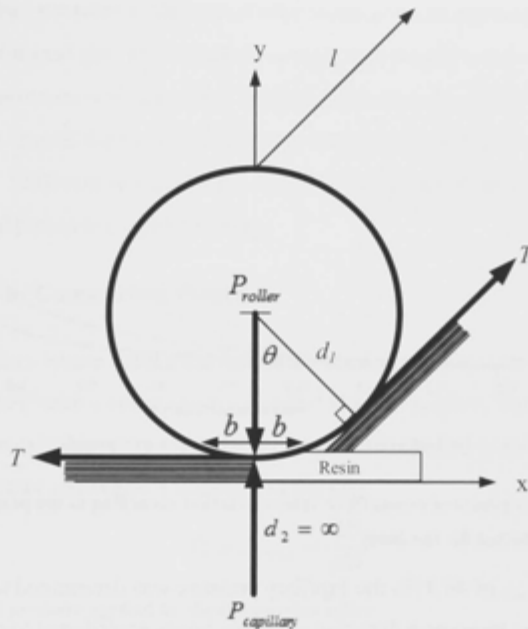
Figure 98 – The impregnation nip point pressure model schematic

Each of the known pressures were calculated accordingly in the following sections and summed in the final impregnation model in section 5.3.4.5.

5.3.4.4.1 Capillary Pressure

The capillary pressure was calculated according to Equation 25 and Equation 26. A calculation of the change in capillary pressure according to the fibre packing volume fraction (inverse of porosity or free space in the dry tow, ε) is shown in Figure 99. For the calculations, the surface tension was assumed to be 44 N/m and the contact angle assumed to be 57° according to the work undertaken by Shotton-Gale [158]. The same filament radius was used as per the permeability calculations 8.5μm [154].
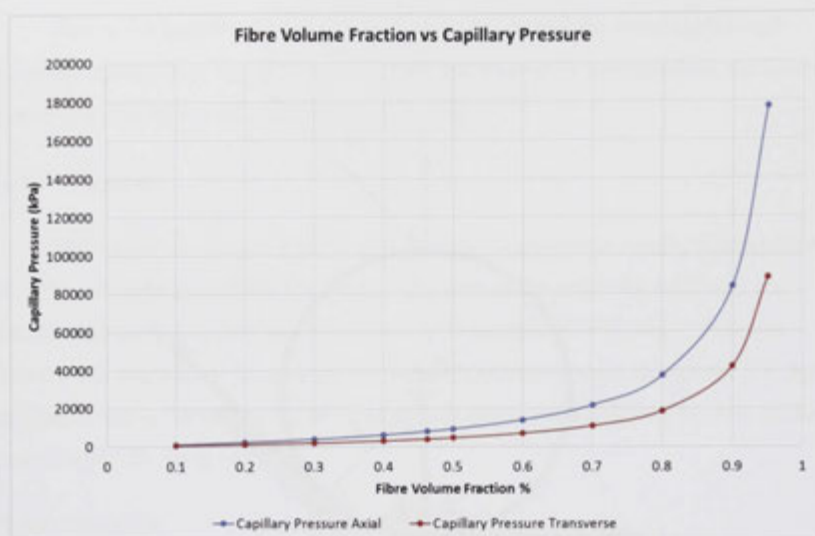
Figure 99 – Capillary pressure versus fibre volume fraction according to the properties of UVAFP and the materials selected for the study

For the $V_{f,dry}$ of 46.31% the capillary pressure was determined to be as below in Equation 37. In the transverse direction capillary forces contributed to a pressure of 4.018kPa and in the axial direction 8.036kPa. As can be seen, the relationship is exactly double from transverse to axial.

$$P_{Capillary} = \frac{4\zeta\cos\theta}{D_E}$$

$$P_{Capillary} = \frac{4\zeta\cos\theta}{\left(\frac{8r_f\varepsilon}{F(1-\varepsilon)}\right)}$$

$$P_{Capillary,trans} = \frac{4 \times 44\cos57}{\left(\frac{8 \times 0.0000085 \times 0.5369}{2(0.4631)}\right)}$$

$$P_{Capillary,trans} = 4.018kPa$$

$$P_{Capillary,axial} = \frac{4 \times 44\cos57}{\left(\frac{8 \times 0.0000085 \times 0.5369}{4(0.4631)}\right)}$$

$$P_{Capillary,axial} = 8.036kPa$$

Equation 37 – Formula for capillary pressure in UVAFP for $V_{f,dry}$ 46.31%

5.3.4.4.2 Applied Pressure

The applied pressure is the sum of all process induced pressures other than capillary and entrapped gas. These include compaction pressure and tow tension pressure. Each pressure was calculated independently in order to derive a complete net applied pressure around the nip point. Pressure is applied to aid laminate consolidation via compaction. Different reinforcement forms will react differently to applied pressure (P) and how said pressure is applied [203].

5.3.4.4.2.1 Roller Compaction Pressure

In processes where cylindrical rollers are used in contact with a flat plane, as in the case of UVAFP with a compaction roller and flat tool surface, Equation 38 [204] can be applied to calculate the maximum pressure [205] applied in the normal direction to the tool surface or transverse z direction of the tow.

$$P_{roller,max} = \frac{2F}{\pi bl}$$

Equation 38 – The pressure applied by the compaction roller

Where l is the contact length, calculated according to the compaction roller length of 25.4mm. b is half the width of the narrow rectangular contact area that occurs between a cylinder and flat plate due to deformations of the roller and tool and calculated according to Equation 39 [205]. This equation only calculates the maximum pressure directly under the roller contact perpendicular and not the elliptical distribution occurring across the width (2b).

$$b = \sqrt{\left(\frac{2F \left[\frac{(1 - v_1^2)}{E_1} + \frac{(1 - v_2^2)}{E_2} \right]}{\pi l \left[\frac{1}{d_1} + \frac{1}{d_2} \right]} \right)}$$

Equation 39 – Contact width of a cylinder on another body

Where E_1 was the elastic modulus, v_1 was the poisons ratio and d_1 the diameter of the first body (cylinder) and E_2 was the elastic modulus, v_2 was the poisons ratio and d_2 the radius of the second body (flat plate). The normal compaction pressure of the compaction roller was taken directly from the ideal setting as determined in Chapter 4

to achieve the nominal uniform thickness, namely 100N and determined according to Equation 38. In this case the roller was considered the first body, the material was a steel inner assembly containing the bearings and a Teflon outer, and therefore Teflon material properties were chosen. The elastic modulus was taken as 0.5GPa [206] and the Poisson's ratio was taken as 0.46 at 23°C [207]. The roller radius was 15mm. The second body was the tool, an aluminium plate (Al2024-T6) was used and therefore the elastic modulus was determined as 72.4GPa and the poisons ratio was taken as 0.33 [208].

$$2b = 0.6913mm$$

$$P_{roller,max} = 7.25MPa$$

Equation 40 – calculated values for the roller contact area width (2b) and the maximum pressure applied in the transverse direction

The roller diameter was 30mm and d_2, the tool surface diameter, in this case this was made infinitely large and the term $\frac{1}{d_2}$ was set at 0. The calculated contact width and pressure are shown in Equation 40.

5.3.4.4.2.2 Tow Tension Pressure

AFP shares similarities to the filament winding process. For filament based processes, tow tension also causes an increase in the pressure exerted on the resin layer as it passes over or under curved surfaces such as compaction rollers, tensioners or drums during impregnation. Chandler et al. [209] described 4 zones in pin impregnation; (1) the entry zone, where the tow approaches the pin at a pre-determined angle commencing contact with the resin; (2) the impregnation zone, where the resin is forced into the tow by the pressure difference on either side of the tow caused by the change in direction over the pin; (3) the contact zone, where resin is applied to the fibres and forced through the thickness of the tow and where the tension is built up as a result of Coulombic friction and viscous drag; and (4) the exit zone, where the tow leaves the pin impregnated with resin. Chandler's model [203] for the pressure build up due to this tension in pin assisted impregnation is shown in Equation 41 [203] where T is the tension of the tow, w is the tow width and $r_{compactor}$ is the radius of the curved surface.

$$P_{tension} = \frac{T}{wr_{compactor}}$$

Equation 41 – Resin film pressure due to tension

The pressure created due to tow tension was calculated according to Equation 41 as $P_{tension} = 395.120 kPa$. The value for tension was taken from the optimal setting as determined in Chapter 4 of 40N, the width was taken as 6.749mm and radius over which the tension acted, namely the radius of the compaction roller, was taken as 0.015m.

5.3.4.5 Degree of Impregnation and Impregnation Time

Following determination of all inputs the Shotton-Gale [158] modified model by Foley and Gillespie [191] was employed to determine infiltration time and the degree of impregnation. Equation 29 was first used to calculate the impregnation time according to Foley and Gillespie's model.

$$t_i = \eta(1 - V_f)T_0^2 \left[\frac{c_1^2 \left(\ln\left(\frac{1}{c_1}\right)^2 + 1 \right) - c_2^2 \left(\ln\left(\frac{1}{c_2}\right)^2 + 1 \right)}{4K_y(\Delta P)} \right]$$

$$t_i = 0.37(1 - 0.4631)0.000291^2 \left[\frac{c_1^2 \left(\ln\left(\frac{1}{c_1}\right)^2 + 1 \right) - c_2^2 \left(\ln\left(\frac{1}{c_2}\right)^2 + 1 \right)}{4 \times 1.527 \times 10^{-12} \times (4018 + 8065866.283)} \right]$$

$$t_i = 1.682 \times 10^{-8} \left[\frac{c_1^2 \left(\ln\left(\frac{1}{c_1}\right)^2 + 1 \right) - c_2^2 \left(\ln\left(\frac{1}{c_2}\right)^2 + 1 \right)}{5.252 \times 10^{-5}} \right]$$

Equation 42 – Impregnation time for UVAFP according to Foley and Gillespie's model

Using this approach the impregnation time was calculated as shown in Figure 100. Under the processing conditions of the UVAFP setup at the selected parameter settings full impregnation of the tow is predicted to be achieved in approximately 0.00032 sec or approximately 1m/sec, which was considered reasonable given the high localised pressures or the roller and capillary effect.

Figure 100 – The impregnation time of the UVAFP tow during processing

The impregnation and time was also calculated by rearranging the degree of impregnation model developed by Gaymans and Wevers as shown in Equation 43.

$$t_i = (D_l)^2 \frac{\eta \varepsilon T_0^2}{2K\Delta P}$$

Equation 43 – Gaymans' and Wevers' derived impregnation time prediction

The resulting impregnation time is shown in Figure 100. Under the processing conditions of the UVAFP setup at the selected parameter settings full impregnation of the tow is predicted to be achieved in approximately 0.00064 sec using Gaymans' and Wevers' model. This is approximately double the time prediction of the Foley and Gillespie model. The two models also differ considerable in the velocity of the predicted flow front. Foley and Gillespie predict slower impregnation at the beginning, accelerating as the impregnation progresses, whereas Gaymans and Wevers predict that the impregnation starts more rapidly than it finishes with full impregnation occurring as an approaching limit. The different rates of impregnation between each model are consequent to the fitting functions used. It was observed that the model of Foley and Gillespie was more appropriate to the UVAFP process, likely due to changes in the pressure front following initial infiltration and flow.

The impregnation times predicted by the model indicated that placement speeds, from the point of view of ensuring adequate wet-out and impregnation of the fibre, could be very fast. That is, the impregnation of the composite or migration of the resin would not be a process speed limiting factor. The impregnation times were translated into residence time of the compaction roller according to the placement speed and the contact width (previously defined as 2b from Equation 40) of the roller. At 0.6913mm in order to meet the minimum residence time of 0.00032 sec according to the Foley and Gillespie model the placement head could move as fast as 2160 mm/sec. While this is an extremely rapid placement rate it assumes constant roller pressure across the compaction contact width as well as maintained tension.

5.3.4.6   Impregnation Trials

It was calculated that to achieve the target V_f of 46.31% for the glass fibre tow, density of 2.62 g/cm^3 and resin, density of 1.046 g/cm^3, the required flow rate need to be approximately 5.14 x 10^{-3} g/mm as determined in Equation 44. Applying this coefficient provides the flow rate according to the velocity.

$$Q = v\rho_r \left[\frac{TEX}{1000000} \times \frac{1}{\rho_f} (1 - V_f) \right]$$

$$Q = v1.046 \left[\frac{2.4 \times 10^{-3}}{2.62} (1 - 46.31\%) \right]$$

$$Q = 5.14 \times 10^{-3} v$$

Equation 44 – Calculation of the nominal volumetric flow rate according to a nominal fibre volume fraction

This was calculated by using the TEX of the glass tow (as explained in Chapter 4, 2400 TEX = 2400 g/km). Therefore, at 1mm/sec, approximately 5.14x10^{-4}g/sec would be required. At 1000mm/sec, approximately 0.514/sec would be required and so on.

Figure 101 shows the setup using the resin spray gun connected to the robot. In the setup the compaction roller did not contact the tool surface and did not come into contact with the resin so that the flow rate and film quality could be assessed. The placement head assembly was covered in plastic film to protect against overspray.

Figure 101 – Resin flow rate calibration trials using the robotised setup

At the commencement of the trials a number of issues were identified that had to be addressed before comparable quality laminates could be produced. These issues included excessive resin flow rate from the spray nozzle, excessive bleed due to over compaction, excessive tow spread to the point of tow breakup, tow fracture due to excessive localised pressure of the compaction roller and lofting of fibres due to tow breakup and sticking of the resin to the roller. To address these issues a number of improvements were made to the experimental setup. These improvements included reduction of the nozzle size to reduce the flow rate as well as reducing the resin delivery pressure, precise tension control of the tow. All improvements were implemented for the manual lay-up trials and carried forward in the automated trials and quantified in the methods in further experiments.
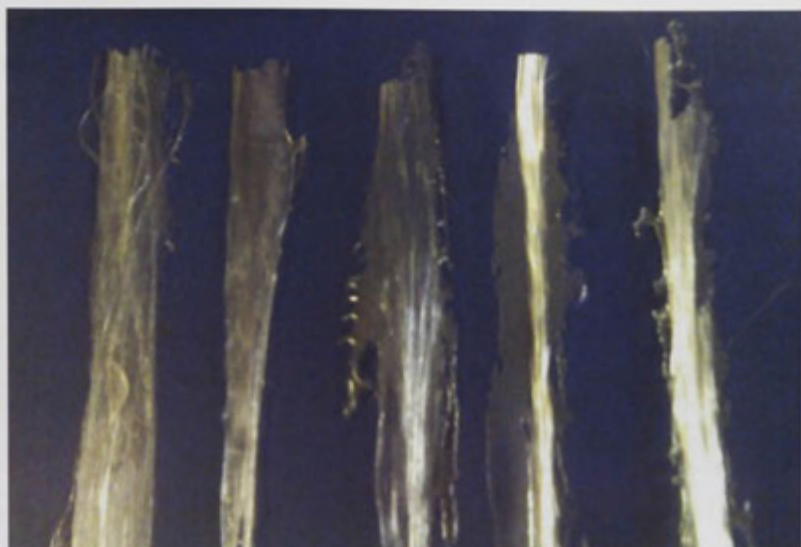
Figure 102 – On-the-fly impregnation trials

Figure 102 shows the results of the first trials by hand and the issues with tow spread and fibre misalignment, excessive resin bleed, excessive resin application and tow breakup from left to right. Due to the lack of die or tooling to constrain resin flow, a large amount of resin was lost out of the side of the tow before the resin had even flowed into the tow stack, as shown in Figure 104.

Figure 103 – Excess resin bleed in impregnation trials

This lost resin can be seen as the large amount of 'flashing' along the edges of the tow. Such a result was unacceptable for an AFP process because the flashing would

inhibit consequent adjacent plies being laid. In the first instance the issue was related to excess resin being applied, saturating the tow and excess being 'squeezed' out, therefore for subsequent runs the resin flow rate (delivered quantity) was reduced.

Figure 104 – The result of the first hand lay-up on-the-fly impregnation trials using the spraying system

It was noted that the resin loss, visible from the spread of resin beyond the tow edge, increased down the length of the placement path in the direction of the compaction roller travel. The resin spread in a moving "wave" that sat just ahead of the compaction roller. While the resin "wave" was advantageous for ensuring tow wet-out, resin loss was extreme, spreading resin almost 4 times the width of the tow as visible in Figure 104 (LHS). Such spread of resin would cause issues for laying adjacent tows, although in systems capable of laying many tows in a collimated manner at the same time, the resin would most likely spread to the other tows. This would mean that the resin spread would cause issues only for each new placement path adjacent a previously laid path and not between every tow.

The issue was eventually resolved by machining a very fine groove into the compaction roller that sealed the fibre tow and resin within the geometry created by the closed volume of the groove. Because the geometry created a void that had to be filled by resin and tow filaments, it would see a lower pressure ramp up if measured locally during pass over by the roller. An advantage of this was that the resin was driven into the tow first and then any excess pushed ahead of the roller. In total, three geometries for the compaction roller were tested. These were no groove, rectangular groove and circular groove.

The groove profiles are shown in Figure 105. The depth, d, width w, and radius, r were set to match the tow width, nominally 6.35mm. A depth of 0.2mm was chosen for the rectangular profile and for the circular groove where the peak of the radius to the tool surface to ensure compaction of the tow as average thicknesses seen in the results of section 4.3, where tow thicknesses were, except in rare occasions always greater than this amount.
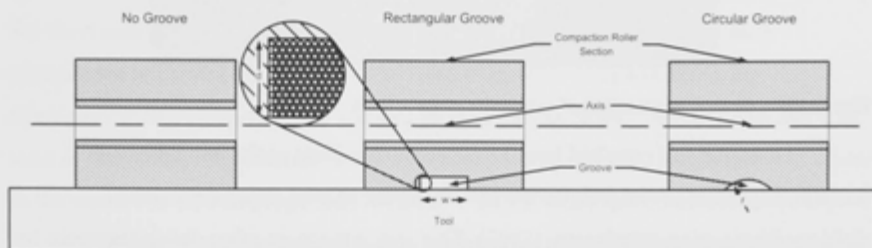
Figure 105 – Compaction roller groove profiles tested to eliminate resin flow

Tow spread was reduced using the groove and tow compaction averaged at the depth of the arc groove as expected. Furthermore voids and excessive resin bleed were also reduced. A detrimental result of the groove profile was the occurrence of a resin flow front that was pushed to the end of the lay-up path and the shaping of the tow rather than just the consolidation. For laying of multiple tows in a collimated placement head such roller design would leave require a gap between each tow to allow the profile edge to contact the tool surface at the edge of each tow.

Figure 106 shows the cross section of the final composite laminate produced in the grooved tool using a matched resin flow rate to desired fibre volume fraction. Multiple sections were made through multiple samples in order to assess the uniformity of wetout and quality. Figure 106 is a representative result of wat was found throughout the sample. The resin-rich interlaminar layer caused by the ply-by-ply lay-up and cure approach can be seen, which is typical of laminated composites produced in such a manner. A number of voids are evident within the fibre tow region but generally there was good wet-out of the fibre by the resin, and a typical fibre distribution pattern with good degree of consolidation and uniformity can be observed.
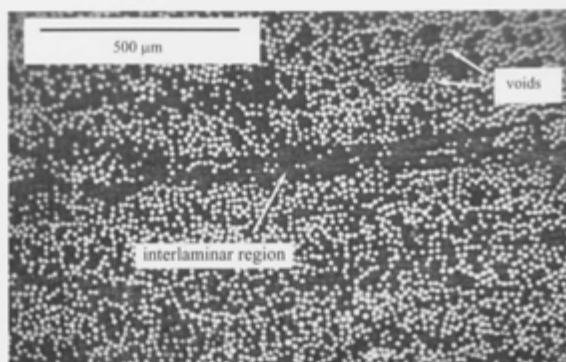
Figure 106 – Optical micrograph of composite cross-section

To ensure full cure had been achieved the hardness of the laminate was measured. Typical techniques for measuring degree of cure involve the use of differential scanning calorimetry (DSC). This technique most often determines cure by the degree of completion of the thermal reactions within the sample. Without measuring the total heat of reaction in uncured samples and then comparing to the residual heat of remaining reaction the degree of cure cannot be calculated accurately except through correlation of thermal properties such as the Tg to degree of cure. Using the residual heat of reaction as an indicator for degree of cure in a photo-cure free radical reaction does not provide an accurate indicator of degree of cure because the reaction is not heat driven in the first place and initiators are not driven by thermal conditions. Therefore just as Tg is used as an indicator for degree of cure, in this work hardness was used just as effectively correlating a mechanical property of the material to degree of cure. Previous work [75] has similarly correlated hardness to degree of cure effectively and easily. While developments have been made in the field of DSC systems fitted with UV sources rather than thermal (termed Photo-DSC [221]) and have been shown to be highly accurate, this sort of analysis was not undertaken in this experiment. Further work examining the thermal behaviour of photo cured composites should be examined to determine the effect of non thermal processes on thermal properties. The average hardness on Rockwell Scale M was 53, with a standard deviation of +3.3. This value is lower than that reported in previous work for UV cured and thermally post-cured vinylester [201]. However, this hardness value is double the value recorded for a

vinylester resin cured for 24 hours at room temperature (without an elevated temperature post cure).

5.3.5 Experiment Conclusions

The resin spraying and compaction roller on-the-fly impregnation trials provided value learning and data required in order to design an optimal on-the-fly impregnation system for the UVAFP prototype. Overall increased lay-up speed was demonstrated by the short impregnation time, thus increasing the productivity of the process in comparison to current AFP technology. Even in Shotton-Gale's thesis in the development of a clean filament winding process and an impregnation model that was used in this study, Shotton-Gale concluded that locating of the impregnation unit closer to the mandrel where impregnation occurred would be a logical improvement [158].

This experiment presented the first experimental results for a new AFP process that uses dry fibre, liquid resin with on-the-fly impregnation and in-situ UV curing. The process shows potential for reducing raw material cost, reducing the number of processing steps and eliminating the need for autoclave post curing. A number of issues were identified during the commissioning stage. The conflicting viscosity requirements for resin pumping/spraying and applying a bead was the most difficult to solve. Cooling the tool was investigated but presented further difficulties to control and may cause unwanted process variations. Spray directly onto the tow might improve this issue removing the need for a uniform bead of resin on the tool, however this was not tested as part of this work. After resolving the commissioning issues, uniform fibre wet-out was observed and a reasonable degree of cure in the resin was achieved with separate delivery of liquid resin and dry fibre. A partially closed strip mould was used in this work to limit resin overflow, however further work will be conducted to obtain acceptable composite quality using open moulds, and at increased placement speeds. This may require some modification of resin formulation and viscosity.

Numerous parameters affected the laid resin characteristics. Varying the nozzle spray size and the pressure behind the resin the flow rate could be accurately controlled. The speed of the lay-up was also important in controlling the lay down of the resin. By matching the robot speed with the projection speed of the resin as it exited the spray nozzle, the resin remained on the surface in a precise bead similar to the width of the

fibre tow. Further, by varying the styrene content of the resin the viscosity could be controlled. Varying the temperature of the resin also affected the viscosity of the resin and how it was delivered. Conflicting considerations in this setup were that the resin viscosity needed to be low enough to be sprayed and delivered to the sprayer, while it was desirable to also form a bead on the mould. To control this, the resin was heated within the pressure pot and the mould was chilled so that the resin forms a bead when it contacted the mould.

The hardness results indicates that UV curing in this AFP process has potential to produce composites with a high degree of cure, using hardness as an indicator of degree of cure, compared to the common room temperature cure method. Further work will investigate the processing parameters required to achieve a hardness value of 80-90 HRM, which is the typical range recorded for the post-cured vinylester sample.

In regards to impregnation the significant effect that process pressures have on the impregnation were evident from the models. A possible further process pressure than could be introduced would be the resin spray impact pressure if the resin spray was aimed directly onto the tow. This would force resin into the tow prior to contact with the tool and compaction, decreasing the penetration depth the compaction pressure would need to impregnate the resin through.

5.4 Summary

Impregnation and consolidation are two distinct actions of impregnation process. In the first instance, impregnation occurs to ensure the resin has fully wet-out the fibre tows filling the free space and voids in order to form the composite construction. In the second instance, consolidation occurs to ensure the lay-up of the preimpregnated plies is intimate, the fibre packing is optimised for maximum mechanical properties due to increased fibre volume fraction and to ensure there is no entrapped air. Functionally impregnation and consolidation can occur in one process, as in the case of the concept presented in this section, optimising impregnation by applied pressures which then also act to consolidate the composite, removing air and maximising the V_f. It has been demonstrated that consolidation and impregnation can be applied on-the-fly to wet-out the fibres and reduce voids and delamination without the need for a separate de-bulking processing step would be necessary for split process approaches.

By eliminating the need for additional post curing steps and constant de-bulking during lay-up and integrating the curing within the same process that is laying (and de-bulking) the composite AFP would provide a complete manufacturing solution, rather than another step in the process chain [47]. By combining the lay-up, consolidation, and curing mechanisms in one system that functions in a continuous but transient manner, a fundamentally novel process is developed in comparison to existing systems that separate the mechanisms into individual machines and processes. Therefore, a thorough understanding of the new processes driving parameters is necessary. Further research to develop the interrelationships of the process and curing and the effect on the performance of the part is needed.

6 AFP Curing and Post-Processes

In this chapter the limitation of AFP systems as placement devices only is addressed and the issues associated with the processes post placement via AFP in order to complete the component manufacture. During composite manufacturing using AFP technology, additional post processing steps are required following the fibre placement step in order to cure the composite, and in some instances an additional post cure in order to realise the maximum material properties. The need for post-processing using AFP is due firstly to the prepreg materials used in AFP and the need for thermal curing and consolidation using ovens, autoclaves or presses (as discussed in Chapter 4); and secondly to the lack of curing mechanisms within the placement system. With the fibre (and resin) placement and the curing as separate steps in the manufacturing process a sequential approach is taken that requires batching, loading and unloading of the entire part as well as additional tooling. By sequencing the manufacture in batches, the cost and time of the finished product are increased considerably. In aerospace, composites curing often requires at least 8 hours in an autoclave. Some convective heating processes can be implemented in continuous production lines such as conveyor ovens however these systems are generally not qualified for use in aerospace applications, have a high degree of process variability and instability and have high energy consumption. In addition the size and cost of the capital equipment is restrictive.

A solution is proposed that combines the ply-by-ply continuous approach of AFP with the curing of the composite to produce a cured component on-the-fly, cured in-situ immediately following placement. By combining the curing with the placement the need for post-processing is eliminated. Section 6.1 introduces the concept of in-situ curing and the techniques that can be applied in this manner. Section 6.2 the background theory of ultraviolet (UV) radiation and its use as an in-situ curing technique is presented. A detailed description of this radiation spectrum range is provided, the control and measurement of UV and then its application in composite curing. Finally, two experimental studies are presented. In section 6.3 the first proof-of-concept experiment examining the use high-intensity UV spot curing is presented. The

results of this study are discussed in the context of the application of high intensity UV curing for the UVAFP prototype. In follow-up, section 6.4 presents the experimental results examining the concept of in-situ curing on-the-fly in a ply-by-ply manner versus the traditional approach of at-once batch are presented. The results and discussion are again provided in the context of UVAFP and how in-situ UV curing could be applied. Both tests provide the first data validating the concept of high intensity UV spot curing and its use as an in-situ curing source. The final section of this chapter summarises the theory, and the results and discussion of the two studies and draws conclusions for consideration in the UVAFP prototype design and programming as previously examined in Chapter 3.

6.1 In-situ Curing

In-situ curing is the process by which the resin matrix of the composite is cured at the point of application in an on-the-fly manner with either the part or the curing source moving in relation to one another as the process progresses. In-situ curing is incremental, meaning that each ply is cured one at a time and the thickness of the part built up. Cross-linking of polymers using radiation sources stems from the work of Charlesby in 1960 [210]. Charlesby observed that when polyethylene was exposed to radiation emanating from a reactor it formed an insoluble gel. Up until that time it had been thought that cross linking could only occur due to the addition of chemical agents with suitable functional groups, sulphur vulcanisation for example [211].

An in-situ approach lends itself to serialised manufacture where the lay-up and cure stages are combined and removes additional process steps, decrease overall cycle times and cost and reduce work in progress. By utilising in-situ curing the maximum dimensions of a single part are only limited by the size of the tool, not to the dimensions of the curing device, for example the diameter of the curing autoclave. Large structures such as aircraft wings, wind turbine blades and vehicle chassis can therefore be manufactured without the need for joins, fasteners or assembly.

Due to the localised application of curing energy, in-situ curing mechanisms generally utilise irradiant energy delivery to initiate cure in high intensity localised to the placement or impregnation system. Some thermal processes can be applied in-situ such as conduction rollers and high intensity lasers but the residual stress, non-uniform

thermal expansion, thermal lag, large equipment and energy efficiency associated with such systems can cause quality concerns and are less efficient. Continuous processes where fibre and resin are combined, consolidated and formed dynamically such as pultrusion, roll forming and filament winding lend themselves to in-situ curing. A number of in-situ irradiation techniques have been examined over the years in composite manufacturing in various applications.

In-situ processes that cure the component using radiation instead of temperature require different resin chemistries that can cure rapidly without requiring long exposures and have appropriate rheology for impregnation at radiating temperature. The approaches that are collectively covered by the term in-situ curing are listed below:

- Ultraviolet (UV) light [75];
- Microwaves [42];
- Hot gas guns;
- High intensity lasers;
- Conduction rollers;
- Infrared (IR) light [74];
- Electron beams [86]; and
- X-ray [211].

The most successful use of in-situ curing has been in highly automated processes that require no manual labour or intervention. As with most radiation curing techniques significant health and safety challenges restrict its implementation to protect personnel and equipment. Electron beam curing, for example, requires large and restrictive infrastructure for radiation protection for operators, the size of the electron beam gun, and the energy required to power the system. Similarly microwave radiation can cause illness or death to humans and therefore requires similar shielding. Lasers pose a threat to operators with the risk of blindness caused by exposure of eyes to the laser beam. UV radiation likewise requires UV blocking shielding for direct line of sight and personal protective equipment (PPE) to protect the skin and eyes of operators.

Table 26 – In-situ curing radiation sources and their safety risks and mitigations

Curing Source	Risk	Mitigations
UV Light	Direct exposure to skin and eyes	Line of sight UV filtering screens, either transparent or non-transparent
Microwaves	Direct and indirect exposure to the body	Closed shielding using microwave absorbing or shielding materials
Lasers	Direct exposure to the body, direct and indirect (reflected) exposure to eyes	Closed shielding using energy absorbing or shielding materials that can withstand high concentrated temperatures, either through dissipation or reflection
IR Light	Direct exposure to the body	Closed shielding using energy absorbing or shielding materials that can withstand high concentrated temperatures, either through dissipation or reflection
Electron Beam	Direct and indirect exposure to the body	Closed shielding using electron beam absorbing materials and de ionisation mechanisms to remove latent/residual radiation sources
X-ray	Direct exposure to the body	Direct shielding using X-ray absorbing materials

These safety issues and the associated risk mitigations are summarised in Table 26. Of all of the radiation sources UV light is the simplest and least expensive source to contain and manage while also allowing close contact by operators and viewing of the process using transparent shielding.

6.1.1 Radiometry

Of the radiation curing mechanisms there is also an associated intensity and dose relationship that is required in order to achieve full cure. Each radiation source works across a different wavelength and thus has a differing penetration rate and depth according to the composite material absorption and transparency. The analysis and measurement of the nature of radiation curing is termed radiometry. Radiometry is a set

of techniques for measuring electromagnetic radiation, including UV radiation. Radiometric techniques characterise the distribution of the radiation's power and are distinct from quantum techniques such as photon counting. For the purposes of UV curing, UV radiometry measures and controls the intensity, irradiance, dose and the absorption of the substrate. The explanations of terms relevant to the calculation of the important parameters in UV radiation are detailed below.

Source Radiant Power (Φ) is the radiant power (W) emitted in all directions by a radiant energy source, often modelled as a point source. Irradiance (E) is defined as the total radiant power from all directions incident on an infinitesimal element of surface area dS containing the point under consideration, divided by dS. The SI unit of irradiance is Wm^{-2}; although, $mWcm^{-2}$ is used more commonly in the literature. For a position at r cm from a point source in a non-absorbing medium, the irradiance is given by:

$$E = \frac{\Phi}{4\pi r^2}$$

Equation 45 – Irradiance from a point source in a transparent medium

The fluence rate (E') is the radiant power passing from all directions through an infinitesimally small sphere of cross-sectional area dA, divided by dA. The SI unit of fluence rate is Wm^{-2}, but $mWcm^{-2}$ or $mWcm^{-2}$ are commonly used. Note that fluence rate and irradiance are similar (same units) but conceptually quite different terms, however, they are the same for a collimated beam. The fluence rate or irradiance is often termed 'light intensity'; this is incorrect. The correct definition of 'radiant intensity' is given below. Radiant intensity is defined as the irradiance per solid angle. SI units for this measure are W/sr (watts per steradian). Dose or Fluence (H') is defined as the total radiant energy from all directions passing through an infinitesimally small sphere of cross-sectional area dA, divided by dA. The UV dose is the fluence rate times the irradiation time in seconds. The SI unit of dose is Jm^{-2}, but often UV dose is given as $mWscm^{-2}$ or the equivalent $mJcm^{-2}$ (since it emphasizes the delivery of energy).
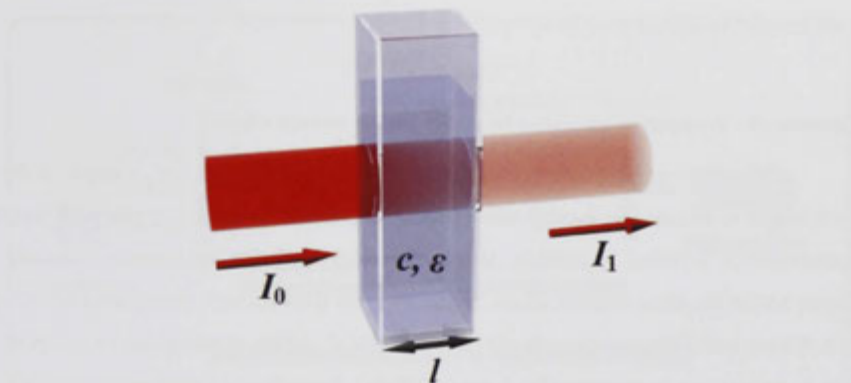
Figure 107 – Beer-Lambert absorption of a beam of light

Absorption is the transformation of light to other forms of energy as it passes through a substance and is defined according to Beer-Lambert's law [212]. The Beer-Lambert law is shown in Equation 46.

$$A(\lambda) = \in (\lambda)cl$$

Equation 46 – Beer-Lambert's law

As an energy beam passes through a material the energy is absorbed. Absorbance quantifies the decrease in the amount of incident energy as it passes through a material.

$$U = e^{-\alpha(\lambda)l}$$

Equation 47 – Attenuation factor for a given source beam

If $\alpha(\lambda)$ is the (napierian) absorption coefficient (cm^{-1}) at wavelength λ and l is the path length (cm), then the attenuation factor, U, for a beam of light, where $\alpha(\lambda)$ is related to the absorbance $A(\lambda)$ at a given wavelength λ, is defined according to Equation 47.

$$\alpha(\lambda) = \left[\frac{A(\lambda)}{l}\right] \ln(10)$$

Equation 48 – Absorption coefficient

Where $\in (\lambda)$ is the molar absorption coefficient (M^{-1}cm^{-1}) at wavelength λ, c is the molar concentration of the absorbing species and l is the path length (cm). The

concept is described graphically in Figure 107 [212]. The transmittance $T(\lambda)$ over the path length l is related to $A(\lambda)$ by

$$T(\lambda) = 10^{-A(\lambda)}$$

Equation 49 – Transmittance equation for energy passing through a body

Often the transmittance is measured for a fixed path length. For example, if the path length is 10 mm, the transmittance should be designated as the '10 mm path length transmittance' (symbol T_{10}) [213]. Absorption of UV radiation by common materials varies across the three classifications. Ordinary glass is considered transparent to UV-A, but opaque to shorter wavelength of UV-B and UV-C. Silica, quartz glass, or Perspex can be transparent to wavelengths down to 200 nm. Radiation at wavelengths smaller than 180 nm is strongly absorbed by the oxygen in air and by most common materials [163].

6.1.1.1 Spectrophotoscopy

Spectrophotoscopy is one of the most common tools used in the science of radiation and absorption analysis. A spectrophotometer is used to determine the extent of absorption of specific wavelengths of light by a material. This analysis is commonly known as *colorimetry*, in contrast to *calorimetry*, where the analysis of heat energy transfer is examined. The internal instruments of a photo-spectrometer include:

1. A stable source of radiant energy (Light);
2. A wavelength selector to isolate a desired wavelength from the source (filter or monochromator);
3. Transparent container (cuvette) for the sample and the blank;
4. A radiation detector (phototube) to convert the radiant energy received to a measurable signal; and a readout device that displays the signal from the detector.

In this way the light source is passed through the monochromators to select the appropriate wavelength of light. This wavelength is then directed to a sample cuvette containing the material under examination and the light is absorbed and transmitted. The detector then determines the energy received and this is compared to the energy output by the light source to determine the absorption. A figure of the setup of a - spectrophotometer is shown below in Figure 108 [214].

Basic Instrumentation of a Spectrophotometer
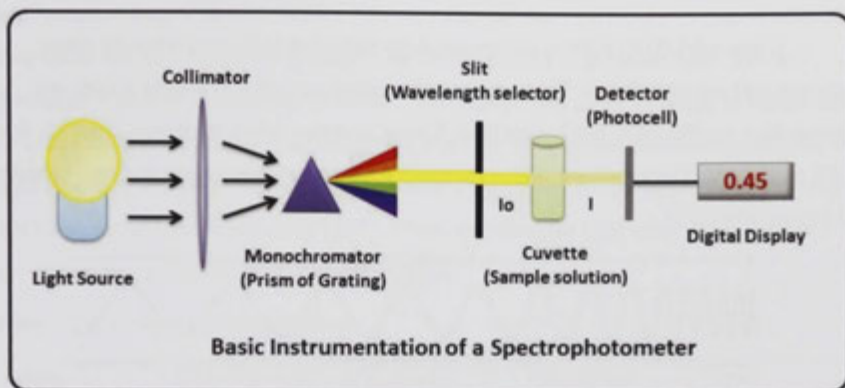
Figure 108 – Principals of a spectrophotometer

The absorption wavelength of a material, which also determines colour properties, uses the Beer-Lambert's law. This explains that absorption increases as a linear and positive function of concentration of a compound, while the percentage of transmittance decreases exponentially. With the need for quicker and cleaner manufacturing processes [46][76], UV-curing technology has the potential to address these requirements due to its clean and rapid results. Various other types of radiation technologies exist that have also been applied to the curing of composites. These include electron beams [2], near infrared and microwave radiation. According to the material selection detailed in Chapter 4, while UV radiation is limited in terms of penetration depth into the substrate, in implementation UV curing offers many advantages when compared with the other types of radiation. These include lower costs of the equipment and lower energy consumption. The radiation produced by UV light is also the least hazardous and is the easiest to produce while meeting national safety requirements [163] of most countries. Due to its simple control and delivery, the ability to concentrate high intensity exposures in a small area, the rapid cure times and the low cost of capital, ultraviolet radiation curing was selected as the in-situ curing source for the UVAFP prototype and is explained in detail in the following sections.

6.2 Ultraviolet Radiation

Ultraviolet (UV) light is electromagnetic radiation with a wavelength range between 400 nm and 10 nm. This wavelength range means that UV light waves are shorter than visible light, but longer than X-rays, corresponding to photon energies from 3 eV to 124 eV. The relative wavelength range on the electromagnetic spectra is shown in Figure 109 [215].
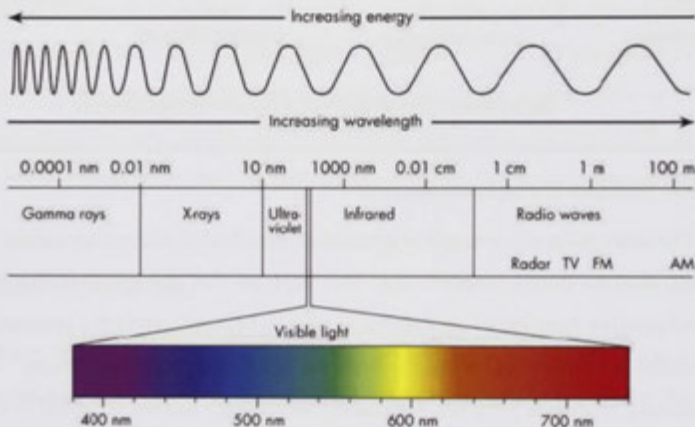
Figure 109 – Light spectra ranges

In radiation energy transfer, decreasing the wavelength increases the energy, however the depth of penetration decreases with a decrease in wavelength. UV radiation is classified by three wavelength ranges, UV-A, UV-B and UV-C and transition wavelength ranges that include extreme UV (EUV). The classifications by wavelength are detailed in Table 27. A large fraction of UV, including all that reaches the surface of the Earth, is classified as non-ionizing radiation. The higher energies of the ultraviolet spectrum from wavelengths about 10 nm to 120 nm, 'extreme' ultraviolet are ionizing, but due to this effect, these wavelengths are absorbed by nitrogen and even more strongly by dioxygen, and thus have an extremely short path length through air [216].

UV light is found in sunlight where it constitutes about 10% of the energy in vacuum. Specialized UV gas-discharge lamps, containing a variety of different gases, produce UV light at particular spectral wavelengths for scientific purposes. Commonly used sources of UV radiation are mercury arc lamps or electrode-less microwave-

powered mercury lamps. Mercury short arc lamps are often used in UV curing applications along with UV LED's. Mercury vapour short arc lamps are gas discharge lamps that use an electric arc through vaporized mercury to produce light. The arc discharge is generally confined to a small fused quartz arc tube. The vapour lamps can be used for lighting purposes with filtering outer bulbs to protect humans from the UV light however the use of such bulbs purely for lighting has been banned in Europe from 2015 and in the USA since 2008 [163]. These are often the light sources in UV spectroscopy equipment for chemical analysis.

Table 27 – UV wavelength classifications

Name	Classification	Wavelength, λ (nm)	Energy per photon (eV)	Type
Ultraviolet A	UV-A	315–400	3.10 – 3.94	Long wave, black light
Ultraviolet B	UV-B	280–315	3.94 – 4.43	Medium wave
Ultraviolet C	UV-C	100–280	4.43 – 12.4	Short wave, germicidal
Extreme Ultraviolet	EUV	121-10	10.25 – 12	

Medium pressure vapour lamps of this type are the most common sources of UV radiation in technology applications. In microwave powered lamps, microwaves are used to generate a mercury vapour that has a characteristic radiation emission range in the UV spectrum. In all instances, the composition of the mercury vapour and the presence of trace elements or halides can be added to vary the spectra according to a desired output peak wavelength or range [163]. Other lamp sources exist such as solid state diodes made from doped semiconductor materials and excimer lasers but these are less common in application. In composite material curing application the UV light source depends on the process and part requirements, but most often flood light systems covering the full surface of the part are used. These systems are generally of low surface irradiance. For continuous or limited size process focal / spot curing systems of high intensity can be used [171]. Numerous studies on the effect of the UV radiation intensity (I_0) on the polymerization kinetics of UV-curable resins have shown that an

increase of intensity leads not only to faster polymerization but also to a more extensive cure, so that the final product contains a lower amount of unreacted functional groups [217]. Therefore there exists much promise for high intensity spot curing of composites.

6.2.1 UV Curing of Composites

There is a large number of studies in the literature examining the UV curing in fibre reinforced composites, utilising both cationic and free radical chemistries but the majority of studies focus on free-radical photo curing using glass-fibre reinforcements due to the UV transparency of the glass fibres, aiding the depth of penetration. Endruweit [163] detailed a number of studies examining the properties of resins cured using UV radiation. The many formulations and differing fibre ply schemes possible with UV curable systems makes a widespread examination of the actual figures for mechanical properties [163] impractical. As with any composite process the curing conditions and exposure setup has a significant impact on the performance on these materials that are extremely sensitive to the UV curing mechanism. However, in all instances, comparable properties to the equivalent thermal cured system were found but with markedly improved curing times for a variety of processes [163][201]. The processes used with UV curing included wet lay-up techniques, vacuum infusion type processes with UV-transparent membranes, pultrusion [170], filament winding and prepreg processes [86][163]. Even curved composite parts have been produced in a pultrusion process [163] where the composite was cured with UV light in-situ as it exited the die. Vacuum assisted resin transfer moulding (VARTM) [218]or vacuum assisted resin infusion (VARI) [219], resin infusion between double flexible tooling (RIDFT) [220] and even prepreg hand-lay-up [173] have all been used with UV curing resins.

Free-radical UV curing provides a convenient "cure on demand" behaviour for their use in composites [221]. This is due to the fast on/off capability of UV light delivery systems and the efficient energy transfer the radiant delivery rather than convective. Most structural adhesive compounds are hardened through the transfer of energy in the form of heat either at room or elevated temperature over a certain gelation period, often many hours. Such thermal lag leads to long cure times and an inability to selectively and locally cure on demand. These resins must be mixed and used within a

certain time (otherwise known as the pot life) before the material expires and is unusable or the mechanical properties following curing are diminished. Typically for UV-curing materials, full cure occurs in a matter of seconds rather than hours [163] as for thermal cured resins, nor is there any requirement to use the dispensed or initiated material within a short time for pot life concerns. The only requirement is to control exposure to light at specific UV wavelengths.

UV curing resins are most often solvent free and therefore are not limited by thermal processes that require large amounts of energy transferred across the entire part and tool to evaporate the solvent which can be extremely slow and inefficient. The type and concentration of the photo-initiator and of the (optional) diluents, the intensity and the duration of the irradiation, and the temperature at which the curing process takes place determines the cross linking density of the reaction. This density determines the mechanical properties of UV-cured resins [163]. The increased speed of cure reduces the window for the release of volatile organic compounds (VOCs) from the resins, such as styrene from vinylester [201]. Since curing starts on the surface of the resin, which is exposed to the radiation first, a 'gelled' skin is produced sealing in unreacted styrene trapped below the surface. In calculating the absorption and depth of cure in UV curable resins, the reactive species are mainly generated in the top resin layer, in which the polymerization starts [163]. As the absorbing photo-initiator in the top layer is consumed in the reaction transparent photoproducts are formed, the incident radiation can then penetrate deeper into the material [163]. Thus, the polymerization front moves progressively through the material thickness [217]. This trapped styrene remains available during further gelation and curing for on-going polymerization. UV curing has already seen rapid adoption in the printing, coatings, water purification, stereolithography, semiconductor lithography and dental industries because of its rapid cure.

6.2.1.1 UV Curing Process Parameters

Bolton [213] examined the significance of refraction and reflection on fluence rates by developing a model that contained multiple point sources in the summation of exposure as a unit area of fluid passed through a linear water purifier using a UV reactor lamp. The model also accounted for both reflection and refraction as a beam of UV

radiation passed through an air/quartz/water interface (as was the case for the purification reactor design). The reflection within the reactor was found to account for only 6.5% in the short T'_{10} 10mm path. However in most practical applications this length is much larger and reflection and refraction can play a much more significant role in concentrated exposure environments. Bolton highlighted the *ideal* fluence or dose calculation is generally determined by multiplying the irradiance by an exposure time, but in reality this can only ever be seen as a theoretical maximum. Bolton's [213] calculation of fluence rate provided a far more accurate view by accounting for variances in the irradiance source across the exposure area and also throughout the exposure period. Coupled with a calculation of the transmittance of the UV light through the medium a 3D view of fluence can be determined.

In free-radical photo-initiated reactions, curing only occurs upon exposure to UV light and therefore the depth of penetration is critical to ensuring complete curing through thickness. In composites the transparency of the fibre places a key role in the depth of penetration. Crivello et al. [222] found that in the case of glass fibre the depth of cure can actually be increased due to the transparency of the fibre to UV radiation. With other common fibres that are not UV transparent, such as carbon and Aramid, the reactants must include a mix of either cationic and free radical or processing must be hybrid, for example in the form of UV curing and thermal curing, to ensure full through thickness cross linking. The use of fillers or pigments in the resin may also interfere with the radiation [163]. UV transparent materials must be used where separation of the composite from the radiation source occurs, for example, UV transparent vacuum bagging materials, glass fibre tooling and glass fibre reinforcements within the composite. In processes where non-opaque materials are used, such as carbon fibre reinforcements, penetration depth becomes an issue and resins can only be B-staged if a free-radical initiator is used or a dual curing initiator or process approach is necessary [167].

The issue of exposure and positioning of the UV lamp has also been explored in the literature [219][222]. Okoli et al., proposed a simple method for locating optimal positions for UV lamps used in the curing of curvilinear composite components manufactured with the Resin Infusion between Double Flexible Tooling (RIDFT) processes. A multivariate optimization model, consisting of continuously differentiable

and two-dimensional integral domain parts for the UV lamps positions, dimensions of the manufactured composite component, and UV power source. The two-dimensional integration aimed to determine and minimise the difference between the required intensity and actual intensity the composite component receives. A Gauss quadrature numerical integration method was used to numerically evaluate the surface integral, and the Davidon-Fletcher-Powell (DFP) algorithm was used for predicting optimum positions for the lamps. Mechanical and rheological properties of the UV cured laminates were compared with catalytically cured laminates [219]. In conclusion to the work, while the model predictions for lamp positions in experimentally validated tests were better that catalytically cured parts, uniform irradiance was not achieved. Without increasing significantly the number of lamps this would be impossible but a good effort was made given a limit on the lamp numbers.

Unluturk, Arastoopour and Koutchma [223] developed a numerical model for calculating UV dose based on a dispersed phase arrangement of the UV sources, known as a dispersed phase model (DPM). The model was used to describe the relationship between the flow patterns of micro-biobial particles in water and residence times of the biobs in a thin-film UV reactor, the 'Cider Sure 1500'. The model was developed along with a UV intensity model, to ensure adequate UV dose delivery in order to kill micro-biobial particles in water used in apple cider production. The results of the model simulations, which included computational fluid dynamics to understand the movement of the particles in the water, showed good agreement with experimental biodosimetry data as well as reasonable agreement with simulation calculated and experimental UV dose values. The model interestingly predicted that most of the particles passing through the UV reactor received a UV dose less than the average value, calculated simply by multiplying the estimated residence time by the nominal average UV intensity. Two models for calculating dose based on lamp position were examined, the infinite line source model and the finite-line source model, In the infinite line source model all light is emitted radially from a line source, while the finite-line source uses sources at specific spacing along a line. The Beer-Lambert's law is used to calculate the irradiated energy through thickness as a function of the absorption of the material. Significant effort was taken to calculate delivered irradiance (mW/cm^2) both in the radial direction and longitudinal directions for the two source models at a particular point in the reactor.

For the infinite line source model a point irradiance formula was determined as per Equation 50.

$$I = I_0 \frac{r_q}{r} e^{-a_i(r-r_q)}$$

Equation 50 – Infinite line source model irradiance

For the finite-line source Equation 51 was used. Dose was calculated by a summing method using the residence time interval and irradiance at specific point coordinates. This was undertaken for 166 particles per simulation. Unluturk, et al. [223] were able to determine the transient irradiance received by the particles and calculate a more accurate dose figure than the standard method used by most of the literature that simply multiple total exposure (based on an average intensity) over the total exposure time. The dose calculated was very different to the one that would be calculated using the standard method and therefore demonstrates the amount of flux and variation in dose that can be seen in dynamic processes.

$$I_\lambda(r,z) = \sum_{i=1}^{n} \frac{\frac{\Phi}{m}}{4\pi l_i^2} \exp[-\left(a_q t_q + a_\lambda(r - r_q)\right)] \frac{l_i}{r}$$

Equation 51 – Finite line source model irradiance

Significantly the irradiance at any given point within the flux field of the UV source changes dramatically depending on the absorbing mediums in between the source and that point. Unluturk, et al. [223] did not calculate the absorption of UV radiation in air however which meant that absorption was only considered to occur in the quartz shielding and the water.

Measuring the reaction rates of photo-polymerising resins presents significant challenges due to the scarcity of equipment established and the ability to gather data fast enough to provide relevant data over the very short time periods of reaction due to the rapid rate of photo-polymerisation. Chartoff and Du [224] developed an advanced reflectance real time infrared (RRTIR) analysis technique which involved time resolved IR analysis by reflected IR radiation while a resin sample is being exposed to a UV laser beam. The technique proved highly effective for quantifying the reaction rates of photopolymerization in the millisecond time range and hence the degree of cure. In the context of stereolithography (SLA), and for analysis of the dark reaction (continued

cure post exposure), the process was able to demonstrate degree of cure advancement beyond exposure with a very tight tolerance on timeframe. Chartoff and Du [224] used the technique to determine the effect of process parameters such as resin composition, temperature, UV exposure intensity and exposure time on real time cure development. The technique allowed isothermal conditions to be set to isolate the polymerisation rate according to the UV exposure only. By changing the temperature however Chartoff noted accelerated photo-polymerisation. The technique and has been used for a large number of resin systems where UV curing is critical, including dental systems, SLA and ink printing [224].

To evaluate the effect of the UV light intensity and temperature on the real time conversion, temperature and conversion of samples undergoing photopolymerization were recorded by RTIR spectroscopy as shown in Figure 110 [217]. Two different light intensities (10 and 80mW/cm^2) and a temperature range up to 100 °C were recorded. The temperature rose as soon as polymerization began and reached its maximum value once the reaction slowed down because of gelation. The temperature later decreased thereafter more slowly as air cooling overtook the small amount of heat evolved at the end of the reaction. The temperature rose faster and was more important for the sample irradiated at high light intensity, reaching a maximum value of 90°C at 80mW/cm^2, compared to 40°C at 10mW/cm^2. By acting on the cure extent through the sample temperature, the light intensity affected the physical properties of UV-cured polymers, in particular the elastic modulus and Tg which both increased as I_0 was increased [217].
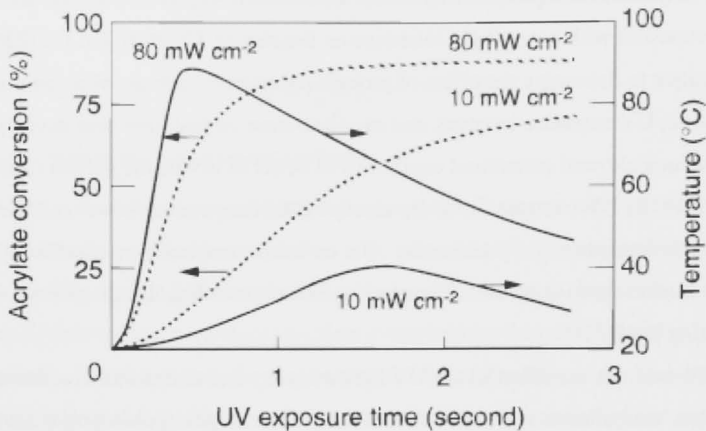
Figure 110 – Influence of the light intensity and temperature and polymerisation/conversion of acrylate exposed to UV light

Importantly, Decker [217] demonstrated the logarithmic nature of the relationship for conversion in vinyl ether and acrylate systems versus exposure time. It was found that at a given exposure time, the conversion rate plateaued and in order to progress the degree of cure much longer exposures were required. On the other hand, although achieving far slower conversion rates, the rate was much closer to a linear relationship for cycloepoxides, methacrylates and glycidyl ether, as shown in Figure 111 [217].
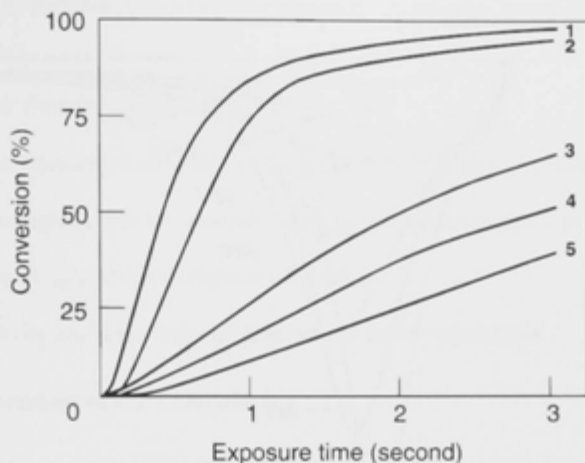
Figure 111 – Polymerisation rates of different resin systems. 1 – arcylates, 2 – vinyl ethers, 3 – cycloepoxides, 4 – methacrylates, 5 – glycidyl ether

Scott, Cook and Forsythe [221] , found that the maximum rate of photopolymerization increased by a factor of 10 as the isothermal cure temperature was varied from 30°C to 90°C. The increased rate was attributed to faster propagation and greater initiator efficiency counterbalanced by a faster termination rate, as shown by the differential scanning calorimetry results in Figure 112 [221].
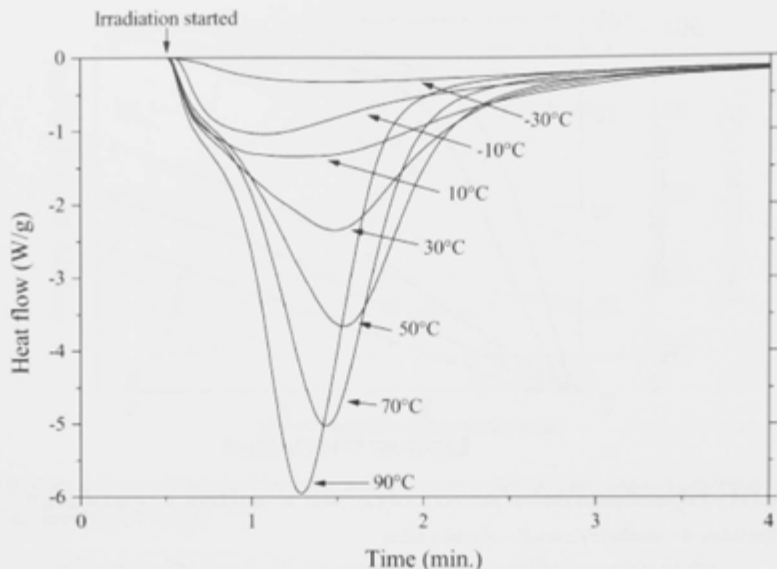
Figure 112 – Isothermal differential scanning calorimetry results for samples cured at various temperatures. Note the increased reaction rate with increasing cure temperature.

Following initial UV exposure and cure, samples were thermally post cured by heating at strict linear rates in a DSC to investigate if any further conversion through 'dark' curing. It was found that the final degree of cure after post cure was independent of the isothermal temperature during the initial cure, and therefore it seemed only the reaction rate was effected. Significantly, the onset temperature for the reduction of mechanical properties was found to increase, suggesting a higher glass transition temperature (Tg) with an increased isothermal cure temperature. This was linked to a proposed increased in the vitrification rate [221] due to the higher molecular mobility and ability for the cure reaction to occur more rapidly. Tg is usually used as an indicator for degree of cure or conversion in polymers however this research suggests that for photo-cured polymers conversion has little or no relationship to Tg, rather it is the thermal conditions that exist at the time of gelation and cure that dictate Tg. For UVAFP this suggests the significance of the heating that could occur during exposure to the UV curing system.

In all circumstances the process parameters must be optimised while ensuring degradation of the composite does not occur due to over exposure or UV ageing [221].

In addition to the parameters explained in section 6.1.1, process parameters important to UV curing are:

- Distance from the source to the substrate, mm

- Specific wavelength of source and absorption wavelength of photo-initiator, μm

- Angle of light source to substrate – flux across exposure area, ° or radians

- Number of light sources (finite or infinite), #

- Reflectivity and refractivity of substrate, % and n respectively

6.2.1.2 Applications of UV Composites

Sunrez Corporation [218] demonstrated the use of UV curing in marine applications for the U.S. Navy. UV cured composites were proposed and tested for the manufacture of military ship hulls. In this application the proposed process was vacuum assisted resin transfer moulding (VARTM) with UV curing. The process used glass-fibre reinforced moulds that had low UV absorption and therefore allowed exposure through the mould. UV cured hull sections were produced showing exceptional productivity and cost benefits over traditional processes such as room temperature curing. Productivity exceeded lay-up and cure rates of 40 lbs per man hour on monolithic skin laminates, 8 lbs per man hour for cored laminates and 10 lbs per hour for stiffened laminates. In comparison to UV prepreg lay-up the UV-VARTM was far more efficient but slightly more expensive. However in comparison to traditional thermal cure processes the technology was extremely economical with a cost of no more than $8USD/lb for cored panels and even less for stiffened and monolithic skins. Laminates had an average of 66% fibre by weight exceeding the fibre volume fraction of currently available UV curing prepregs that have an average of 58% fibre by weight.

UV cured epoxy and polyester composite patches have also been shown to offer a strong, durable and cost effective alternative to ambient temperature and thermal cured prepregs in the repair of impact damage sites [225] and large composite structures [226] as well as joining techniques. Pang et al. [227] and Peck et al. [228] studied composite pipe joints and both reported satisfactory mechanical properties for the UV-cured joints compared to room temperature cured joints. Peck, et al. [228], examined

pipe joints manufactured using glass fibre, vinylester resin and UV curing at three different intensities 80, 35 and 15 mW/cm² (in total 36 joints were produced). The effect of UV light intensity on the internal pressure rating, the ultimate bending load, and stiffness was evaluated based on experimental test results. Peck, et al. [228], used a UV light array of relatively low intensity used six 160W fluorescent bulbs at distances that resulted in surface irradiance averages of 80 mW/cm². Likewise, the variation of irradiance based upon the placement of the bulbs on three evenly spaced fixtures on a circular radius from the substrate meant the transient exposures could not be qualified. There was a direct correlation observed between increased light intensity and increased residual mechanical properties. A lack of exposure and therefore low degree of cure and non-uniform curing were found to be the largest determiners of mechanical performance and highlighted the concern of exposure dosage and uniformity for performance certainty. There exists several factors for optimization of UV curing resins that Peck raised, including the concentration of photo-initiators, intensity of UV light used for curing, type of monomer and the presence of oxygen in the curing environment. The total UV radiation required to effect cure is characterized by the dosage, measured in J/cm². This is a product of the two main processing parameters, the UV intensity (or irradiance) measured in W/cm² and the exposure time. A dosage in the range of 7.5-12 J/cm² can be sufficient to cure relatively thin (~0.8mm) composites [222].

6.3 Experiment 6: The Effects of High Intensity UV and Curing Speed on Material Properties

In continuous processes, such as UVAFP, the rate of reaction is critical in determining the total processing time. Research has shown that by increasing intensity of the UV light source, the rate of reaction in photo initiated resins increases dramatically [167][211]. In the case of this work, high intensity UV light is defined as intensities above 5W/cm². At such intensities cure occurs in a matter of seconds rather than minutes [63] by using focused spot curing to provide localised control [229]. High intensity UV light equipment requires greater safety controls in order to protect operator's skin and eyes. However, as UV light can easily be contained by simple filtering screens implementation is relatively simple in comparison to other curing mechanisms allowing it to be used in a variety of applications. Spot curing systems

exist commercially and are often utilised in dental, adhesive and dye curing processes [229] in close proximity to human operators with the risks of exposure easily managed. Furthermore, in spot curing systems that utilise high intensity UV light the temperatures during exposure can be elevated significantly within the localised exposure area [221]. It has been shown that these elevated temperature conditions can aid in further increasing the speed of cure but with the risk of degradation by burning, oxidisation and/or chemical temperature property degradation.

A number of studies have been conducted to evaluate the effect of UV light intensity on the curing rate in order to accelerate the total curing time [167][230][231][232][233][234][235][236]. However, most of these studies have been in the field of dentistry research, using UV curing resins for dental filling and adhesive applications, not structural composites [228] and at low intensities due to the application within a patient's mouth. Other studies examining the effects of UV intensity is in purification systems or reactors using the light to kill micro-biobial organisms or ink and dye printing. Much of this research is focused on dose control version application conditions (angle, refraction etc.) but again use relatively low UV intensities, in the order of mW/cm^2 [228][237]. While these references provide good data on the calculation, control and monitoring of UV dose, little research has been conducted at higher intensities, up to 25 W/cm^2, to examine the curing speeds possible using high intensity UV curing within continuous structural composite processes. This experiment examines this possibility for use in the UVAFP prototype and provides an understanding of the overall effect on the final material properties of the composite depending upon dose and intensity.

6.3.1 Experiment Aim and Hypothesis

The aim of this experiment was to determine the effect of the dose (intensity over time) on the degree of cure of bulk vinylester resin and understand how this translates as to achievable mechanical properties in a glass fibre reinforced vinylester resin composite. It was hypothesised that by using high intensity UV light the dose will be increased, therefore leading to a higher degree of cure over a shorter amount of time than using 'standard intensity' ranges. Resin hardness was used as a direct measure of degree of cure across a range of exposure intensities and times to provide a qualitative

assessment of the degree of cure of the resin. The hardness was measured at least three times at both the incident and bottom tool surfaces in order to gauge the depth of penetration according to the intensity and the average taken. The interlaminar shear strength test was chosen as the mechanical property measure for a laminated composite sample cured using the determined ideal exposure time from the bulk curing resin tests as it induces delamination failure at the mid-plane of the composite, and is therefore sensitive to the resin performance [73].

6.3.2 Experiment Method

Swancor 901-35 bisphenol-A epoxy vinylester resin [238] was used in this trial due to lack of availability of the resin chosen according to the work of Chapter 4 (Ashland Derakane's 411-350 vinylester). The Swancor vinylester resin was selected for its similar properties and formulation to Ashland's Derakane 411-350 vinylester resin. The resin was formulated with 0.5 parts per hundred (pph) ratio by weight of phosphine oxide-based photo-initiator (Irgacure 819, Ciba Specialty Chemicals). The bulk resin was poured into a 10 mm diameter cylindrical mould (made of machined Teflon) to a depth of 8 mm. The mould was placed under a high-intensity UV spotlight (Omnicure 2000) that emitted UV light in the UVA/UVB range through a fibre optic light guide. Intensity was measured at the orifice (distance = 0mm) using an Exfo R2000 Radiometer. The diameter of the aperture at the tip of the guide was 5mm and the distance from the tip to the surface of the resin was 20 mm. Only the top surface of the resin (termed the incident surface) was exposed to the UV light. Samples were exposed to the irradiance levels between 3 and $25W/cm^2$, each over an increasing exposure period from 5 to 60 seconds, thus providing a variety of doses.

6.3.3 Experiment Results and Discussion

The total UV radiation required to effect cure was characterized by the dosage, measured in J/cm^2. This was a product of the two main processing parameters, the UV intensity (or irradiance) measured in W/cm^2 and the exposure time. A dosage in the range of 7.5-12 J/cm^2 has been shown to be sufficient to cure relatively thin (~0.8mm) composites [222]. By using the high intensity UV light the hypothesis of the experiment was proven correct, with higher dosages leading to faster cure. It was shown that the

dose was the primary driver in the degree of cure achieved and not time as an independent variable because of any rate restricted properties of the chemistry. In thick structures, previous work has shown that a dosage of 375 J/cm^2 [75] is necessary before the hardness of vinylester resin is the same for both the incident and non-incident surfaces of an 8 mm thick sample. Due to use of a similarly deep sample depth, a similar range of total dosage was applied in this experiment.

Rockwell hardness testing (scale M) of the bulk resin samples was conducted according to ASTM D785-89. A minimum of 3 readings were taken from the incident and non-incident surfaces of each sample.
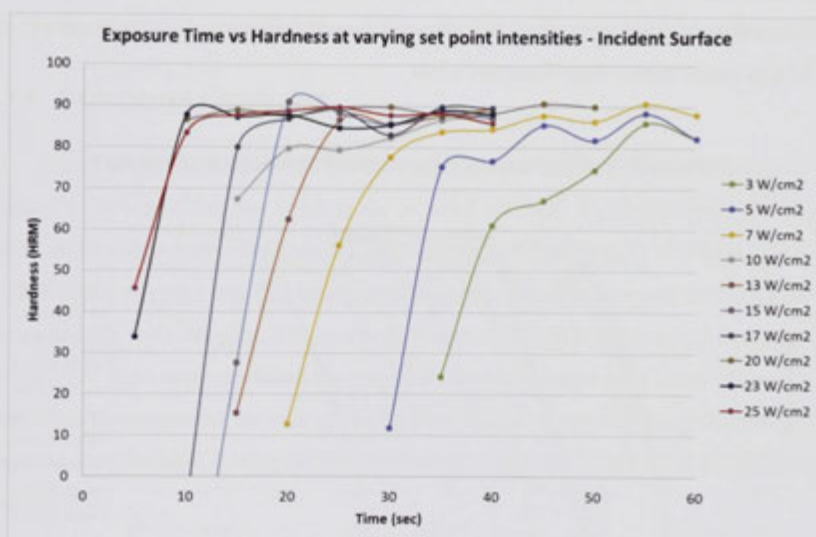
Figure 113 - Rockwell hardness (scale HRM) for bulk resin as function of exposure time for the incident surface

The average hardness results for the incident surface are shown in Figure 113. Hardness measurements could only be taken upon gelation and sufficient surface structure existed, therefore sufficient exposure had to be applied before the hardness could be measured, as such no data exists from zero up. In all cases an exponential relationship exists showing that within a very short time step (usually less than 5 seconds) from the time that the resin gelled and a hardness measurement could be taken the degree of cure progressed rapidly.

Figure 114 shows the Rockwell hardness versus exposure time at various intensities at the bottom surface (8mm depth). During the early stages of cure and where the depth of penetration had not yet reach the bottom surface sufficiently, a hardness measurement could not be taken for both the incident and bottom surface. In the measurement of hardness a sufficiently hard substrate and depth of cure must have occurred otherwise readings would be impacted by the supporting stand. Therefore at low cure levels not all data could be used and the lack of measurable hardness suggested that the bottom face cure was not developing consistently through the thickness. The variance in data and the lower conformity to a clear exponential relationship is clear in the bottom surface hardness data. This is attributed to the depth of penetration of the light into the resin and generally lower cure levels at this depth versus the incident surface as described by Beer-Lambert's law.
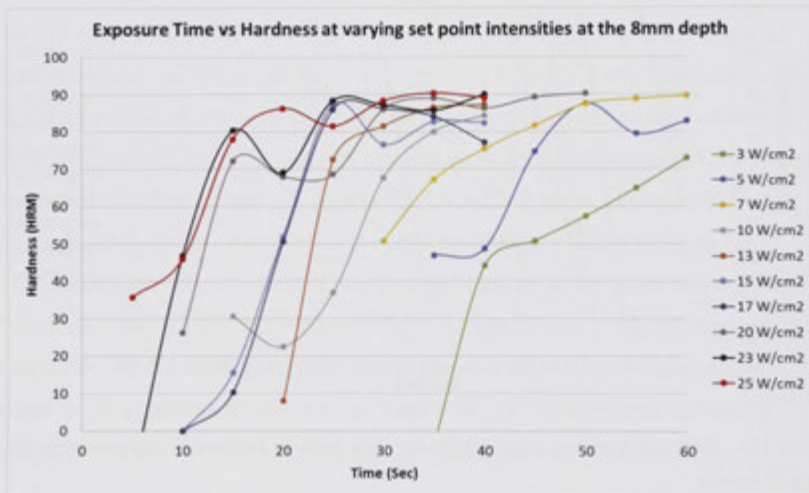
Figure 114 – Rockwell hardness (scale HRM) for bulk resin as function of exposure time at 8mm depth (the bottom surface against the tool)

Except at medium to low intensities (3, 5 and 7 W/cm^2), it was clear that 15 sec of exposure was required before the hardness was within scatter. This was relatively the same for both the incident and non-incident surfaces of the 8 mm thick sample. At 25 W/cm^2 this corresponded to a dosage of 375 J/cm^2 and reflected the time dependent aspect of penetration rate as important in UV curing in time dependent processes.

Above the 30 second exposure period, almost all high intensities samples achieved hardness levels on both the incident and bottom surface close to 90 HRM. The similarity in hardness gives a qualitative indication that the degree of cure is similar on both surfaces and the exponential nature of the rate did not, within scatter, increase the hardness and hence degree of cure significantly above this time. The maximum hardness values were in the range 85-90. Previous work reported a hardness value of 90 for vinylester resin that were room temperature cured for 24hrs and then received a thermal post-cure treatment of 90°C for 4 hours [239], a total cure cycle of 28hrs not including de-mould times. This thermal post-cure was recommended by the resin manufacturer to attain maximum properties. Therefore, the hardness results for the UV-cured resin in the current study indicate that a high degree of cure has been attained.

6.3.4   Experiment Conclusion

Much of the research on UV curing composites to date has been conducted at relatively low intensities and doses in the order of mW/cm². Exposure times in the range 10-30 minutes are therefore required [201]. Using the high intensity UV light achieved a high degree of cure up to 420 times faster than room temperature and thermal post curing in bulk resin samples. The in-situ approach of UVAFP using a high intensity (25 W/cm²) UV light source reduced the required exposure time to only several seconds. This result demonstrated the cure speed for the UVAFP process and materials could be dramatically increased leading to faster placement rates and higher productivity of the process.

The depth of penetration was shown to be sufficient to cure an 8mm thick sample. Ply thicknesses in composite are generally in the order of 0.2 to 0.4mm thick and as such cure at such shallow depths could be easily achieved allowing for the possibility to increase the processing speed even faster. Given the ply-by-ply nature of UVAFP lay-up with very thin plies applied each time, exposure is repeated across the laminate and therefore with each ply the degree of cure is proposed to progress even further for the previously laid plies, particularly for those plies deeper within the laminate. Only the top ply would receive a single dose and therefore this final pass could be slowed to ensure a minimum exposure level so as to maximise the speed for previously laid plies. This could therefore mean that the overall process speed could be further increased.

The interlaminar shear strength of the composite sample showed equivalent properties to the thermally cured reference sample cured for over 28 hrs and demonstrated the process was relevant and applicable to composites and not just bulk resin. In fact, by visual observation it appeared from the relative hardness of each ply immediately after exposure that the degree of cure was very high and perhaps aided by the addition of glass fibres which have a high UV transparency.

In the bulk resin curing trials by using directly perpendicular exposure from a light guide UV distribution across the sample was relatively even due to the small sample size and stationary light guide orifice. In dynamic processes the flux in intensity across the exposure area would affect the delivered dose and would need to be characterised. In testing the hardness of the bulk resin samples the hardness deviation was very small indicating good uniformity across the exposure area. Across the composite sample produced using a moving light source hardness measurements showed greater deviation indicating the greater variance across the exposure area and the effect of the dynamic light source. Further work will be conducted to optimise the processing parameters and dosage to rapidly cure thin layers of composite with high intensity UV light while achieving acceptable mechanical and thermal properties.

6.4 Experiment 7: The Effect of Curing On-the-Fly in a Ply-by-Ply Manner versus Bulk Curing At-Once

Greer, McLaurin, and Ogale [16] examined the reinforcement of photo-curing resins with continuous carbon fibres in an automated desktop photolithography unit (ADPU) developed at Clemson University, USA. In this proof of concept study, continuous fibres were added in-situ to the photo-resin to obtain composite samples containing over 20 % of the fibre volume fraction. The specimens produced in the semi-automated desktop prototype had much improved tensile strength by at least a factor of 2 as compared to that of the pure photo-resins without fibre reinforcement. As carbon fibres are non-transparent to UV light and inhibit the depth of penetration, full cure could not be totally achieved in a single step. However, it was noted that the photo-resin could be cured enough to develop sufficient green strength in the composite samples that would allow a free-standing thermal post-cure, if a dual cure resin was used. The ADPU system successfully produced single strip carbon fibre samples with in-situ resin

application. Samples however had poor width uniformity due to the irregularity of the supply tows, as well as poor thickness uniformity due to the high resin content and lack of compaction. A dual-curing resin was used in this study however it appears from the results that the properties of the resin were compromised by the chemistry. With a thermal post cure beyond 2 hours, conversion was progressed to a high level but brittleness became an issue for mechanical performance. These issues while critical for industrialisation did not detract from the evident success in the in-situ build-up of composites and curing on-the-fly.

Beyond the research of Clemson little research exists examining the effect of curing on-the-fly using a ply-by-ply manufacturing approach as applied the composite materials. Following the initial scoping experiments detailed in section 6.3 using high intensity UV curing in a static setup, the same high intensity system was applied in an in-situ manner curing on-the-fly and ply-by-ply to assess the application of the approach to the UVAFP prototype and understand the processing limits. The technique was compared to the traditional approach of curing the composite in bulk at-once at the end of the lay-up of the entire laminate.

6.4.1 Experiment Aim and Hypothesis

The aim of this experiment was to understand the effect on the material properties by comparing a ply-by-ply lay-up and cure approach with a traditionally laid up composite, complete with all plies laid and then cured "at-once". It was hypothesised that applying the curing mechanism source (in this case the UV light) in a ply-by-ply, in-situ approach will result in equivalent mechanical properties to a traditional at-once thermal cured composite processing.

6.4.2 Experiment Method

Two 10-ply laminates of dimensions 80 x 80 mm were manufactured by hand lay-up with a Derakane 411-350 vinylester resin formulated with 0.5 parts per hundred (pph) by weight ratio of Ciba Specialty Chemicals Irgacure 819 photo-initiator [162]. The fibre reinforcement used was a unidirectional E-glass (Owens Corning R25, 300 g/m²). Both laminates were cured using a high intensity spot curing system by Exfo called the Omnicure S2000 [202]. The Omnicure S2000 contained a high intensity 200

Watt mercury short arc UV light that emitted light in the UVA/UVB range, with light directed by an iris through a fibre optic light guide. This light guide had an orifice diameter of 5mm. Laminates were cured at an intensity setting of $20W/cm^2$, which was measured using an Omnicure radiometer placed on the aperture at the tip of the light guide. The UV light guide was attached to a small industrial robot (ABB IRB1600), as shown in Figure 116, and a path program was written that passed over the laminate ensuring complete exposure of the entire surface area of the laminate.
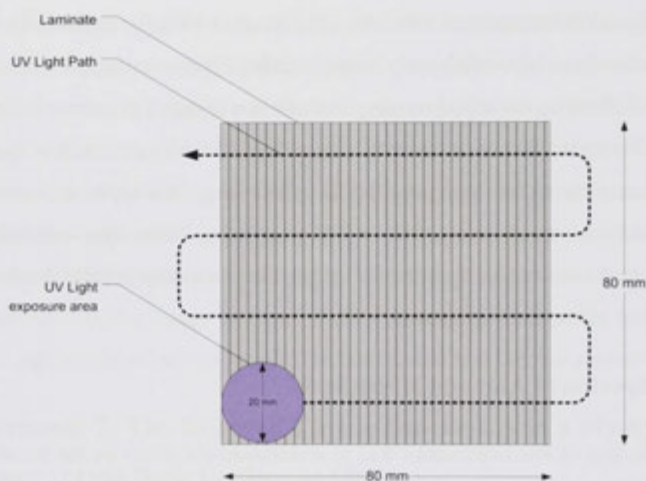
Figure 115 – UV light exposure method

The distance between the surface of the laminate and the aperture at the tip of the light guide was 20 mm forming a UV exposure area 20 mm in diameter.

Figure 116 – Image of the UV light mounted onto the end of an ABB IRB1600 industrial robot passing over the laminate

For the first laminate, all 10 plies were laid-up, consolidated with a wet lay-up compaction roller and then exposed to UV light all at once with a single pass of the robot arm at a tool centre point (TCP) speed of 1.5 mm/s. The cycle time was approximately four minutes. For the second laminate, each ply laid by applying a film of resin onto the previous ply surface followed by the placement of dry fibre on top of the wet resin. Following this placement the fibre tows were compacted into the resin using a wet lay-up compaction roller, (similar to a fibre placement process). Each ply was then immediately exposed to the UV light prior to lay-up of the next ply. For each exposure, the robot arm speed was 600mm/s and the cycle time was less than 1 second. The exposure was only enough to give a low tack, b-staged surface prior to laying of the next ply. Upon lay-up of the final ply, the laminate was then exposed with the TCP speed set to 3 mm/sec, to give a final cure exposure of just over 2 minutes to ensure full cure – the total cure cycle time (excluding lay-up) was approximately 2 minutes and 15 seconds. This approach was intended to simulate an automated, ply-by-ply composite placement process whereby a partially cured ply produces a tacky surface to promote chemical bonding with the next ply.

A qualitative assessment of the degree of cure of each laminate was then made using the Rockwell Hardness test (scale M), according to ASTM D785. Following hardness testing a centre-loaded interlaminar shear tests were conducted on samples from each laminates according to ASTM D2344. The average sample length was 50mm

and width 7mm. Samples were tested on a mechanical testing machine (Instron model 4505) in a 3-point bending fixture with a cross head speed at 1.3mm/min. The span length to thickness ratio was 5:1 and the loading pin diameter was 6.35 mm as recommended by ASTM D2344. A minimum of 5 samples were tested for each laminate. The interlaminar short beam shear strength (τ_{sbs}), in MPa, was evaluated according to Equation 15.

Where P is the maximum load, w specimen width and t is the thickness of the specimen. Microscopy of the fracture surfaces was undertaken on a Cambridge S360 electron microscope. Samples were coated with a thin layer of gold prior to examination.

6.4.3   Experiment Results and Discussion

The hardness of the resin-rich surfaces directly exposed to the UV light (incident) and on the mould (non-incident) is given in Table 28. The hardness values are in the range 85-90, which is are consistent with hardness of vinylester resin cured conventionally at room temperature and thermally post-cured at 90°C for 4 hours [201][201].Within scatter, there is no significant difference in results between surfaces or between laminates. Therefore, it can be concluded applying the curing mechanism in a ply-by-ply in-situ approach does result in equivalent properties proving the hypothesis and that a high degree of cure can been achieved with the ply-by-ply approach.

Table 28 – Average (± standard deviation) laminate thickness, fibre-volume fraction (V_f), hardness and interlaminar short beam shear (ILSS) strength.

Laminate	Thickness (mm)	V_f (%)	Surface hardness (HRM)		ILSS (MPa)
			Incident	Non-incident	
Ply-by-ply	4.88 ±0.18	24 ±0.9	91.98 ±7.10	85.15 ±5.20	51.18 ±2.52
At once	5.25 ±0.36	22 ±1.1	91.63 ±7.66	87.49 ±5.28	50.49 ±1.91

All samples exhibited shear-induced mode II delamination along the mid-plane, which is the typical failure mode for the interlaminar shear test [242]. Electron micrographs were again taken in the assessment of samples. The typical fracture morphology observed for each laminate are shown in Figure 117. The deformation features between the fibres were classified as "hackle marks". Hackle marks, caused by

the coalescence of micro-cracks initiated by shear loading were present in the resin between the fibres of both samples. These marks are commonly observed for mode II shear failure [240][241] and are also similar to those observed in thermally post-cured glass-fibre/vinylester counterpart [201]. The consistency of the morphology between samples supports the shear strength results, and the conclusion that the ply-by-ply process produces laminates of comparable quality to the bulk laminate. The shear strength results and hackle mark morphology presented here are also similar to those reported for thermally post-cured glass-fibre/vinylester counterparts subjected to the same interlaminar shear [201]. This observation supports the conclusion that a high degree of cure has been achieved with the high-intensity UV light.
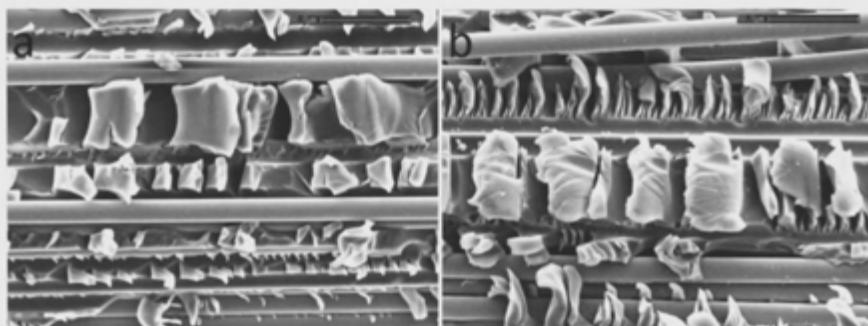
Figure 117 - Fracture surface micrographs from (a) ply-by-ply composite and (b) bulk composite short beam shear samples.

Localised heating at the exposure area during curing at slow speeds (in the at once sample and for the final ply of the ply-by-ply) was observed but quantitative assessment is not presented in these results. This heating could enhance resin reactivity but may also cause localised thermal stresses.

6.4.4 Experiment Conclusion

This experiment demonstrated that the ply-by-ply curing approach could be applied to the UVAFP process and achieve comparable mechanical properties to a traditional at once thermally cured composite of the same fibre and resin using a different initiator, while resulting in a faster cure speed due to the thin ply depth each exposure had to penetrate and the incremental increase of exposure with each

subsequent ply. The results of this preliminary study are of immediate significance, ultimately indicating the possible to increase production rate. The potential for reduction in cycle times is clear. Laminates that were cured in minutes versus hours for the conventional room temperature and thermal post-cure stages for thermal processes.

While a B-stage initial cure was used in the ply by ply approach for this experiment, the intended mode of operation in the complete UVAFP system would be to achieve full or near to full cure in each pass. That being said further work could consider the B-stage only approach with the view to increase the lay down rate. This should be investigated in future work.

Furthermore, relatively rapid cure can be achieved with well-known and commercially available, relatively low-cost materials. The only difference in the case of the composite used here is the formulation of the vinylester resin with a photo-initiator to initiate the free radical cure mechanism instead of a peroxide catalyst. The ply-by-ply procedure also demonstrates the concept of an automated composite placement process with rapid in-situ UV curing. Automation can enable higher productivity and improve accuracy and repeatability of fibre placement and orientation. The b-staging of the resin through brief UV exposure provides integrity to the ply and minimizes ply movement or resin run-off when the next ply is placed, while still allowing for chemical bonding with the resin in the next ply. Thicker laminates could be manufactured by partially curing each layer prior to placement of the next layer. The accumulated UV exposure or an increased dosage via a final UV exposure would achieve full resin cure.

The rapid curing of photo-initiated resins with UV radiation offers the potential to drastically reduce the curing time. Processing times of glass-fibre and photo-initiated resin composites are orders of magnitude quicker than room temperature or thermal cure counterparts [75] with a relatively low power (400 W) and low intensity (2 mW/cm^2) UV light. Mechanical properties are unaffected by layering and secondary bonding, and solvent emissions are reduced [76]. Furthermore, curing of the resin occurs only on exposure to UV. This allows time for precise fibre placement and orientation, complete wet-out of fibres and removal of trapped air. This has further benefits in the lay-up of large single piece components where pot life and processing windows can be an issue if the lay-up is slow. UV curing is not a novel technology for composite materials processing but its adoption in AFP could offer major productivity

gains as already demonstrated in application in a number of different advanced composite manufacturing techniques.

6.5 Summary

A significant body of knowledge exists around the use of in-situ curing techniques in various applications however limited application of the technology has been seen in composites and in particular in automated manufacturing processes. In order to eliminate the need for post-curing as an additional step in the composite manufacturing process when using AFP the concept of using UV curing applied in-situ in a ply-by-ply manner was proposed and tested. First, the cure rate versus the intensity was tested accordingly with a direct measure of the degree of cure using resin hardness. Second, a comparison to traditional at-once bulk curing approaches was made using high intensity UV light in a ply-by-ply approach. The shear strength result and the observed fracture behaviour supports the conclusion that a high degree of cure and mechanical performance can be attained with high intensity UV curing. The results of the experiments of this chapter are also significant in that it shows the potential for high speed UV curing technology in automated composite fabrication processes that could eliminate time consuming ambient cure and post-cure stages. This concept can be termed in-situ curing [76]. For composite layers less than 1 mm thick, full cure could be achieved with shorter exposure times and lower dosages than those reported here. UVAFP combines curing and individual tow lay-up and consolidation into the one process while still being able to accurately and discretely control the through thickness orientation of every fibre.

The resin hardness and the composite interlaminar shear results indicated that rapid, high intensity UV curing can provide equivalent resin dependent properties compared to conventionally cured composites. Comparable properties can also be achieved in laminates manufactured using an integrated ply-by-ply and UV curing process. This shows potential for automated processing of composites with significantly reduced cycle times compared conventional thermal curing methods.

Further work needs to be done to rapidly cure thin layers of composite with high intensity UV light while achieving acceptable mechanical and thermal properties in the ply-by-ply process. Placement models will be required to understand the thermal history

of the process and the residual stresses, given the rapid cure. It is also important optimize the processing parameters, such as UV intensity and exposure time in order to maximise mechanical properties and depth of cure.

7 Degree of Cure Process Model

A current limitation of the AFP process is the lack of publically available data to model the process and discern process capacity critical information for process assessment. Chapter 3 identified the critical design parameters of an AFP machine dictating reach and access in order to maximise the flexibility and usability of AFP on complex parts. Chapter 4 identified suitably inexpensive, easily handling and rapidly curing materials which would drive the recurring price down. Impregnation of the fibre and resin chosen has been shown in Chapter 5 to occur incredibly fast, thanks to the localised pressure of the compaction roller, the capillary effect, the form of the glass fibre tow (primarily due to the fibre diameter and V_f). Chapter 6 examined the use of UV curing in the UVAFP process conditions including use of localised high intensity UV light applied on-the-fly and curing in a ply-by-ply manner. In each of the chapters each process limitation and experiment has looked at a singular aspect of the UVAFP process in order to optimise the UVAFP prototype and characterise the process steps. However, no work has been done as yet combining these results and looking at the model as a system in a holistic manner. This chapter therefore aims to examine the critical capacity driver for UVAFP – the speed of lay-up and the degree of cure of the resin by bringing together the learning of previous chapters. The result is a predictive degree of cure model looking to maximise rate while maintaining quality.

Section 7.1 describes the current literature and types of models developed to predict and characterise AFP and how it could be applied to UVAFP. Section 7.2 presents the relevant literature available examining the specific process conditions associated with UV curing. Section 7.3 presents Experiment 7, the development of a predictive model for the degree of cure model based on the primary process parameters, placement speed, set point intensity and the height of the UV light from the incident surface. Section 7.4 provides a summary of the modelling work and the context for further modelling work to examine the quality issues associated with temperature and degradation that can occur using high intensity UV light.

7.1 Process Modelling of the AFP Process

During lay-up, tows or fibres are pulled from a creel system that guides the fibre to the placement head on the end of the articulation device that also provides compaction force. Within the placement head fibres are tensioned, fed, cut, clamped and restarted (CCR). At the nip point the fibre is heated and cooled as required compacted in place and in some instances inspected inline. It is evident that the AFP process involves a number of individual operational steps. With so many operations in one system, complexity is inevitable. In order to simplify models usually only 1 or 2 operations are addressed based on significance to the end result, usually this is the heat transfer and the compaction [32]. Generic models exist that examine the process fundamentals; with particular attention being paid to thermoplastic fibre placements where in-situ consolidation requires accurate heat control.

Over the years of development, process modelling of the standard AFP process has expanded from 2D [142] to 3D looking at edge effects from adjoining tows and previously laid plies [243]. In these models, the most critical independent process parameters are temperature, pressure and time. The most critical quality measures are the mode I fibre driven properties such as tensile and compressive strength and modulus, mode II resin driven properties which include flexural strength and modulus, hardness, operating temperatures as well as the quality such as void content and degree of impregnation. The mode II properties, are predominantly related to degree of conversion or degree of cure of the resin and the curing conditions. A majority of the research on AFP process modelling has focused on identifying and optimizing these critical process parameters of temperature, pressure and time [27][32][38][47][114]. Accurate process models can be used to predict the degree of cure, thermal degradation, thermal history, consolidation and melding adhesion (for thermoplastics) and localised stresses accurately enough to characterise materials manufactured using the process and control quality.

Alici, et al. [244] highlighted the complexity associated with the modelling of the AFP process by developing a tenth order parametric model of a robotic fibre placement system, using a step response experimental setup to verify the model. The results showed the dynamic nature of fibre placement and the complexity in quantifying a model with a high number of process parameters. This conclusion is common to many

studies [245] and most have therefore focused on limiting the scope of the model to the main process parameters of tacking heat and compaction force.

7.2 Process Modelling of UV Curing

The modelling of UV curing is derived from a number of independent and dependent variables determining the delivery of the incident energy and the effectiveness of the energy in curing the photo-initiated resin. These are broadly covered by the dose, the absorption and penetration and wavelength reactivity of the initiator.

UV dose is the critical factor that determines the degree of cure in photo-initiated resins. Dose is generally calculated through simple averaging of the irradiance (W/cm^2) multiplied by time, dt [222][246][247][248][249]. However, this method only calculates a 'step-wise' mean dose, negating irradiance flux across the exposure area, absorption by the air, reflection and refraction and is not accurate for the exact determination of dose. Bolton [213][250], used this value as an 'ideal maximum' only and outlined the significance of reflection, refraction and the distribution of the UV light in determining actual dose delivery in UV reactors for water filtration applications. Comparisons of the different methods for calculating the dose, such as average, peak average and Gaussian distribution versus time show large variation in dosage value.

The interchangeable use of the terms 'irradiance' and 'power', in the calculation of dose, leads to some confusion on the actual definition of the term. In this work, irradiance was measured in W/cm^2 and as such, dose was calculated as J/cm^2 and is inversely proportional to speed [251]. Dose is derived from the exposure time and irradiance energy. As per the last experiment, the cured properties can be based on dose alone because this value describes the total energy delivered, photons per unit area, to hit the surface. But, as a lone parameter, dose tells us little about the process setup of the actual independent process parameters (such as speed, irradiance, height and set point intensity). As such irradiance at the source, distance and irradiance at the incident surface, absorption and speed need to be analysed before the dose can be predicted.

7.3   Experiment 8: Degree of Cure Predictive Model for UVAFP

Given the lack of available data for existing systems and the critical need for process models that relate process parameters to degree of cure as a final quality measure, an experimental approach was undertaken to build a predictive degree of cure model for UVAFP. A parametric map of the UVAFP process was created to identify the independent and dependent variables and to inform the areas of necessary research. The parametric map is shown in Figure 118.
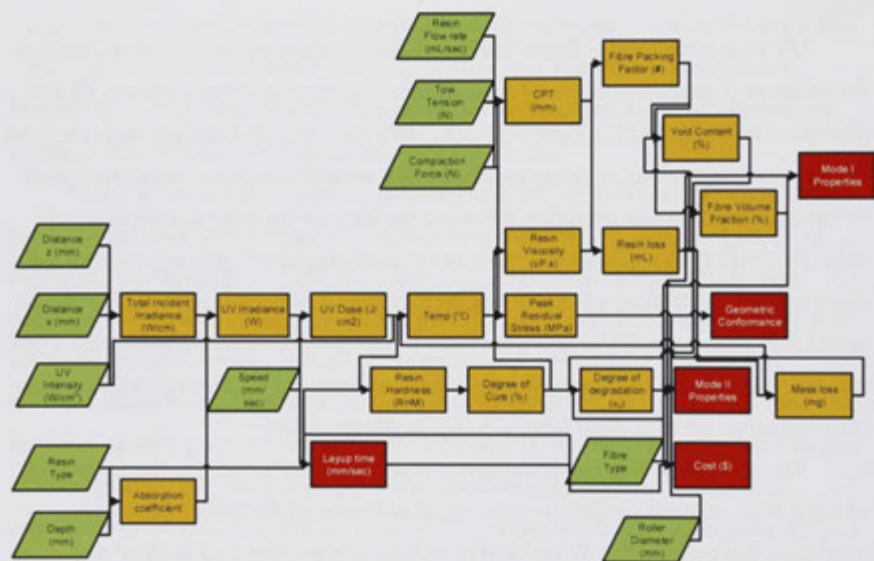
Figure 118 – UVAFP parametric map from independent process parameters to dependent quality criteria

Independent process parameters are shown in green, calculated or dependent in amber and quality output parameters in red. As shown in Figure 118, the independent process parameters of the UVAFP process are directly controllable with wide range and increments. Calculated or dependent parameters can be controlled indirectly to reach target outputs. While a significant amount of work has been done in modelling in-situ consolidation mechanisms in thermoplastic AFP processes [32][13], little is known about in-situ curing for thermoset resins and the unique irradiation curing dependencies of UVAFP. Some models do exist that characterise dosage delivery in processes outside

the field of UVAFP, such as in electron beam (EB) AFP and UV water purification reactor modelling [213]. However, these do not capture the transient irradiance delivery and its effect on the final dose. Precise control of dose and irradiance are critical to ensuring final properties and process integrity. The reaction rate of photo-initiation occurs in seconds, rather than the minutes and hours in thermal processes. Only by accurately characterising the output of the UV source and its interaction with the photo-initiated resin can such integrity be guaranteed in dynamic processes to ensure final material properties. As a part of this thesis a prototype UVAFP system was developed and integrated with 6 degrees of freedom industrial robot (Chapter 3). The prototype (as shown in Figure 119 [7]) was developed to capture the effect of the primary parameters on the final degree of cure in this work to develop the predictive model.
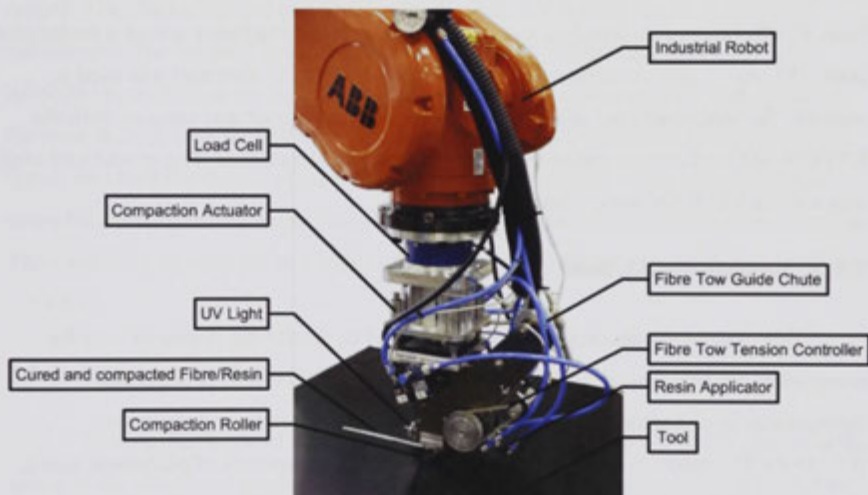
Figure 119 - New AFP process with in-situ UV curing prototype

7.3.1 Experiment Aim and Hypothesis

The aim of this experiment was to develop a model that could predict the degree of cure based upon the independent process parameters to optimise the process settings for maximising process efficiency (maximum speed) while maintaining quality (maximum degree of cure). In order to achieve this the UV dose had to be accurately characterised during the dynamic and transient UVAFP process. It was hypothesised

that testing the height of the UV light (distance to the incident surface from the source), the set point intensity of the UV light (at the source orifice) and the speed of the placement head the dose of UV light can be accurately modelled and related directly to degree of cure of the composite.

7.3.2 Experiment Apparatus

The materials used in this study were Owen's Corning SE1200-2400TEX E-glass roving [154] and Derakane 411-350 vinylester by Ashland Chemical [162] with a fixed ratio of 0.5% by weight (wt%) of Irgacure 819 (IC819) [252], a bisacylphosphine oxide (BAPO) photo-initiator by CIBA Chemical. IC819 undergoes a free radical reaction that causes cure only when exposed to UV light. The UV light was a Lumen Dynamics spot curing system, Omnicure S2000 [202]. Irradiance measurements were taken using an Exfo R2000 radiometer which is specified to capture total irradiance across wavelengths from 250 nm – 1 μm. A surface irradiance sensor (the EXFO Sitecure) was used to measure the total irradiance at the incident surface. This sensor was coupled with the EXFO R2000 radiometer and also measured the overall irradiance. The mould tool used was a white PTFE flat plate 12mm thick.

7.3.3 Experiment Method

This experiment presents a parametric model to predict the degree of cure for composites produced using an Automated Fibre Placement (AFP) process that incorporates in-situ ultraviolet (UV) curing and on-the-fly resin impregnation (UVAFP). The model is based on the primary process parameters of placement speed, set point intensity and the height of the UV light from the incident surface. Experimental data was collected to characterise the UV light output spectra and absorption wavelengths of the resin, the incident irradiance, the dose delivered at varying speeds and the hardness of the resin as a direct indicator of final degree of cure. Fitting analyses were used to model these phenomena and predict the degree of cure of the composite produced in UVAFP according to the independent process parameters. The model was validated with comparisons to manufactured samples.
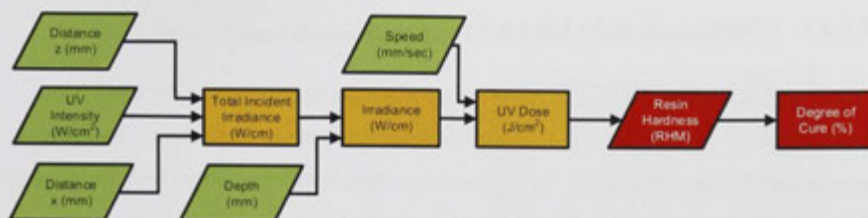
Figure 120 - Analytical model for the UV AFP process

The modelling process involved definition of each calculation in the model steps in order to produce the final series of simultaneous equations (presented in section 7.3.3) and these equations were then consolidated to form a final mathematical model. The overall modelling approach is shown schematically in Figure 120. The effectiveness of the UV light to cure the resin was confirmed by measuring the spectral output. The absorption and penetration depth of the UV light in the resin was then determined. The incident irradiance delivered by the UV light was measured and modelled according to the height, position and set point intensity of the light. Finally, the dose delivered by the UVAFP process was calculated, in relation to the placement speed, and then the degree of cure of the resin was correlated to this calculated dose using hardness measurements. The degree of cure was then modelled according to dose. The modelling process led to a series of simultaneous equations (as explained in section 7.3.4.6).

7.3.4 Experiment Results and Discussion

Testing the height of the UV light, the set point intensity of the UV light and the speed of the placement produced results that were able to be used to accurately define the effect of each parameter independently and together on the dose of UV light delivered to the incident surface. Furthermore, the dose was then able to be related directly to the degree of cure of the composite during UVAFP processing and a predictive model for the degree of cure was created. The results are presented below for each of the characterisations leading towards the final model. Each characterisation built the foundation data and equations for the next analysis.

7.3.4.1 Effectiveness of the UV Light

A photo curing reaction is triggered by exposure to UV light at the absorption wavelength of the initiator. Therefore the first experiment undertaken was designed to ensure the effectiveness of the UV light used in the UVAFP prototype with the selected Irgacure 819 photo-initiator. Spectral analysis of the UV output of the light was performed using a spectrophotometer to ensure peak outputs matched the peak absorptions of the initiator. The manufacturer's specifications [252] for the photo initiator Irgacure 819 indicates an activation wavelength of 365 nm, as shown in the inset of Figure 121 [229]. The spectral analysis result is shown in the main image of Figure 121. The UV light produced three peak outputs at varying wavelengths, one of which was at the peak absorption wavelength of the photo initiator trigger the reaction at 365 nm. This result indicated the light system provided UV light energy at the sufficient activation wavelength of the photo initiator and would be an effective curing light source.

The remaining peaks at 405 and 435nm while not necessarily matching the peak absorption could be seen as useful by contributing to heating of the composite. The generated heat was theorised to assist cross-linking by aiding molecular mobility due to the subsequent decrease in viscosity of the resin at the higher temperature [8]. The heat could also be a contributor to the final thermal properties of the resin such as the glass transition temperature [8][224], due to the increased temperature of the resin at which cure occurred.
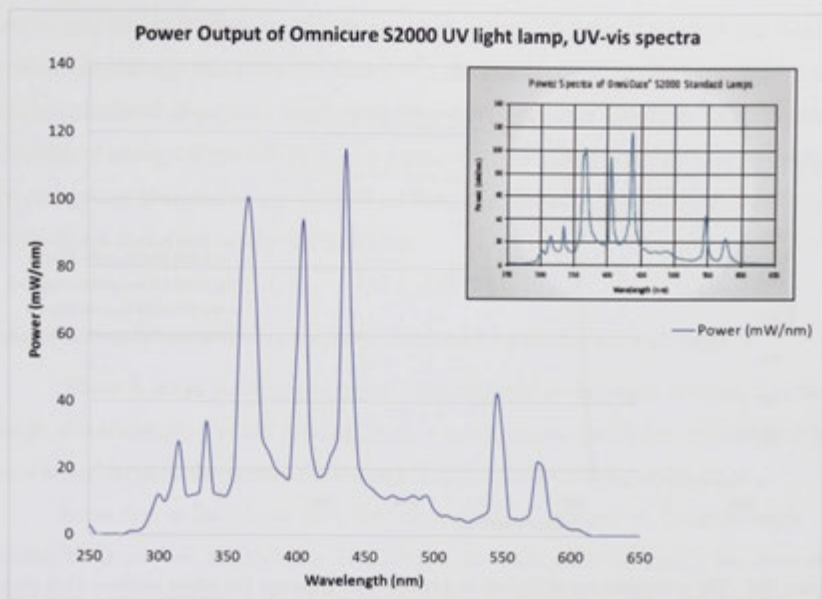
Figure 121 - Power spectra output of the Omnicure S2000 high intensity UV curing system as measured, with the manufacturer spectral output for the UV light by Lumen Dynamics (inset)

7.3.4.2 Absorption and Penetration Depth of the UV light

To determine the absorption coefficient and the effective penetration depth of the UV light in the resin at the activation wavelength (365nm), the transmittance of the resin across the UV-visible wavelength range was measured. The transmittance was measured in both cured and uncured samples in two different sample cuvettes (results shown in Figure 122) using a Perkin-Elmer Lambda spectrophotometer. The measurement of uncured and cured samples would show the change in transmittance through thickness as the reaction initiated and cross linking started from the incident surface and progressed into the laminate.

Low transmittance (high absorption) was observed from approximately 250nm to 425nm in all samples. Above approximately 425nm noticeable differences were observed between cured and uncured states, as well as between the different cuvettes used. The reflection of the cuvettes and resin was determined separately as necessary to calculate the absorption coefficient of the resin only.
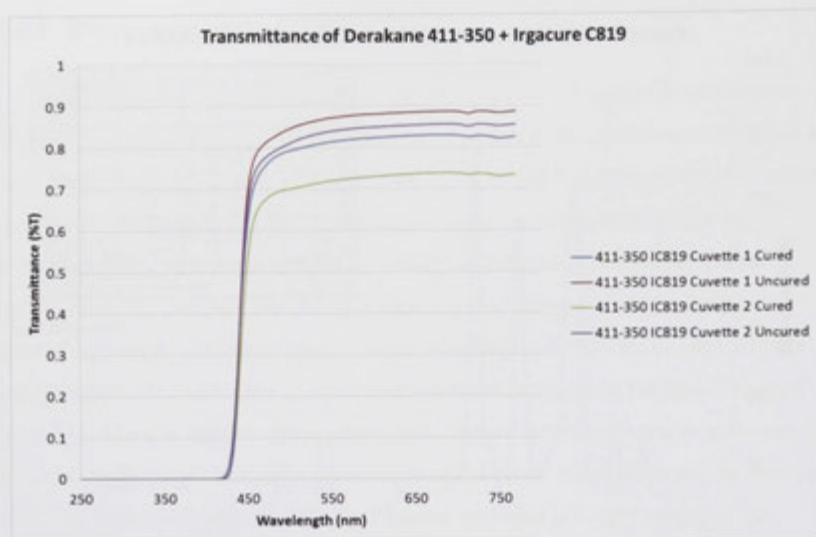
Figure 122 - The transmittance of Derakane 411-350 with Irgacure 819 photo initiator over the UV-vis spectra

At the peak activation wavelength of the photo-initiator, 365nm, the transmittance of UV light in the resin was measured to be very low, approximately 0.809 (Figure 122). Thus according to Equation 52, the absorption coefficient was calculated to be 1.65618.

$$A = 1 - T - R \qquad T = 0.0001164 \ \& \ R = 0.1908$$
$$A = 0.8090$$
$$T = 1 - R - A$$
$$T = 1 - R - (1 - e^{-\alpha d})$$
$$T = 1 - R - (1 - e^{-\alpha}) \ because \ d = 1cm \ as \ per \ cuvette \ depth$$
$$T = e^{-\alpha} - R$$
$$\ln(T + R) = -\alpha$$
$$\alpha = -\ln(T + R)$$

Equation 52 – Definition of Transmittance and the calculation of the absorption coefficient

Where T is the transmittance of the material measured as the percentage of incident energy transmitted through the sample, A, is the absorption of the material, R is the total reflectance, related directly to the reflectance of the cuvette containing the

sample, α is the absorption coefficient per cm depth and d is the depth from the incident surface. The through thickness irradiance was calculated using the Beer-Lambert's law and the calculated absorption coefficient. Beer-Lambert's law, Equation 53, defines the reduction of energy of the UV light as it passes through a medium. The law stipulates that energy not absorbed at the incident surface, and not reflected, is transmitted through the thickness and absorbed by the substrate.

$$I_\lambda = I_{0\lambda}(e^{-\alpha d})$$

Equation 53 – Beer-Lambert's law for energy absorbance versus depth at wavelength, λ.

Where I_0 is the incident energy or dose delivered to the upper surface, I_λ is the energy at wavelength λ at the defined depth, α is absorption coefficient at wavelength λ, and d is the depth of the composite through thickness from the incident surface.

According to Beer-Lambert's law, as applied in Equation 54, the maximum penetration depth was calculated to be 6.03mm, at which point the energy becomes less than $1/e$ or approximately 37% of the incident energy. Because of the exponential nature of the Beer-Lambert law, the delivered energy rapidly decreases beyond this point. The depth of a single ply glass fibre composite processed using UVAFP is generally no more than 0.25mm. Therefore, previously laid plies will experience cure advancement with each subsequent ply lay-up up to a built up thickness on top of approximately 6mm or 24 plies. This would be a relatively thick laminate and therefore for standard composite structures – of no more than 3mm the light exposure would lead to a well cured and high performing component. This is ignoring the effect of the fibre reinforcement.

$$I = I_0 e^{-\alpha d}$$

$$\frac{I}{I_0} = e^{-\alpha d}$$

$$T = e^{-\alpha d}$$

$$d = \frac{-\ln(T)}{\alpha}$$

$$d = \frac{1}{\alpha} \; where \; I = \frac{1}{e}$$

Equation 54 – Maximum penetration depth, d, according to transmittance where the energy is equivalent to $1/e$ or 37% of the energy on the incident surface

In trial laminates incorporating glass fibres, the depth of penetration was vastly increased. Laminates of thicknesses up to 12mm with a 50:50 fibre volume fraction were cured to full hardness upon exposure to the UV light. The glass fibres have a higher transparency to UV light than the resin and therefore allowed further penetration through the laminate and possible benefits from scattering reflection and refraction that could distribute the UV radiation energy, as also reported by Crivello [222]. Using Equation 52 to Equation 54 the measured transmittance, absorption and the penetration depth results are summarised in Table 29. These results were used in the final model to calculate the irradiation delivery through the thickness of the composite, thus adding the second dimension to the model, the depth, as measured in mm.

Table 29 – Transmittance, reflection and absorption data for Ashland's Derakane 411-350 vinylester with Irgacure 819 photo initiator in its uncured and cured states

Parameter	Uncured	Cured
Wavelength (nm)	365	365
$T_{average}$ (/1)	0.0001164	5.8300 x 10^{-5}
$R_{average}$	0.1908	0.1923
A (/1)	0.8091	0.8076
α (cm^{-1})	1.6562	1.6484
Penetration depth where $I = e^{-1}$(cm)	0.6038	0.6067
Penetration depth where $I = \frac{I_0}{3}$ (cm)	0.7270	0.7304

7.3.4.3 Incident Irradiance of the UV Light

Precise control of dose and irradiance are critical to ensuring final properties and process integrity. In order to accurately characterise the delivered dose as a specific aim of the experiment, the incident irradiance distribution of the UV light was recorded at varying set point intensities. The set point intensities were measured as irradiance at the orifice of the light guide using the Radiometer, while the incident irradiance was measured using a surface UV sensor positioned at the surface height. The incident distribution was determined as a function of the distance between the light orifice and the incident surface, referred to as the height (z, measured in mm) and the horizontal

displacement relative from the lights normal axis (x, measured in mm). The results are shown in Figure 123.

UV Irradiance Distribution for 5W/cm² at various Heights

UV Irradiance Distribution for 10W/cm² at various Heights
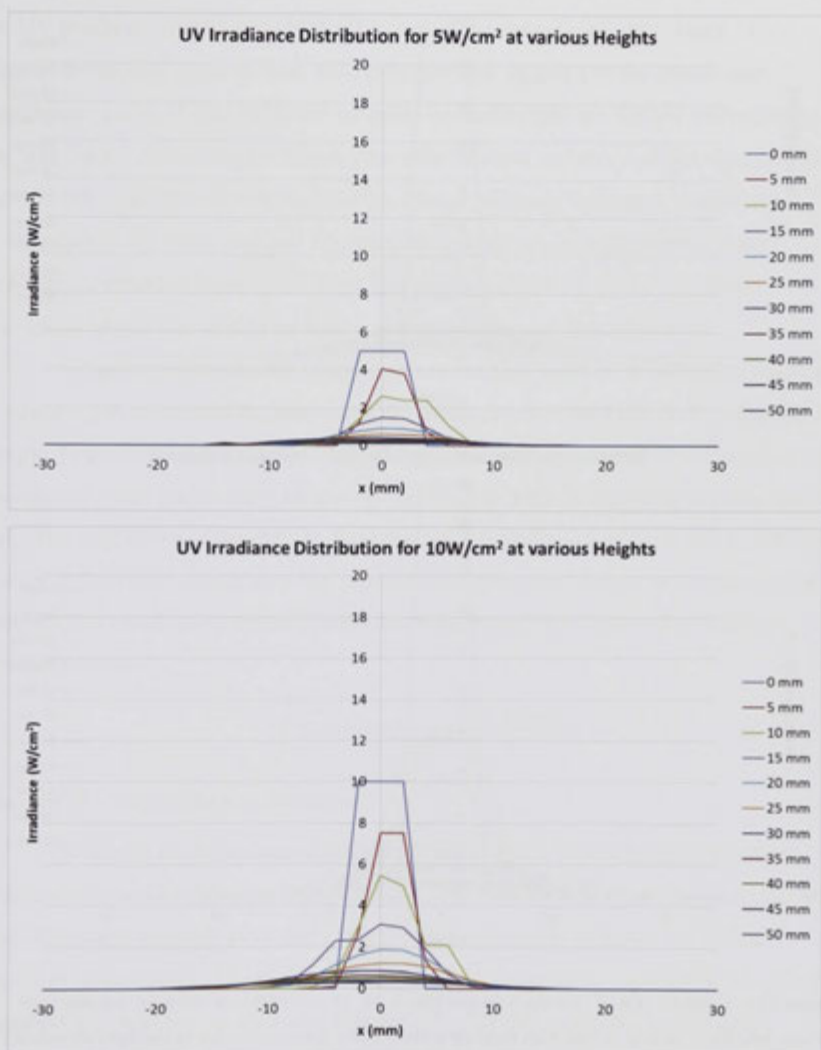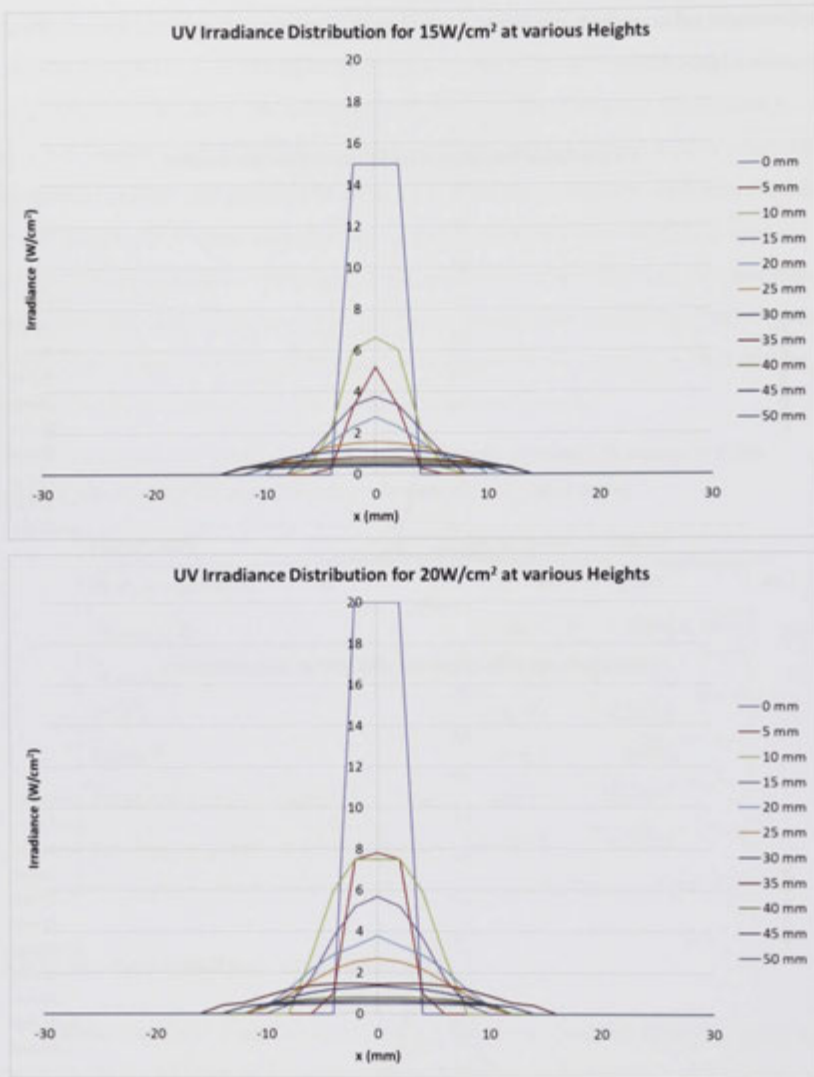
Figure 123 - Contour plot of radiation output (for 5, 10, 15 and 20W/cm² set point intensity) at various heights (z in mm in-line with light direction) and x (perpendicular to the light direction)

The irradiance curves in Figure 123 show the Gaussian distribution of irradiant light with the light being moved vertically above the stationary sensor, the origin (0,0). The curves indicate a clear reduction in incident irradiance the higher the source is but with greater distribution of the energy. Of interest though is the resultant curves for the

10mm and 5mm heights with sources of 15 and 20W/cm². For these two source intensities more radiance is achieved at the 10mm height as opposed to the 5mm height. This is particularly visible in the 15W/cm² plots. Furthermore, at this source intensity the UV irradiance distribution is equal to that of the 0mm height plot which refers to directly at the light guide orifice. This indicates that, in terms of the production application, using 15 and 20W/cm² set point intensities provide the UVAFP prototype the best energy delivery up to 10mm above the incident surface. Another aspect noted is that the UV irradiance distribution for the 15 and 20W/cm² sources is a more even distribution at the 10mm height. This may have implications with respect to the exposure time and ultimately the dose. The trends therefore indicate a possible maximum height that should be used in order to maximise dose efficiency.

Following measurement of the incident irradiance and its distribution, the total irradiance was calculated by integrating the irradiance as a function of dx, using the simple Trapezoidal rule (Equation 55). This technique was selected as it simplifies the calculation while maintaining an appropriate level of error in capturing the area under the point wise curve of the data. In Equation 55, x is defined as a range and a and b are values in this range. Integrating the incident irradiance with respect to dx reduced the independent variables of the data as the normal distance was captured by the total irradiance value.

$$\int_{a}^{b} f(x)dx \approx (b-a)\frac{f(a)+f(b)}{2}$$

Equation 55 – Trapezoidal area calculation

To model the behaviour of the total irradiance as a function of height and irradiance, over 150 different fitting functions were tested and scored based on the least sum of squared absolute error and a target of 6 coefficients, effecting the fitting equation 'smoothness'. Using the scoring study a full quadratic logarithmic transform equation was selected, as shown in Equation 56. The full quadratic logarithmic transform fit achieved the least sum of squared absolute error with a high R^2 value of 0.90985 and a Root Mean Squared Error (RMSE) of 0.07257.

$$I_0 = a + b(\ln(hI_{set} + i)) + c(\ln(iz + k)) + d(\ln(hI_{set} + i)^2) + f(\ln(jz + k)^2)$$
$$+ g(\ln(hI_{set} + i))(\ln(jz + k))$$

Equation 56 – Total irradiance, I_0, full quadratic logarithmic transform fit equation, where I_{set} is the set point irradiance (W/cm²) and z is the height from the incident surface (mm)

The coefficients of the transform function are detailed in Table 30.

Table 30 – Full quadratic logarithmic transform coefficients

Coefficient	Value
a	-0.6331
b	-4.0204
c	0.4502
d	453.7568
f	-0.01298
g	-9.4963
h	0.0009516
i	1.04656
j	0.8979
k	0.1273

The as recorded and predicted total irradiance values were surface plotted as shown in Figure 124. A noticeable difference between the actual and predicted surfaces was observed at the 5mm to 10mm and 35mm height ranges. At these heights an inflection or flux in the intensity is apparent. This effect could be explained by lens distortion of the light orifice and non-collimated light scattering from the liquid filled light guide causing non-perpendicular light to hit the substrate. These effects could have therefore caused irradiance concentrations at the respective heights.
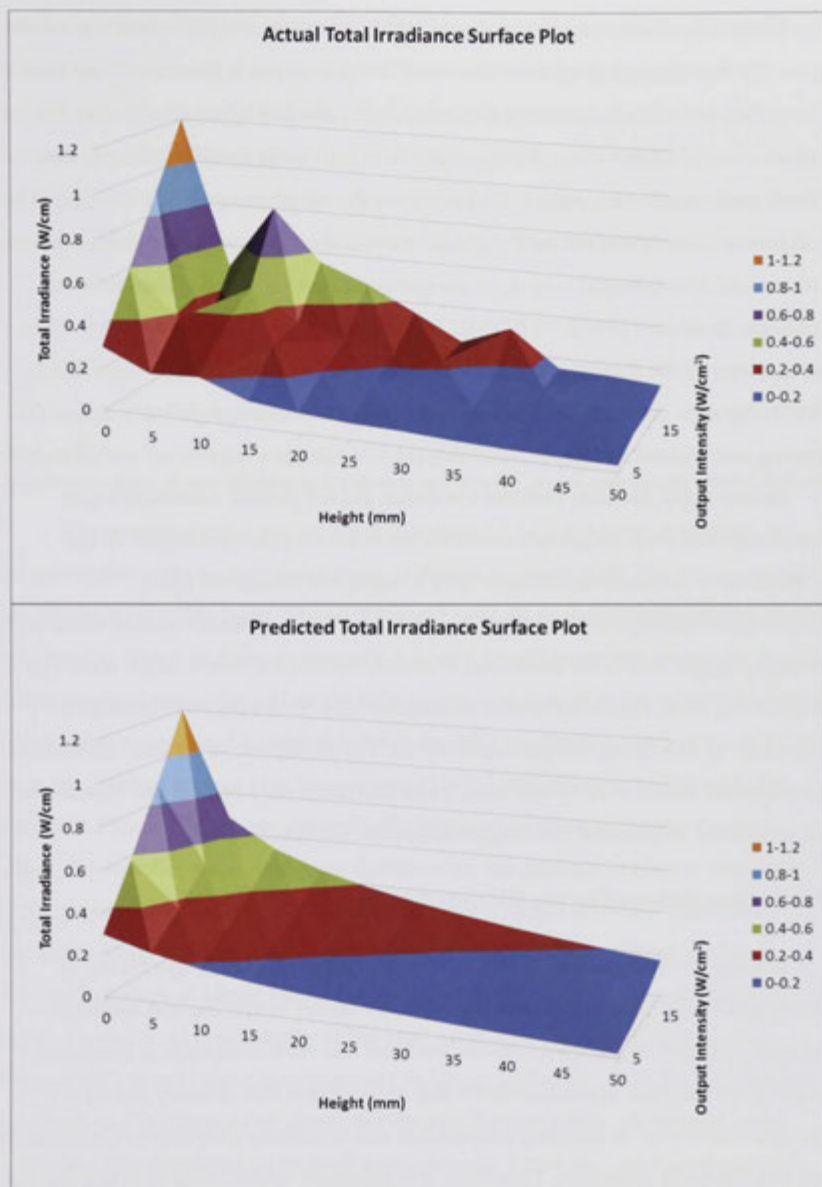
Figure 124 – Irradiance as recorded (top) and calculated surface plot (bottom), irradiance as fitted using full quadratic logarithmic transform surface fit.

Previous studies [230] have often used only the peak irradiance measured at the orifice of the light or directly under the light multiplied by the exposure time (providing

a step function) to determine the total irradiance. However, it is clear from the results in Figure 123 that the peak irradiance decreases dramatically as a function of distance, and the distribution area increases. The Gaussian distribution of light indicates that the total irradiance, as calculated using this approach, is significantly less than the standard methods peak irradiance average, the average or the set point irradiance multiplied by the exposure time. While the model did not capture the fluxes or inflections at the 5mm to 10mm and 35mm height ranges, in comparison to previous techniques used in calculating irradiance [246][247][253][254], the prediction accuracy is improved as demonstrated by the RMSE and R^2 values achieved. The full quadratic-logarithmic function captures the transient irradiance levels and non-uniform delivery across the exposure area instead of simply modelling the UV light in a 'step-wise' on/off manner.

Interestingly, the total incident irradiance did not present a constant linear relationship with each height increment for the same set point irradiance. In the literature, air is generally assumed to have a negligible absorption [224] [239][246][247][253][255], meaning that no loss of total irradiance should occur with increasing height, that is the same total is merely distributed over a larger area. The results of this work found that over a distance of only 50mm the total irradiance dropped by up to a factor of approximately 10. The absorption of air and reflectance and scattering that occurs even in spot curing systems is not only evident but impacts the total irradiance, even at the low heights above the incident surface.

7.3.4.4 Dose delivered by the UVAFP Process

For the UVAFP process as well as stereolithography (SLA), dye curing in printing and water treatment, where the exposure source is moving and localised application of the UV energy on the uncured tow and resin composite is important, capturing the transient irradiance levels and non-uniform flux delivery across the exposure area is vital in ensuring a repeatable and accurately dose is provided to ensure consistent material properties. Therefore, it is necessary when trying to determine the dose, to take into account the transient irradiation effects, non-perpendicular exposure, reflection, refraction and focal effects as well as the changing velocity of the placement head as it articulates through complex paths to ensure normal orientation to the tool surface. It was therefore considered important to build on the above results, in relation

to height above the incident surface and the incident distribution findings for total irradiance by combining them with the effect of UVAFP lay-up speed.

To do this, first, the definition had to be clearly articulated and correctly measured. The dose delivered by the UV light, D (J/cm^2), was calculated according to the velocity of the placement head over the composite substrate by dividing the total incident irradiance by the speed of the UVAFP head. This is shown in Equation 57.

$$D = \frac{I_0}{v}\left(\frac{W/cm}{cm/sec}\right)$$

$$D = \frac{J}{cm^2}$$

Equation 57 – Dose, D as a function of irradiance and velocity, v and appropriate units calculation

The measured dose, according to Equation 57, as a function of velocity at various heights and set-point irradiances, is shown in Figure 125. The results graphed were obtained by using 5, 10, 15 and 20W/cm^2 light sources at various heights ranging from 0mm to 50mm in 5mm increments. For each height increment above the incident surface the dose was measured as the light source was moved at the velocities shown. The negative exponential relationship between velocity and dose for any given height above the incident surface is to be expected [251]. The results are in line with the findings at Figure 123, in that generally the higher the source above the incident surface, the less direct the irradiance and likewise, the greatest irradiance was observed at 10mm versus the as expected 5mm height. Interestingly, the 5mm height also delivered a lower dose than the 15mm height at 15 and 20 W/cm^2. For the 5 and 10W/cm^2 intensity at 10mm height the light delivers the same dosage as the 5mm height. However, as the intensity of the light source increases to 15W/cm^2 and 20W/cm^2, the dose is significantly greater at 10mm versus the 5mm height between 0 and 10mm/sec velocity. After 10mm/sec the plot flattens and the difference is not significant. It is apparent that beyond approximately 5 mm/sec, the dose decreases significantly. This trend may indicate a possible maximum speed of 5mm/sec in order to achieve a minimum of UV dose delivery.

5W/cm² Dose vs Velocity at various Heights

10W/cm² Dose vs Velocity at various Heights
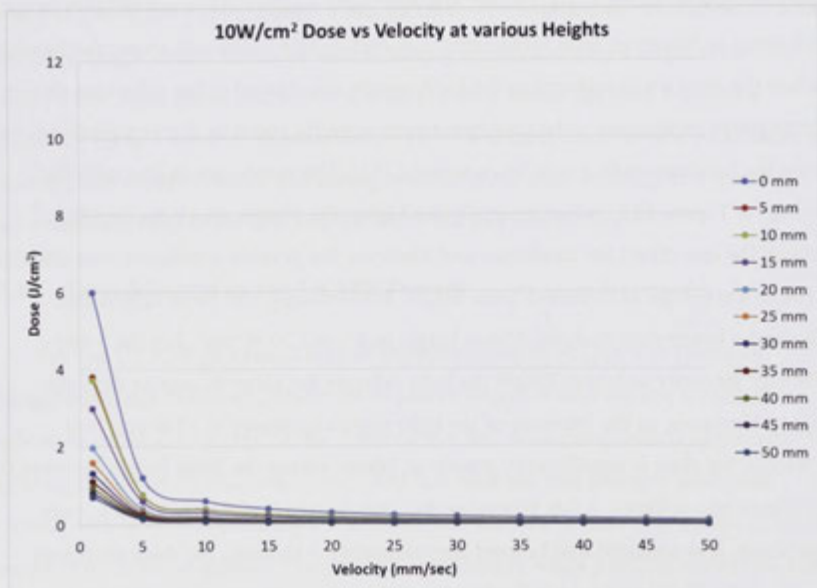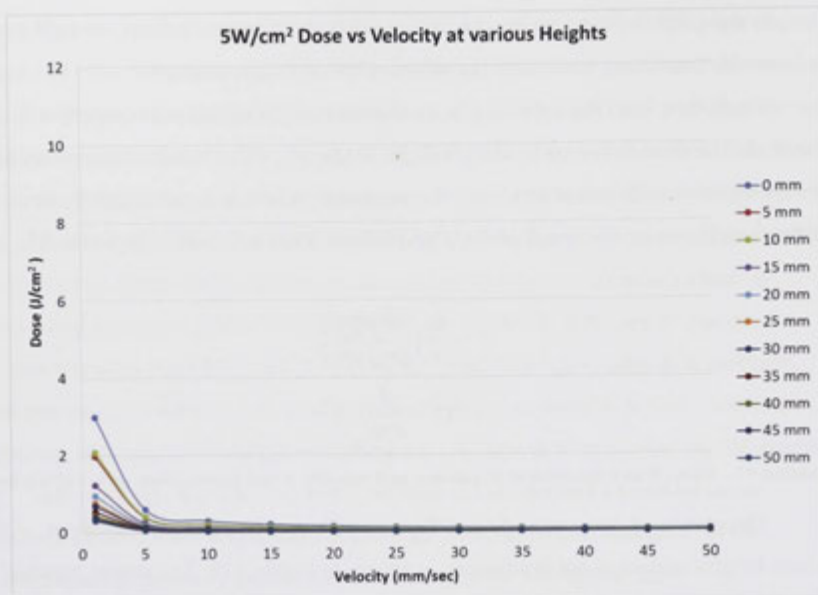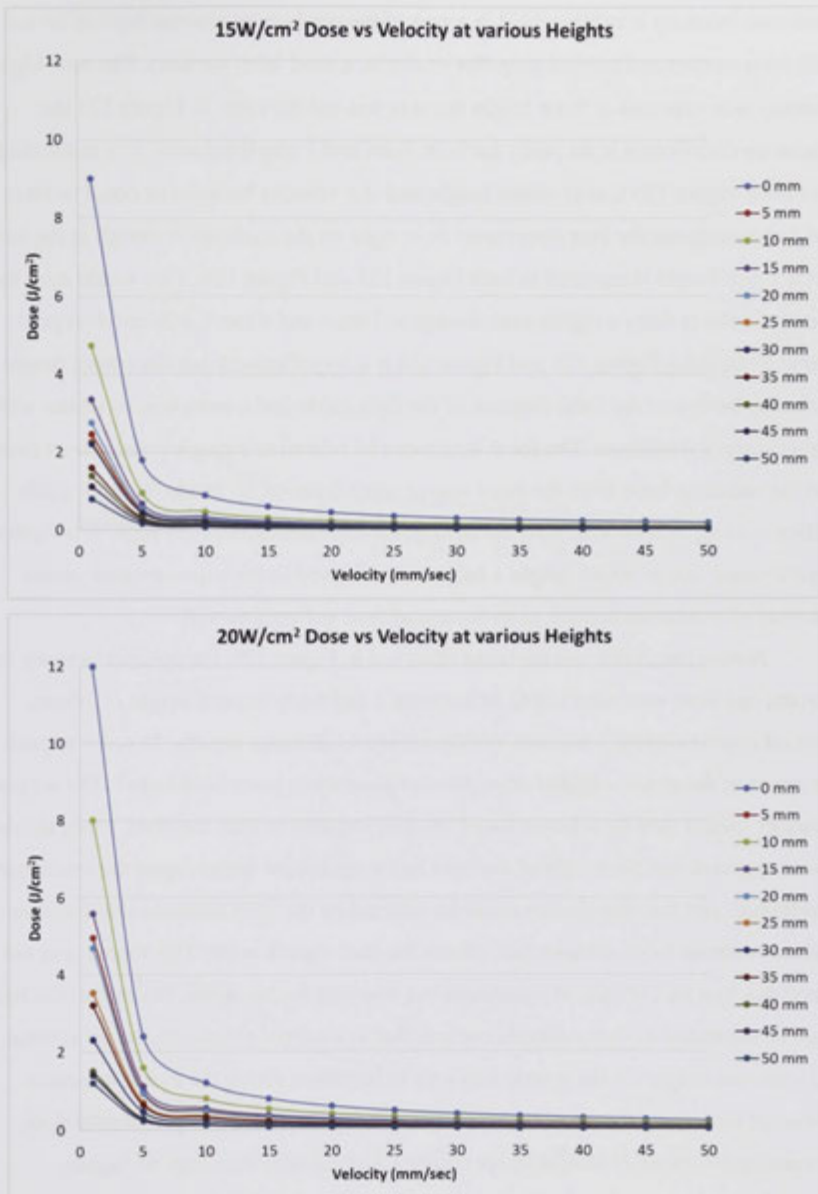
Figure 125 – Dose vs Velocity at various heights and set-point irradiances.

The dose, as a function of height at various velocities and set-point irradiances is also shown in Figure 126. As expected, at 0mm height above the incident surface, the

maximum intensity is achieved but in terms of the production process this has issues with resin contact and surface prep (for example, a dead level surface). The next highest intensity was expected at 5mm height but this was not the case. In Figure 123 the irradiance distribution is on parity for both 5mm and 1 mm irradiance. It is interesting to note from Figure 126 that at 10mm height and at a velocity between or equal to 1mm and 5mm/sec gives the best dose (apart from right on the surface). A trough in the trend at the 5 mm height is repeated in both Figure 125 and Figure 126. This would raise the question, why is there a higher peak dosage at 10mm and a much reduced dosage at 5mm? Examining Figure 123 and Figure 124 it is hypothesised that the 10mm height peak may be due to the focal distance of the light guide and a reduction of scatter with a higher surface irradiance. The focal length can be related to a single point source model and the radiating lines from the point source some distance up inside the light guide orifice causing reflection around the light guide that concentrates the light. It is further hypothesised that at 10mm height a balance is achieved in the exposure area versus intensity of irradiance leading to an increased dose delivery overall.

Noting the above and the trend observed in Figure 126, the optimal velocity for maximising dose was observed to be between 1 and 5mm/sec at a height of 10mm. Beyond approximately 5 mm/sec, the dose starts to decrease rapidly. In order to push the speed of the process higher other process parameters must be changed. The set point intensity should then be selected based on dose required to cure the resin. From the data it was apparent that the height of the light had a significant impact upon the irradiance distribution and this distribution could be effected by the light direction and location and an observed focal distance that effects the dose significantly. This theory was not tested due to a lack of optical equipment but warrants further work. Given that the light must be separated from the sample surface, that is it cannot practically be set at 0mm, the optimum height for the source was seen to be 10mm above the incident surface. Although increasing the set point intensity logically has a direct impact on the dose, increasing the intensity should be approached with caution. Not only do higher intensities present a safety risk but there is also a risk of degradation of the composite. Further experiments are needed to determine if there is a peak source value that provides optimal compromise between cure and UV exposure management.

5W/cm² Dose vs Height at various Velocities

10W/cm² Dose vs Height at various Velocities
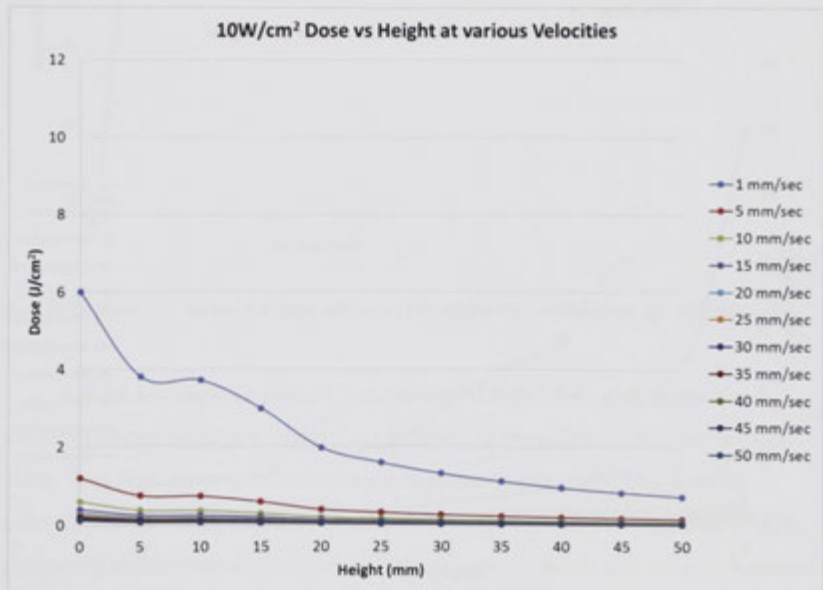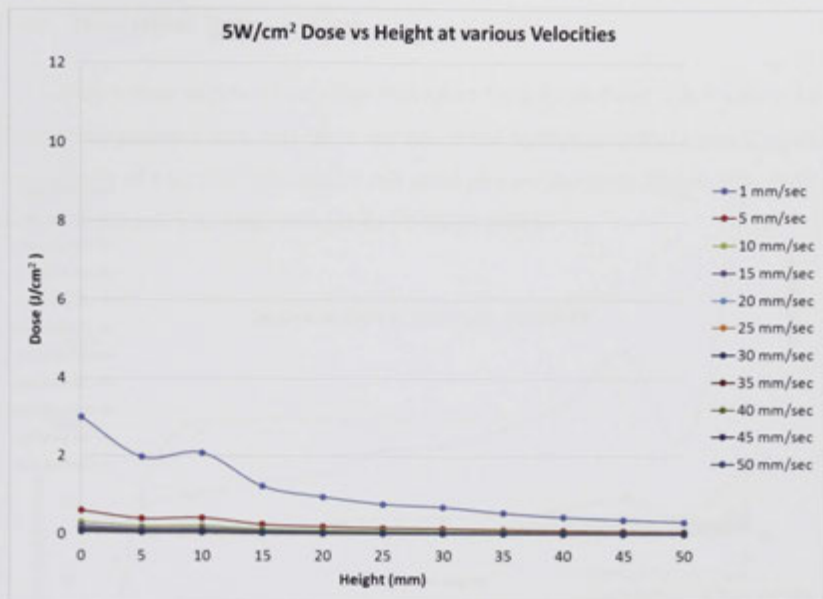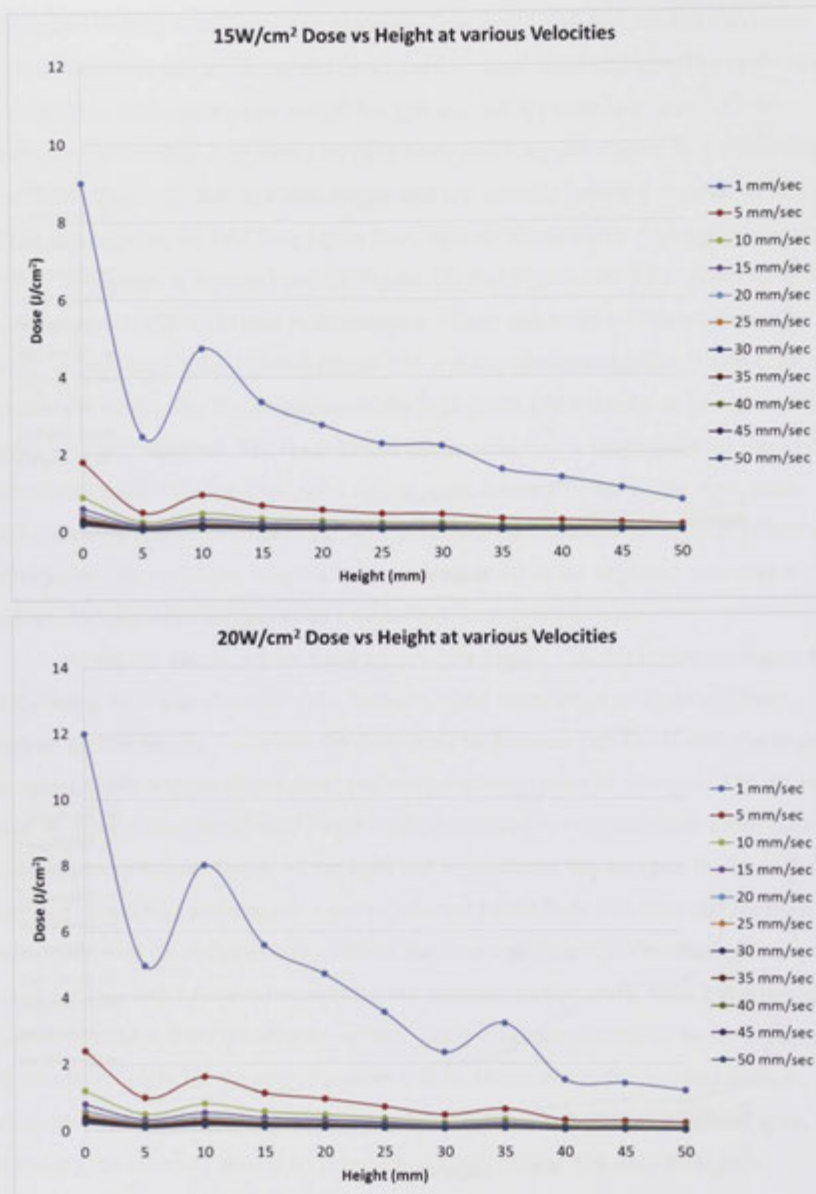
Figure 126 – Dose vs height at various velocities and set-point irradiances

7.3.4.5 Dose versus Degree of Cure

Dose versus degree of cure data was taken from Experiment 6 in Chapter 6.3. The intensity and time data was taken and converted to dose in order to provide a dose versus degree of cure plot. The results and trend plot are shown in Figure 127. The reference hardness was determined to be 90 HRM [201].
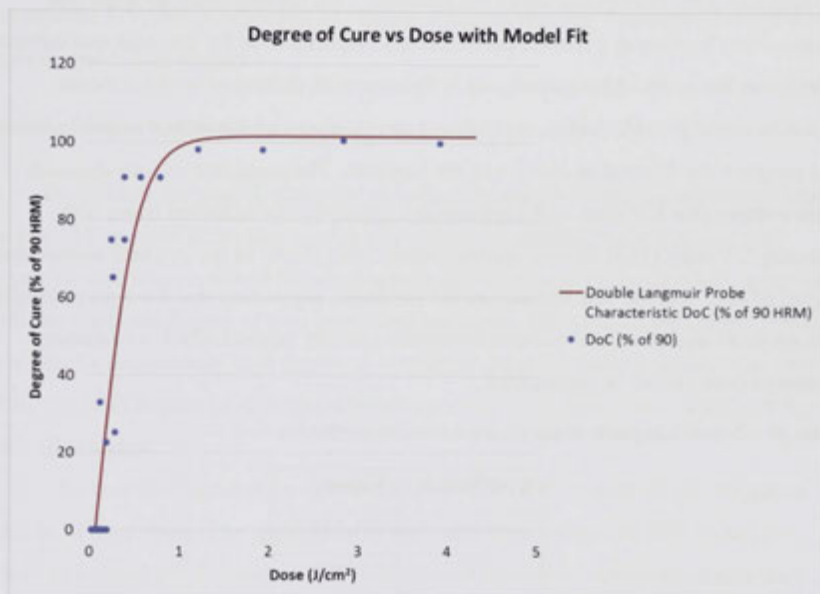
Figure 127 - Hardness versus UV dose delivered (J/cm) for the incident surface of bulk resin samples

A Double Langmuir Probe Characteristic (DLPC) fitting equation was undertaken to predict degree of cure as a function of dose delivered to the incident surface. This equation was selected based on observations of the how the data presented. The DLPC fit achieved an RMSE of 12.91698 and R^2 value of 0.87919, significantly higher than a maximum R^2 vale of approximately 0.8 using polynomial fits. The DLPC fit equation is shown in Equation 58 and the trend plotted in Figure 127.

$$\% \ cure = \varrho \ tanh(\tau D + \varphi)$$

Equation 58 – Double Langmuir Probe Characteristic curve fit for degree of cure, % cure, as a function of UV dose, D (J/cm²)

The coefficients are defined in Table 31. Due to the nature of the DLPC function and the coefficients used, beyond approximately 1.1 J/cm² the model predicts a degree of cure above 100%. Greater than 100% cure is of course not possible, but at doses above this the DLPC could indicate over exposure and possible over-heating, leading to burning and thermal degradation of the laminate. This finding could indicate that 1.1J/cm² can be seen as a theoretical maximum required dose for the resin and initiator selected in this work. Alternatively, as is the case with thermoset resins the over exposure could provide further crystallinity development of the matrix as in a post cure and progress the thermal properties of the laminate. The rapid rate of cure $d_{\%cure}/dt$, demonstrates that UV cure with high process speeds can be achieved using high intensity UV light [163]. Below approximately 250 mJ/cm² at the incident surface the degree of cure was too low to measure the hardness, suggesting that for a given height and set point intensity there exists a maximum velocity beyond which a minimum degree of cure cannot be guaranteed.

Table 31 – Double Langmuir Probe Characteristic fit coefficients

Coefficient	Value
ϱ	101.6187
τ	2.3081
φ	-0.1638

The resin hardness, and as related herein, the degree of cure, were shown to be highly sensitive to changes in dose below approximately 1.1 J/cm². As such, accurate calculation of the dose is vital to ensuring the cure properties of the composite.

7.3.4.6 The Degree of Cure Predictive Model

The degree of cure was modelled by solving the simultaneous equations for penetration depth, incident irradiance, according to the speed and dose. The simultaneous equations were Equation 52, Equation 53, Equation 56, Equation 57 and Equation 58. The final model is shown in Equation 59 and predicts the degree of cure at the depth d, according to the height z, the velocity v and the set point intensity I_{set}.

$$\% \, cure = \varrho \times \tanh\left(\tau \frac{a + b(\ln(hI_{set} + i)) + c(\ln(iz + k)) + d(\ln(hI_{set} + i)^2) + f(\ln(jz + k)^2) + g(\ln(hI_{set} + i))(\ln(jz + k))(e^{-\alpha d})}{v} + \varphi\right)$$

Equation 59 – The cure kinetic model for UV-AFP, providing the degree of cure, % cure.

The coefficient e is the exponential and the absorption coefficient $\alpha = 1.65618$ and the variables I_{set}, v and d represent the set point intensity, the velocity and the depth respectively. Other coefficients are fully defined in Table 30. The following sections detail the development of the simultaneous equations that were developed to characterise UVAFP in Equation 59. This is achieved through a process of experimental analysis and fitting studies.

7.3.4.7 Model Validation

To validate the model, a number of bulk resin samples were manufactured using the UVAFP process according to a variety of process parameter settings and their degree of cure was measured (by measurement of their hardness) to confirm accordance with the predicted degree of cure (predicted hardness). The process parameters were set to achieve a consistently high degree of cure at the incident surface, in this case above 95%. The high degree of cure was selected to ensure a hardness value could be taken from all samples.

To measure hardness by the standard, ASTM D785 – scale M, the thickness must be at least 8mm. The application of resin and fibre by the UVAFP prototype achieved a cured ply thickness (CPT) of 0.25mm. Therefore, sample thickness was supplemented with a substrate of known hardness 90 HRM up to the 8mm minimum requirement. By using the known hardness substrate, the UVAFP cured resin the reduction in hardness of the resin could be shown as a percentage of the 90 HRM, the reference hardness used in correlating hardness to degree of cure. This approach could not be benchmarked however and therefore it was considered that in the future further testing using alternative methods for determining degree of cure should be used.

Table 32 – Model validation parameters, predicted versus actual degree of cure

Parameter	Units	Trial 1	Trial 2	Trial 3	Trial 4
Set point Irradiance, I_0	W/cm2	20	15	10	5
Height	mm	10	10	10	10
Velocity	mm/sec	0.81	0.65	0.49	0.33
I_0 (calculated)	W	0.5412	0.4042	0.2848	0.1833
$D_{incident}$ (predicted)	J/cm^2	0.4790	0.4755	0.4827	0.4825
Hardness$_{incident}$	Mean HRM	84.9	87.5333	89.3667	84.4667
% cure$_{incident}$ (predicted)	% of 90 HRM	95.6862	94.8733	96.5650	96.5159
% cure$_{incident}$ (actual)	% of 90 HRM	94.3330	97.2590	99.2960	93.8520
Error	% of actual	1.4100	-2.5100	-2.8300	2.7600
Hardness$_{non-incident}$	Mean HRM	57.3667	57.8333	55.1	55.5333
% cure$_{non-incident}$ (predicted)	% of 90 HRM	57.60146	57.06416	58.1824	58.1499
% cure$_{non-incident}$ (actual)	% of 90 HRM	63.740	64.259	61.222	61.704
Error	% of actual	-10.66%	-12.61%	-5.22%	-6.11%

Table 32 provides the experiment setup information in the first section including the calculated irradiance and predicted dose for this setup. The second section then provides the incident surface predicted versus actual data including the error and the third provides the same information for the non-incident surface at the 0.25mm CPT depth. The results did demonstrate the confidence of the model for the incident surface and would allow for the optimisation of process parameters in real time based on the desired mechanical properties and achievable processing rates. In automated processes such as UVAFP where lay-up rate can be numerically controlled in real time, the degree of cure could be calculated on-the-fly during processing based on actual speeds. In the manufacture of complex parts where geometry would require compound manipulation of the robots position, accelerations and decelerations of the placement head speed could be controlled in real time to ensure a uniform degree of cure in the fastest possible time is achieved.

7.3.4.8 Error Analysis

As can be seen in Table 32, the predicted degree of cure had no more than a 3% error when compared to the actual measured degree of cure at the incident surface, and no more than 13% difference in comparison to the actual measured degree of cure at the non-incident surface. The results show the reduced accuracy of the model for the non-incident surface. This reduction in the accuracy can be related to the increased scattering and reflection and refraction of the UV as the depth increases and likewise the changing temperature through the thickness. Previous studies have shown that UV curing can also be effected by the capping of volatiles with the formation of a cured skin at the incident surface, which could also affect the degree of cure prediction accuracy [201].

The limitations of the model must be acknowledged. The modelling approach provided is empirical, and applicable to a complex physical situation. However, the application of this model is limited to the specific materials used in this study. Likewise, throughout this study, a white PTFE flat tool approximately 12mm thick was used for the manufacture of the samples. This tool was used throughout all sampling as the cure rates of the resin were observed to change significantly depending upon the choice of tool material. This could be explained by the different thermal properties of the tool

either influencing the temperature of the composite during curing or the dose by either absorbing or reflecting energy back into the resin or a combination of both. This observation would indicate that in the process design and system set up, the tool material may need to be factored into calibrating the cure process. This is an area for further study.

7.3.5 Experiment Conclusions

This experiment presented the testing and creation of a predictive model for the degree of cure in the UVAFP process. The input variables of the model included the process setup parameters of set point intensity, height of the UV light from the incident surface and the speed of processing. The predicted degree of cure was based upon experimental results and fitting analyses characterising first, the UV output and conformance to the photo-initiator activation wavelength. Second, the absorption and penetration depth of the UV irradiance through the thickness of the resin was determined. Third, modelling of the transient and Gaussian like distribution of irradiance on-the-fly was determined. Fourth, the dose, as a function of the irradiance and speed was calculated. And finally, the degree of cure according to the dose delivered was determined. The model was then validated by confirming the actual degree of cure and predicted degree of cure in manufactured laminates. The impact of this model is in the ability to predict and control the degree of cure based on the independent process variables, ensuring quality and or repeatability as well as tailoring the material properties. Although a speed limitation using the current setup of 5 mm/sec was found, it is believed this could be increased based on material chemistry changes and variation of other settings as previously discussed. Future work should compare layup rates to autoclave processes based on scaled designs laying down multiple tows. In any case, the results showed that it is possible to achieve a high degree of cure with in-situ UV curing in AFP and that it is possible to eliminate one of the primary limitations of the current process, the need for autoclave post curing.

Stowe [251] described irradiance as a consideration of process design and dose as a consideration of process control. In developing the UVAFP prototype, the design demanded that irradiance should only be applied to a single tow by a single UV light, hence the need for a spot curing system. At the same time the system was designed to

harness a high intensity source providing process control choice in terms of the dose. Many UV light systems are fundamentally limited by the choice or design for low intensity sources. In comparison to other UV light sources, spot curing systems have very high peak irradiances compared to the total dose delivered. Common calculation techniques using simply the peak irradiance divided by the speed would therefore yield vastly different values for the dose than using the actual Gaussian distribution integral as found in this work. In considering process control it is evident from Figure 126 that speed control has the most significant influence on dose.

With this process model, real time control of parameters may be implemented in order to ensure final quality. Further, while the model was applied to an AFP process, the approach can also be applied to other processes such as stereolithography, printing and water treatment reactors where transient radiation dose calculation is important. The data and model proved that a high degree of cure can be achieved using UVAFP in a single continuous process in seconds rather than minutes. Laminates were manufactured exhibiting a high degree of cure as a function of mechanical hardness to composites processed in thermal cure cycles [75]. The UVAFP process offers significant efficiency advantages by eliminating the single largest bottleneck to the current AFP process, the need for autoclave post curing.

During the development of the model, it has been found that current techniques used for calculating dose vary significantly and generally overestimate the dose needed. In high-speed processes using on-the-fly curing, such as AFP with in-situ UV curing, consistent and accurate calculation of the dose is critical in predicting the degree of cure and ensuring quality. Future work should include real time dose measurement including the reflectance as published by Chartoff and Du [224]. Measurement instruments such as reflectance real time infrared (RRTIR) or in-situ cure monitoring using fibre optics could improve the accuracy of results and provide insight into cure rates [224]. Heat generation observed during irradiance using the high intensity UV spot curing system could also have an effect on reaction rate and final T_g [248] and should be investigated further. Likewise, this work negated the influence of fibres in the curing behaviour of the composite. The effect of the glass fibres on UV penetration, the refractive and reflective influence on the surface boundaries and the effect of the substrate tool surface on UV absorption should be examined in future work.

7.4 Summary

To make accurate and effective production decisions on the implementation of AFP technology and fully understand the effect of process parameters, accurate process models are required that account for the process costs, timing and throughput (otherwise known as production capacity), quality and lifecycles. These models require validated experimental data that can and should be supported by research institutes working in the field. Furthermore, for new state-of-the-art processes, models need to include qualification cycles that are necessary to provide the necessary verification of the quality of the parts produced. In composite manufacturing the most critical drivers are the lay-up, consolidation and curing kinetics. The ability to predict cycle times is vital in costing and business case development to justify the new process and capital investment.

Experimental data was collected to characterise the UV light output spectra and absorption wavelengths of the resin, the incident irradiance, the dose delivered at varying speeds and the hardness of the resin as a direct indicator of final degree of cure. Regression analyses are used to model these phenomena and predict the degree of cure of the composite produced in UVAFP. The model was validated with comparisons to manufactured samples. The results demonstrated that it is possible to achieve a high degree of cure with in-situ UV curing in AFP and that it is possible to eliminate one of the primary limitations of the current process, the need for autoclave post curing.

There are some important considerations in modelling the UVAFP process related to the final material properties for use in design tools such as finite element models. During processing the structure is laminated, consolidated and cured ply-by-ply, therefore gaps, overlaps and wrinkles can cause variation through the thickness of the material and collimating of fibres adjacent previously cured laminates generates resin rich breaks through the ply. It has been previously shown that the ply-by-ply curing process does not affect material properties as long as good adhesion between plies occurs. Therefore, the continuous layered structure of UVAFP laminates can be modelled with repeated unit cells, ply-by-ply. This type of micro model requires dense meshing and is computationally intensive. An alternative that is perhaps less computationally intensive for more complex application loading situations is to model the material as a continuum including all plies [256].

A material advantage of using free-radical photo-initiators in the resin is that it allows for precise cure control as the reaction only progresses when UV light is applied to the laminate [7]. By using a spot curing system the cure can be controlled accurately on-demand (because of the extremely fast response time for on/off delivery of the UV light versus time absorbing thermal systems that have large thermal inertias to overcome). Additionally, by curing in local areas through spot curing, wet edge and melding techniques that could be applied to joining processes [257]. Lackey, et al. [171][246][247][253] and Di Pietro and Compston [7][63][72][73], demonstrated the rapid speed of curing using high intensity UV light while maintaining comparable mechanical performance qualities to composites cured with traditional thermal cures [7][230]. With such rapid curing rates, the overall cycle time [247] and the emission window of volatile organic compounds (VOC) [7] can be significantly reduced. This is of huge benefit to production processes were seconds are critical in achieving throughput as well as reducing environmental risks associated with using resins.

8 Thermal and Degradation Process Model

This chapter investigates the thermal behaviour of the composite during UVAFP process. Section 8.1 provides a summary of the most relevant literature on the thermal modelling of the standard AFP process, mainly concerned with thermoplastic AFP where in-situ heat application is common. Section 8.2 details the relevant literature on degradation modelling during AFP processing. Again, primarily concerned with thermoplastic AFP. Section 8.3 covers the experimental work of this chapter where the thermal behaviour and degradation behaviour of the UVAFP process is characterised. A model to predict the temperature response of the glass fibre vinylester composite during processing using the UVAFP process was developed in order to minimise any possible degradation that could have occurred as a result. The model was based on the same primary process parameters for the UVAFP process as determined in Chapter 7; the placement speed, the set point intensity of the UV light, and the height of the UV light from the incident surface. The thermal and degradation modelling of this chapter lends heavily on the in-situ consolidation and heat modelling work done to develop thermoplastic AFP systems although the source of the heat in this instance is generated through the radiant energy of the UV light and the heat does not contribute to consolidation except to aid wet-out and flow by reducing the viscosity somewhat of the resin as it is processed at the nip point. Finally, section 8.4 summarises the results in context of the work of previous chapters and the concerns around degradation and possible contribution of heat to the UVAFP process.

8.1 Thermal Modelling in AFP Processes

A number of heat transfer models exist for the thermal history in thermoplastic AFP [32][114][144][145][146]. The literature most commonly focuses on two techniques to model thermal history. The first, a quasi-steady state is assumed and the problem is reduced to a steady-state heat transfer analysis using Eulerian techniques. The second, a transient state is assumed and a dynamic heat conduction equation using Lagrangian techniques is applied. Commonly, these models produce temperature

profiles or meshes using finite element methods to predict the thermal gradient and region of heating to ensure adequate adhesion of the new ply to the previously laid ply has occurred. Models exist that are 1D, 2D and 3D and generally show significant thermal gradients across the lay-up nip point depending upon speed, heat input and the environment or preheating conditions [58].

Although much of the work has been focused on thermoplastics, Hassan, et al.[58], developed a 3D heat transfer model of the thermoset automated fibre placement process. The model employed a Lagrangian formulation utilizing 8 brick nodes and the 2 x 2 x 2 integration rule and included heat conduction in 3D including through the tool and losses to the environment. An equation for the degree of cure was proposed based upon the rate of heat evolved during reaction and the total heat of reaction. Further, an equation for the rate of reaction was proposed based on the type of reaction and reaction order. This function incorporated rate constants determined by Arhennius type expressions including the activation energy and gas constant. By neglecting diffusion of chemical species and convection of the fluid the degree of cure at any point in the lay-up could be determined by integrating the cure rate with respect to time. Composite ring structures were manufactured to validate the results with thermocouples integrated between the plies of the rings. The recorded experimental data was compared with a finite element model for the rings. With optimisation of the coefficients through an iterative comparison to the actuals and the model, the produced data correlated well with the recorded data. The Lagrangian model successfully predicted the thermal behaviour of the thermoset fibre placement process using convective heating techniques in transient scenarios and showed the necessary experimental approach needed to develop accuracy in the model.

Costen [114], developed a 3D model of the thermal heat transfer for thermoplastic AFP in steady state using a 'Green' function. A finite width tape was modelled on an infinitely wide substrate and the glass transition temperature of the weld interface between the tape and substrate was used to determine the cooling incursion rate inwards from each edge of the tape caused by premature heat loss. The work identified the significant influence of environmental edge effects and the influences of heat loss through the substrate and adjoining tows and the challenge in regulating uniformity in localised heating processes. Specifically, in thermoplastic lay-up where heating and

cooling are critical to the melding bond adhesion, the variances in temperature across a single tow showed a considerable challenge in assuring quality of melding in such a process. This addressed a gap in research for diffusive thermal edge effects, specifically where a newly placed tape contacts the cooler substrate. Costen was able to compensate for premature edge cooling to help achieve uniform weld strength and crystallinity across the width of the tape.

Lee [32] focused on the modelling of the two key parameters in the AFP process, namely, the heating and compacting of towpreg. These were identified as the two critical process parameters in dictating final quality by a functional block diagram approach. A linear one-dimensional model was first developed for the towpreg. Thereafter a two-dimensional heat transfer model between the towpreg heating sources was developed. A partial differential equation was established with boundary conditions and initial settings to solve the quasi steady state model. Using this model a number of heating techniques were investigated. Rigid contact heating was identified as one of the most efficient heating methods. Rigid contact involves conduction of the cure heat energy through the compaction roller itself instead of a convective heating gun. This said, rigid rollers present limitations previously discussed in terms of adherence and conformance to complex surfaces. This would mean that most likely these types of heaters could only be used on simpler geometry or further research is required to develop conductive conformable rollers. To further investigate the rigid contact heating model.

Lee [32] developed a 2D finite element model and validated the model in an experimental setup using a Pyrex tube coated in Teflon with a filament coil inside. Various heating controllers were used to test overshoot and response time. In all cases response time was less than a second and overshoot was minimised to within ±2.5°C from the desired temperature with the use of a proportional and derivative (PD not PID) controller and active cooling. Lee also analysed the compaction force accuracy of pneumatic compaction systems like those used currently in commercial systems as well as ways to optimise the control accuracy. Lee [32] combined mechanical springs and dampeners with a pneumatic cylinder to improve compaction force variation in a dynamic environment. Interestingly, it was found that the main source of force fluctuations came from the motion system itself (either a robot or gantry), not the force

control actuated within the AFP head. This suggested that the rigidity and stiffness of robotic systems are factors that influence the optimization of AFP process parameters.

Tierney and Gillespie [147][258] utilised an experimental placement rig to perform a parametric AFP study on a thermoplastic-based composite. The authors showed a significant difference in the performance properties of autoclave cured and consolidated composites, and composites manufactured using AFP technology and cured in-situ. The study highlighted the placement speed limits on thermal dependent processing, showing a clear reduction in properties when the placement speed exceeded a certain material and process setup maximum. A series of integrated sub-models were developed for predicting the heat transfer and void entrapment dynamics within the laminate allowing the through thickness void percentage to be calculated using a relationship determined from the process parameters. The model was used to quantify the relationships between variation in quality of incoming material and final void content gradients. It was found that the gradient of the final void content relationship increased dramatically through the thickness as determined by the processing conditions.

As thermoplastic consolidation relies on heat to melt the polymer and allow adhesion to occur, many studies have been conducted looking at the characterisation of the thermal viscoelastic aspects of the process at the lay-up point. Most models of the thermal heat transfer are only 2D and do not capture the diffusion of heat between the newly laid tow and the cooler tow beside it. However, some 3D modelling has been undertaken. Sonmez & Hahn [146] also examined the effects of heating and consolidation in thermoplastic fibre placement. Quality measures included the interlaminar bond strength, weight loss through thermal degradation, and crystallinity of the final composite part. The paper developed models for stress, heat transfer, crystallinity, degradation and bonding based on experimental results. These models and their relations were used to develop a processing window similar to other works in the field by Steeg, Schledjewski & Schlarb [259], and Sandusky, Marchello, Baucom & Johnston [260].

Sonmez, Hahn and Akbulut [123] also developed a thermo-viscoelastic finite element model to predict residual stresses induced during the processing conditions of thermoplastic tape placement. A previously developed heat transfer model [146] was

employed and given the viscoelastic behaviour, this model's predictions correlated closely with experimental data. The process was modelled in a quasi-steady state with the reference origin of the model located at the compaction roller axis. Both unidirectional and cross ply laminates were produced using tape placement to validate the model. The model was limited to flat laminates assumed to and the roller assumed to be as wide as the laminate, mimicking a single tape width lay-up.

8.2 Degradation Modelling in AFP Processes

In 1997, Sonmez and Hahn [261] analysed the online consolidation of thermoplastics in tape placement and possible degradation that could occur due to overheating. The overriding degradation mechanism considered was mass loss rather than inadequate cross-linking. A maximum mass loss of 0.01% was assumed as reasonable, beyond which property reduction starts to occur. This limit was then applied as a degradation constraint in the thermal model as a restriction in optimisation studies and the development of ideal processing limits. Sonmez and Akbulut [262] also developed a process optimisation scheme for thermoplastic tape placement. The objectives of this work were to minimise the peak tensile residual stress and thermal degradation while increasing the productivity of the process by optimising for the maximum placement speed. Two quality measures were used, namely, the bond strength and the thermal degradation level. Previously developed models [261] were used to determine the temperature distribution, residual stresses, bond quality and thermal degradation. Previous model used a Nelder-Mead, zeroth-order search algorithm to minimise the objective functions based on the major process parameters (identified in their previous works), these were, the temperature of the hot gas to heat and melt the thermoplastic, the velocity of the roller, the preheating temperature of the tape and the heated length to overall length ratio for the tape. The optimisation scheme used a penalty weighting according to degradation limits, bonding limits and residual stress limits, all calculated according to the thermal distribution. The optimisation scheme allowed the process parameters to be balanced based upon a number of conflicting requirements, namely ensuring adequate temperature was reached in the laminate to allow for bonding but not exceeding temperature limits which would

degrade the material. This work again used the same constraint assumption for thermal degradation through mass loss as used in past work of Sonmez [261].

Other studies [263] have found that stresses accumulate gradually during successive lay-down of layers effecting quality and likewise the speed had an immediate effect on quality. Both parameters could be optimised based on changes to the process variables of temperature of the hot gas to heat and melt the thermoplastic; the velocity of the roller; the preheating temperature of the tape; and the heated length to overall length ratio for the tape. The model was sophisticated enough to provide a clear optimisation according to quality for the small number of variables for each goal but did not allow the two objective measures of residual stress and speed to be combined. The optimisation for residual stress reduction allowed acceptable stress levels to be achieved but led to the lay-up speed becoming unacceptably long. Likewise, the speed optimisation lead to unacceptable residual stress levels, which would result in micro cracking. The authors suggested simply laying the thermoplastic tow at a speed sufficient for minimal bonding to maintain shape and keep residual stresses acceptable and then using a post processing technique such as an autoclave to progress the bonding fully. This suggestion of course would destroy one of the key advantages of thermoplastic AFP, in-situ manufacture of the component.

Chung, Seferis and Nam [144] investigated the thermal degradation behaviour of polymeric composites to predict the effect of thermal cycling on the matrix performance. Degradation was measured by monitoring the mass loss of carbon fibre and epoxy laminates in both isothermal and dynamic conditions. This mass loss was considered a reasonable measure for thermo-oxidative degradation, with oxidative degradation being considered the most significant factor for environmental deterioration of composites. Chung, et al. found that loss rates were geometry dependant and anisotropic. A model was developed for the mass loss as a sum of the weight losses times the surface area in the fibre direction, the surface area normal to the fibres in the transverse direction and the surface area normal to the fibres in the through-thickness direction. These directions are detailed in Figure 128 [144].
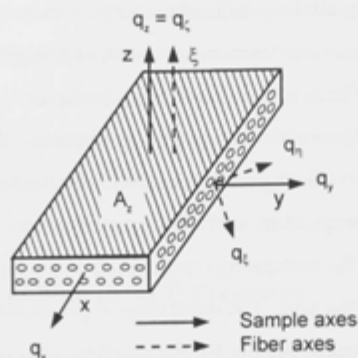
Figure 128 – Chung, et al. geometry definition

The model considered surface dependent oxidative degradation based on the shrinking core model as defined below in Equation 60.

$$q_i = D_{Ei} t^{n_i}$$

Equation 60 – Chung et al. surface dependent shrinking core model for thermal weight loss degradation

Where the subscript i refers to either ξ, η or ζ. ξ refers to the fibre direction, η, normal to the fibres in the transverse direction and ζ, denotes normal to the fibres in the through-thickness direction (to the resin rich surface). n_i is a time exponential factor; and D_{Ei} is an effective diffusion coefficient that may be described by an Arrhenius expression with activation energy E. If the weight loss is limited by the diffusion, then value of n_i was 0.5; if it was limited by the reaction kinetics, n_i was 1. If the rate was not limited by a single step, the experimentally determined constant D_{Ei}, was used for both the thermal degradation reaction and the diffusion. The model successfully predicted the mass loss rates in isothermal cycling conditions with step wise (instantaneous change gradient), finding that the higher the surface to volume ratio the greater the loss suffered by the laminate. The model did not cover transient thermal cycling conditions such as those experienced during the AFP process.

8.3 Experiment 9: Thermal Modelling and Degradation Constraints of the UVAFP Process

Chapter 7 focused on the development of a predictive model for the degree of cure of composites produced using the UVAFP prototype. As an obvious conclusion, in order to maximise the degree of cure, the speed and height should be set at a minimum and the intensity at the maximum. However, this could lead to degradation and possible effects on mode II properties can occur due to thermo-oxidative effects. Therefore, this chapter now takes the next step and examines the temperature during the same processing and the effect this temperature has on the composite and the degradation that may occur due to overheating.

Based on the work by Chung, Seferis and Nam [144], thermo-oxidative degradation was proposed to be directly proportional to the mass loss of the laminate during curing which is related to the peak temperature of processing and the time of exposure. In Figure 118, the link between process parameters and degradation and residual stresses were considered. The same parameters that drive dose delivery also drive the temperature in the laminate. Due to the differing absorption and transmittance of different materials so too does the resin and fibre type and the depth at which the results are being measured. Therefore the degree of cure model and the thermal and degradation model are directly related.

In the UVAFP process, UV energy is applied on-the-fly within the placement head, directly after the point of application. By using photo-initiated resins the process is thought to be independent of temperature profiles and therefore not effected by issues such as thermal mass, conductivity and heat transfer issues and instead depends upon the dose of energy at the appropriate wavelength delivered to the part. Dose is affected by UV intensity, the height or distance of the source and substrate, the placement speed or exposure time and the absorption of the resin and therefore initiation and reaction windows are significantly shorter. Previous chapters have characterised the UVAFP process and the unique conditions around the high-intensity dynamic application of UV energy and its effect on the degree of cure of the composite. However none of these chapters considered the impact of the temperature on the process.

While a significant amount of work has been done in modelling standard thermoset AFP processes [250][264][32] where thermal curing occurs in a separate process step after placement, little is known about thermoset AFP processes employing in-situ curing mechanisms. Some transient models exist that characterise UV systems used in dynamic processes, such as in UV water purification reactor modelling [254], but these do not capture the transient dose delivery and the high-intensity localised application in spot curing process such as the case with the UVAFP prototype. Often, UV modelling research focuses on the effects of reflection, refraction and the light is only modelled as a stepwise function. This calculates dose delivery in an on/off state and does not capture the varying irradiance levels the sample may undergo. In the context of UVAFP exposure can be less than a second and the cure can occur immediately after lay-up at that specific location. With such short exposure windows at high intensities, a clear understanding of the actual dosage levels and cure kinetics as well as the significant variations in stress due to localised thermal differentials is necessary for accurate modelling. Therefore this experiment was undertaken to provide further robustness to the UVAFP process model and add constraints to the model to optimise productivity by maximising the process speed and efficiency while minimising degradation.

8.3.1 Experiment Aim and Hypothesis

The aim of this experiment was to characterise the thermal response of the substrate to the process parameters of Experiment 7 and be able to avoid degradation of the composite caused by process parameter combinations that would lead to overheating of the composite. It was hypothesised that testing the height of the UV light, the intensity of the UV light and the speed of the placement will define the temperature during processing and the degradation of the composite during UVAFP.

In addition, as it was hypothesised that the temperature during processing would vary significantly during processing, another aim of the experiment was to investigate and understand if the thermal properties (Tg and residual heat of reaction) of the composite would be effected by different thermal processing conditions even if the driving curing mechanism was photo-curing. It was further hypothesised that the Tg of the resin would be increased as the peak temperature during exposure increased. It was

also hypothesised that inversely, as the peak temperature during exposure increased the residual heat of reaction would decrease.

8.3.2 Experiment Apparatus

The constituent materials used in this study were Owen's Corning SE1200-2400TEX E-glass roving and Derakane 411-350 vinylester by Ashland Chemical [162] with a fixed ratio of 0.5 wt% of Irgacure 819 (IC819), a bisacylphosphine oxide (BAPO) photo-initiator by CIBA Chemical [252]. IC819 undergoes a free radical reaction when exposed to UV light [252]. The UV light used in the UVAFP system was a Lumen Dynamics spot curing system, the Omnicure S2000 [202]. Irradiance measurements were taken using an Exfo R2000 radiometer [202] which is specified to capture total irradiance across wavelengths from 250 nm – 1 µm. To measure the total irradiance at the incident surface, a surface irradiance sensor by EXFO, called a *Sitecure* sensor, was used. This sensor was coupled with the EXFO R2000 radiometer and also measured the overall irradiance [202].

8.3.3 Experiment Method

The experiment method involved a series of characterising studies during UVAFP processing. The experiment setup is shown in Figure 129.
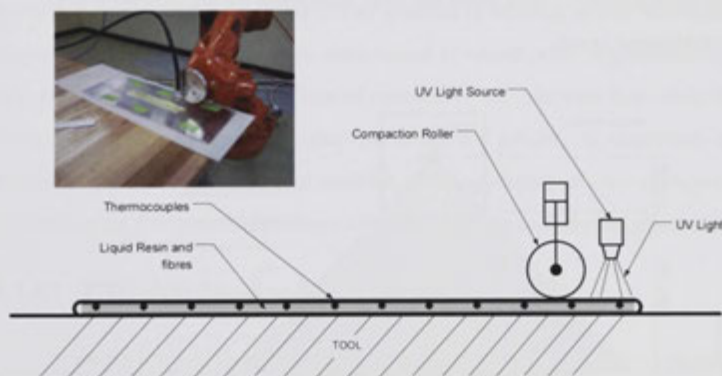
Figure 129 – Robot high intensity UV curing setup using for measuring temperature during exposure

First, the placement speed was varied at two set point intensity levels (5 and 10 W/cm^2) and a single light source height of 5mm were used to determine the effect on the temperature ramp up and down, peak temperature and overall exposure of the laminate. 5mm height was chosen in order to try and present the worst case in concentration of intensity. Temperature data was collected in real time with thermocouples placed on the surface of the tow during processing. The second study then examined the effect of the height of the UV light, from 5 to 50mm in 5mm increments, on the temperature in the laminate (again examining the ramp up and down in temperature, the peak temperature and overall exposure). This was done at a single velocity of 10mm/sec and two set point intensities of 5 and 10W/cm^2 intensities. The data from these two studies was used to produce a model to predict the temperature based upon the independent process parameters.

Another study was undertaken examining the mass loss of the composite according to dose and temperature using the thermal model. The experimental set-up is shown below in Figure 130. A static setup was used with the UV light remaining stationary above the composite sample so that the loss could be measured in real time. The scales used in the experiment had an accuracy of ±0.005 g. The dose was calculated based upon the results of Experiment 7 capturing the non-uniform irradiance across the surface and using the trapezoidal technique to calculate the actual irradiance and then calculating of the actual dose. The step wise approach often used in the literature was not used as this method simply multiplies the peak irradiance by the exposure time giving an over estimated result.
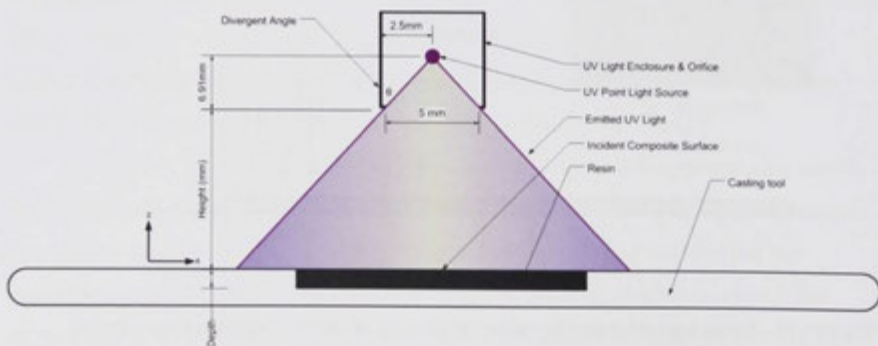
Figure 130 – Mass loss measurement experimental setup

The mass loss data was then used to determine the temperature and dose limits of the processing window as predicted by the thermal model in order to avoid degradation by mass loss. The predictive model with degradation limits was then related to the degree of cure model in order to develop a processing window providing both upper and lower limits for process parameter combinations.

Because of the observed temperature variation that could be seen during UVAFP processing, a final study was also undertaken to examine the temperature impact of processing on thermal properties such as glass transition temperature (Tg) and the residual heat of reaction remaining in the cure. This data was gathered using differential scanning calorimetry (DSC) on cured, uncured and partially cured samples.

8.3.4   Experiment Results and Discussion

The results for each characterising study are recorded in the following sections in the order they were undertaken. The results are combined at two stages, first in creating the predictive thermal model and then in the predictive degradation model. The height and the set point intensity of the UV light and the speed all effected the temperature and degradation by mass loss. Therefore the hypotheses of the experiment were met. Each parameter had a differing impact on the peak temperature achieved, the temperature ramp up and cool down rates and the period of elevated temperature exposure which in turn effected the mass loss and therefore degradation differently. With the experimental data an accurate predictive thermal model was created and likewise temperature limits were determined at which point degradation by mass loss occurred. The Tg and residual heat of reaction results showed that while the Tg of the composite remained constant regardless of the UV processing conditions and temperature, the residual heat of reaction and thus degree of cure changed significantly depending on the peak temperature and thermal exposure during processing.

8.3.4.1   Placement Speed and Temperature in UVAFP

Single tows of the glass fibre reinforcement and the photo-initiated resin were laminated with thermocouples embedded on the incident surface of the top ply in order to measure the temperature during UVAFP processing at various speeds, heights and UV set points. The compaction roller and UV light were then passed over the lay-up

according to the UVAFP process and the temperature recorded over time. The resulting temperature plots are shown in Figure 131 and Figure 132. Figure 131 shows the temperature at the incident surface with varying placement speeds, for set point intensities of $5W/cm^2$ and $10W/cm^2$ and a height of 5mm. With increasing speed the peak temperature decreases and likewise the temperature ramp up rates and elevated temperature period decreases. Increasing the set point wattage from $5 \ W/cm^2$ to $10W/cm^2$ had a significant effect on peak temperature and temperature ramp up rates, almost doubling the peak temperature for the same speed. The peak temperature measured at the slowest speed for this study, 10mm/sec, was 53.2°C for $10W/cm^2$ which was achieved in less than 1 second of exposure. Ramp rates recorded were recorded as high as approximately 68°C/min and as slow as 15°C/min. In all cases, ramp up rates were significantly faster than traditional convective thermal processes such as ovens or autoclaves. The efficiency and speed of this heat transfers suggests that UV lights could also be used for thermally catalysed resins that are not photo-initiated, similar to infrared heating lamps for an efficient non-contact heat source.
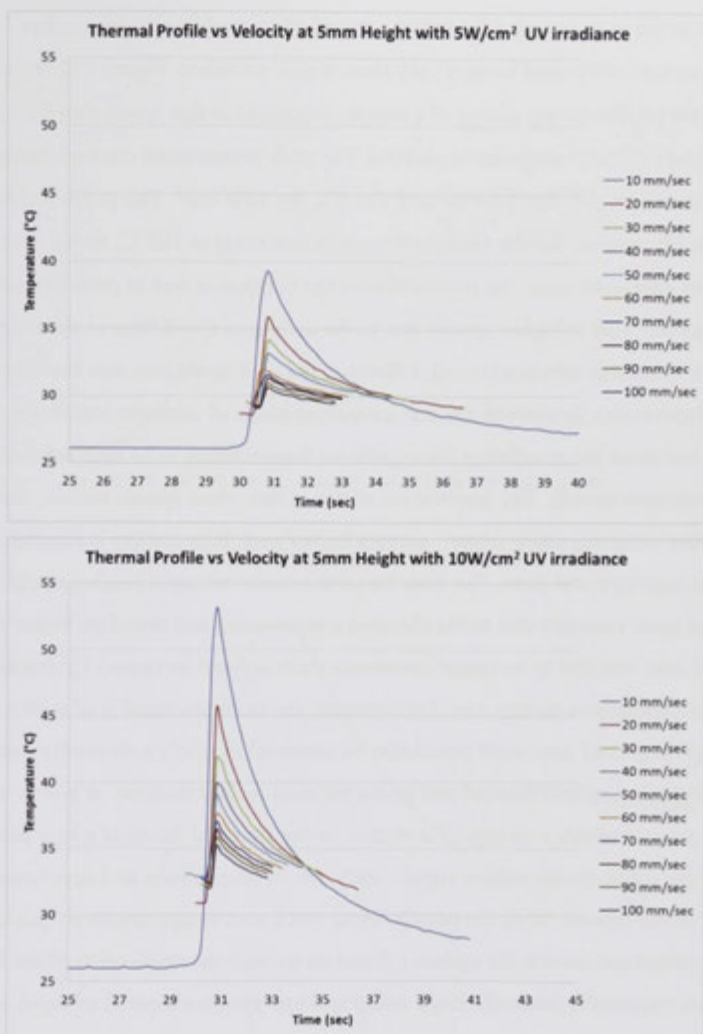
Figure 131 – Temperature during cure of sample with 5 and 10W/cm² intensities at speeds from 10mm/sec to 100mm/sec

Beyond 10mm/sec in speed, peak temperatures did not exceed 55°C, well below the service temperature published for the resin system when catalysed using 6% MEKP and CoNap catalysts and cured for 24 hours at room temperature, followed by a post cure for 2 hours at 120°C.

In order to understand the heating threshold of the UV system another experiment was performed using a very slow speed, 1mm/sec. Figure 132 shows the temperature profile during curing of a sample processed at this speed also for both $5W/cm^2$ and $10W/cm^2$ set point intensities. The peak temperature reached during processing was 81.3°C for $5W/cm^2$ and 132.9°C for $10W/cm^2$. The published heat distortion temperature for the vinylester resin in this study is 105°C, hence exceeded at $10 W/cm^2$. As can be seen, the period of time the composite was at peak temperatures was far greater than at higher speeds due to the increased dwell time at slower speeds where the same unit area is exposed. Likewise, the cool down rate was much slower. These temperatures far exceed any service temperatures of common vinylester resin systems and show the possibility for significant temperatures to be reached during very slow placements speeds. The implication of this is that when speeds reduce, the temperature ramp up, while slower, a much higher peak temperature is reached due to increased exposure and dose. The benefits of this observed rapid heating could include decreased resin viscosity due to the elevated temperatures and therefore better wet-out, increased cure rate due to increased molecular mobility and increased Tg due to elevated temperatures during cure. Furthermore, the heat generated is of such a range that a high degree of cure itself could also be achieved in solely a thermally initiated resin or even in a hybrid thermal and photo initiated resin. Likewise, at points in the UVAFP process where a change of direction or the start and finish of a new placement path occurs, robot speeds reduce significantly due to acceleration and deceleration capacity of the motors. With the possibility to reach such temperatures so quickly, the need to control and switch the system off and on to limit the application of the UV light only when required is essential. High speed aperture systems capable of rapid opening and closing are available on most spot cure systems and would be necessary to protect the composite. This finding indicates the significance of the temperature profiling in order to ensure thermal degradation is not occurring at slower process speeds.
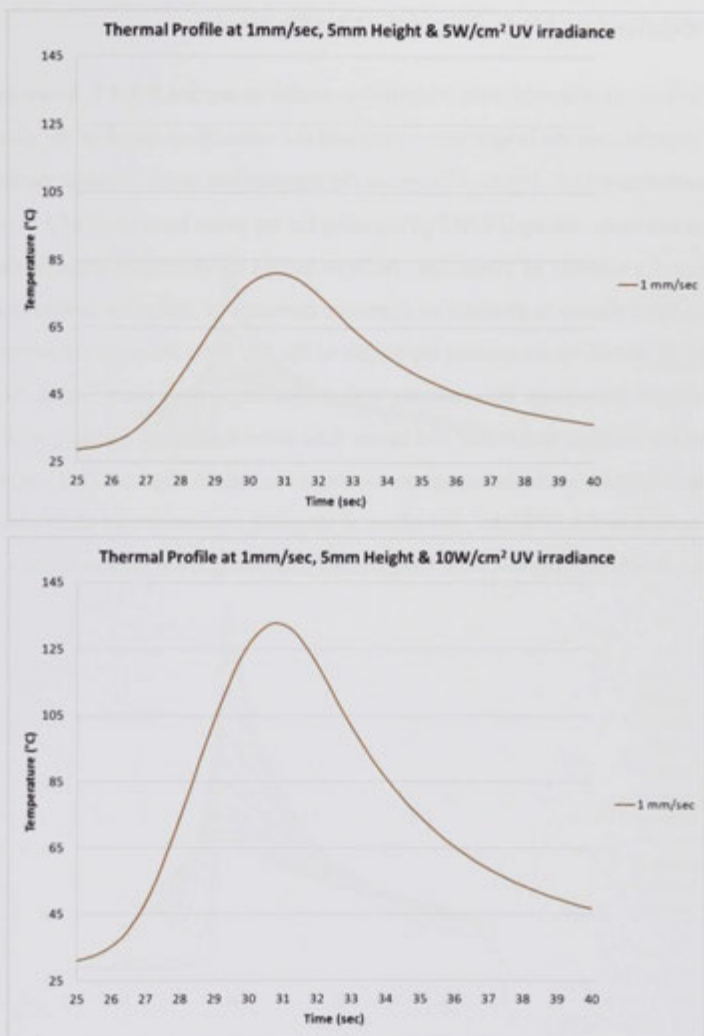
Figure 132 – Temperature during cure of sample with 5W/cm² and 10W/cm² intensity at 1mm/sec and 5mm height

Cooling ramp down rates after exposure ceased were noted to be similarly rapid as with the ramp up. No active cooling mechanism was used in the experimental setup. Therefore, only loses to the surrounding laminate, tool and environment could have caused the cooling rate. This demonstrated the highly localised exposure and control of the UV application at the 5mm height.

8.3.4.2 Height of the UV Light and the UVAFP Process

Further experiments were undertaken similar to section 8.3.4.1, however for this series of experiments the height was varied and the velocity or speed of the placement head remained constant. Figure 133 shows the temperature at the incident surface of the composite substrate during UVAFP processing for set point intensities of 5 W/cm^2 and 10W/cm^2 and a velocity of 10mm/sec. At 5mm height the divergent angle of the light source has been shown to produce an exposure diameter of 10mm up to 40mm at 50mm height. As expected, by increasing the height of the UV light the peak temperature and heat up rate are decreased. This concurs with the findings of Chapter 7, that showed by increasing the incident irradiance and hence dose were decreased. Further, with increasing height an increased exposure area was seen, as in Figure 133. Comparing the 5W/cm^2 results to the 10W/cm^2, the effect of set point irradiance was show also to be significant in determining the peak temperature increasing from approximately 39°C to 53°C.
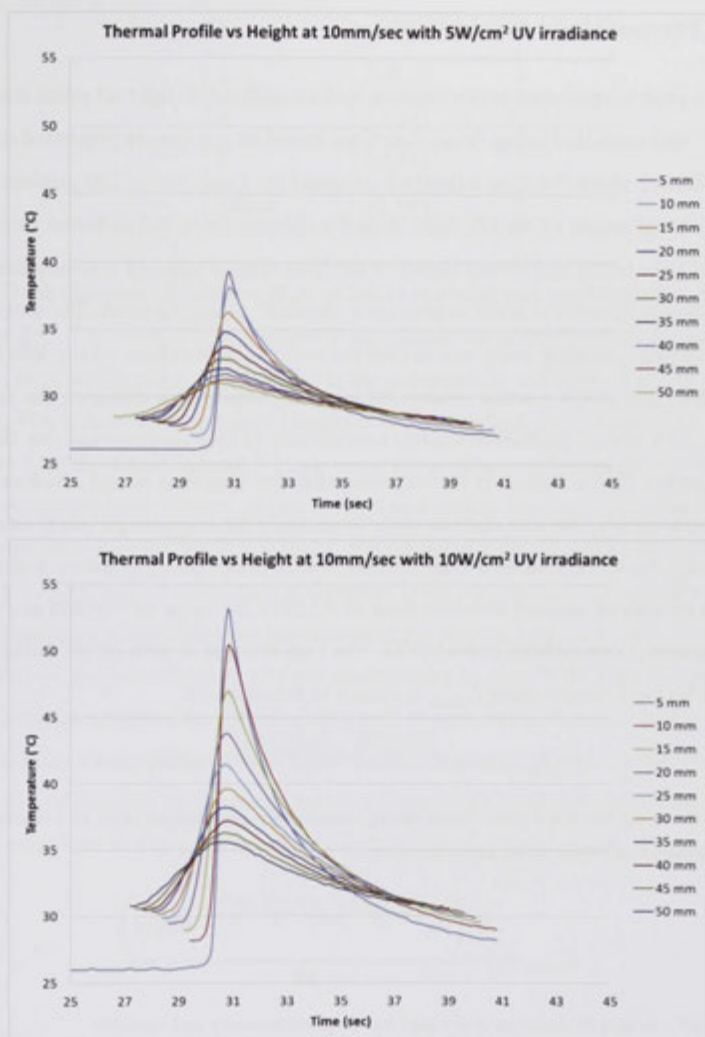
Figure 133 - Temperature during cure of sample with 10W/cm² intensity at heights from 5-50mm

As per the results of the speed analysis in section 8.3.4.1, again the heat up rates, even at the maximum height of 50mm, were significantly higher than most convective heat up techniques used in the curing of thermoset resins such as autoclaves and ovens.

8.3.4.3 Thermal Model Development

The peak temperature at the incident surface with a UV light set point intensity of 10W/cm² was modelled using fitting functions based on previously presented data, from sections 8.3.4.1 and 8.3.4.2, as a function of speed for 1 mm/sec to 100 mm/sec as and as a function of height of the UV light from 5 to 50mm. Over 300 different fitting equations were tested and scored based on the least sum of squared absolute error and a target of 6 coefficients (in order to provide a 'smooth' fitting surface). The aim of fitting approach using a scoring study was to find the best fitting function, taking into account all variables using only a scalar change for intensity, rather than changing the actual fit function. This was so predictive models needed only to take into account one fitting function rather than a library. It was expected that this approach would result in decreased accuracy, but was done in order to simplify the complex physical situation.

Using the scoring study a Log-Normal A with offset fitting equation was selected based on its sum of squared absolute error of 3.35944, R^2 value of 0.99864 and a Root Mean Squared Error (RMSE) of 0.55773. The Log-Normal A with offset fitting equation for peak temperature T_{peak} is shown in Equation 61.

$$T_{peak} = ae^{\left(\frac{ln(v)-b}{c}\right)^2 + \left(\frac{ln(h)-d}{f}\right)^2} + \text{offset}$$

Equation 61 – Log-Normal A with Offset fitting equation for peak temperature as a function of speed and height at 10W/cm² set point intensity

$$T_{peak} = \frac{W\left(ae^{\left(\frac{ln(v)-b}{c}\right)^2 + \left(\frac{ln(h)-d}{f}\right)^2} + \text{offset}\right)}{10}$$

Equation 62 – Scaled fit equation to account for set point intensity as a variable

The fitting equation was then scaled according to the fourth independent variable, the set point intensity as per Equation 62. Where the coefficients and are defined in Table 33, v is the velocity, h is the height and W is the set point intensity scaling coefficient, either 5 W/cm² or 10 W/cm² as per this study.

Table 33 – Full quadratic logarithmic transform coefficients.

Coefficient	Value
a	6086.7618

b	-13.2240
c	4.6074
d	1.6343
f	1.1884
Offset	33.1841

Three dimensional surface plots of the as recorded and modelled data are shown in Figure 135. The surface-fitting model is significant because it predicts the dependent variable, peak temperature, with respect to the independent variables of height and velocity. The actual versus predicted surfaces show excellent conformance for $10W/cm^2$ with very little deviation beyond 1°C, however the scaling coefficient did not provide robust correlation for 5 W/cm^2. At low heights and speeds the model failed to predict peak temperatures within 15°C. Likewise, at high heights for all speeds deviation was above 10°C. The lack of correlation at the outer lying temperatures (both higher and lower) immediately highlights the limitations of the scaling approach. Only having two data points on the intensity is an obvious shortcoming in data. With a third data point for intensity the nature of the relationship would present itself. With the data collected the scalar error shows either that the scalar was too high a coefficient or that the relationship of intensity on the temperature is actually not linear but exponential. This was not examined in this work but should be considered in future work.
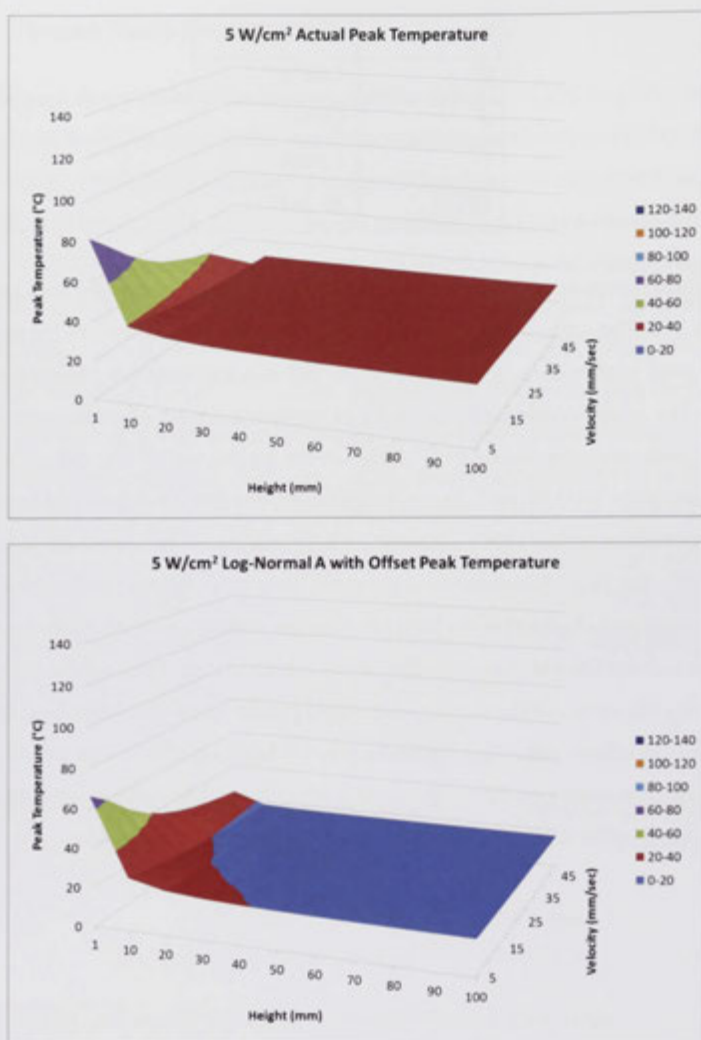
Figure 134 - Peak temperature as recorded and fitted using log-normal A with offset surface for 5W/cm²
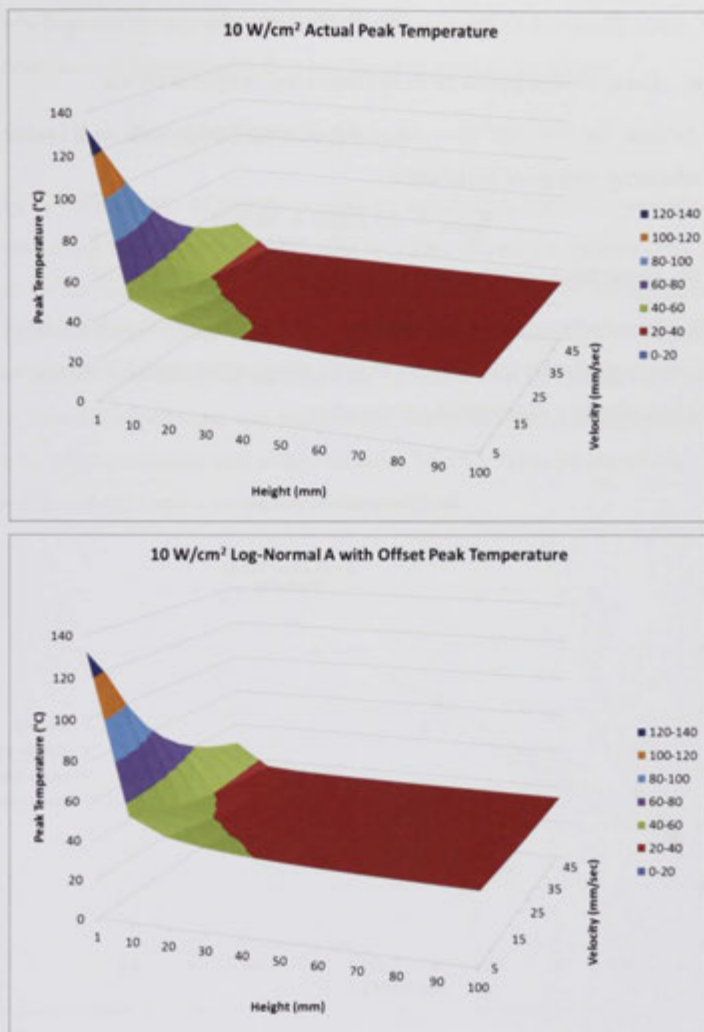
Figure 135 – Peak temperature as recorded and fitted using log-normal A with offset surface for 10W/cm²

With the available dataset the temperature could be compared to the actual dose delivered and not just the parameter settings. The results are shown in Figure 134 and Figure 136. The relationship in both cases (5 and 10W/cm²) show close correlation to positive linear fittings. For 5W/cm² the relationship is described in Equation 63 with an R^2 value of 0.9721, indicating very good correlation.

$$T_{peak} = 23.379D + 31.174$$

Equation 63 – Linear fitting equation for Peak temperature vs Dose at 5W/cm²

Likewise, for 10W/cm² the relationship is described in with an R^2 value of 0.9776, indicating very good correlation.

$$T_{peak} = 23.205D + 36.036$$

Equation 64 - Linear fitting equation for Peak temperature vs Dose at 10W/cm²

This linear relationship is in contrast to the independent variable relationships of height to peak temperature and velocity to peak temperature, which both more closely correlated to a negative exponential relationship.
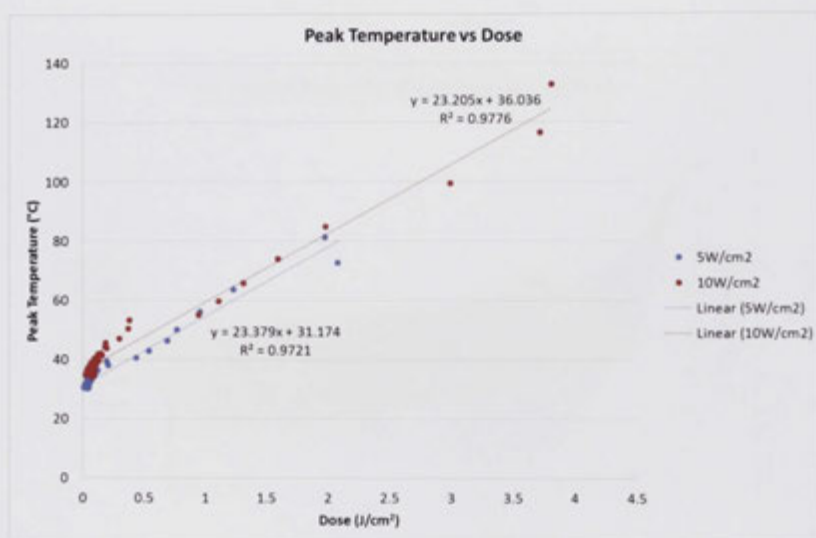
Figure 136 – Peak temperature vs dose

The predictive model developed for peak temperature as a function of height, velocity and set point intensity is significant because it enables UVAFP process parameters to be setup in order to maximise the thermal properties by reducing the residual heat of reaction in order to aid in Tg development and resin flow due to decreased viscosity and at the same time. When used in conjunction with the degree of cure predictive model (Chapter 7) the parameter settings can be used to ensure

excessively high temperatures are not seen by the composite that could cause degradation through thermo-oxidative mechanisms such as mass loss.

8.3.4.4 Mass Loss during the UVAFP Process

As a direct indicator of thermo-oxidative degradation, mass loss was measured during processing via UV curing [144]. The set point intensity, exposure area, resin depth and the resin initial temperature were kept constant and only the height of the UV light from the incident surface was changed. Only 3 height settings were investigated due to the limited availability of the data logging scales used to measure real time mass loss at the time the experiment was undertaken. The initial resin temperature prior to exposure for all experiments was measured to be 24.8°C. Table 34 shows the experiment test matrix and a summary of the results.

Table 34 – Mass loss test matrix and results

Experiment	Depth (mm)	Set Point Intensity (W/cm^2)	Distance (mm)	Incident Surface Diameter (mm)	Incident Area (m^2)	Surface Irradiance (W/cm)	Exposure Time (sec)	Total Dose (J/cm^2)	Total Mass Loss (%)	Peak Temperature (°C)
1	8	10	10	12	0.045239	0.34403	470	161.6941	24.53	160.3
2	8	10	15	12	0.045239	0.27056	470	127.1632	10.89	155
3	8	10	20	12	0.045239	0.17151	470	80.6097	4.2	135.9

Mass loss can be expressed in various forms that combine initial composite mass (m_0), transient composite mass (m), normalized mass (m/m_0), extent of mass loss ($\alpha = 1 - m/m_0$) and total mass loss ($Q = m_0 - m = \alpha m_0$) [144]. Each expression can be easily compared to another using the constant initial mass (m_0). In this study, normalised mass loss was calculated to express the change in the mass as a percentage. This normalised mass is defined as the ratio between initial weight and the weight of specimen corresponding to a given stage of the degradation process. The results are shown in Figure 137.
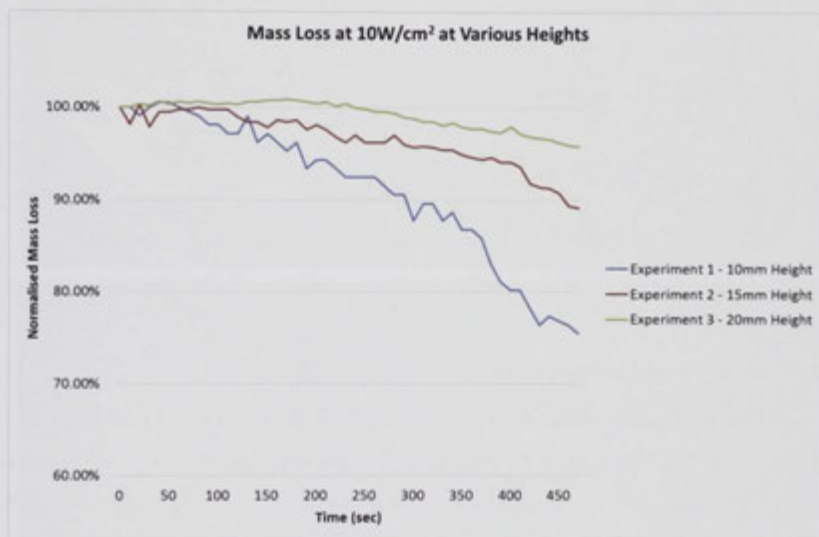
Figure 137 – Mass Loss results over time in static exposure setup

Increasing the height of the UV light and therefore reducing the incident irradiance decreased the rate at which the mass loss occurred. As presented in section 8.3.4.2, with increasing height, the peak temperature reached during transient exposure decreased. Because of the static setup used in this experiment in order to deliver the UV radiation over an extended period of time, direct comparison to temperatures measured in transient experiments are not representative. Therefore, temperatures were recorded during exposure in order to compare mass loss to temperature. The experiments were run up to the point where the temperature rise rate slowed at the thermocouple. It was thought that the heating stabilised due to environmental heat losses but also possible

burning and release of the heat energy. Static temperature measurements were taken for all heights investigated in Experiment 7 and 8 and not just 10, 15 and 20mm as per the mass loss measurements. The results are presented in Figure 138.
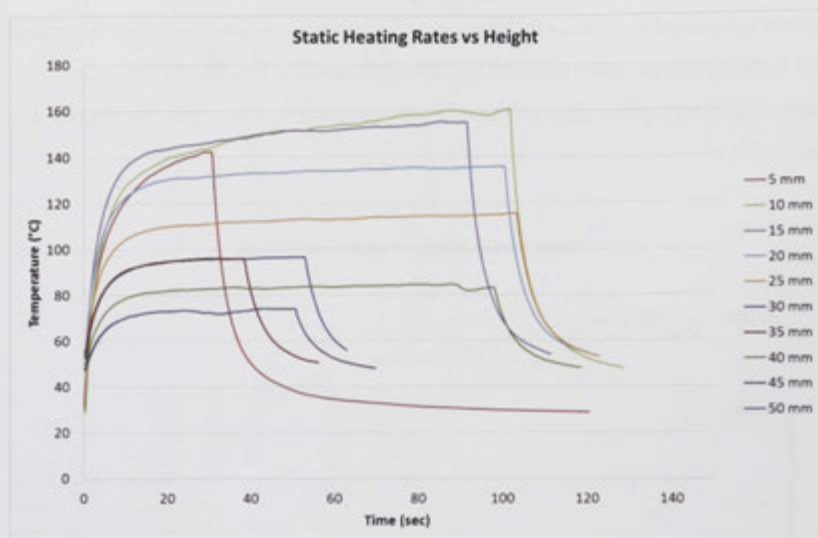
Figure 138 – Static exposure temperature ramp up

The results showed that in all cases, mass loss increased with increasing exposure time (increasing dose) and by increasing the intensity the rate and total mass loss also increased. This result concurred with previous thermo-degradation models by Chung [144]. It was observed that due to the non-uniform irradiance delivery, mass loss was concentrated in the high irradiance area immediately under the light source orifice. Figure 139 shows the sample from Experiment 1 produced in the static mass loss experiment exposed to over 5 minutes of UV light at 5mm height and 10W/cm² set point intensity. This was undertaken to assess what effect extreme exposure would have. As can be seen, in this extreme scenario the incident surface experienced significant thermal degradation through thermo-oxidative means (burning) with smoke and even flames produced. This experiment showed what might happen if, for example, the UVAFP head might stop with the UV light still on. The high intensity and focus of UV spot curing systems can be seen with a clear circular area matching the exposure diameter at 5mm height. For such charring and consequent auto-ignition to occur,

temperatures above 420°C would need to have been reached [160] according to the manufacturer's material safety datasheet (MSDS). Interestingly the damage did not penetrate deep into the sample. The depth of charring appeared to be no more than 1mm deep.
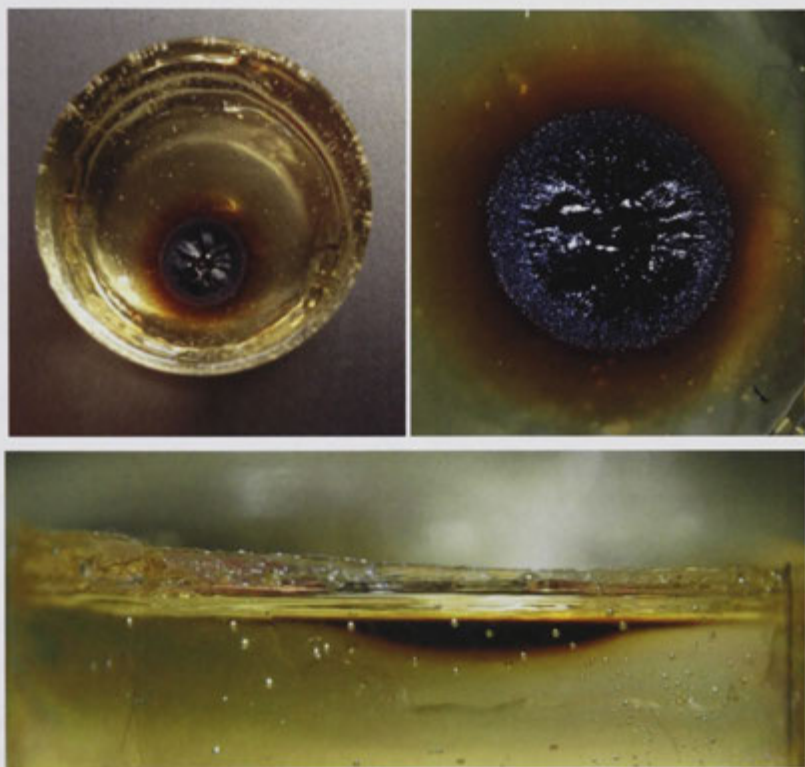
Figure 139 – Mass loss sample showing signs of thermal degradation (top left), close-up of degraded area (top right) and cross section showing depth of degradation (bottom)

Vinylester resins (VER's) are typically manufactured via reaction of bisphenol-A epoxy resins with acrylic or methacrylic acids. The reaction product is highly viscous, so VER's are diluted by adding a low molecular weight co-monomer, usually styrene [265]. During the reaction volatile organic compounds (namely, the styrene) are released in small but not insignificant quantities and evaporates from the sample contributing to a degree of mass loss that is not related to any degradation of the resin. The small amount of styrene mass loss can be seen during early exposure after ramp up

of the temperature of the sample, especially given the elevated temperatures measured during the experiment setup.

8.3.4.5 Degradation Model

Mass loss was compared to the dose directly using the real time dose calculation and the real time mass loss data, as shown in the scatter graph below, Figure 140.

Mass Loss vs Dose

$y = 1E-05x^2 - 0.0004x + 0.005$
$R^2 = 0.9323$

Figure 140 –Mass loss vs dose, including 2D trend line fitting

The figure shows a second order polynomial negative relationship with mass loss, Q, defined by Equation 65, where the total mass loss is Q and the dose is D. The calculation of this dose is shown in with a defined y intercept of 100% at x = 0. The correlation to the trend was high with an R^2 value of 0.9312.

This result is in contrast to the result found by Chung [144] that showed a negative exponential relationship with rapid mass loss early during exposure then slowing. Although these tests were undertaken after full cure had been achieved according to the manufacturer's instructions and after drying (in order to remove moisture absorbed and surface) which differs greatly to the mass loss mechanisms during curing and cross linking.

$$Q_{\%} = 1.1104 \times 10^{-5}D^2 - 2.8748 \times 10^{-4}D$$

Equation 65 – Mass loss versus Dose

Previous studies demonstrated that sample geometry affects the degradation behaviour of polymers and their composite systems. This is predominantly driven by the surface area to volume ratio of the composite [144]. Furthermore, the reinforcing fibres change the heat conduction, dissipation through the composite and therefore effect the degradation rate behaviour of polymer composites under elevated temperature in an air environment due to the very anisotropy nature of the continuous fibre reinforced laminate [144]. Thermo-oxidative degradation by mass loss can be related to mass loss per unit area (g/cm^2) as q_i, although the composite substrate was orthotropic, previous studies [144] have found that degradation is anisotropic and therefore the mass loss is different in all directions. In this experiment mass loss progression and direction were considered only from the incident surface downwards through the thickness of the resin.

In relation to the temperatures observed during degradation testing, a second analysis was undertaken comparing temperature to mass loss for the available data. The results are shown in Figure 141. Due to the nature of the data, a fitting function or trend line was not applied. The relationship did appear quadratic in nature, although this was not tested. If this observation is accurate and significant this could suggest a physical reasoning based on diffusion limiting behaviour. This would be interesting for future analysis. The commencement of mass loss can be seen once temperatures exceed 120°C. At this temperature it is most likely constituent ingredients are boiling off, particularly the VOC's including the styrene and mass loss commences. Therefore, degradation can also be said to occur due to constituent loss not just thermo oxidative effects.
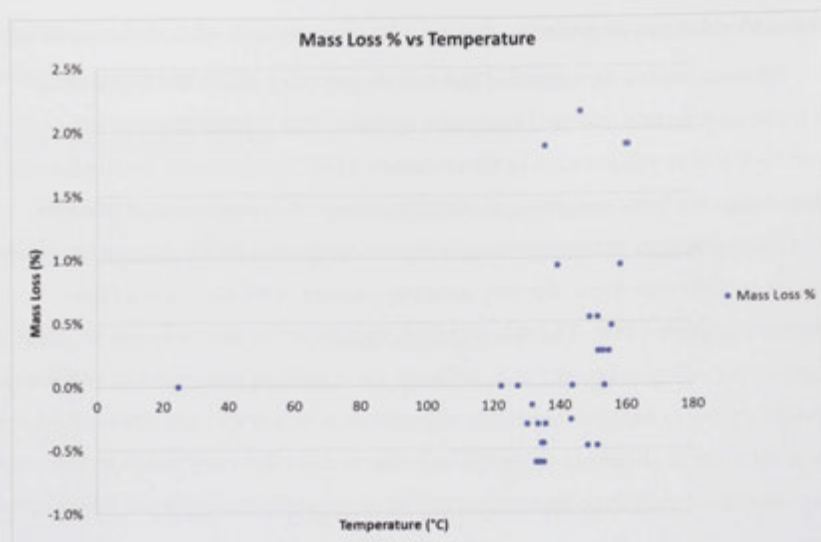
Figure 141 – Mass loss versus Temperature

8.3.4.6   Degradation and Degree of Cure (DoC)

In Chapter 7 [266] a model to predict the degree of cure was developed based upon the same independent variables, height, speed and intensity. The model used the mechanical property of hardness as a direct relation to degree of cure and was able to predict hardness through thickness using the Beer-Lambert law of absorption to determine the dose as a function of depth. The model allowed for the optimisation of process parameters to drive a required degree of cure related mechanical property, namely hardness. In process control considerations for UVAFP this work is crucial for ensuring quality and maximising productivity. The model did not however include any consideration for temperature and degradation, leading to the possibility that the composite could be exposed to excessive irradiance causing mass loss and thus degradation due to the lack of constraint around peak exposure temperature during processing.

With the work presented here in Chapter 8, the dose could now be constrained in order to determine the optimal process parameters to ensure maximum DoC without causing mass loss beyond a desired amount of dose (J/cm).

In the comparison of mass loss and temperature it is also evident that certain products are lost above 120°C as well as the start of possible thermo oxidative degradation. Therefore, this temperature should also be provided as an upper limit on temperature which can be applied to the thermal model developed in section 8.3.4.3 when calculating thermal impact on process parameter combinations.

8.3.4.7   Glass Transition Temperature

Differential scanning calorimetry (DSC) experiments were undertaken on the select samples from the experiments in sections 8.3.4.1 and 8.3.4.2. This was to assess the thermal properties of the laminates and identify possible effects caused by the temperature variation observed depending upon UV light height and intensity as well as the placement speed. The experiment test matrix and results are detailed in Table 35.

Table 35 – DSC sample process parameters

Sample Number	UV Set-point Intensity	UV Light Height	Placement Speed	Peak Temperature during Curing	Tg	Residual Heat of Reaction	Series in Figure 142
#	W/cm^2	mm	mm/sec	°C	°C	mJ	Colour
1	10	5	1	132.9	52.97	44.27	Blue
2	10	5	10	53.2	52.76	106.8	Red
3	10	5	20	45.6	52.85	140.97	Cyan
4	10	5	30	41.9	51.17	187.61	Brown
5	10	5	40	39.9	51.88	270.27	Purple

The cured samples were exposed to a standard 10°C/min ramp up in the DSC from room temperature (approximately 25°C) to 200°C. The results of the DSC scans are shown in Figure 142.
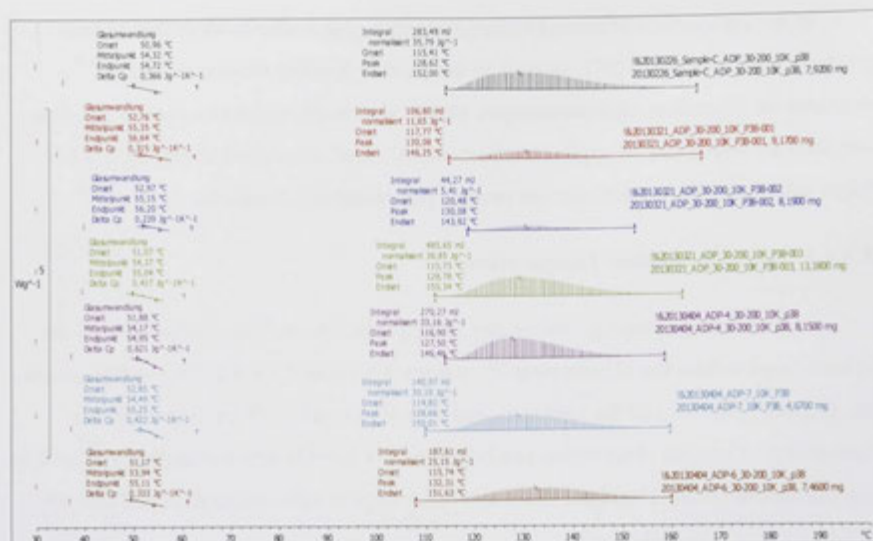
Figure 142 – DSC plots taken for a number of samples produced using UVAFP at varying speeds, heights and set point intensities

It should be noted that environmental UV light could have been significant in the results of these studies. The time between manufacturing samples and testing was in the order of months due to the lack of access to a DSC in a timely manner. In order to undertake these studies the author had to attend a testing facility in Germany after manufacturing the samples in Australia. Samples were kept in 'dark environments' using aluminium foil wrapping as well as storage in an opaque sealed container for most of the period, but it is unclear if the time between exposure and cure and testing had an effect. This is suggested as future work. In any case, the DSC results showed consistent phase change indicating the Tg temperature around 50°C, where an evident change in the resin heat absorption occurred. The second observed reaction with onset usually around 110°C was an exothermic reaction of the resin, suggesting further curing and residual unreacted bonds forming. Because the resin did not contain a thermally activating catalyst it appeared that an auto-catalysation reaction made possible purely by the addition of the heat during DSC analysis occurred. Significantly, the while first phase change Tg's observed for each sample, appear to not be related to the peak temperature achieved during cure the amount of residual heat of reaction did. This result has multiple implications. First, that while UV curing is considered a thermally

independent process, the temperature achieved as a by-product of the localized irradiant energy has a direct effect upon temperature dependent material properties such as the residual heat of reaction. Residual heat of reaction is often used as a qualitative measure of the degree of cure of a resin system when compared to the total heat of reaction and therefore the result shows an effect caused by the peak temperature achieved during curing using UVAFP. By optimizing the process parameters in order to control the peak temperature achieved during exposure a laminate of comparable mechanical and thermal properties to a fully thermal cured sample could be achieved.

Scott et al. [8], examined the effects of temperature on the changes in the styrene, methacrylate, and radical concentrations during photopolymerization of vinylester resins by using FTIR and ESR spectroscopy. As in this study, the photo initiator Irgacure 819 was used but at a concentration of 0.25 wt % and added styrene was supplied by Huntsman Chemical. After UV curing of samples and post curing at 180 °C for 1 hour, a Perkin-Elmer 1600 spectrometer was used to record the FTIR spectra. An increase in the isothermal cure temperature raised the polymerization rate of both methacrylate and styrene species due to the increased propagation rate and initiator efficiency. The degree of conversion also increased with increased isothermal cure temperature because the resin was able to cure further before the onset of vitrification. While propagation was able to proceed to higher conversions at raised isothermal cure temperatures, bimolecular termination also continued which resulted in lowered concentrations of trapped radicals in the network with increased cure temperature [8].

The free-radical UV curing of VERs is diffusion-controlled. Towards the end of the cure reaction, methacrylate group consumption ceases, while consumption of the smaller, more mobile styrene groups continues for some time before ceasing [265]. Eventually, vitrification of the network occurs and all reactive groups are frozen in the matrix, giving place to the previously reported effect that VERs do not achieve 100% conversion immediately a defined "full" cure [8]. Once the network is vitrified, post-cure above the glass transition temperature (Tg) is necessary to increase molecular mobility and allow full cure to occur [265].

Figure 143 presents three DSC plots at 10°C/min up to 200°C, an uncured VER Derakane 411-350 reacted with an MEKP thermal initiator, black, a cured VER Derakane 411-350 reacted with Irgacure 819 photo initiator (0.5 %wt) after processing

in UVAFP (at 10W/cm² set point intensity, with the UV height at 10 mm and the speed at 50mm/sec), red, and finally the same sample after a 1 hour post cure at 100°C, orange. The thermally cured sample produced a total heat of reaction calculation of 6648.62 mJ. The residual heat of reaction of the UV cured only sample was 1152.92mJ, indicating an approximate degree of cure of 76%, however with a Tg still around the 40°C range. The UV cured and thermal post cured sample showed very little residual heat of reaction, approximately 14.23 mJ suggesting an approximate degree of cure above 99%.
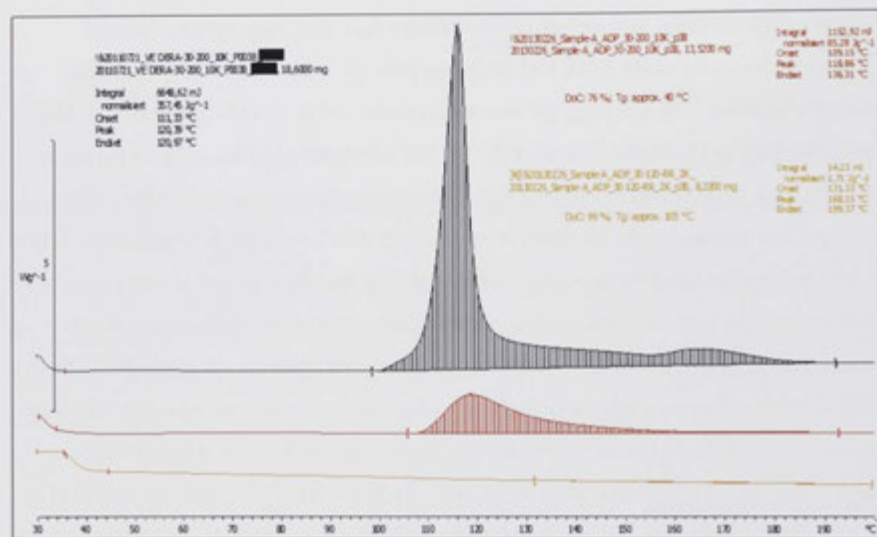
Figure 143 – A thermal cure MEKP catalysed sample, a UV cured sample and a UV cured sample with post cure DSC plots

As discovered in the previous experiment and in concurrence with the findings of Scott [8] and Cardona [265], the UV only cured laminate produced residual heat of reaction during DSC analysis, suggesting only partial cure in regards to thermal properties and only after post-cure above the Tg further molecular mobility could occur and full cure could be achieved leading to the very low residual heat of reaction.

In work investigating the effect of isothermal conditions on reaction rate of UV curing systems, a clear relationship between increased isothermal temperature and increased reaction rate were found. This concurs with the results of this experiment.

While not directly measure the relationship between temperature and irradiance intensity were consistent and it has been previously found that increasing the intensity, while also increasing the overall dose, increases the reaction rate. The findings of this experiment did conflict with some previous findings looking at the isothermal conditions during UV curing [8][265], in that the Tg did not seem to be effected although only a limited number of samples were tested and no investigation of the precise nature of the low temperature phase change at 40-50°C was made.

8.3.5 Experiment Conclusions

During the UVAFP process radiant energy delivered by the UV light source contributes to rapid localised heating of the composite. This heating could both aid in processing and degrade the finished composite properties. It was hypothesised that by controlling the height and set point of the UV light and the placement speed, the temperature experienced by the substrate during processing could be indirectly controlled using a predictive model. This predictive model could then be used to maximise the temperature to aid in fibre wet-out and thermal properties while ensuring degradation did not occur. Both hypotheses were proven successfully in the experiment. The impact if this is that by using the model any degradation can be minimised, increasing the robustness and quality control of the process and defining a precise operating window.

Elevated temperatures during processing were also found to not only benefit wet-out, by reduction of the viscosity (observed only – not measured) cure rate and reduce residual heat of reaction by decreased resin viscosity, increased molecular mobility and heightened cure cross linking at elevated temperatures. The predictive model was demonstrated to have very good correlation (less than 1°C variation) at 10 W/cm^2 but due to the scaling coefficients used was less accurate at a set point intensity of 5 W/cm^2 due to the simple scaling coefficient used. The published distortion temperature for Derakane 411-350 is 105°C, only with a speed of 1mm/sec and at a distance from the incident surface of less than 15mm did the temperature exceed 100°C. In most cases this combination of process parameters would never be utilised. Due to the regular rapid speed of the UVAFP process, the high intensity UV lamp does not excessively heat the composite as other techniques (for example, laser, EB or hot gas gun) do. This model

was approached empirically, and applicable to a complex physical situation. Therefore, this model is limited to the specific materials used in this study.

Degradation has been demonstrated to occur due to the temperature and dose delivery of the UV light source. At a speed of 1mm/sec and at a distance from the incident surface of less than 15mm did the temperature exceed 100°C. In most cases this combination of process parameters would never be utilised. Due to the regular rapid speed of the UVAFP process, the high intensity UV lamp does not excessively heat the composite as other techniques do. This reduced temperature means that the risk of thermal degradation is reduced and that the issues of shrinkage due to rapid cooling and different thermal expansion coefficients are minimised.

The outcome of this analysis was the ability to select and optimise process parameters to achieve the desired degree of cure on-the-fly while managing the degradation (by mass loss) of the composite. In processes such as UVAFP where industrial robots are utilised for the articulation of the placement head, accelerations and decelerations of the robot can vary the placement speed significantly, thus varying cure. By knowing the processing lower limits the placement speed, UV light intensity and height settings can be adjusted accordingly.

The analysis of thermal properties (Tg and residual heat of reaction) of the composite in comparison to the dose and temperature of processing showed that while the peak temperature of processing had little to no effect on the Tg in the UV cured resin it did effect the residual heat of reaction and the calculated degree of cure. The impact of this finding is that the temperature could be controlled to vary the residual heat of reaction and thus degree of cross linking which could have an impact on mechanical properties not measured in this experiment, for example hardness and flexural strength and modulus.

Future work should consider a number of additional experiments to fill gaps in the data set. The modelling approach provided is empirical, and applicable to a complex physical situation. However, the application of this model is limited to the specific materials used. Further, additional mass loss measurements according to all UV light heights as consistent with Experiment 7 process settings and the dynamic temperature measurements in this experiment. Further, the experiment data only considered temperature in one dimension at the incident surface, temperature readings were not

recorded for previously laid plies or in the in-plane direction for adjoining tows. Temperatures through thickness would vary as a function of depth and repeat exposure (due to the absorption of the UV light and penetration depth exceeding that of 1 ply) and therefore the mobility of chemical chains and likewise temperature at which cross-linking would occur would vary through each cured ply thickness.

While previous research [72] has shown no effect using a ply-by-ply curing approach the non-uniform thermal history of the composite requires further analysis to understand possible sensitivities. In all at once thermal cures such as in an autoclave or oven, thermal distribution uniformity through across the entire part thickness is far greater but through thickness distribution is far greater. In UVAFP the thicknesses of each ply is very thin and therefore thermal variation through thickness is less indicating greater control in the process and hence material properties.

Future work should also investigate the viscosity change or dynamic viscosity and rheology during processing according to the temperature range seen in this experiment. While elevated temperatures are known to reduce viscosity such data would aid in the formulation of accurate impregnation models (Chapter 5) and allow for temperature targeting for optimal wet-out and not simply degradation avoidance.

8.4 Summary

The thermal considerations during UVAFP were investigated in this chapter. These considerations included both the use of temperature in order to aid in processing and controlling or predicting degradation due to overheating as well as the thermal property of residual heat of reaction. Previous work has found significant effects of the temperature on the composite in thermal driven processes as well as the possible degradation these temperature can also cause. However, due to the novelty of the UVAFP process and use of a photo-initiator, little was understood about the behaviour and effect of the composite in regards to temperature and thermal properties during dynamic UV curing applied in-situ in a ply-by-ply manner. This chapter presents the first work of this kind and adds to the body of knowledge on UVAFP in supporting predictive models to allow for accurate process control and planning as well as quality control by avoiding degradation.

Most references were taken from thermoplastic material processing where dynamic application of heat is critical to final quality, but little conclusions could be carried over in terms of final material and part quality due to the use of photosetting vinylester resin. The low viscosity of the VER's at room temperature coupled with their rapid cure and low cost, make them prime candidates for composites in transportation and infrastructure. Vinylester has a long historical utilisation in marine applications and other structures and exhibits good fire retardant properties. A final predictive model with degradation limits placed on temperature and dose was constructed and added to a previously developed models optimising the degree of cure (Chapter 7). This was to ensure that the speed was not set too slow and the dose was not set too high to maximise the temperature of the composite during processing without causing degradation. Although the results of this work implied constraining the processing window for UVAFP, the work still demonstrated the high mechanical properties that could be achieved and the rapid processing speeds of UVAFP in order to address the demands of the composite industry for fast, and efficient processes for the production of high quality composites.

9 Conclusions and Future Work

This chapter presents the final conclusions for the body of work undertaken for this thesis. Section 9.1 summaries the key findings of this research in terms of component design, material selection and process optimisation and how the limitations of Automated Fibre Placement (AFP) were identified and overcome. Section 9.2 summarises the new knowledge developed from this thesis. Section 9.3 proposes future work as a continuation of this research and what could be done in order to progress the development of the UVAFP technology. Section 9.4 is the final summary of the thesis.

9.1 Summary of Research Outcomes

This thesis has addressed a number of gaps in the literature relating to AFP, composite materials, UV curing, and the combination and integration of these technologies. First, the design considerations for placement head devices and the reach and access of these placement heads in defining the complexity of the parts that can be laid-up. This applies not only to AFP but also to technologies such as stereolithography, 3D printing and other additive manufacturing techniques. Second, using raw constituent materials such as dry fibre tows and liquid resin, and the issues associated with using such materials in high tech automated systems. This includes dimensional stability, uniformity of the raw material, environmental conditions and handling systems. Third, applying high intensity UV photo-curing along with on-the-fly resin impregnation in combination with AFP technology. Fourth, using flexible industrial robots in such applications and utilising their six degrees-of-freedom to produce complex parts. Finally, the modelling of such dynamic and transient processes with a small processing window operating at high speeds and the impact this has on the material quality. This includes impregnation, consolidation, curing and the ultimate thermal and mechanical properties. The limitations of AFP and the process used to demonstrate the feasibility of using UVAFP as a manufacturing process for composite materials were defined and addressed within this thesis. The three key areas of focus were design, material, and process as described in the following sections

9.1.1 Design of Automated Fibre Placement Systems

Whilst many recent advances in AFP for composite production are commercial in confidence, it is generally acknowledged that current AFP systems are limited in their reach and access due to the design of the placement head. Until now the literature had not addressed the multi-body kinematics and dependencies in surface following applications, and therefore the packaging of AFP devices was not optimised and were often cumbersome with geometry limiting designs. This thesis focused on reducing the size of the AFP placement head in order to increase its reach and accessibility within the lay-up tool. The sizing dimensions of clearance angle, head width and roller diameter were found to strongly influence reach and access as defined by minimum radii and arc length of this minimum radii. The results enabled the design envelope for the UVAFP prototype to be clearly defined to maximise reach and access. The impact of this part of the thesis will be to make the technology more versatile to facilitate the production of complex shapes by all AFP processes. The design of the UVAFP system was purposefully modular so as to allow scaleability for increased production. The scaleability of the design could be made through simple addition by stacking of the tow feed and cure mechanisms similar to other CCR systems using angular offsets to create package envelope for processing equipment. Certainly the reach and access of any increased scale would likely be reduced, but the design could be developed so that placement head sizing could be changed swiftly depending on the scale of the part.

While industrial robots have seen increasing utilisation throughout the manufacturing industry their role has been limited to pick and place or point-to-point applications. Little literature exists on the performance of robots in surface following applications with dynamic tool centre point loads. It was found that by decreasing the arm extension, decreasing feed rate, increasing spindle speed, and decreasing the point filtering for the path generation of industrial robots, the path following accuracy was increased. The outcome was to increase the versatility through compact design as well as increase the degrees of freedom. Utilising the 6th degree of freedom on industrial robots may lead to the possibility of producing more complex parts. Furthermore, industrial robots are far more economical than large gantry systems. Using these robots reduces the cost of the technology and makes it more accessible to the market.

9.1.2 Material Selection and Development

Current AFP materials, while optimised for weight are only available in a select few composite combinations (fibre and resin) and are very expensive. Limited information was available in the literature relating to dry fibre tows and liquid resin used in automated handling and lay-up. In addition, there was little information on systems maintaining the fibre as a continuous form and impregnating the fibre at the nip point upon lay-up for the final part form. Further, while UV curing exists in many industrial applications, no references were found to exist for UV curing applied in-situ in an AFP system. It was found that controlling the tension and compaction force of the lay-up process decreased the width and thickness variability of dry glass fibre tows allowing them to be readily used in automated systems such as UVAFP. It was shown that both tension and compaction force had an optimal setting in controlling noise and variability to nominal target dimensions which was within the tolerances for automated handling systems such as feed rollers and guide chutes. Dry fibre tows offered greater flexibility in terms of the resins they can be impregnated with but also the architecture of lay-up and are far more inexpensive than towpreg.

It was demonstrated that by using glass fibre and vinylester resin impregnated on-the-fly and cured in-situ using UV, the resulting composite was comparable in terms of mechanical properties if not improved properties to aluminium, steel and composites manufactured by traditional hand laid-up thermally cured techniques. The impact of this is that glass fibre and vinylester processed according to the UVAFP process can be considered as a structural material and offers weight savings currently required to meet target emissions for vehicles.

9.1.3 Process Optimisation for Resin Impregnation and Curing

To meet the stringent requirements of weight targets for new vehicle structures, production processes capable of producing components efficiently and cost effectively for large scale applications need to be industrialised. While AFP currently offers an automated solution with the benefits of a full CAE approach, the process is slow and includes many pre and post process steps. The majority of the literature was found to focus on current or outdated AFP devices and due to the proprietary nature of this field,

little information on alternate AFP based systems, their internal workings and new concepts was discovered. Furthermore, it appears that the scope for AFP is still mostly focused on the lay-up step of the manufacturing process. While additive manufacturing techniques such as 3D printing and sterolithography utilise similar mechanisms in the manufacture of components in a ply-by-ply manner, little research exists that examines the effect of the selection of materials on the approach and characterises the material properties (degree of cure for example) based on processing parameters. This thesis explored the use of dry glass fibre tows and on-the-fly resin impregnation, therefore reducing the impregnation time in comparison to existing AFP processes. It was shown that impregnation time, often a limiting factor to production rates for composites was not in the case of UVAFP a limitor. High lay-up speeds were calculated as possible using on-the-fly resin impregnation (up to 2160 mm/sec), an increase of over 400% in comparison to current benchmarks averaging 500mm/sec layup speeds, leading to high production rates.

The use of high intensity UV light resulted in an increase in UV dose over a shorter period of time and meant that the degree of cure could be increased or the required exposure time could be reduced. In Experiment 6 in Chapter 6 it was demonstrated that the production rate could be increased by reducing the curing time as the resin conversion rate was incredibly fast. This means that higher productivity can be achieved at lower costs.

In Experiment 7, the curing mechanism was applied in a ply-by-ply in-situ approach resulting in equivalent V_f, surface hardness and ILSS to glass fibre vinylester composite cured using conventional thermal processing. Further, when the UV light was applied in a ply-by-ply in-situ approach, the cure time was measured to decrease further by 43.75% and the degree-of-cure was increased by 1.3% (as measured indirectly by the interlaminar shear strength). This demonstrated that higher productivity and lower costs can be achieved with UVAFP.

Analytical modelling of the process using fitting functions was used to predict the performance of the process and the effect on the final degree of cure of the component. The effect of the height of the UV light, the intensity of the UV light and the speed of the placement the dose of UV light and degree of cure of the composite during UVAFP was accurately modelled. The impact of this model is the ability to

predict and control the degree of cure to ensure quality. Used in one way, the model could determine material properties. And in the other way, be used to ensure material properties are in accordance with to process conditions. That is, assigning a speed to determine the degree of cure (DoC) or in situations where the speed cannot be controlled, assigning the DoC required to determine the speed.

The temperature during processing and whether increased temperatures led to degradation of the composite during UVAFP was also investigated. The influence of the height of the UV light, the intensity of the UV light and the speed of the placement all had an effect on temperature profile during processing. A model was developed in order to predict the temperature and process limits prescribed to ensure degradation did not occur. The impact of the model is the ability to control the temperature and minimise degradation during UVAFP processing according to the independent process parameters. This ultimately provided an optimal operating window for future application of the technology.

9.2 Research Outcomes

This thesis aimed to build upon the knowledge and understanding surrounding AFP as a state-of-the-art process, and how to progress the technology further. This thesis research started as a design, test and build approach project to understand the influence of the design of AFP systems, the materials and processes. This meant that it was necessary to build a robust process prototype. Therefore a large amount of the research of this project was invested in designing the prototype. This presented a number of challenges which were time consuming, yet ensured that the results from the subsequent experiments were both reliable and industrially relevant. The design, mechanisation and implementation of a working AFP prototype built from simple sketch pad concepts, was absolutely vital in gaining an in depth understanding on the process, the dependencies and even quality control. This opportunity gave the author a wealth of experience not just in testing and experimentation but also design, automation and control systems.

Throughout this work effort was made to ensure a consistent experimental design and procedure was applied and that all tests performed captured data accurately and in a representative manner to draw production conclusions, even if the UVAFP prototype

only produced single tow lay-ups. However, inevitably errors were present throughout the experimental work due to the nature of the technology and the novelty of the system. Sensors used in the control system were calibrated and used according to manufacturer's instructions, and some designs after testing could have been improved. A number of valuable lessons were learned that can be applied to the development of the next generation of fibre placement prototype. During commissioning and testing, it became apparent that the UVAFP prototype design required improvement, although budget and time did not allow for such changes. As such, workarounds had to be applied. For example, the cut clamp restart (CCR) system had to be supplemented during sample manufacture with manual cutting of the tows at the end of each run as the restart roller coating material sheared the tow apart and therefore had to be deactivated. Likewise, while the 6 degree-of-freedom load cell provided great insight into the forces at play during surface following not just the normal loads. The device was difficult to integrate as a real time closed loop sensor due to its configuration and the lack of expertise of the author in electronics and control systems. Therefore, an open loop pressure regulation system was used and a specific pressure within the actuator was correlated to a specific normal force. The responsiveness of the force control system was not tested nor optimised due to lack of time and funding to purchase additional equipment. Any engineering design effort would usually allow for multiple prototypes and iterations of design, especially with a new technology. Therefore, these limitations are not surprising, serving as good learning for the author and the field

Whilst there were many advantages, there were also some limitations resulting from the design of a fully integrated system. In some instances the integrated system actually restricted the amount of data that could be gathered in comparison to a standalone test set-up using a design of the subsystem or sub process alone. In the end the data was gathered but no opportunity existed to feedback the learnings into the prototype design to develop the technology.

During this thesis mechanical and test specimens were the focus of sample production, therefore only requiring flat tools. Future experiments should investigate shaped tooling to produce a shaped part using the UVAFP prototype to test reach and access rather than just the modelling work (as undertaken in Chapter 3). A noticeable issue in the literature were the dimensions assigned to the measurement of irradiance

and the calculation of dose. The most commonly used dose measure throughout the literature was simply the irradiance multiplied the exposure time which ignores flux within the exposure aperture and also the losses associated with the refraction of light beams. Furthermore, the measurement of irradiance using W/cm^2 as collected from most radiometers with variable input diameters as well as no reference information as to the surface area of the measurement sensor. This was cause for great confusion and could be an area of future research in terms of radiation sensors. In the end, the dose had to be calculated with length term due to the 2D approach to the characterisation.

The choice of glass fibre was necessary due to the nature of the UV cure reaction and lack of dark curing reactant in the resin formulation. Glass fibre is not the highest performance advanced structural fibre and this material restriction inevitably limits the technology in its current to intermediate weight/performance structures or large scale structures such as wind energy generation or marine. For these applications, glass fibre was considered to offer a competitive cost to performance balance. That said, the UVAFP process could be applied to other advanced fibres, such as carbon fibre and preliminary tests not presented in this thesis showed positive results. Future work should consider investigating use of such fibres in the process to expand its scope.

UV radiation as a controlled source was also a problem due to the fact that sunlight contains UV radiation and eliminating all sunlight from the experiment environment was impossible. The relative dose of UV radiation at the absorption wavelength though was considered very low in comparison to the amount applied by the spot curing system and therefore ignored except in the DSC studies of Chapter 8. Furthermore, in many instances data sets were more than 3D (sometimes up to 6D) and therefore regression analysis and model generation was difficult. Often data was simplified to 3D in order to take advantage of known surface fitting functions [267]. By doing so some of the data resolution and interrelationship conclusions were lost.

The appropriate selection of the calculation technique and/or fitting function used to generate models was also a possible limitation of this research. Modelling was applied using a scoring algorithm for many fitting functions [267] in order to determine the best fit, but in many instances the parameters being related by the fitting function had to be connected through assumed causal relationships (for example hardness to degree of cure) as the equipment was not available (or even existed) to test the end

measure directly. This was particularly true given the use of a photo curing as the curing mechanism. In most of the literature measurement of performance and quality relies on thermal systems and thermal measures. Since starting this thesis photo-DSC's have become wider spread, assumingly as a consequence of the same issues faced by this author. Although, it must be said that the DSC studies undertaken present very interesting results, measuring thermal properties and effects of non thermal processes.

9.3 Future Work

During the undertaking of this work nine experiments were undertaken with a number of recommendations made throughout regarding future work. Some recommendations were considered in subsequent studies and addressed, while others remain open at the conclusion of this body of work. These include:

- Expansion of the placement head design experiment to investigate in a simulated environment an appropriate design envelope in 3D for a placement head capable of producing a representative complex 3D part.

- Expansion of the current datasets to examine 3D issues associated with adjoining tows, and 3D geometry.

- Investigation of the UVAFP process using different fibre and resin combinations such as carbon fibre with UV and thermal hybrid curing epoxies as well as comingled glass and carbon fibre using only UV curing resins for example.

- Expansion of the current models to finite element modelling for real time prediction. This would increase the robustness of the model for simulations over a greater range of parameter settings.

- Further development of the path following experiment using the UVAFP prototype and a 3D tool and measuring the surface conformance of the part off the tool, taking into account the residual stresses caused by the process and materials.

- Further investigation of the thermal properties of UV cured composites and the effect of processing parameters such as transient temperature conditions on mechanical and thermal properties.

- Investigation of the time effect of VOC release and also the possibility of cure progression beyond exposure to the spot curing system simply by exposure to sunlight.

- Inclusion of further mechanical property testing on UVAFP produced samples to build a larger material card dataset.

- Further experimental verification of the damage model by testing the bond strength of laminate samples removed from formed parts.

Whilst development of the technology on its own is crucial to improvement and increased use of AFP, composites manufacturing faces larger challenges surrounding the many feed-in steps and manual operations required to supply such a production line. The level of automation in surrounding processes and complete production line integration likewise need to be addressed. This said, the challenges do not just remain on the manufacturing side; designers and analysts must shift their design and engineering practises. This should be approached keeping in mind the strong connection between part and process these materials have, and to ensure that their implementation is not simply 'black metal', but fully utilises the advantages of the materials keeping in mind the process. Future research is therefore required across all three lightweighting drivers, during design, in the materials and processes. This includes those feeding into and out of the UVAFP process.

In addition to the future work recommended above, there are three main areas that require immediate investigation. While in this research glass fibres and vinylester resin were selected due to their transparency to UV light, ready availability, intermediate properties and low cost, many advanced structures require the use of higher performance materials such as carbon fibre and epoxy. The UVAFP process could be applied to these materials but new resin formulations would be required. This would affect the impregnation and cure time and new fibres, such as carbon fibre, that are not transparent to UV light, would require that a new curing agent be used that could function in dark curing resins as well as possible hybrid curing systems. Future work should investigate these possibilities. Particularly hybrid curing systems due to the thermal behaviour observed using high intensity light and the high dose application.

This would require little to no modification of the prototype and further expand the scope of the technology according to one of the existing aims of the research.

As part of this research, a laboratory scale prototype was designed and tested in a flexible robotic work cell. The establishment of, and access to, such laboratory scale work cells will be crucial in the development of AFP technology in the future and the material and curing mechanisms that are associated with part production [46]. Furthermore, one of the most critical issues today is whether large general purpose AFP and ATL machines are the optimal solution for production or whether part-specific machines with limited flexibility but increased throughput are the best option. These purpose built machines could utilise the components, design features and technology of generic AFP and ATL systems, but be tailored for making only one part, more quickly, with less investment. This topic alone should be the focus of future work, linking back to the drivers for weight reduction from the perspective of specific design, materials and process for specific parts or generic design rules, material options and flexible processes.

Placing dry fibres not only addresses the cost issue associated with prepregs but allows users to manufacture dry fibre performs for liquid moulding processes, such as resin transfer moulding (RTM). Through control of the fibre/resin ratio a user can create a structure with very low resin content (the resin only acts as a binder) or with selective application of binder in localised areas. Laying the 'dry' fibre onto a mould means that the formed shape is 'preformed' as per the designer's specification. Limited research exists on dry fibre placement for preforming, particularly with selective binder application and should be investigated further.

9.4   Final Remarks

While vehicle weight has a cost in a carbon market economy, there is a limit to what the market will pay for lightweighting. This is based on the investment versus the impact on emissions reductions and the cost of the emissions. This cost drives the innovation lifecycle and currently the cost of emissions is only increasing. As such, all efforts of this thesis aimed to have an impact upon the recurring and non-recurring costs associated with making lightweight vehicle components. The outcomes of this thesis were demonstrated time savings, efficiency improvements, reduced material costs and

improved versatility of reduced capital based on the current benchmark. Ultimately, for the technology to be implemented in industry, further development and research must be undertaken to drive its maturation. Furthermore, efforts must also be continued to reduce the cost of making the raw materials, increasing material options, addressing production integration and scalability, driving down energy consumption, and improving design practices for components to maximise the return from the material and process. Development of the industry itself must continue as the technology is proliferated. This will help create a competitive environment of vendors rather than sole source technologies.

Even with these developments and improvements, composites still face a hard sell for industry. Henrichsen and Bautista [59] stated that in general, composite structures are still vastly more expensive compared to conventional metallic structures. This is a comparison between materials with knowledge bases that differ by centuries. Change will not occur instantly and economies cannot be created overnight which would see composites compete head-to-head with metals in large industries such as the automotive. The UVAFP process is an exciting new technology that offers significant improvements and cost saving to the current AFP benchmark and this thesis has proven the concept as viable and provided robust process knowledge and models for further development [9][268][269][270].

10 References

[1] Department of Climate Change and Energy Efficiency 2009, *Australian National Greenhouse Accounts - National Inventory by Economic Sector*, Canberra, Australia, viewed 15 October 2009, <http://www.environment.gov.au/climate-change/greenhouse-gas-measurement/publications/national-inventory-economic-sector-2009>.

[2] United Nations 2015, *Framework Convention on Climate Change UNFCCC*, Bonn, Germany, viewed 12 December 2012, <http://unfccc.int/kyoto_protocol/items/2830.php>.

[3] Warren, DC 2013, *Lightweighting Composites and Low Cost Carbon Fibre*, Oak Ridge Research Laboratories, USA.

[4] Composites World 2009, *Carbon fibre market will reach $2.4 billion by 2014*, viewed 26 May 2009, <http://www.compositesworld.com/news/report-carbon-fibre-market-will-reach-24-billion-by-2014.aspx>.

[5] McCarville, D, Guzman, J, Rotter, D 2008, 'Automated Material Placement: Industry Overview', *SAMPE Conference 2008*, USA.

[6] McCarville, D 2009, 'Evolution of and Projects for Automated Composite Material Placement Equipment in the Aerospace Industry', Thesis (Ph.D.), Walden University, Walden, USA.

[7] Di Pietro, A, Compston, P, Gresham, R, Hovland, G 2009, 'Rapid robotic fibre placement with in-situ ultra-violet curing', *1st International Conference on Sustainable Automotive Technologies*, RMIT University Publishing, Australia, pp. 73-78.

[8] Scott, T, Cook, W, Forsythe, J, Bowman, C, Berchtold, K 2003, 'FTIR and ESR Spectroscopic Studies of the Photopolymerization of Vinyl Ester Resins', *Macromolecules*, vol. 36, pp. 6066-6074.

[9] Schlimbach, J, Mitschang, P 2006, 'Process based cycle time estimation for Thermoplastic tape placement', *Journal of Thermoplastic Composite Materials*, vol. 19, pp. 507.

[10]   Coriolis Composites 2011, *Coriolis Composites: Home*, viewed 31st
         September 2011, <http://www.coriolis-composites.com>.

[11]   Boeing 2009, *Modular Head Lamination Device and Method*, US Patent
         Number 2009/0078361.

[12]   Lichtenwalner, P 1993, 'Neural-Network based control for the Fibre
         Placement Composite Manufacturing Process', *Journal of Materials Engineering
         and* Performance vol. 2, no. 5, pp. 687.

[13]   Ahrens, M 1998, Robotic based thermoplastic fibre placement process,
         Industrial Robot, vol. 25, no. 5, pp. 27.

[14]   Reinforced Plastics 2008, 'Fiber Placement Systems for Airbus A350
         XWB', *Reinforced Plastics Magazine*, pp. 15, viewed 11 November 2012,
         <http://www.mag-ias.com>.

[15]   Yan, L, Chevy Chen, Z, Shi, Y, Mo, R 2014, 'An accurate approach to
         roller path generation for robotic fiber placement of free form surface
         composites', *Robotics and Computer Integrated Manufacturing*, vol. 30, pp.
         277–286.

[16]   Wang, C & Sun, CT 1997, 'Thermoelastic behavior of PEEK
         thermoplastic composite during cooling from forming temperatures', *Journal of
         Composite Materials*, vol. 31, pp. 2230-2248.

[17]   Gresham, J 2006, 'The Influence of Temperature on the Stamp Forming
         of Fibre Metal Laminates', Thesis (M.Phil.), Australian National University,
         Canberra, Australia.

[18]   Composite Plastics 2012, *Benefits of Composites*, viewed 27 March
         2012, <http://composite.about.com/od/aboutcompositesplastics/tp/Benefits-Of-
         Composites.html>.

[19]   Composites World, 2014, Composite leaf springs: Saving weight in
         production suspension systems, viewed 17th July 2016,
         <http://www.compositesworld.com/articles/composite-leaf-springs-saving-
         weight-in-production-suspension-systems>.

[20]   Gurit 2010, *Infusion Brochure*, Gurit, UK, viewed 22 June 2013,
         <http://www.gurit.com/files/documents/Infusion_brochure_2010.pdf >.

[21]   Strong, BA 2008, *Fundamentals of Composite Manufacturing: Materials, Methods and Applications: Second Edition,* Society of Manufacturing Engineers, USA.

[22]   Easy Composites 2013, *Beginners Guide to Out of Autoclave Prepreg Carbon Fibre*, viewed 19 October 2013, <http://www.easycomposites.co.uk/Beginners-Guide-to-Out-of-Autoclave-PrePreg-Carbon-Fibre.aspx>.

[23]   Quickstep Technologies 2013, *Resin Spray Transfer for Automotive Manufacturing*, viewed 21 August 2013, <http://www.quickstep.com.au/Projects/Resin-Spray-Transfer-for-Automotive-Manufacturing>.

[24]   Grimshaw, M, Grant, C, Diaz, J 1996, 'Advanced technology tape laying for affordable manufacturing of large composite structures', *46th International SAMPE Symposium*, California, USA, pp. 1003-1015.

[25]   De Vlieg, R, Jeffries, K, Vogeli, P 2007, 'High-Speed Fibre Placement on Large Complex Structures', *SAE International Aerofast Conference*, SAE International, California, USA.

[26]   Hulcher, B, Marchello, J, Hinkley, J, Johnston, N 1999, 'Dry Ribbon for heated head automated fibre placement', *44th International SAMPE Symposium and Exhibition*, California, USA.

[27]   Towell, T, Johnston, N, Grenoble, R, Marchello, J, Cox, W 1996, 'Thermoplastic Fibre Placement Machine for materials and Processing Evaluations', *41st International SAMPE Symposium and Exhibition*, p. 1701-1711.

[28]   Crothers, P, Drechsler, K, Feltin, Herszberg I, Kruckenberg T 1997, 'Tailored Fibre Placement to minimise Stress Concentrations', *Composites Part A*, vol. 28, pp. 619-25.

[29]   Brouwer, WD, van Herpt, ECFC, Labordus, M 2003, 'Vacuum injection moulding for large structural applications', *Composites Part A,* vol. 34, pp. 551–558.

[30]   Hardesty, E 1972, 'Design and construction of a fully automated tape placement machine for aircraft structures', *Journal of Composites*, vol. 3, pp. 248-53.

[31]   Leininger, J, Penn, S 2005, 'Boeing orders new Cincinnati machine composite tape layers for 777 and 787 production', *Cincinnati Lamb: PR05-14*, Cincinnati, USA.

[32]   Lee, M 2004, 'Heat Transfer and consolidation modelling of composite fibre tow in fibre placement', Thesis (Ph.D.), *Virginia Polytechnic Institute and State University*, Virginia, USA.

[33]   Britnell, D, Tucker, N, Smith, G, Wong, S 2003, 'Bent pultrusion—a method for the manufacture of pultrudate with controlled variation in curvature', *Journal of Materials Processing Technology*, vol. 138, no. 1-3, pp. 311-315.

[34]   Barth, J 1990, 'Fabrication of complex composite structures using advanced fibre placement technology', *35th International SAMPE Symposium and Exhibition*, California, USA, pp. 710-720.

[35]   Composites World 2009, 'MTorres to supply fibre placement, machining equipment for A350', viewed 17 August 2009, <http://www.compositesworld.com/news/mtorres-to-supply-fiber-placement-machining-equipment-for-a350>.

[36]   Beckwith, S 2008, 'Filament Winding vs Fibre Placement Manufacturing Technologies', *SAMPE Journal*, vol. 44, no. 2.

[37]   Goldsworthy, WB 1974, *Geodesic path length compensator for composite-tape placement method*, US Patent US3810805.

[38]   Grant, C, Martin, J 2003, 'Automated Processing Technology for Composites: Current Status and Vision for the Future', *SAMPE Journal*, Long Beach, California, USA, pp. 888-895.

[39]   Kitson, L, Johnston, B 2007, 'Fibre Placement Technology Advancements at Boeing Helicopters', *American Helicopter Society 51st Annual Conference*, Fort Worth, Texas, USA, pp. 69.

[40]   Reinforced Plastics 1995, 'Fibre placement finds footbridge role', *Elsevier Science*, London, UK.

[41]   Composite Machines Company Inc. 1999, 'WOW! A filament wound Boat', *Coriolis Composites*, vol. 7, viewed 11 March 2008, <https://www.coriolis-composites.com>.

[42]   Lind, A, Wear, F, Kurz, J 1992, 'Microwave Heating for Fibre Placement Manufacturing of Carbon Fibre Composites', *DTIC Online Database*, USA.

[43]   Littlefield, A, Hyland, E, Andalora, A, Klein, N, Langone, R, Becker, R 2005, 'Design, Fabrication and Testing of a Thermoplastic Composite overwrapped Gun Tube', *SAMPE Journal*, ADC PR-21, viewed 7 August 2007, <https://www.automateddynamics.com>.

[44]   Gruber, M, Lamontia, M, Waibel, B 2001, 'Automated Fabrication processes for large composite aerospace structures: A trade study', *SAMPE 2001*, Long Beach, USA, vol. 1, no.11.

[45]   Becker, R, Nettles, A, Bucinell, R, Langone, R, Mondo, J 2001, 'Fabrication of PEEK / Graphite composite cryogenic fuel line', *Proceedings of the SAMPE Conference 2001*, Long Beach, USA.

[46]   Bannister, M 2001, 'Challenges for Composites into the next Millennium – a reinforcement Perspective', *Composites Part A*, vol. 32, pp. 901-910.

[47]   Evans, D, Vanigilia, M, Hopkins, P 1989, 'Fibre Placement process study', *34th International SAMPE Symposium*, California, USA, pp. 1822-33.

[48]   Northrop Grumman Corporation 1990, 'Automated Pre-preg Tow Placement for Composite Structures', *The 35th International SAMPE Symposium*, California, USA, pp. 734-45.

[49]   SAMPE 2011, 'Conference Program and Exhibitor's Guide'. *ASM Aeromat Conference*, Long Beach, California, USA.

[50]   Buckingham, R, Newell, G 1996, 'Automating the manufacture of Composite Broadgoods', *Composites Part A*, vol. 27, pp. 191-200.

[51]   Jarvis, S, Wilcox, K, Chen, X, McCarthy, R, Sarhadi, M 1986, 'Design of a handling device for composite ply lay-up automation', Brunel University, Brunel, UK.

[52]   Ewald, G 1985, 'Access / ATLAS II, Two Stage Tape Placement System', *30th International SAMPE Symposium*, SAMPE, Long Beach, California, USA, pp. 565-78.

[53]   Kinard, J, Colton, J 2000, 'Material Systems for rapid manufacturing of composite structures', *Polymer Composites*, vol. 21, no. 6, pp. 918-31.

[54]   Forest Line 2009, 'News: Forest line Dual Stage ATLAS machine used on Boeing 787 Wing Skins in Japan', viewed 15 May 2009, <http://www.forest-line.com/anglais/produits/fiche.asp?IDMach=25&Langue=2>.

[55]   Fibreforge Corporation 2009, *System and Method for the rapid, automated creation of advanced composite tailored blanks*, US Patent Application Number US2009/0101277 A1.

[56]   Land, I 1996, 'Design and Manufacture of Advanced Composite Aircraft Structures Using Automated Tow Placement', Thesis (Ph.D.), *Massachusetts Institute of Technology*, Boston, USA.

[57]   Grove, SM 1988, 'Thermal modelling of tape laying with continuous carbon fibre reinforced thermoplastic', *Composites,* vol. 19, no. 5, pp. 367–75.

[58]   Hassan, N, Thompson, J, Batra, R, Hulcher, A, Song, X, Loos, A 2005, 'A Heat Transfer Analysis of the Fibre Placement Composite Manufacturing Process', *Journal of Reinforced Plastics and Composit*es, vol. 24, no. 8, pp. 869.

[59]   Henrichsen, J, Bautista, C 2001, 'The Challenge of Reducing both airframe weight and manufacturing cost', *Aircraft Technologies – Air and Space Structures,* Europe, vol. 3, no. 3.

[60]   Olsen, H, Craig, J 1993, 'Automated composite tape lay-up using composite devices', *Robotics and Automation Conference: IEEE*, pp. 291-97.

[61]   Criss, J, Watkins, S, Holmes, S 1998, 'In-situ Advanced Fibre Placement of thermosetting prepregs'. *30th International SAMPE Symposium*, Long Beach, California, USA, pp. 654-64.

[62]   Hutchins, J 1999, 'Fibre Placement of staged Thermoset Material', *AHS International Forum: Proceedings*, pp. 806-17.

[63]   Di Pietro, A, Compston, P, Hovland, G 2008, 'Toward Rapid Robotic Fibre Placement with in-situ UV Curing', *1st Annual International Conference on Sustainable Automotive Technology (ICSAT),* RMIT Press, Melbourne, Australia.

[64]   Enders, M, Hopkins, P 1991, 'Developments in the fibre placement process', *36th International SAMPE Symposium and Exhibition*, Long Beach, California, USA, pp. 778-90.

[65]   Goodman, D, Byrne, C, Yen, A 2000, 'Automated tape placement with in-situ electron beam cure', *SAMPE Journal*, vol. 36, no. 2, pp.11-17.

[66]   Goodman, D, Weidman, D, Byrne, C, Bykanov, C 2001, 'Automated tape placement with in-situ electron beam cure – A viable Process', *46th International SAMPE Symposium*, Long Beach, California, USA, pp. 2127-39.

[67]   Grenoble, R, Marchello, J, Belvin, H 1996, 'Alternative ribbon cross sections for automated fibre placement'. *The 28th International SAMPE Technical Conference*, California, USA, pp. 1003-1015.

[68]   Cano, R, Belvin, H, Hulcher, A 2001, 'Studies on Automated Manufacturing of High performance Composites', *The American Helicopter Society: Structure Specialist Meeting*, NASA Langley Research Center, USA.

[69]   Burgess, J, Wilenski, M, Belvin, H, Cano, R, Johnston, N 2001, 'Development of a cure-on-the-fly Automated tape placement machine for EB curable pre-pregs', *SAMPE Journal*, USA, vol. 13.

[70]   Cincinnati Milacron 1989, *Compliant Presser Member for Fibre Placement Machine*, US Patent Number 4869774.

[71]   Wang, X 2007, 'Modelling of in-situ laser curing of thermoset matrix composites in filament winding', Thesis (Ph.D.), *University of Nebraska*, Nebraska, USA.

[72]   Di Pietro, A, Compston, P 2009, 'Automated Fibre Placement with in-situ Ultraviolet Curing: Concept Testing', *2nd Annual International Conference on Sustainable Automotive Technology (ICSAT)*, Germany.

[73]   Di Pietro, A, Compston, P 2011, 'Shear properties of a glass-fibre/vinylester composite cured with high intensity ultraviolet light for use in automated manufacturing processes', *Advanced Composite Letters*, vol. 20, no. 2, pp. 52-55.

[74]   Calawa, R, Nancarrow, J 2007, 'Medium Wave Infrared Heater for High Speed Fibre Placement', *SAE International AeroFast Conference*, California, USA.

[75]   Di Pietro, A, Compston, P 2009, 'Resin Hardness and interlaminar shear strength of glass fibre/vinylester composite cured with high intensity ultraviolet (UV) light', *Journal of Material Science,* vol. 44, pp. 4188-4190.

[76]   Di Pietro, A, Compston, P, Gresham, R, Hovland, G 2008, 'Automated Fibre Placement with in-situ UV Curing', *Meeting the Challenges to Sustainable Mobility,* RMIT University Publishing (ISBN 9781921426155), Victoria, Australia.

[77]   Pasanen, M 2007, 'Advances in In-situ fibre placement of Thermoplastic Matrix composites for commercial applications', *Automated Dynamics Corporation,* NY, USA.

[78]   Mantell, S, Wang, Q, Springer, G 1992, 'Processing thermoplastic composites in a press and by tape laying – experimental results', *Journal of Composite Materials,* vol. 26, no. 16.

[79]   Tessnow, K, Hutchins, J, Carlson, D, Pasanen, M 1994, 'Low cost Thermoplastic helicopter tailboom development', *50th American Helicopter Society Annual Forum,* USA.

[80]   Felderhoff, K, Steiner, K. 'A new compact robotic head for thermoplastic Fibre Placement', *38th International SAMPE Symposium,* California, USA, pp. 138.

[81]   Shih, P 1997, 'On-line consolidation of Thermoplastic Composites', Thesis (Ph.D.), *Virginia Polytechnic Institute and State University,* Virginina, USA.

[82]   Leon, G, Hall, J, Kelly, J, Coffenberry, B, Cirino, M 1995, 'Affordable thermoplastic processing of marine structures', *Composites Manufacturing,* vol. 6, pp. 193-199.

[83]   Hulcher, A, Banks, W, Pipes, R, Tiwari, A 2001, 'Automated fibre placement of peek / IM7 Composites', *The 46th International SAMPE Symposium – Materials and Processes Odyssey,* California, USA, pp. 1998-2012.

[84]   Coffenberry, B, Hauber, D, Cirino, M 1993, 'Low cost alternative in-situ consolidated thermoplastic composite structures', *38th International SAMPE Symposium and Exhibition,* California, USA, pp. 1640.

[85]   Lamontia, M, Funck, S, Gruber, M 2003, 'Manufacturing flat and cylindrical laminates and built up structures using automated thermoplastic tape laying, fibre placement and filament winding', *SAMPE Journal*, vol. 39, no. 2, pp. 30-38.

[86]   Shirinzadeh, B, Cassidy, G, Oetomo, D, Alici, G, Ang, M 2007, 'Trajectory Generation for open contoured structures in robotic fibre placement. Robotics and Computer Integrated Manufacture', vol. 23, pp. 380-394.

[87]   Belhaj, M, Deleglise, M, Comas-Cardona, S, Demouveau, H, Binetruy, C, Duval, C, Figueiredo, P 2012, 'Dry Fibre Placement of Carbon Fibrous Preforms'. *Composites: Part B*, vol. 10, pp.1016, viewed 14 June 2013, <http://dx.doi.org/10.1016/j.compositesb.2013.01.014>.

[88]   Wakeman, M, Hagstrand, P, Bonjour, F, Bourban, P, Manson, J 2002, 'Robotic tow placement for local reinforcement of glass mat thermoplastics (GMTs)', *Composites Part A*, vol. 33, pp. 1199-1208.

[89]   Feltin, D, Gliesche, K 2001, 'Tailored Fibre Placement – Cost effective preforms for high loaded composites'. *The 46th International SAMPE Symposium and Exhibition*, California, USA, pp. 2463-71.

[90]   Rudd, C, Tuner, M, Long, A, Middleton, V 1999, 'Tow placement studies for liquid composite moulding', *Composites Part A*, vol. 30, pp. 1105-1121.

[91]   Akao, Y 1994, '*Development History of Quality Function Deployment, The Customer Driven Approach to Quality Planning and Deployment*', ISBN 92-833-1121-3, Asian Productivity Organization, Minato, Tokyo Japan, pp. 339.

[92]   Cincinnati Machine LLC 2006, *Fibre Placement Machine*, US Patent Number 0249256.2006.

[93]   Cincinnati Machine 2010, *Rotary Clamp Mechanism for Fibre Placement*, US Patent Application Number US2010/0276087.

[94]   Cincinnati Machine 2008, 'Charger Series Tape Layer and VIPER Fibre Placement Systems', *Automated Composite Processing*, viewed 1 August 2008, <www.cinmach.com>.

[95]   MAG Cincinnati 2007, 'Viper Fibre Placement System', *MAG Cincinnati Inc.*, viewed 19 August 2007, <www.cinmach.com>.

[96]   Coriolis Composites 2010, *A Fibre Application Machine provided with flexible fibre conveying tubes arranged within a cold sheath*, Internation Patent Number WO2010/049424 – A1.2010.

[97]   Coriolis Composites 2008, *Fibre Applicator Head Including Systems for Cutting Individual Fibres*, International Patent 2008/132299.

[98]   Stamen, J, Rudberg, T, Brock, J 2012, 'Automated Lay-up of High-Angle-Range Carbon Composite Parts with Static Tools', *Composites Manufacturing, Society of Manufacturing Engineers Conference*, Mesa Arizona, USA.

[99]   McAfee, A 1990, 'On the appropriate level of Automation for Advanced Structural Composites Manufacturing for Commercial Aerospace Applications', Thesis (Ph.D.), *Massachusetts Institute of Technology*, Boston, Massachusetts, USA.

[100]   Debout, P, Chanal, H, Duc, E 2010, 'Tool path smoothing of a redundant machine: Application to AFP', *Journal of Computer Aided Design*, vol. 43, no. 2, pp. 122-132.

[101]   Faubion, G 2010, 'AFP Kinematics for High Speed Lay-up', *Composites Manufacturing, SME Conference*, San Diego, USA.

[102]   ElectroImpact 2014, 'ElectroImpact: Home', *ElectroImpact*, viewed 24 July 2014, <www.electroimpact.com>.

[103]   Rower, J 2010, 'Robot Driven Automatic Tapehead for Complex Composite Lay-ups', *AMAF, SAE*, USA.

[104]   ImageJ Software Portal, 'ImageJ', *NIH*, viewed 3 January 2013, <http://imagej.nih.gov/ij/>.

[105]   Kim, BC, Potter, K, Weaver, PM 2012, 'Continuous tow shearing for manufacturing variable angle tow composites', *Composites: Part A*, vol. 43 pp. 1347–1356.

[106]   Groppe, D 2000, 'Robots improve the Quality and Cost-Effectiveness of Composite Structures', *Industrial Robot*, vol. 27, no. 2, pp. 96-102.

[107]   Ingersoll Machine Tools Inc. 2006, *Compact Fibre Placement Apparatus*, European Patent Application Number 06119534.3.2006.

[108]   Black, S 2009, 'Automating wind blade manufacture: Composites Technology Case Study, *Composites World*, viewed 11 January 2014, < http://www.mmsonline.com/articles/automating-wind-blade-manufacture>.

[109]   Inside Manufacturing Magazine 2013, 'New Equipment brings tape placement within reach of smaller shops', *High Performance Composites*, viewed 1 Jan 2007, < http://www.compositesworld.com/articles/new-equipment-brings-tape-placement-within-reach-of-smaller-shops>.

[110]   Abdalla, F, Mutasher, S, Khalid, Y, Sapuan, S, Hamouda, A, Sahari, B, Hamdan, M 2007, 'Design and fabrication of low cost filament winding machine', *Journal of Materials and Design*, vol. 28, pp. 234-239.

[111]   Cano, R, Belvin, H, Johnston, N, Hulcher, A 2011, 'A prototype research laboratory for automated fabrication of high performance composites', *46th International SAMPE Symposium*, California, USA, pp. 2037.

[112]   Steiner, K, Faude, E, Don, R, Gillespie, J 1994, 'Cut and Re-feed Mechanisms for Thermoplastic Tape Placement', *39th International SAMPE Symposium*, California, USA, pp. 2627-2636.

[113]   Lamontia, M, Gruber, M, Waibel, B, Cope, R, Hulcher, B 2000, 'Conformable compaction system used in automated fibre placement of large composite aerospace structures', *Technical Brief SBIR Phase I & II - Low Cost Processing of Large Composite Structures*, Contract NAS1-00019, Report Number 99-1 Phase 1 25.03-5390A, USA.

[114]   Costen, R 2000, 'Thermal Edge effects model for automated tape placement of thermoplastic composites', *45th International SAMPE Symposium and Exhibition*, vol. 45, no. 1, pp. 721-733.

[115]   Groppe, D 2003, 'Robots speed lay-up of Composite Materials', *Journal of Reinforced Plastics*, vol. 47, no. 4, pp. 44–47.

[116]   Ren, S, Lu, H, Wang, Y, Fu, H 2007, 'Development of PLC based Tension control system', *Chinese Journal of Aeronautics*, vol. 20, pp. 206-271.

[117]   Lamontia, M, Gruber, M, Funck, S 2003, 'Developing a contoured deposition head for in-situ laying and fibre placement', *International SAMPE Symposium and Exhibition*, California, USA, pp. 2063-2076.

[118]   Morey, B 2009, 'Innovation drives composite production',
         Manufacturing Engineering Magazine, vol. 142, no. 3.

[119]   Evans, D 2008, 'Fibre Placement', *ASM Fibre Placement Chapter*,
         Cincinnati Machine, viewed 1 June 2008, <www.cinmach.com>.

[120]   Anglani, A, Nucci, F, Spagnolo, A 2002, 'Filament Winding: An
         Integrated Simulation Environment for Automated Cell Programming ',
         *Advanced Manufacturing Systems and Technology International Centre for
         Mechanical Sciences*, vol. 437, pp. 481-489.

[121]   Starnes, J, Dexter, H, Johnston, N, Ambur, D, Cano, R 2006, 'Composite
         Structures and Materials Research at NASA Langley Research Center', *NASA
         Langley Research Center*, USA.

[122]   Thuis, B 2005, 'Automating Aerospace manufacture', *Reinforced Plastics*
         vol. 20.

[123]   Sonmez, F, Akbulut, M 2007, 'Process optimization of tape placement
         for thermoplastic composites', *Composites: Part A*, vol. 38, pp. 2013–2023.

[124]   Schiemer, J, Di Pietro, A, Compston, P, Hovland, G 2009, 'Accuracy
         assessment of 3-axis robotic milling of polymer foam', Internal Report,
         Australian National University, Canberra, Australia.

[125]   Pan, Z, Zhang, H, Zhub, Z, Wang, J 2006, 'Chatter analysis of robotic
         machining process', *Journal of Materials Processing Technology*, vol. 173, pp.
         301–309.

[126]   Chen, YH, Hu, YN 1999, 'Implementation of a Robot System for
         Sculptured Surface Cutting', *International Journal of Advanced Manufacturing
         Technology*, vol. 15, pp. 624–639.

[127]   Simoes, A, Coole, TJ, Cheshire, DG, Pires, AR 2003, 'Analysis of multi-
         axis milling in an anthropomorphic robot, using the design of experiments
         methodology', *Journal of Materials Processing Technology*, vol. 135, pp. 235–
         241.

[128]   Fowlkes, WY, Creveling, CM 1995, *Engineering methods for robust
         product design: using Taguchi methods in technology and product development*,
         Addison Wesley, Reading, Massachusetts, USA

[129]   Kalyanasundaram, S 2006, 'Design of Experiments', Systems Engineering Lecture Slides, *The Australian National University*, viewed 18 February 2006.

[130]   Dremel Inc. 2009, *Dremel Product Specifications*, viewed 18 June 2009, <www.dremel.com>.

[131]   Ferretti, G, Magnani, G, Rocco, P 1999, 'Force Oscillations in Contact Motion of Industrial Robots: An Experimental Investigation', *IEEE/ASME Transactions on Mechatronics*, vol. 4, no. 1, pp. 86-91.

[132]   Matsuoka, S, Shimizu, K, Yamazaki, N, Oki, Y 1999, 'High-speed end milling of an articulated robot and its characteristics', *Journal of Materials Processing Technology*, vol. 95, pp. 83-89.

[133]   Meier, R 1986, 'An advanced control system for composite material placement', *Interational SAMPE Syposium*, California, USA; pp. 822-831.

[134]   Siemens PLM 2015, *FiberSim*, viewed 11 January 2015, <http://www.plm.automation.siemens.com/en_us/products/fibersim/>.

[135]   CGTech 2014, CGTech: Composite Applications, viewed 28 December 2014, <http://www.cgtech.de/products/composite-applications/>.

[136]   Wu, K, Tatting, B, Smith, B, Stevens, RS, Occhipinti, G, Swift, J, Achary, D, Thornburgh, R 2009, 'Design and Manufacturing of Tow-steered Composite Shells Using Fiber Placement', *American Institute of Aeronautics and Astronautics*, NASA Press, USA.

[137]   Temmen, H, Degenhardt, R, Raible, T 2006, 'Tailored Fibre Placement Optimisation Tool', *25th International congress of aeronautical Sciences (ICAS)*, Congress of Aeronautical Science, Germany.

[138]   Enders, M 1991, 'The Fibre Placement Process', *8th International SAMPE Conference on Composite Materials (ICCM8)*, California, USA, pp. 1-11.

[139]   Steiner, K, Wiest, G 1993, 'Algorithms for computer aided robotic filament winding', *25th International SAMPE Technical Conference*, California, USA, pp. 725-735.

[140]   Sonmez, F, Hah,n H, Akbulut, M 2002, 'Analysis of Process-Induced Residual Stresses in Tape Placement', *Journal of Thermoplastic Composite Materials*, vol. 15, pp. 525.

[141]   Shirinzadeh, B 2000, 'Robotic Fibre placement process planning and control', *Journal of Assembly Automation*, vol. 20, no. 4, pp. 313-320.

[142]   Shirinzadeh B, Alici, G, Foong, C, Cassidy, G 2007, 'Fabrication process of open surfaces by robotic fibre placement', *Robotics and Computer Integrated Manufacturing*, vol. 20, pp. 17-28.

[143]   Sun, W, Mantell, S, Stelson, K 2001, 'Demonstration of Bond Quality Improvement for closed Loop Control of Thermoplastic Tape-laying', *Journal of Composite Materials*, vol. 35, pp. 57.

[144]   Chung, K, Seferis, J, Nam, J 2000, 'Investigation of thermal degradation behavior of polymeric composites: prediction of thermal cycling effect from isothermal data', *Composites: Part A*, vol. 31, pp. 945–957.

[145]   Grove, SM 1988, 'Thermal Modeling of Tape Laying with Continuous Carbon-Fibre-Reinforced Thermoplastics', *Composites*, vol. 19, pp. 367–377.

[146]   Sonmez, F, Hahn, H 1997, 'Analysis of the online consolidation process in thermoplastic composite tape placement', *Journal of Thermoplastic Composite Materials*, vol. 10, no. 6, pp. 543-572.

[147]   Tierney, J, Gillespie, J 2006, 'Modeling of in-situ strength development for the thermoplastic tow-placement process', *Journal of Composite Materials*, vol. 13.

[148]   Demmeler Machinenbau 2008, 'Demmeler', viewed 22 January 2008, <http://www.demmeler.com/en/home.html>.

[149]   Bowler, M, Oltman, T, Yates, D, Van Swearingen, S 1999, 'New technology for fuselage fabrication', *Automated Fastening Conference & Exposition*, Nashville, TN, USA.

[150]   Toso, YMP 2003, 'Effective Automated Tape Winding Process with On-Line Bonding under Transient Thermal Conditions', Thesis (Ph.D.), *Technische Wissenschaften ETH Zürich*, Switzerland, Nr. 14983.

[151]   ASTM 2014, ASTM D578-05, viewed 2 November 2014, <www.astm.org/DATABASE.CART/HISTORICAL/D578-05.htm>.

[152]   Owens Corning Reinforcements 2015, High Performance Brochure, viewed 13 January 2014, <www.ocvreinforcements.com/hp/docs/HP_Brochure.pdf>.

[153]   Gay, D, Hoa, SV, Tsai, SW 2002, *Composite Materials: Design and Applications*, CRC Press Content: 552, Australia.

[154]   Owens Corning 2012, 'Single End Rovings - Type 30', Product Datasheet, *OCV Reinforcements*.

[155]   Owens Corning 2011, 'Composite Materials - Composite Solution Guide', *OCV Reinforcements*, Pub. No. 100360-E, USA.

[156]   Fowlkes, WY, Creveling, CM 1995, *Engineering Methods for Robust Product Design, Using Taguchi Methods in Technology and Product Development*, Addison and Wesley, USA.

[157]   The Michigan Chemical Process Dynamics and Controls Open Textbook 2015, *Design of Experiments*, viewed 13 June 2012, <https://controls.engin.umich.edu/wiki/index.php/Design_of_experiments_via_t aguchi_methods:_orthogonal_arrays>.

[158]   Shotton-Gale, NEH 2012, 'Clean Filament Winding: Process Optimisation', Thesis (Ph.D.), *University of Birmingham*, Birmingham, UK.

[159]   Gupta, KM 2014, *Engineering Materials: Research, Applications and Advances*, CRC Press, USA.

[160]   Ashland Chemical Co. 2004, 'Derakane 411-350 Product Technical Datasheet', *Ashland Chemical Co.*, CWT-DS-344 Rev. 1, viewed 21 July 2015, < http://www.ashland.com/Ashland/Static/Documents/APM/Derakane%20411%2 0350%20tds.pdf>.

[161]   Ashland Chemical Co. 2013, 'Derakane MOMENTUM 411-350 Epoxy Vinyl ester resin Technical Data Sheet', *Ashland Chemical Co.*, viewed 21 July 2015, < http://www.ashland.com/Ashland/Static/Documents/APM/DERAKANE%20M OMENTUM%20411%20350%20TDS.pdf >.

[162]   Allen, N 1996, 'Photoinitiators for UV and visible curing of coatings: Mechanisms and properties', *Journal of Photochemistry and Photobiology A: Chemistry*, vol. 100, pp. 101-110.

[163]   Studer, K, Decker, C, Beck, E, Schwalm, R 2003, 'UV-curable
         formulations for UV-transparent optical fiber coatings: Acrylic resins', *Program
         in Organic Coatings*, vol. 48, pp. 92.

[164]   Endruweit, A, Johnson, M, Long, A 2006, 'Curing of composite
         components by ultraviolet radiation: A review', *Polymer Composites*, vol. 27,
         no. 2, pp. 119-128.

[165]   Noren, GK 2000, 'Cationic UV-Curable Formulations Containing
         Hydroxy Functional Fluoropolymer Resins', *Journal of Coatings Technology*,
         vol. 72, no. 905, pp.53-60.

[166]   Chen, J & Soucek, MD 2003, 'Ultraviolet Curing Kinetics of
         Cycloaliphatic Epoxide with Real-Time Fourier Transform Infrared
         Spectroscopy', *Journal of Applied Polymer Science*, vol. 90, pp. 2485–2499.

[167]   Golaz, B, Michaud, V, Leterrier, Y, Manson, JA 2012, 'UV intensity,
         temperature and dark curing effects in cationic photo curing of cycloaliphatic
         epoxy resin', *Polymer*, vol 53, no. 10, pp. 2038-2048.

[168]   Chartoff, R 2006, 'Thermal characteristics of thermosets formed by
         photocure', *Journal of Thermal Analysis and Calorimetry*, vol. 85, no. 1, 213–
         217.

[169]   Narayanan, V, Scranton, A 1997, 'UV Curing of Composites', *RadTech
         Report*, vol. 11, no. 6, pp. 25.

[170]   Compston, P, Dexter, D 2008, 'The effect of ultraviolet (UV) light
         postcuring on resin hardness and interlaminar shear strength of a glass-
         fibre/vinylester composite', *Journal of Material Science*, vol. 43, pp. 5017-5019.

[171]   Lackey, E, Inamdar, K, Worrel, L, Al-Akhdar, W, Wostratzky, DA 2001,
         'Demonstration and Development of Filament Winding Using Photoinitiated
         Resins', *RadTech Report*, vol. 15 no. 36-42.

[172]   Gupta, A & Ogale, A 2002, 'Dual curing of carbon fiber reinforced
         photoresins for rapid prototyping', *Polymer Composites*, vol. 23, no. 6, pp.
         1162–1170.

[173]   Stachurski, Z, Coman, F, Compston, P 2004, *Reinforced Polymer
         Composition*, International Patent WO 2004/050750 PCT/AU2003/001617.

[174]   Nawy, EG (eds) 2001, *Fundamentals of high-performance concrete - Second Edition*, John Wiley and Sons, ISBN 978-0-471-38555-4.

[175]   Yu, H, Longana, ML, Jalalvand, M, Wisnom, MR, Potter, KD 2015, 'Pseudo-ductility in intermingled carbon/glass hybrid composites with highly aligned discontinuous fibres', *Composites Part A: Applied Science and Manufacturing*, vol. 73, pp. 35–44.

[176]   Ogale, A 2006, 'Investigations of sewn preform characteristics and quality aspects for the manufacturing of fibre reinforced polymer composites', Thesis (Ph.D.), *Institut fur Verbundwerkstoffe*, Germany.

[177]   Hull, D, Clyne TW 1992, *An Introduction to Composite Materials*, Part of Cambridge Solid State Science Series, Cambridge University Press, Cambridge, ISBN: 9780521388559.

[178]   Amico, SC & Lekakou, C 2002, 'Axial impregnation of a fiber bundle. Part 1: Capillary Experiments', *Journal of Polymer Composites*, vol. 12, no. 2, pp. 249-263.

[179]   Carman, PC 1937, 'Fluid flow through granular beds', *Transactions of the Institution of Chemical Engineers*, vol. 15, pp. 150-166.

[180]   Cai, Z & Berdichevsky, AL 1993, 'An improved self-consistent method for estimating the permeability of a fibre assembly', *Journal of Polymer Composites*, vol. 14, no. 4, pp. 314-323.

[181]   Berdichevsky, AL & Cai, Z 1993, 'Preform permeability prediction by self consistent method and finite element simulation', *Journal of Polymer Composites*, vol. 14, no. 2, pp. 132-143.

[182]   Bruschke, MV and Advani, SG 1993, 'Flow of generalised Newtonian fluids across a periodic array of cylinders', *Journal of Rheology*, vol. 37, no. 3, pp. 479-498.

[183]   Gebart, BR 1992, 'Permeability of Unidirectional Reinforcements for RTM', *Journal of Composite Materials*, vol. 26, no. 8, pp. 1100-1133.

[184]   Zeng, X, Brown, LP, Endruweit, A, Matveev, M, Long, AC 2014, 'Geometrical modelling of 3D woven reinforcements for polymer composites: Prediction of fabric permeability and composite mechanical properties', *Composites: Part A*, vol. 56, pp. 150–160.

[185]   PPG Industries Ltd UK 2015, *Fibre Glass - Home*, viewed 12 January 2015, < http://www.ppgfiberglass.com/Home.aspx>.

[186]   Foley, ME & Gillespie, JW 2005, 'Modelling the effect of fibre diameter and fibre bundle count on tow impregnation during liquid moulding processes', *Journal of Composite Materials*, vol. 39, no. 12, pp.1045-1065.

[187]   Ahn, KJ & Seferis, JC 1991, 'Simultaneous measurements of permeability and capillary pressure of thermosetting matrices in woven fabric reinforcements', *Journal of Polymer Composites*, vol. 12, no. 3, pp.146-152.

[188]   Williams, JG, Morris, CEM, Ennis, BC,1974, 'Liquid flow through aligned beds', *Polymer Engineering and Science*, vol. 14, no. 6, pp. 413-419.

[189]   Lam, RG & Kardos, JL 1989, 'The permeability and compressability of aligned and cross plied carbon fibre beds during the processing of composites', *ANTEC 1989 Technical Papers, SPE*, pp. 1408-1412.

[190]   Binetruy, C, Hilaire, B & Pabiot, J 1998,'Tow impregnation model and void formation mechanisms during RTM', *Journal of Composite Materials*, vol. 32, pp. 223-245.

[191]   Foley, ME & Gillespie, JW 2005, 'Modelling the effect of fibre diameter and fibre bundle count on tow impregnation during liquid moulding processes', *Journal of Composite Materials*, vol. 39, no. 12, pp.1045-1065.

[192]   Gaymans, RJ & Wevers, E 1998, 'Impregnation of a glass fibre roving with a polypropylene melt in a pin assisted process', *Journal of Composites: Part A*, vol. 29, pp. 663-670.

[193]   Miaris, A 2010, 'Continuous impregnation of Carbon Fibre Rovings', *JEC Magazine*, vol. 56, France.

[194]   Entec Composites Machine Inc. 2015, 'Resin Baths', viewed 21 July 2015, <http://www.entec.com/resin.html>.

[195]   Faustel 2015, 'Labmaster Coating Methods', USA, viewed 21 July 2015, <http://www.faustel.com/convertingequipment/modularsystems/labmaster-pilot-line/labmaster-coating-modules/>.

[196]   Waeco Group 2015, 'Litzler Hotmelt Prepreg System - S-Wrap Technology', viewed 21 July 2015, <http://www.waeco1.com/home/s-wrap/>.

[197]   ToolingU 2015, 'Curtain Coating', viewed 21 July 2015,

<http://www.toolingu.com/definition-680140-106673-curtain-coating.html>.

[198]   All4-GP Process Solutions 2010, 'Printed Circuit Board Newsletter', viewed 10 September 2011, <http://all4-gp.us/userfiles/file/news/all4-pcb-newsletter2010Spray.pdf>

[199]   Aerospace and Advanced Composites 2013, 'Liquid Composite Moulding', viewed 18 January 2014, <http://www.aac-research.at/products/products_AAC_CompositePolymer_lcm_en.html>

[200]   Mills, A 2001, 'Automation of Carbon Fibre Preform manufacture for Affordable Aerospace Applications', *Composites: Part A*, vol. 32, pp. 955-962.

[201]   Compston, P, Schiemer, J, Cvetanovska, A 2008, 'Mechanical properties and styrene emission levels of a UV-cured glass fibre / vinylester composite', *Composite Structures*, vol. 86, no. 1-3, pp. 22-26.

[202]   Excelitas 2015, 'Omnicure S2000 Product Brochure', viewed 25 March 2015, < http://www.excelitas.com/Downloads/OmniCure-S2000-Brochure.pdf >.

[203]   Bates, PJ & Charrier, JM 1999, 'Effect of process parameters on melt impregnation of glass roving', *Journal of Thermoplastic Composite Materials*, vol. 12, pp. 276-294.

[204]   University of Utah 2015, 'Mechanical Engineering: ME EN 7960 – Precision Machine Design – Contact Stresses and Deformations', viewed 7 February 2015, <http://www.mech.utah.edu/~me7960/lectures/Topic7ContactStressesAndDeformations.pdf>.

[205]   Budynas, R & Nisbett, K 2014, *Shigley's Mechanical Design Engineering*, McGraw-Hill Series in Mechanical Engineering 10th Edition, McGraw-Hill, USA.

[206]   Engineering Toolbox 2015, 'Young's Modulus', viewed 7 February 2015, <http://www.engineeringtoolbox.com/young-modulus-d_417.html>

[207]   DuPont 2015, 'PTFE Handbook', viewed 7 February 2015, <http://www.rjchase.com/ptfe_handbook.pdf>.

[208]   Matweb 2014, viewed 20 September 2014,
          <http://matweb.com/search/datasheet.aspx?MatGUID=79cd55e17b2648409398
          393c4e47bb45>.

[209]   Chandler, HW, Devlin, BJ & Gibson, AG 1992, 'A model for the
          continuous impregnation of fibre tows in resin baths with pins', *Journal of
          Plastics, Rubber, and Composites Processing and Application*, vol. 18, no. 4,
          pp. 215-220.

[210]   Charlesby, A 1960, 'Atomic radiation and polymers', *Pergamon*, New
          York, USA.

[211]   Clough, 2001, 'High energy radiation and polymers - a review of process
          and applications', *Nuclear Instruments and Methods in Physics Research: Part
          B*, vol. 185, no. 1-4, pp. 8-33.

[212]   Li, X 2009, 'Computational Analysis of Ultraviolet (UV) reactors',
          Thesis (Ph.D.), *Rochester Institute of Technology*, USA.

[213]   Bolton, J 2000, 'Calculation of fluence rate distributions in an annular
          reactor: significance of refraction and reflection', *Journal of Watwer Research*,
          vol. 34, no. 13, pp. 3315-3324.

[214]   Heda, N 2015, 'Spectrophotometry', viewed 21 July 2015,
          <namrataheda.blogspot.com>.

[215]   NASA 2015, 'REMSENS597K', viewed 22 April 2015,
          <https://wikispaces.psu.edu/display/RemSens597K/E>

[216]   HPS.org 2008, 'HPS.org', viewed 8 November 2011, <www.hps.org>.

[217]   Decker, C 1998, 'The use of UV radiation in polymerisation', *Polymer
          International*, vol. 45, no. 2, pp. 133-141.

[218]   Livesay, M 1999, 'UV-VARTM Fabrication of Low cost composite
          Structures', *International SAMPE Conference*, Long Beach, California, USA.

[219]   Yuan, Q, Yang, M, Mai, Y 2000, 'Ultraviolet Curing of Glass Fibre
          Reinforced Polyester Composites', *Advanced Composite Letters*, vol. 9, no. 5,
          pp. 341.

[220]   Adewuyi, O, Okoli, O, Jack, D 2009, 'Optimisation of lamp positioning
          in the UV curing of 3D composite components manufactured using the RIDFT
          process', *Proceedings of the 17th ICCM*, Edinburgh, UK.

[221]   Scott, T, Cook, W, Forsythe, J 2002, 'Photo-DSC cure kinetics of vinyl ester resins. I. Influence of temperature', *Polymer*, vol. 43, pp. 5839–5845.

[222]   Crivello, J, Narayan, R, Sternstein, S 1997, 'Fabrication and Mechanical Characterization of Glass Fibre Reinforced UV-Cured Composites from Epoxidized Vegetable Oils', *Journal of Applied Polymer Science*, vol. 64, pp. 2073.

[223]   Unluturk, S, Arastoopour, H, Koutchma, T 2004, 'Modeling of UV dose distribution in a thin-film UV reactor for processing of apple cider', *Journal of Food Engineering*, vol. 65, pp. 125–136.

[224]   Chartoff, R & Du, J n.d., 'Photopolymerisation reaction rates by reflectance real time infrared spectroscopy: application to stereolithography resins', Rapid Prototype Development Lab and Center of basic and applied Polymer Research, *University of Dayton*, Dayton, Ohio, USA.

[225]   Britnell, D, Tucker, N, Smith, G, Wong, S 2003, 'Bent Pultrusion – a method for the manufacture of pultrudate with controlled variation in curvature', *Journal of Material Processing Technology*, vol. 138, pp. 311-315.

[226]   Li, G & Ghebreyesus, A 2006, ' Fast repair of damaged RC beams using UV curing FRP composites', *Composite Structures*, vol. 72, no. 1, pp. 105-110.

[227]   Pang, S, Li, G, Jerro, D, Peck, J 2004, 'Fast joining of composite pipes using UV curing FRP composites', *Polymer Composites*, vol. 25, pp. 298-306.

[228]   Peck, J, Li, Q, Pang, S, Stubblefield, M 2004, 'Light intensity effect on UV cured FRP coupled composite pipe joints', *Composite Structures*, vol. 64, pp. 539-546.

[229]   Excelitas 2005, Omnicure S2000 Output Charts, viewed 25 June 2015, <http://www.excelitas.com/Downloads/OmniCure-S2000-Brochure.pdf>.

[230]   Endruweit, A, Johnson, MS, Long, AC 2006, Curing of composite components by ultraviolet radiation: A review, *Polymer Composites*, vol. 27, pp. 119-128.

[231]   Peinado, C, Salvador, EF, Alonso, A, Corrales, T, Baselga, J, Catalina, F 2002, 'Ultraviolet curing of acrylic systems: real-time fourier transform infrared, mechanical, and fluorescence studies', Journal of Polymer Science - Part A: *Polymer Chemistry*, vol. 40, pp. 4236–4244.

[232]   Jonsson, S, Hasselgren, C 2015, 'Secrets of the dark', Fusion UV
         Systems, USA, viewed 1 June 2015, <http://www.fusionuv.com>.

[233]   Scherzer, T, Decker, U 1999, 'Real-time FTIR-ATR spectroscopy to
         study the kinetics of ultrafast photopolymerization reactions induced by
         monochromatic UV light', *Vibration Spectroscopy*, vol. 19, pp. 385-398.

[234]   Kindernay, J, Blazkova, A, Ruda, J, Jancovicova, V, Jakubıkova, Z
         2002, 'Effect of UV light source intensity and spectral distribution on the
         photopolymerization reactions of a multifunctional acrylated monomer', *Journal
         of Photochemistry & Photobiology Part A: Chemistry*, vol. 151, pp. 229–36.

[235]   Soppera, O, Croutxe-Barghorn, C 2003, 'Real-time fourier transform
         infrared study of the free-radical ultraviolet-induced polymerization of a hybrid
         sol–gel. II. The effect of physicochemical parameters on the
         photopolymerization kinetics', *Journal of Polymer Science - Part A: Polymer
         Chemistry*, vol. 41, pp. 831–40.

[236]   Harris, JS, Jacobsen, PH, O'Doherty, DM 1999, 'The effect of curing
         light intensity and test temperature on the dynamic mechanical properties of two
         polymer composites', *Journal of Oral Rehabilitation*, vol. 26, no. 8, pp. 635–
         639.

[237]   Li, G., Pourmohamadiam, N., Cygan, A., Peck, J., Helms, J., Pang, S.,
         'Fast repair of laminated beams using UV curing composites', *Composite
         Structures*, vol. 60, pp. 73-81

[238]   Swancor Industries Co. Ltd 2013, 'Swancor 901-35 Epxoy Vinylester
         Resin Datasheet', viewed 30 June 2013, <
         http://www.swancor.com/en/goods.php?act=view&no=5>.

[239]   Cvetanovska, A, Compston, P 2004, 'Degree of cure and tensile
         properties of vinylester resin cured with ultraviolet light'. *Journal of Materials
         Science*, vol. 39, pp. 1791-1793.

[240]   Compston, P, Jar, P-YB, Burchill, PJ, Takahashi, K 2001, 'The effect of
         matrix toughness and loading rate on the mode II interlaminar fracture toughness
         of glass-fibre/vinyl-ester composites', *Composite Science and Technology*, vol.
         61, pp. 321-333.

[241]   Freidrich, K, Walter, R, Carlsson, LA, Smiley, AJ, Gillespie, JW 1989, '
          Mechanisms for rate effects on interlaminar fracture toughness of carbon/epoxy
          and carbon/PEEK composites', *Journal of Material Science*, vol. 24, pp. 3387-
          3398.

[242]   Pantano, V, Compston, P, Stachurski, Z, Jar, P 2002, 'Effect of matrix
          toughness on the shear strength of brittle and rubber-modified glass-
          fibre/vinylester composites', *Journal of Materials Science Letters*, vol. 21, 771-
          773.

[243]   Lichtinger, R, Hörmann, P, Stelzl, D, Hinterhölzl, R 2015, 'The effects of
          heat input on adjacent paths during automated fibre placement', *Composites Part
          A: Applied Science and Manufacturing*, vol. 68, pp. 387-397.

[244]   Alici, G, Shirinzadeh, B, McConville, A, Foong, C, Ang, M 2002, 'A
          mathematical model for a pneumatically actuated robotic fibre placement
          system', *Robotica*, vol. 20, pp. 545-551.

[245]   Smith, A, Anthony, D 1992, 'Robotic Fibre Placement in the fabrication
          of complex thermoplastic structures', *International SAMPE Electronics
          Conference*, Toronto, Canada, pp. 399-407.

[246]   Lackey, E, Inamdar, K, Worrel, L, Al-Akhdar, W, Wostratzky, DA 2001,
          'Demonstration and Development of Filament Winding Using Photoinitiated
          Resins', *RadTech Report*, vol. 15, no. 36.

[247]   Lackey, E, Vaughan, J, Patki, R 2003, 'Enchanced pultrusion using
          photocure to supplement the standard thermal cure', *Composites 2003,
          Convention and Trade Show, Composites Fabricators Association*, California,
          USA.

[248]   Jacob, S & Dranoff, J 1970, 'Light intensity profiles in a perfectly mixed
          photoreactor', *A.I.Ch.E. Journal*, vol. 16, pp. 359-363.

[249]   Geveke, D, Boyd, G & Zhang, H 2011, 'UV Penetration depth in liquid
          egg white and liquid whole egg', *Journal of Food Processing and Preservation*,
          pp. 1745-4549.

[250]   Ahrens, M, Mallick, V, Parfrey, K 1998, 'Robotic based thermoplastic
          fibre placement process', *International Conference on Robotics and Automation*,
          Belgium.

[251]   Stowe, R n.d, 'Practical aspects of irradiance and energy in UV curing', White Paper, *Fusion UV Systems* viewed 23 July 2015, <www.fusionuv.com>.

[252]   Ciba Speciality Chemicals 2013, 'High lights! Radiation curing with resins and photoinitiators for industrial coatings and graphic arts: Laromer®, Irgacure®, Lucirin®, Darocur®', viewed 2 February 2013, <www.basf.com/group/corporate/en/general-info:/Brand+Irgacure>.

[253]   Lackey, E, Vaughan, J, Patki, R 2003, 'Utilisation of photocure techniques in conjunction with thermal cure – for increasing productivity of the pultrusion process', *RadTech Report*, USA.

[254]   Bolton, J 2000, 'Calculation of UV fluence rate distributions in an annular reactor: significance of refraction and reflection', *Water Research Journal*, vol. 34, no. 13, pp. 3315-3324.

[255]   Adewuyi, OS, Okoli, OI 2009, 'Optimisation of lamp position in the UV curing of 3D Composite Components Manufactured using the RIDFT Process', *Proceedings of the 17th International Conference of Composite Materials*, Scotland, UK.

[256]   Styles, M 2008, 'Characterisation of the Flexural Behaviour of Aluminium Foam Composite Sandwich Structure', Thesis (Ph.D.), *The Australian National University*, Canberra, Australia.

[257]   Livesay, M 1997, 'Low Cost Manufacturing Processes using UV Cure Resins', *Composites '97 Manufacturing & tooling Conference Advisory Committee Liquid molding Session: Emerging Low Cost manufacturing Processes for UV Cure Resins*, USA.

[258]   Tierney, J, Gillespie, J 2003, 'Modeling of Heat Transfer and void Dynamics for the thermoplastic tow-placement process', *Journal of Composite Materials*, vol. 37, pp. 1745.

[259]   Steeg, M, Schledjewski, R, Schlarb, A 2006, 'Automation Implementation and process development of thermoplastic tape placement for 3D parts', *SAMPE Journal*, vol. 42, no. 5, pp. 18-24.

[260]   Sandusky, D, Marchello, J, Baucom, R, Johnston, N 1992, 'Customized ATP Towpreg', *24th International SAMPE Technical Conference*, California, USA, pp. 591-605.

[261]   Sonmez, F, Hahn, H 1997, 'Analysis of the On-Line Consolidation Process in Thermoplastic', *Journal of Thermoplastic Composite Materials*, vol. 10, pp. 543.

[262]   Sonmez, F, Akbulut, M 2007, 'Process optimization of tape placement for thermoplastic composites', *Composites: Part A*, vol. 38, pp. 2013–2023.

[263]   Heider, D, Piovoso, MJ, Gillespie, JW 2003, 'A neural network model-based open-loop optimization for the automated thermoplastic composite tow-placement system', *Composites Part A*, vol. 34, pp. 791–799.

[264]   Hassan, N, Thompson, J, Batra, RC, Hulcher, A, Song, X, Loos, A 2005, 'A Heat Transfer Analysis of the Fibre Placement Composite Manufacturing Process', *Journal of Reinforced Plastics and Composites*, vol. 24, no. 8, pp. 869.

[265]   Shacklford, J & Alexander, W 2001, *Materials Science and Engineering Handbook 3rd Edition*, CRC Press, Australia.

[266]   Cardona, F, Rogers, D & Van Erp, G 2007, 'Investigation by TGA--FTIR of the Effect of Styrene Content and Thickness on the UV-curing of Vinylester Resins', *Journal of Thermoplastic Composite Materials*, vol. 20, pp. 601.

[267]   Phillips, J 2013, 'Fitting Toolbox', viewed 23 January 2013, <www.zunzun.com>.

[268]   Barlow, D, Howe, C, Clayton, G, Brouwer, S 2002, 'Preliminary study on cost optimisation of aircraft composite structures applicable to liquid moulding technologies', *Composites Structures*, vol. 57, pp. 53–57.

[269]   Kumar, J, Kendall, E 1999, 'Complexity Based Cost Estimation Model for Composite Aerospace Structures', Internal Report, *Cooperative Research Centre for Advanced Composite Structures*, CP 99004, Australia.

[270]   Neoh, ET 1995, 'Adaptive Framework for Estimating Fabrication time', Thesis (Ph.D.), *MIT*, Department of Mechanical Engineering, USA.

11 Appendices

11.1 Appendix 1

Quality Functional Deployment (QFD) for the design of the UVAFP placement head as undertaken in the work of Chapter 3.

Table 36 - The pairwise comparison for the prioritisation of the UVAFP prototype requirements.

High Order \ Low Order	Low cost	Produce complex parts	Lightweight	Controllable / Adjustable Process parameters	Varying material systems	Minimise waste	High Quality Laminates / Minimise voids	Varying width fibre rovings	Durable	Detachable Unit - easily swapped	Modular	Not restrict motion of Robot	Lay on complex Contours	Easy to keep clean	TOTAL	Percentage
Low cost		0	0	0	0	0	0	0	0	0	0	0	0	0	0	0
Produce complex parts	1		1	0	1	1	0	1	1	1	1	1	1	1	11	12.087912 09
Lightweight	1	0		0	1	0	0	1	0	1	1	0	0	0	5	5.4945054 95
Controllable / Adjustable Process parameters	1	1	1		1	0	0	1	1	1	1	1	0	1	10	10.989010 99
Accept varying material systems	1	0	0	0		0	0	0	1	1	1	0	0	0	4	4.3956043 96
Minimise waste	1	0	1	1	0		0	1	1	1	1	1	0	1	9	9.8901098 9
High quality Laminates / Minimise voids	1	1	1	1	1	1		1	1	1	1	1	1	1	13	14.285714 29
Accept varying width fibre rovings	1	0	0	0	1	0	0		1	1	1	1	0	1	7	7.6923076 92
Durable	1	0	1	0	0	1	0	0		1	1	0	0	0	5	5.4945054 95
Detachable Unit - easily swapped for another tool	0	0	0	0	0	0	0	0	0		1	0	0	0	2	2.1978021 98
Modular	1	0	0	0	0	0	0	0	0	0		0	0	0	1	1.0989010 99
Not restrict motion of Robot	1	0	1	0	1	0	0	0	1	1	1		0	1	7	7.6923076 92

Lay on complex Contours	1	0	1	1	1	1	0	1	1	1	1	1		1	11	12.087912 09
Easy to keep clean	1	0	1	0	1	0	0	0	1	1	1	0	0		6	6.5934065 93
													TOTAL	91	

11.2 Appendix 2

The UVAFP prototype build process is documented pictorially below.

Figure 144 – The pneumatic compaction actuation platform (top left), pneumatic compaction control system (top right), the resin spray tank (bottom left), the mounted pneumatic control system
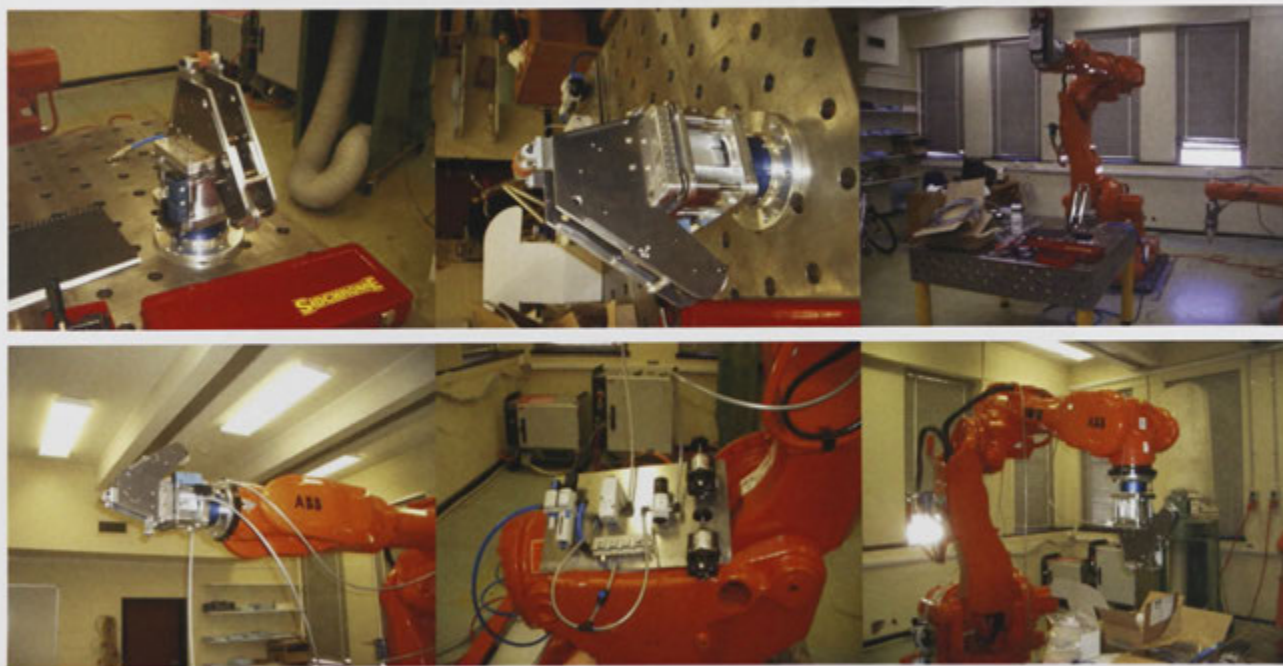
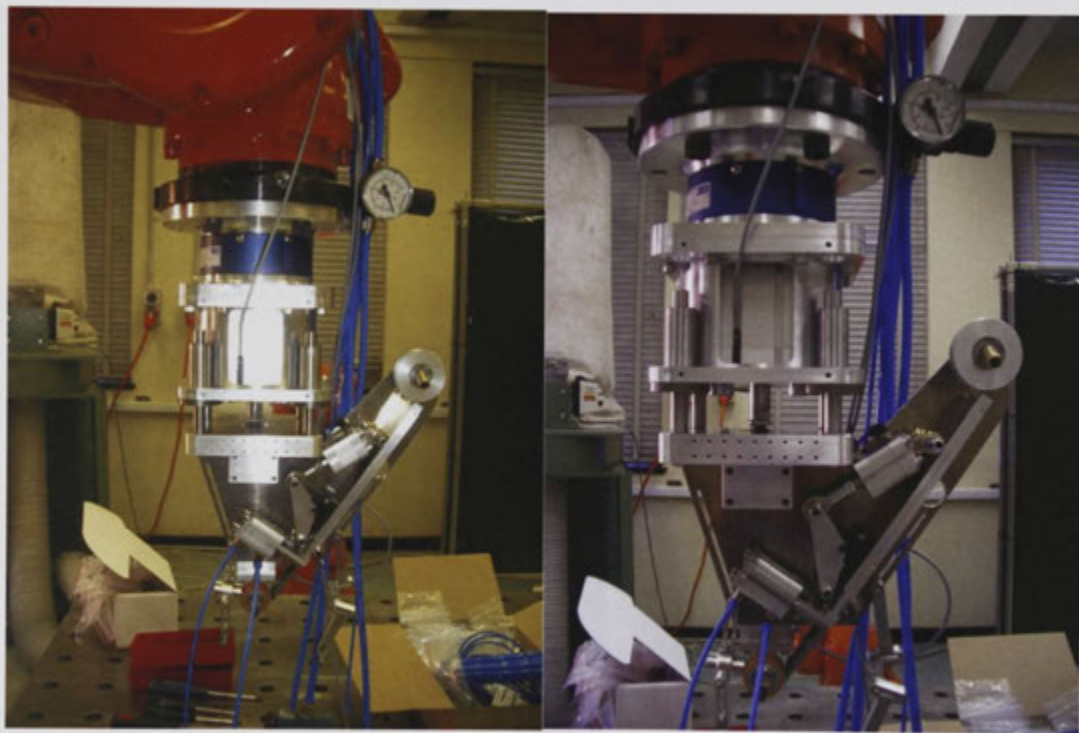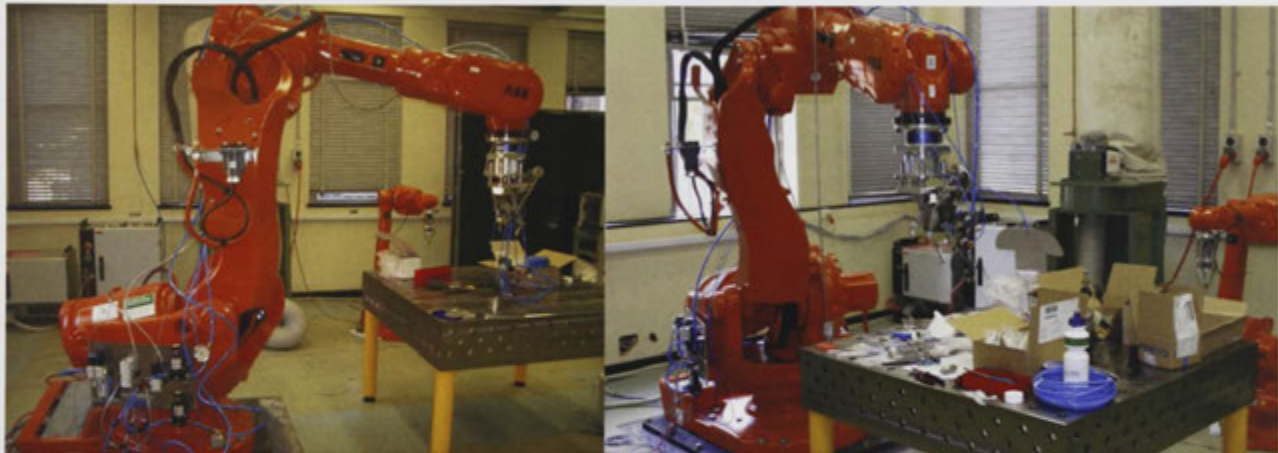Figure 145 – The prototype assembly and build in stages from top to bottom

Figure 146 – The placement head during build

Figure 147 – The prototype build showing the blue resin feed lines and placement head

The spray system design is shown schematically below. The bill of materials for the system is shown in Table 37.

Table 37 – UVAFP Spray System bill of materials

QTY	PRODUCT CODE	DESCRIPTION
1	B1/8JJAUCO-SS+SUJ2-SS	Small JJAU spray gun.
1	22140-1-304SS	Pressure tank stainless steel 3.8 litres
2	10222U+EBO9921+ 530.9312973.23	Precision air regulators c/w mounting brackets & gauges for atomizing air & pressure tank air.
1	11438-50+26383-1/8-60	Air regulator & gauge for cylinder air.
1	52A11DOBDMDDAJ1JM	Atomizing air solenoid 24Vdc x ¼".
1	36A-ACA-JDAO-2KJ	Cylinder air solenoid 3/2 x 1/8" x 24Vdc.
1	74A-015	Y-strainer ½" for liquid.

11.3 Appendix 3

Table 38 – Resin properties

Property	Units	Test Method	Swancor 901-35 vinylester resin [238]	Nuplex Polyplex 62-311 (F62311)	Standard Epoxy	Ashland Derakane 411-350 Vinylester Resin	Ashland Derakane MOMENTUM 411-350 Vinylester Resin
Cost	($US/kg)		4	3.8	6 to 20	5.2	6.4
Viscosity (uncured @ 25°C)	mP.s		2500	300		370	370
Kinematic Viscosity	cSt					350	350
Density	g/ml	ASTM D-792/ISO1183	1.06 +/- 0.02	1.1	1.2	1.046	1.046
Styrene Content	%		45	47-51		45	45
Hardener (as used to generate properties)	name		6% Cobalt: 0.4phr, 100% DMA: 0.05phr, Andonox LCR: 1.2phr @25°C.	MEKP-NR20		NOROX MEKP-925H	NOROX MEKP-925H

Cure cycle			24 hrs @ RT then 2 hrs at 105°C	50 mins @ RT		24hrs @ RT then 2 hrs @ 120°C	24hrs @ RT then 2 hrs @ 120°C
Elastic Modulus	MPa				4500		
Cured Tensile Strength (@ 25°C)	MPa	ASTM D-638/ISO 527	75-96	74	130	86	86
Cured Tensile Modulus (@ 25°C)	GPa	ASTM D-638/ISO 527	3.309-3.585			3.2	3.2
Cured Tensile Elongation (@ 25°C)	%	ASTM D-638/ISO 527	5.0-6.0	4.0	2	5.0-6.0	5.0-6.0
Cured Flexural Strength (@ 25°C)	MPa	ASTM D-790/ISO 178	117.2-137.9	130		150	150
Cured Flexural Modulus (@ 25°C)	GPa	ASTM D-790/ISO 178	3.102-3.447	3.0		3.4	3.4
Cured Heat Distortion Temperature (@ 25°C)	°C @ 1.82 MPa applied stress	ASTM D-648 Method A/ISO 75	105-110			105	105
Cured Barcol Hardness (@ 25°C)	Barcol	ASTM D-2583/EN59	35			35	35
Cured Glass Transition Temperature (Tg)	°C	ASTM D-3419/ISO 11359-2	110	110	80-200	120	120

Volume Shrinkage after cure	%		7.5-8	7-8		7.8	7.8
Heat Capacity (@ 25°C)	kJ/kgK				1.0	1.046	1.046
Thermal Conductivity (@ 25°C)	W/mK				0.2	0.1297	0.1297
Heat of Reaction (@ 25°C)	kJ/kg					60	60
Convective Heat Transfer Coefficient	W/m²/m°C						
Surface Roughness ks	Mm						